Exploring the Dynamics and Distributions of Mercury and Organomercury Species in Soils: Microcosm experiments and Field Studies.

Inauguraldissertation
der Philosophisch-naturwissenschaftlichen Fakultät
der Universität Bern

vorgelegt von

Lorenz Gfeller
von Röthenbach im Emmental

Leiter der Arbeit:
Prof. Dr. Adrien Mestrot, Universität Bern
Prof. Dr. Moritz Bigalke, Technische Universität Darmstadt

Exploring the Dynamics and Distributions of Mercury and Organomercury Species in Soils: Microcosm experiments and Field Studies.

Inauguraldissertation
der Philosophisch-naturwissenschaftlichen Fakultät
der Universität Bern

vorgelegt von

Lorenz, Gfeller
von Röthenbach im Emmental

Leiter der Arbeit:
Prof. Dr. Adrien Mestrot, Universität Bern
Prof. Dr. Moritz Bigalke, Technische Universität Darmsadt

Von der Philosophisch-naturwissenschaftlichen Fakultät angenommen.

Bern, 31.08.2023

Dekan
Prof. Dr. Marco Herwegh

"Dass das physische und geistige Leben des Menschen mit der Natur zusammenhängt,

hat keinen andren Sinn, als dass die Natur mit sich selbst zusammenhängt,

denn der Mensch ist ein Teil der Natur."

- Karl Marx

To all the people,

who bore with me,

during an intensive and uncertain time.

And to my past self,

for standing up again.

Acknowledgements

First and most importantly I would like to thank my primary supervisor, Adrien Mestrot. He has done a great job in supervising me as one of his two first PhD Students. He succeeded in constantly providing an open ear and a positive working culture, while building up a new group and organizing funding for future projects. Thank you for encouraging me to continue my path even in challenging times, to be independent and to learn from mistakes.

Moritz Bigalke, my secondary supervisor, thanks for your expertise and splendid edits to improve my publications. You contributed a great part to my personal and professional development.

Jaime Caplette the PhD buddy and home slice at my side for sharing a lot of experiences, mental breakdowns, all the insider jokes and great laughs.

Thanks to the Swiss National Science Foundation (SNSF) for allowing me to work fully funded four years on this project.

Thanks to all those great lab and office companions and those who have let me use their facilities or helped with experiments. Daniela Fischer, Patrick Neuhaus and Maarika Bischoff for being so good and helpful colleagues in the cLab of the Institute of Geography. Andreas Weber for the endless seeming hours while sampling in the lab. Isabelle Worms, Aline Frossard and Vera Slaveykova for their expertise in qPCR and AF4 analyses. Alexandra Foetisch and Tobias Stalder for the nerdy R and the calming nicotine sessions. Teresa González de Chávez and Evelyne von Wyl for the great discussions and philosophical deep dives – this was nice. Karen Viacava for providing a calm mind when I was frustrated. Hang Guan for showing me the way to properly prepare Hot Pot and being a nice office buddy for a long time. Martin Imseng, Miquel Coll and Sabnam Mahat for great off-work time, parties and concerts. Klaus Jarosch and Tobias Sprafke for the hard but fair discussions about soil types and geological processes. Moritz Köster and Jennifer Herschbach for the introduction in the first few months at the institute. And to Isabelle Geissbühler and Saliba F. Saliba for providing splendid infrastructure at the Institute of Geography.

Diese Danksagung soll aber nicht enden ohne, dass ich den Menschen ab von der Arbeit danke, die mir von allen am meisten am Herzen liegen. Vielen Dank an meine Eltern Walter und Margaretha, dass Ihr mir die Werte auf den Weg gegeben habt, die mich heute auszeichnen, und mir viel Zeit und Möglichkeiten gegeben habt mich zu entwickeln. Vielen Dank an meine Brüder Hannes und Frank für die bedingungslose Unterstützung und die Petanque-Spiele im Lorraine Park. Danke Dosch, Amélie, Mänu, Rowan, Flüpu, Mädy, Leonie, Robin, Meret, Doris, Sarah, Jönu, Hannah, Lina, Marä, Nicä, Paul, Nora, Roman, Stibe, Marc, Lüku, Tashi, Remo, Eva, Katja, Marius, Mättu, Ninil, Rapha und Cécile für alle Gespräche, das Lachen und die Tränen.

Und vorallem, Danke Barbara! Die Zeit während des Doktorats war eine Berg- und Talfahrt. Es ist wahnsinnig schön zu sehen, dass wir uns - trotz konstanter Veränderung und schwierigen Zeiten - immer noch auf Augenhöhe begegnet sind.

Danke für all dein Verständnis, deine Offenheit und dass du mich genommen hast, wie ich bin. Alles gute auf deinem Weg.

Contents

List of Figures

List of Tables

Chapter 3

Chapter 4

Supplement B

Supplement C

Summary

Mercury (Hg) is a pollutant of global concern due to its ubiquitous presence in the environment, ongoing anthropogenic emissions, and its toxic effects on the human nervous, digestive, and immune systems. The toxicity of Hg and its uptake in biota depend on the chemical speciation, with methylmercury (MeHg) representing the most relevant species for bioaccumulation and biomagnification. One significant anthropogenic source of Hg in the environment are historical emissions from chlor-alkali and acetaldehyde-producing chemical plants. Often, their legacy sites exhibit exceptionally high concentrations of Hg but are poorly characterized regarding MeHg and natural mercury methylation. One reason for this is the existing challenges in MeHg analysis in highly polluted substrates. However, analyzing such soils is critical to evaluating potential environmental risks. Polluted soils with high levels of Hg are potential point sources to downstream ecosystems. Repeated flooding (e.g., redox cycling) and agricultural activities (e.g., organic matter addition) may influence the fate and speciation of Hg in a soil system. The formation and aggregation of colloids and particles affect both Hg mobility and its bioavailability to MeHg-forming microbes.

This thesis aimed i.) to assess the differences in regional distribution of Hg and MeHg among landuse types in a alpine mountain valley ii.) to improve and test existing methods for MeHg extraction and analyses of highly contaminated soils and iii.) to assess the influence of anthropogenically induced disturbances such as flooding, and manure application on net-methylation and mobility of Hg in in agriculturally used soils. We addressed these questions by studying soils from agricultural fields and grove sites in the region of Visp, Switzerland. This model site hosts both contaminated and uncontaminated fields and areas that are regularly subjected to flooding.

i.) We observed significant correlations between Hg and soil organic carbon (OC) in the topsoil (R^2 = 0.73, $p < 0.05$). Furthermore, the Hg enrichment factors in the topsoils (0 to 10 cm) were highest in both grassland ($EF_{Hg/Al}$: -36.2 to 1429; median = 323; n = 38) and tree groves ($EF_{Hg/Al}$: 599 to 3676; median = 1163; n = 10). The correlation between Hg and OC, along with the $EF_{Hg/Al}$ profiles, suggests atmospheric deposition as the primary pathway. The absence of a spatial pattern may be attributed to varying wind directions and seasonal temperature inversions in the valley. While the topsoils of grasslands and tree groves exhibit similar levels of Hg, the latter display significantly higher net-methylation potential (MeHg/Hg: 0.28 - 19.1%; median = 3.6%; n = 10) compared to grasslands (MeHg/Hg: 0.18 - 2.4%; median = 0.53%; n = 40), indicating a higher input of readily available Hg, greater bioavailability of Hg, and/or enhanced microbial activity.

ii.) Further, we found that during extraction of MeHg from soil, false positives from artificial methylation may be corrected for by a simple constant correction factor. Methylation factors from iHg spiking were in the range of (0.0075 ± 0.0001%) and were consistent across soils and sediment matrices. Analyzing contaminated soils in the abovementioned area, we suggest that MeHg was anthropogenically deposited and not naturally formed *in-situ* in two out of three highly contaminated locations. Our line of evidence consists of 1) the concomitant detection of ethyl mercury EtHg, 2) the elevated MeHg concentrations (up

to 4.84 µg kg^{-1}), and 3) the absence of hgcA genes at these locations. The combination of Hg speciation and methylation gene (hgcA) abundance analyses proved to be tools suited to assess Hg pollution pathways at Hg legacy sites.

iii.) We conducted a flooding-draining experiment on Hg-polluted floodplain soils from the abovementioned agriculturally used area. The experiment included two 14-day flooding periods and one 14-day draining period, with natural organic matter added to two soils with varying Hg and organic carbon levels. Manure addition resulted in accelerated release of Hg to the soil solution, fast sequestration of Hg, and increased the particulate and colloidal Hg pool bound to dissolved organic matter and Hg^{II} bound to inorganic ligands. The experiment showed net MeHg production during the first flooding and draining period, and subsequent decrease in absolute MeHg concentrations. Manure addition did not significantly change net MeHg production. Our results suggest manure addition may promote Hg sequestration by complexation on large organic matter components and formation of inorganic HgS(s) colloids in Hg-polluted fluvisols with low levels of natural organic matter.

Zusammenfassung

Quecksilber (Hg) ist ein Schadstoff von globalem Interesse aufgrund seiner ubiquitären Präsenz in der Umwelt, der fortlaufenden anthropogenen Emissionen und seiner toxischen Auswirkungen auf das menschliche Nerven-, Verdauungs- und Immunsystem. Die Toxizität von Hg und seine Aufnahme in Biota hängen von der chemischen Speziation ab, wobei Methylquecksilber (MeHg) die relevanteste Spezies für Bioakkumulation und Biomagnifikation darstellt. Eine bedeutende anthropogene Quelle von Hg in die Umwelt sind historische Emissionen und Altlasten der Chlor-Alkali- und Acetaldehyd-produzierenden Industrie. Bekannterweise zeigen diese Altlasten außergewöhnlich hohe Konzentrationen von Hg, sind aber hinsichtlich MeHg und natürlicher Quecksilbermethylierung schlecht charakterisiert. Ein Grund hierfür sind die bestehenden Herausforderungen bei der MeHg-Analyse in hochkonzentrierten Substraten. Die Analyse solcher Böden ist jedoch entscheidend, um potenzielle Umweltrisiken zu bewerten. Böden mit hohen Hg-Konzentrationen sind potenzielle Quellen für nahegelegene Ökosysteme. Wiederholte Flutungen (z.B. Redoxzyklen) und landwirtschaftliche Aktivitäten (z.B. Zugabe von organischem Material) können die Mobilisierung und die Speziation von Hg in einem Bodensystem beeinflussen. Die Bildung und Aggregation von Kolloiden und Partikeln beeinflusst sowohl die Mobilität von Hg als auch dessen Bioverfügbarkeit für MeHg-bildende Mikroben.

Diese Disertation hat zum Ziel, i.) die kleinräumigen Unterschiede in der Verteilung von Hg und MeHg zwischen verschiedenen Landnutzungstypen in einem alpinen Bergtal zu untersuchen und zu bewerten, ii.) bestehende Methoden zur Extraktion und Analyse von MeHg in stark kontaminierten Böden zu testen und bekannte analytische Artefakte zu korriegieren, und iii.) anthropogene Einflüsse - wie die Anwendung von Düngemitteln oder Überschwemmungen - auf die Netto-Methylierung und Mobilität von Hg in landwirtschaftlich genutzten Böden zu bewerten. Diese Fragen wurden anhand von Böden aus landwirtschaftlichen Feldern und Waldstandorten in der Region Visp untersucht. Dieser Modellstandort umfasst sowohl kontaminierte als auch unkontaminierte Felder und Gebiete, die regelmäßig Überschwemmungen ausgesetzt sind.

i.) Es wurden signifikante Korrelationen zwischen Hg und dem organischen Kohlenstoffgehalt (OC) im Oberboden beobachtet (R^2 = 0,73, $p < 0,05$). Darüber hinaus waren die Hg-Anreicherungsfaktoren in den Oberböden (0 bis 10 cm) sowohl in Grasflächen ($EF_{Hg/Al}$: -36,2 bis 1429; Median = 323; n = 38) als auch in Baumhainen ($EF_{Hg/Al}$: 599 bis 3676; Median = 1163; n = 10) am höchsten. Die Korrelation zwischen Hg und OC sowie die $EF_{Hg/Al}$-Profile legen eine atmosphärische Ablagerung als Hauptpfad nahe. Das Fehlen eines räumlichen Musters gegenüber einer historischen Quecksilberemissionsquelle könnte auf wechselnde Windrichtungen und saisonale Temperaturinversionen im Tal zurückzuführen sein. Während die Oberböden von Grasflächen und Baumhainen ähnliche Hg konzentrationen aufweisen, zeigen letztere ein signifikant höheres Netto-Methylierungspotenzial (MeHg/Hg: 0,28 - 19,1 %; Median = 3,6 %; n = 10) im Vergleich zu Grasflächen (MeHg/Hg: 0,18 -

2,4 %; Median = 0,53 %; n = 40), was auf einen grösseren Anteil von bioverfügbarem von Hg für Hg methylierende mikrobielle Gemeinschaften und/oder eine gesteigerte mikrobielle Aktivität in Baumhainflächen hinweist.

ii.) Während der Extraktion von MeHg aus Bodenproen konnten falsch positive Ergebnisse durch einen konstanten Korrekturfaktor berichtigt werden. Die Methylierungsfaktoren durch Hg-Spiking lagen im Bereich von (0,0075 ± 0,0001 %) und waren bei verschiedenen Böden und Sedimentmatrizes konsistent. Die Untersuchung kontaminierter Böden in den oben genannten Gebieten legen nahe, dass MeHg in zwei von drei untersuchten, Hg-kontaminierten Standorten abgelagert wurde und nicht natürlich vor Ort gebildet wurde. Darauf hindeutend sind i) der gleichzeitigen Nachweis von Ethylquecksilber (EtHg), ii) die erhöhten MeHg-Konzentrationen (bis zu 4,84 µg kg^{-1}) und iii) die Abwesenheit von hgcA-Genen an diesen Standorten. Die Kombination von organischer Hg-Speziationsanalytik und Analysen der Methylierungsgene (hgcAB) wurden als geeignete Werkzeuge zur Beurteilung der Ablagerungshistorie in organo-Hg kontaminierten Altlasten bewertet.

iii.) weiter wurden Flutungs-Abflutungs-Experiment an Hg-belasteten Auenböden aus dem oben genannten landwirtschaftlich genutzten Gebiet durchgeführt. Das Experiment umfasste zwei 14-tägige Flutungsperioden und eine 14-tägige Abflutungsperiode, wobei natürliches organisches Material zu zwei Böden mit unterschiedlichen Hg- und organischen Kohlenstoffgehalten hinzugefügt wurde. Die Zugabe von Dünger führte zu einer beschleunigten Freisetzung von Hg in die Bodenlösung, einer schnellen Bindung von Hg und einer Zunahme des Hg-Gehalts in Partikeln und Kolloiden, in denen Hg an organische Polymere und anorganische Liganden (HgS) gebunden waren. Das Experiment zeigte eine Netto-MeHg-Produktion während der ersten Flutungs- und Abflutungsperiode und eine anschließende Abnahme der absoluten MeHg-Konzentrationen. Die Zugabe von Dünger veränderte die Netto-MeHg-Produktion nicht signifikant. Die Ergebnisse deuten darauf hin, dass die Zugabe von Dünger die Bindung von Hg durch Komplexierung an große organische Verbindungen und die Bildung von anorganischen HgS(s)-Kolloiden in Hg-belasteten Fluvisolen mit geringem Gehalt an natürlichem organischen Material fördern kann.

1. Introduction

The purpose of this introduction is to provide a comprehensive overview of the behavior of mercury (Hg) in the environment, with a particular focus on methylation and soils. It will also introduce basic knowledge about Hg, its global cycle, the challenges of analyzing organic Hg species - such as methyl mercury (MeHg) - in soil matrices and will supply an overview of microbial Hg transformations in the environment. Finally, the goals and knowledge gaps that are addressed in this thesis will be outlined. The following chapters will include more specific introductions but may also include some repetition of material presented in this chapter.

1.1 The element Mercury and its chemical species

Mercury (Hg) is a transition metal with the atomic number 80 classified in group 12 and period 6 of the periodic table. On earth, natural Hg consists of seven stable isotopes with comparably even distributed natural abundances (^{196}Hg – 0.15 %, ^{198}Hg – 9.97 %, ^{199}Hg – 16.87 %, ^{200}Hg – 23.10 %, ^{201}Hg – 13.18 %, ^{202}Hg – 29.86 %) and is present in three prevalent oxidation states (Hg^0, Hg^I, Hg^{II}).

In its elemental form (Hg^0), it has a melting point of -38.83° C and a boiling point of 365.62° C. Thus at room temperature of 20 °C, it is liquid and has a relevant vapor pressure of 0.264 Pa (Lide, 2004). In the natural environment, Hg^0 can therefore exist in the gaseous or liquid state. Gaseous elemental mercury (GEM) is the dominant form in the atmosphere, and most natural waters are nearly saturated or supersaturated with respect to atmospheric Hg^0 (Fitzgerald et al., 2007).

Hg^{II}, or divalent Hg, is present in inorganic (e.g., HgS, Hg^{2+}) and organic forms (e.g., methyl mercury). These compounds vary in their toxicity, solubility. Compared to Hg^0, Hg^{II} is more common in soils, sediments, or water than in the atmosphere. Due to the chalcophile character of Hg, it is often associated with sulfide minerals or R-SH functional groups (thiol group) in organic molecules. The common Hg sulfide minerals cinnabar (HgS) and meta-cinnabar (ß-HgS) have an exceptionally low solubility and are the thermodynamically favored form of Hg under sub-oxic condition.

Methylmercury also called mono methylmercury (MeHg or CH_3Hg) is significantly more toxic than Hg^0 or Hg^{II} as it can pass the blood-brain boundary (Langford and Ferner, 1999). Due to its lipophile character MeHg remains and bioaccumulates in organisms and biomagnifies up the food chain. Like this, MeHg. can make up more than 95% of Hg in fish (Chen et al., 2008). It is therefore of particular interest because of its role in the biological cycling of Hg and its toxicity.

Dimethyl mercury (DMHg or $(CH_3)_2Hg$), is a highly volatile and toxic compound, with a toxicity level greater than that of MeHg. Accidental exposure to as little as 100 µl of DMHg on the skin has been shown to be lethal, as exemplified by the death of a scientist due to such exposure. (U.S. Department of Labor, 1998). While it is believed to be present in the atmosphere at very low concentrations, it is thought to be widely distributed in the deep ocean (Bank, 2012). The role of DMHg in the global biogeochemical cycle of Hg, and its potential for bioaccumulation, remains poorly understood. Despite the scientific community's continued focus on MeHg, recent research efforts have aimed at increasing our understanding of DMHg in the environment (West et al., 2022; Lian et al., 2021).

Ethyl mercury (EtHg or C_2H_5Hg) is a product of the chemical industry. It is highly toxic and is utilized as a preservative in vaccines, although concerns about its neurotoxic potential have led to its discontinuation in most vaccines (Geier et al., 2015). To date it is still under debate if EtHg does occur naturally in the environment (Mao et al., 2010). Mainly it is an anthropogenic compound that has also been utilized as a laboratory reagent (Geier et al., 2015). Trace amounts of EtHg may be present in the environment as a result of its use in industrial applications (Tomiyasu et al., 2017) or its application as a fungicide (Skerfving and Copplestone, 1976), however to date it has been environmental contaminant of relatively low scientific interest.

Phenylmercury (PhHg or C_6H_5Hg) is an artificially synthesized compound. In the past it was used as fungicide or pesticide applications (Hintelmann et al., 1995) but has been banned in Europe (José Manuel Barroso, 2012).

In short, Hg is present in various organic and inorganic species and can be found in all environmental compartments, from the upper troposphere (Lyman and Jaffe, 2012) to the deep peridotites of the Earth's mantle (Canil et al., 2015). It is encountered in organisms on land (Weiss-Penzias et al., 2019) or in the oceans (Lavoie et al., 2013) and because of its high toxicity and long residence time in the atmosphere, Hg is the first toxic trace metal to have legally binding international regulations for its emission, use, and trade: the UN Minamata convention. Its potential to harm human health and the environment has led to the implementation of these regulations to reduce Hg exposure and prevent its negative impacts (UNEP, 2019). Despite this, millions of people continue to be exposed to Hg through a diet high in fish in general, or in specific contaminated areas (Matsumoto et al., 1965; Zheng et al., 2019). The environmental implications of its anthropogenic emissions and its toxicity urge scientist until today to unravel the high complexity of its nature.

1.2. Technical applications and anthropogenic sources of Hg to soils.

Despite its toxic effects on human health, Hg's various physical and chemical properties make it ideal for a wide range of technical applications. This includes its use in elemental Hg measuring instruments such as thermometers, manometers and in determining the pore size distribution and volume of porous materials (Abell et al., 1999). It is used in electronic switches and relays because of its liquid state and high electronic conductivity compared to other liquids ($1{,}04 \cdot 10^6$ $A \cdot V^{-1} \cdot m^{-1}$) or in thermometers due to its high thermal expansion coefficient (60.4 µm $(m \cdot K)^{-1}$) (Lide, 2004).

Mercury can form alloys (amalgams) with various metals (e.g. gold, copper, silver). The viscosity of these amalgams varies depending on the proportion of Hg in the alloy, which allows for a wide range of technical applications. For example, dental amalgams are used to fill cavities (Eagles-Smith et al., 2018). While the use of dental amalgam has decreased in developed countries in recent decades, it is still widely used globally (Eagles-Smith et al., 2018). Amalgamation was also commonly used in historic gold mining to extract gold from fine-grained materials. Currently, Hg is still used in small-scale artisanal gold mining. Although, it has been replaced by cyanide as a solvent in commercial gold mining, small-scale artisanal gold mining remains the largest anthropogenic source of Hg to the environment to date (UNEP, 2017). Hg from gold mining is mainly released as GEM to the atmosphere. While the mining and smelting process of the Hg ore cinnabar (HgS) releases both Hg^0 and accounts for the dispersion of solid HgS in the vicinity of the mining sites (Higueras et al., 2003).

Numerous industrial processes within the chemical industry use Hg, including the chlor-alkali process (Wängberg et al., 2003; Hissler and Probst, 2006), the production of acetaldehyde and the synthesis of vinyl acetate (Malta et al., 2017). These application are based on Hg's ability to act as a catalyst, or as a cathode metal agent (Malta et al., 2017; Lakshmanan and Murugesan, 2014). Historically, chemical industries and Hg mining have released Hg into the atmosphere, hydrosphere, and

soils in their surrounding areas (Horowitz et al., 2014). These industries, along with associated legacy sites, are significant contributors to Hg pollution as point sources. Compared to the mining industry, the release of Hg from chemical processes is not limited to the forms of Hg^0 or HgS, but also includes ionized Hg^{2+} or organic-Hg species such as MeHg (Hintelmann et al., 1995; Fujiki and Tajima, 1992; Matsumoto et al., 1965), EtHg (Hintelmann et al., 1995; Tomiyasu et al., 2017) and PhHg (Hintelmann et al., 1995) which are posing higher risks to human health.

Even though emission sources and legacy sites are commonly identifiable, remediation efforts are often insufficient due to financial or political constraints. When addressing the distribution of Hg in a site, the characterization of organo Hg species often falls short. This lack of information leaves uncertainties about the sources, pathways, and potential risks of the Hg source open. Therefore, when investigating contaminated sources, it is crucial to analyze not only total Hg content but also organo Hg speciation.

1.3. The global cycle of mercury

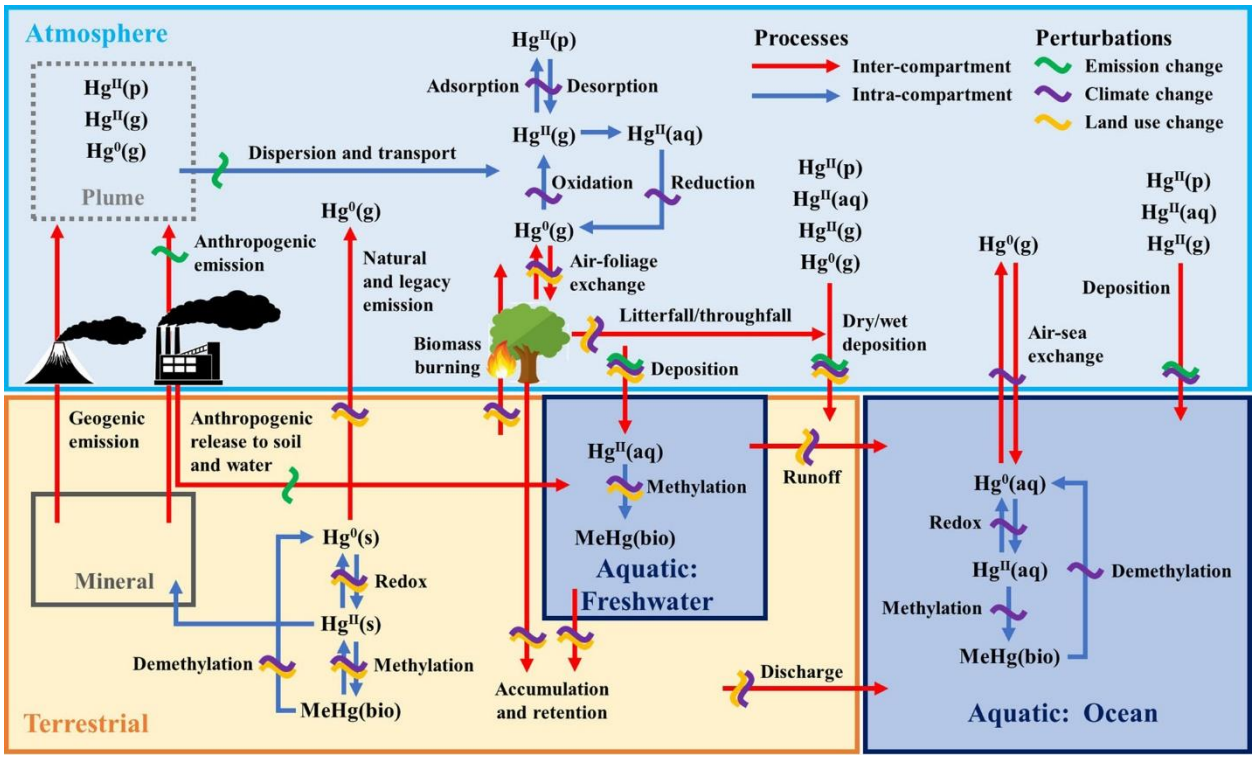

Figure 1 - 1 Obrist et al. 2018: Critical processes of global importance for Hg cycling, including fluxes between major environmental compartments. Perturbations of Hg processes and fluxes show predicted impacts due to changes in emission, climate, and land use.

One of the key differences between Hg and other organic pollutants is that Hg is a compound that cannot degrade or decompose and constantly recycles through the environment. Specifically, Hg that is deposited in soils, lakes, wetlands, or oceans may eventually be re-released to the atmosphere (Fig.1). This continual cycling of Hg through the environment and biota makes it challenging to track and understand its movements and impacts.

1.3.1. Lithosphere – Forms – Pool size

The earth's interior is depleted in Hg with respect to the bulk earth and biggest Hg pools are found on earth's surface. The primitive upper mantle was estimated to have 0.4 to 0.6 µg kg^{-1} Hg based on fresh xenolith samples. In turn, the abundance of Hg in the crustal samples varies from 0.9 to 8 µg kg^{-1} and correlates with S and Cu but no other element indicative of magmatic differentiation (Canil et al., 2015). Organic rich shales show concentrations (100-200 µg kg^{-1}) which are around one magnitude higher than sandstones, limestones igneous rocks (10-30 µg kg^{-1}). This distribution is the consequence of Hg's strong affinity to natural organic matter (Beckers and Rinklebe, 2017). Both mantle and crustal rocks are active sources to the earth's atmosphere, surface, and upper crust through hydrothermal (Roberts et al., 2021) and volcanic (Nriagu and Becker, 2003) activities until today. Whereas arc volcanism shows a three times higher Hg flux than non-arc vulcanism (e.g., ocean ridge or hotspots). Approximately 98 % of the Hg emitted by volcanos is released as Hg^0 or GEM (Edwards et al., 2021). The remaining part is emitted as ionized Hg^{2+} and rapidly binds to solid particles (Fig.1), which then disperse and are transported through the atmosphere. To our knowledge, no well elaborated estimate about Hg pool in the earth's mantle and crust have been made.

1.3.2. Atmosphere – Forms – Pool size

In the atmosphere, Hg is largely composed of Hg^0 (>98%), while various gaseous molecular Hg^{II} species (GOM) and particulate bound mercury (PBM) make up rather small fractions (Fu et al., 2016; Kentisbeer et al., 2014). In the form of GOM, Hg residence times range from days to weeks, and as Hg^0 (GEM) residence times range from several months up to a year (Driscoll et al., 2013). Driscoll et al. 2013 estimated the global pool of Hg in the atmosphere to be approximately 5.0 Gg, and annually, global Hg emissions to the atmosphere range from 6500 to 8200 Mg, with 4600 to 5300 Mg coming from natural processes and sources (primary geogenic plus secondary emissions). Primary anthropogenic sources contribute 1900 to 2900 Mg per year, while primary natural (geogenic) inputs are 80 to 600 Mg per year.

The atmosphere is an important pathway for Hg between environmental compartments (e.g., soils, sediments, the aquatic environment) and facilitates the redistribution and transport Hg from point sources to remote unpolluted areas. Atmospheric Hg deposits on the land surface through wet and dry deposition mechanisms. Wet deposition is dominated by GOM; GEM does not contribute significantly to wet deposition due to its relatively low solubility in rainwater (Bishop et al., 2020; Schroeder and Munthe, 1998). On the other hand, dry deposition involves the direct sorption of Hg^{2+} and Hg^0 to surfaces. This includes uptake by vegetation (Fu et al., 2016; Wohlgemuth et al., 2021; Wang et al., 2016a) and settling of atmospheric particles. Dry deposition though plants and vegetation is considered a significant sink for atmospheric Hg to the terrestrial environment (Jiskra et al., 2018). For the deposition over the ocean, latest evidence using natural stable isotope ratios state that the contributions of wet (Hg^{II}) and dry deposition (Hg^0) are approximately equal (Jiskra et al., 2021). However, it is still a matter of debate whether the marine environment serves as net sink or net source of atmospheric Hg.

On a political level, the long residence time and transboundary transport of Hg were major factors in the development and implementation of the Minamata Convention, an international treaty designed to protect human health and the environment from the effects of Hg (UNEP, 2017).

1.3.3. Ocean water – Forms – Pool size

The marine environment (ocean waters) represents the second largest pool of Hg in the environment, after to the terrestrial pools. Driscoll et al. estimated that the world's oceans carry a sum of about 157 Gg of Hg with 2.9 Gg, 134 Gg, and 220 Gg distributed in Surface Ocean, Intermediate Water, and the Deep Ocean, respectively. The authors highlighted that the Hg size pool in the Surface Oceans were mainly dominated by anthropogenic emissions of the last 150 years (Driscoll et al., 2013). Sources of Hg to the oceans are the atmospheric exchange and the export of Hg from freshwater ecosystems. The main sinks are deep and shallow ocean sediments (Sunderland and Mason, 2007).

In the ocean Hg is mainly present in four forms; Hg^0, MeHg, DMHg and inorganic Hg^{II}, the latter is mostly present as Cl or reduced sulfur complexes or bound to dissolved organic matter (DOM) (Han and Gill, 2005). Total Hg concentrations in the oceans are typically low and range between 100 - 400 pg L^{-1}. The organo Hg species are in the range of 0.04 – 40 pg L^{-1} and 7.5 – 105 pg L^{-1} for DMHg and MeHg, respectively. MeHg concentrations are the result of the methylation and demethylation processes in these environments. For example, MeHg concentrations in ocean surface waters are generally lower due to photochemical UV-degradation of MeHg (Bank, 2012). Although ocean water MeHg concentrations are relatively low, MeHg is an important part of the biogeochemical cycle, since phytoplankton may bioaccumulate MeHg, resulting in concentrations approximately 10,000 times higher than those found in their natural aquatic environment (Pickhardt and Fisher, 2007). This transfer of MeHg from natural waters to phytoplankton is the most significant bioconcentration of MeHg in aquatic food chains at any trophic level and is crucial since the majority of MeHg present in fish at higher trophic levels is acquired through dietary intake (Bank, 2012).

1.3.4. The terrestrial system: Soils and Fresh water – Forms – Pool size

The global pool of Hg in soils is a subject of debate, with estimates ranging widely. In 2013, it was estimated that Hg in organic topsoil was approximately 200 Gg, while mineral soils held approximately 800 Gg. The surface soil Hg reservoir is believed to respond faster to environmental changes (e.g. anthropogenic Hg emissions, climate change) compared to the mineral soil pool, which is considered highly recalcitrant (Driscoll et al., 2013). In 2018 attention has been drawn to the permafrost regions. First estimates claimed that the Northern Hemisphere permafrost region contains 1656 ± 962 Gg Hg in the three upper soil meters which approximately doubled the global Soil Hg pools (Schuster et al., 2018). According to this recent estimate, the terrestrial compartment and soils in particular represent by far the largest pool of Hg. The authors further estimated that 793 ± 461 Gg Hg would be still frozen in the permafrost raising questions about the evolution of Hg mobility and speciation in

response to climate change in these regions. Current climate models estimate that the emissions of the permafrost pool in the form of Hg^0 would be in the order of today's anthropogenic emissions using the RCP85 climate projection (Schaefer et al., 2020). To our knowledge, there are no estimates for the effect of climate change on the transformation of Hg to MeHg in polar regions.

According to Beckers and Rinklebe, 2017, estimates of background Hg concentrations in soils vary between ~10-200 μg kg^{-1}. European soils are at the lower end of this estimate with median concentrations of 23 μg kg^{-1} (Panagos et al., 2021). The wide span of estimates reflects the high heterogeneity of soil Hg on local and regional scales. For example, it was found that soil Hg concentration may change with vegetation type, elevation and latitude (Obrist et al., 2011; Zhou et al., 2021).

Soils may be both sink and source of Hg to atmospheric and aquatic compartments (Fig. 1-1). Pathways of Hg to soils include dry deposition of GEM by incorporation into plant material and soil organic matter (Obrist et al., 2011), wet deposition of gaseous oxidized mercury (GOM) by cloud water and rain as well as deposition of dust from close anthropogenic point sources (Guédron et al., 2013; Hissler and Probst, 2006). To date, dry deposition of Hg is considered the most important pathway of Hg on a global scale. After deposition, Hg may be reemitted by Hg^0 reduction. The exchange of GEM between terrestrial surfaces and the atmosphere is comprised of emissions from soil and vegetation surfaces, geogenic activity, biomass burning, and Hg^0 dry deposition to surfaces. The net flux of Hg^0 between land and the atmosphere is the sum of these processes. However, accurately measuring the real-time net Hg^0 flux remains a significant challenge due to high levels of uncertainty in observations (Bishop et al., 2020). Although the once deposited Hg may be reemitted, a significant part of Hg has been accumulated in the terrestrial environment over time. Especially organic rich soils are subjected to these depositions. A global model suggested that atmospheric Hg deposition has increased the Hg concentration of upper organic soil layers by 20% since the onset of industrialization (Smith-Downey et al., 2010).

The Hg released from soils freshwater aquatic systems (Driscoll et al., 2013). Factors such as the size, topography, elevation, land cover, and land use of a watershed play a role in determining the amount of Hg that is deposited on the land surface and subsequently transported to aquatic ecosystems (Bishop et al., 2020). Although, Arctic regions today show the highest maximal runoffs for Hg (112.24 μg m^{-2} yr^{-1}) and MeHg (0.480 μg m^{-2} yr^{-1}) respectively. Median Hg runoffs are still highest for Urban areas (≈ 5 μg m^{-2} yr^{-1}) followed by Agriculture (≈ 3 μg m^{-2} yr^{-1}), Upland Forest (≈ 2 μg m^{-2} yr^{-1}). Anthropogenic disturbances such as deforestation have been shown to mobilize Hg and MeHg from forest soils to the aqueous phase, often associated with DOM (Kronberg et al., 2016; Ukonmaanaho et al., 2016). Further, during flooding events Hg sorbed to Mn or Fe-oxy-hydroxide surfaces maybe mobilized due to the reductive dissolution of these minerals, for example during flooding events (Gygax et al., 2019; Poulin et al., 2016).

In soils, Hg is present in three predominant forms: elemental Hg^0, inorganic Hg^{II}, and MeHg. Although, Hg^{II} generally represents the largest fraction, Hg^0 may make up significant amount of Hg in contaminated soils (Biester et al., 2002a) or soils

in regions with geological activities (e.g. hydrothermal or volcanic) (Schlueter, 2000). The speciation of Hg^{II} in a soil is primarily governed by the prevailing biogeochemical conditions. Numerous factors, such as the abundance of natural organic matter (NOM), the redox conditions, and the resulting speciation of S, Fe, or Mn, can significantly influence the speciation of Hg. For example, in NOM rich boreal peatlands and forest soils, Hg is primarily bound to thiol-groups of NOM (Hg-NOM), associated with FeS(s), found as cinnabar (HgS(s)) or meta-cinnabar (ß-HgS(s)), which are the thermodynamically most favored forms of Hg in these environments (Skyllberg et al., 2006; Skyllberg and Drott, 2010; Biester et al., 2002a). On the other hand, in with low NOM levels, Hg sorbed onto the surfaces of Mn -, Fe -, and Al-oxy-hydroxides may play a significant role in Hg speciation and retention (Guedron et al., 2009; Gfeller et al., 2021).

There is a consensus that the inorganic speciation of Hg plays a crucial role in its reactivity, mobility, and methylation potential. Also the size and crystallinity of Hg (nano-)particles is thought to have a crucial for their mobility and availability for methylation (Graham et al., 2012; Tian et al., 2021). In a soil system, freshly deposited Hg may undergo various speciation changes such as transforming from a soluble form (e.g., $HgCl_2$) to a strongly chelated (e.g., Hg-NOM) form or become sorbing or coprecipitating on and in particles (both particulate NOM and mineral particles) (Figure 1-2). This process is commonly referred to as "aging" (Aiken et al., 2011). For example, metallic colloids form during biomineralization processes triggered by soil reduction, or during precipitation that occurs within the root zone. These colloids have the potential to incorporate toxic trace elements such as Hg. The formation of HgS occurs in environments with present free reduced S species (Poulin et al., 2017; Gerbig et al., 2011). However, the direct formation of colloidal β-$HgS_{(s)}$ from Hg-NOM has been suggested as mechanism in oxic upland soils (Manceau et al., 2015). Also, the coprecipitation of Hg into metallic Cu particles and different metal sulfides has been observed (Hofacker et al., 2013). Poulin et al. 2017 found that the size of newly formed HgS nano particulates depends on the ratio between DOM and free sulfide (HS^-) in solution. Higher DOM concentrations my cap the growth an aggregation of nano particulate HgS (Gerbig et al., 2011). Other metal sulfide, oxide, or carbonate colloids exhibited similar reactions to DOM (Aiken et al., 2011; Deonarine et al., 2011). The impeding effects of DOM on the formation of β-HgS(s) particles could potentially enhance Hg mobility and availability to microorganisms that produce MeHg (Section 1.4.) (Deonarine and Hsu-Kim, 2009; Graham et al., 2012; Ravichandran et al., 1998). Also the crystalline structure has an effect on the bioavailability of HgS colloids. Tian et al., 2021 observed that the changes in surface structure during HgS nano particulate aging significantly influenced the bioavailability of these colloids for sulfate reducing bacteria. Thus, analyzing inorganic Hg speciation in soil and soil solution is crucial when studying mobility and methylation in a field setting.

To determine the inorganic speciation of Hg in solid matrices like soils or sediment, sequential chemical extractions (Bloom et al., 2003) and thermal desorption pyrolysis (Biester and Scholz, 1997) are among the most frequent methods used. However, while these methods are widely applied, they are unable to determine specific Hg species. Instead, they address operationally defined fractions. The results of such analytical procedures have to be interpreted with care, since the specimen's matrix may

significantly influence the methods. Despite the availability of alternative methods such as extended x-ray absorption fine structure (EXAFS), high detection limits still are limiting their practical application. Therefore, these methods are more commonly employed in laboratory experiments at higher concentrations (Song et al., 2018).

In summary, compared the atmosphere or aqueous systems, the soil compartment has not been as extensively studied and is often addressed as an intermediate pool for aquatic runoff with respect to Hg cycling. Nevertheless, the distribution of MeHg or the transformation of Hg to other species (GEM, MeHg) in the soil system is an important variable that needs to be addressed. The discovery of previously unknown Hg reservoirs in permafrost regions (Schuster et al., 2018) and growing evidence supporting the crucial role of vegetation in global Hg cycling (Obrist, 2012; Jiskra et al., 2018) have shed light on the importance of soils and the terrestrial environment in the global Hg cycle particularly given the uncertainties surrounding the impact of climate change on Hg cycling and transformation processes. Additional research on Hg cycling, particularly with regards to methylation of Hg in soil, will be necessary in the future to enhance our understanding of the risks associated uncertainties climate change and anthropogenic perturbations.

1.4. (Bio)-geochemical transformations of Hg

1.4.1. Methylation/Demethylation

The concentrations of MeHg measured in an environmental matrix represent snapshots in a dynamic competition between methylation of Hg^{II} and demethylation of MeHg. Methylation and demethylation processes can occur via biotic and abiotic processes, with the former being considered the primary mechanism for methylation. Mercury methylating microorganisms have been identified to be mostly anaerobe microbial species such as sulfate reducers (SRB), Fe reducers (FeRB), archaea and some firmicutes (Gilmour et al., 2013). However, recent research has shown that even cyanobacteria (Grégoire and Poulain, 2018) maybe involved in Hg methylation. The high scientific effort in this field of study leads to a swift identification of novel methylating microorganisms. It is established that Hg methylators share the common gene pair *hgcAB* (Parks et al., 2013), but only a small fraction (>2%) of microbial sequences from a global assessment do carried the gene pair (Podar et al., 2015). Both genes of this pair are vital for this methylation pathway. Removing *hgcA*, *hgcB*, or both genes stop microorganisms from producing MeHg (Parks et al., 2013) . Further, a rate-limiting process for Hg methylation is the uptake of Hg^{II} into the methylating organism (Sect. 1.4.1). Possible uptake pathways by methylating bacteria include both passive diffusion of neutral or charged species, and active transport through a transmembrane protein pump (Hsu-Kim et al., 2013).

While Hg methylation has been well studied, there has been less research focused on MeHg demethylation. Grégoire and Poulain, 2018 have been reviewing the advances in the different microbial transformation pathways. These include both reductive demethylation and oxidative demethylation pathways. The reductive demethylation is conducted by bacteria carrying the *mer*-operon which is more prominently know for the reduction of divalent Hg^{II} and thereby involves detoxification. In this

operon, the *merB* gene is responsible for encoding an organomercury lyase (MerB), which breaks down MeHg into inorganic Hg^{II} and CH_4 (Parks et al., 2009). Oxidative demethylation is not involved in Hg detoxification mechanisms and is a non-specific process that is linked to the metabolism of C1 compounds (e.g. Methanol (CH_3OH) or Formic acid (HCOOH)). Oxidative demethylation leads to the production of Hg^{II} and CO_2 (Hsu-Kim et al., 2013). Additionally, MeHg can be degraded though photodegradation by UV-light. Photodegradation is the primary pathway of MeHg degradation in surface water, comprising up to 80-83% of the demethylated MeHg in certain areas (Du et al., 2019).

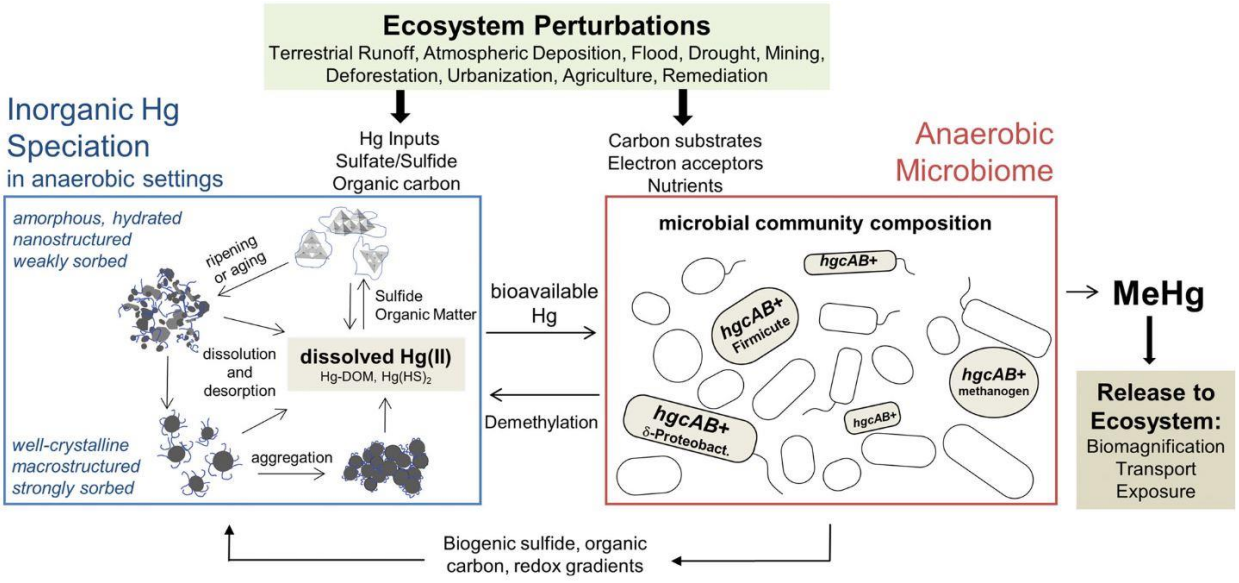

Figure 1 - 2 after Hsu-Kim et al., 2018: A schematic figure of the interplay between inorganic Hg speciation and microbial activity in the scope of Hg de-/methylation. Changes to ecosystems can change factors that contribute methylation in the environment. These factors include the availability of inorganic Hg, the community structure and activity of methylators and demethylators as well as the conditions for abiotic demethylation. Under anaerobic conditions, Hg is mostly associated with particles that contain sulfides and natural organic matter. The availability of Hg in these particles can vary depending on ageing and crystallinity. MeHg production rates depend on the growth and productivity of microorganisms that express hgcAB gene.

1.4.2. Methylation in the environment

In short, the ability of an environmental system to actively transform Hg to MeHg depends on two factors: the presence and activity of the methylating microbial community (which is influenced by geochemical conditions), and the speciation of Hg^{II}, which affects the availability of Hg to the community (Fig. 2). Numerous environments have been shown to exhibit methylation potential and/or the presence of methylation microbial communities, including regularly flooded paddy soils (Zhao et al., 2016; Rothenberg and Feng, 2012), floodplains (Poulin et al., 2016; Frohne et al., 2012), sediment-water interfaces in both marine (Stoichev et al., 2018; Muresan et al., 2007) and freshwater (Ullrich et al., 2001), as well as anoxic (Capo et al., 2022b; Capo et al., 2022a) and even oxic water (Díez et al., 2018; Gallorini and Loizeau, 2022) columns. Moreover, *hgcAB* carrying microbial communities have even been found in extreme environments, such as soda lakes, hypersaline and hyper sulfidic waters, saltern microbial mats, and hydro-thermal sites (Podar et al., 2015). This suggests that MeHg methylation could be possible in such environments, provided that the speciation of Hg allows for its biological uptake.

The bioavailability of Hg to microbes depends on the chemical speciation of Hg. It may be taken up as Hg^{2+}, complexed with DOM, neutral sulfur, or chloride complexes (e.g., $HgCl_2$, $Hg(HS)_2$) or in a particulate fraction (e.g., particulate organic matter (POM) or HgS particles) (Hsu-Kim et al., 2013). However, the rates at which Hg is methylated vary with its speciation and particle size fraction. For example, dissolved Hg^{2+} and Hg^{II} complexed by labile DOM are methylated at faster rates compared to Hg bearing inorganic nanoparticles (e.g., FeS(s), HgS(s)), complexed particulate organic matter (Hg–POM), or larger inorganic particles (Chiasson-Gould et al., 2014; Graham et al., 2013; Rivera et al., 2019; Zhang et al., 2012; Jonsson et al., 2012; Hofacker et al., 2013; Zhang et al., 2019).

In this scope, the significance of DOM, in the cycling, bioavailability and methylation of Hg must be emphasized. DOM is a mix of organic molecules of different, mass (Remucal et al., 2012), origin, or degradability (Vähätalo et al., 2010) dissolved in the aqueous phase. It is the most reactive fraction of carbon in the earths system and contains a complex structure of functional groups such as thiol-, carboxyl-, amine- or sulfide-groups. Due to the chalcophile character of Hg, thiols are the environmentally most relevant functional group for Hg interaction (van Liem-Nguyen et al., 2017; Skyllberg, 2008). Depending on its molecular composition and degradability, DOM may promote Hg methylation rates, as i) it acts as an electron donor that may enhance microbial activity (Chiasson-Gould et al., 2014; Bouchet et al., 2018), ii) inhibit the formation of less available HgS aggregates (Graham et al., 2012, 2013; Hsu-Kim et al., 2013; Aiken et al., 2011) or iii) depending on the microbial species – even act as a shuttle for Hg^{II} (Zhao et al., 2017; Schaefer et al., 2011; Schaefer and Morel, 2009). Further, the presence of DOM may increase methylation, especially when there is a high thiol content, which can prevent the formation of large and poorly bioavailable HgS aggregates (Graham et al., 2013). On the other hand, Pham et al., 2014 demonstrated that the bioavailability of Hg decreases over time since HgS particles agglomerate and become more crystalline even in the presence of dissolved organic matter (DOM), leading to a decrease in Hg methylation. As well, larger DOM molecules (a.k.a. humic substances) inhibit Hg^{II} uptake by forming large complexes which strongly sorb Hg (Zhang et al., 2019). Field studies have indicated that the composition and origin of DOM can impact Hg methylation rates (Bravo et al., 2017; Drott et al., 2007). For instance, a study by Bravo et al. (2017) found that in lake sediments, DOM derived from terrestrial sources resulted in slower methylation rates than DOM from phytoplankton sources.

1.4.3. Methylation in soils

Compared to aquatic environments, the body of research on the methylation of Hg in soils is comparatively small. Most of the existing research has been conducted on periodically or constantly flooded and often contaminated soils such as wetland fluvisols (Windham-Myers et al., 2014; King et al., 2002; Poulin et al., 2016), rice paddy soils (Liu et al., 2014; Yin et al., 2018), and peat soils (Åkerblom et al., 2020). Due to their redox oscillation, these environments may serve as hotspots for Hg methylation (Bigham et al., 2017; Marvin-DiPasquale et al., 2014). During saturated conditions, the MeHg production in soil

may be stimulated by the reduction of iron and sulfate, and the metabolization of labile organic matter that have been accumulated during aerobic periods.

The availability of Hg for methylation in soils is thought to be linked to Hg dissolved in the soil solution, underscoring the importance of its partitioning between the solid and the aqueous phase. The release of Hg into the soil solution has been associated with the mobilization of NOM (Kronberg et al., 2016; Eklöf et al., 2018), copper (Cu) nanoparticles (Hofacker et al., 2013), or the reductive dissolution of Fe- and Mn- oxyhydroxides (Poulin et al., 2017; Gfeller et al., 2021; Gygax et al., 2019). Several studies have reported a rapid decline in dissolved Hg following its release during flooding in different riparian settings (Hofacker et al., 2013; Poulin et al., 2016; Gygax et al., 2019). Possible pathways for this decrease are Hg^{II} reduction to Hg^0, sorption to recalcitrant NOM, formation of less mobile metacinnabar β-HgS(s) or co-precipitation of Hg in sulfides (e.g., FeS(s)) or metallic particles. In this scope, it has been demonstrated that, if sulfate-supply and sulfate-reduction are high, the precipitation of Hg may inhibit the microbial uptake and thus methylation rates (Benoit et al., 1999). Also, Hg bound to NOM has been demonstrated to transform to colloidal β-HgS(s) even under oxic condition (Manceau et al., 2015). Soil wetting and drying cycles may increase the breakdown of organic matter for example by manganese oxidation/reduction cycles (Jones et al., 2018; Sunda and Kieber, 1994; Ma et al., 2020), which in turn increases the DOM and potential DOM fraction in soil solution. This may further increase partitioning of soil-bound Hg into the porewater phase and increased DOM concentration, both of which have been shown to enhance Hg methylation in reservoirs (Eckley et al., 2017).

Often efforts have focused on remediation (O'Connor et al., 2018), land use (Lima et al., 2017; Marvin-DiPasquale et al., 2014), and ecosystem perturbation practices, such as deforestation (Kronberg et al., 2016), fertilization (Zhang et al., 2018), or amendments that may influence the methylation process (Wang et al., 2021a; Vlassopoulos et al., 2018; Liu et al., 2016). For example, the addition of organic amendments in the form of DOM, such as manure (Gygax et al., 2019), rice straw (Liu et al., 2016; Wang et al., 2019), or biochar (Wang et al., 2021a; Eckley et al., 2021), may have both enhancing and diminishing effects on Hg methylation rates. Others report that amendments of organic matter did not have a major impact on the net MeHg production in paddy soils (Zhu et al., 2016; Liu et al., 2016). On the other hand, amendments of Mn oxides (Vlassopoulos et al., 2018) or nitrate (Matthews et al., 2013) to sediments, soils or the water column were also shown to inhibit MeHg formation and mobilization by shifting the redox conditions from iron, sulfate reducing conditions to manganese reduction or denitrification. Studies have reported the promotion of both Hg demethylators and Hg reducers following organic amendments (Hu et al., 2019), as well as the increase in Hg methylators (Tang et al., 2019; Wang et al., 2020). Additionally, microbial community shifts can occur not only due to organic amendments, but also as a result of elevated Hg concentrations (Frossard et al., 2018).

Anthropogenic amendments, wetting-drying cycles and the involved redox oscillations do have major influences on Hg methylation in soils. However, methylation is not necessarily restricted to classical environments of sulfate and iron reduction

(Gallorini and Loizeau, 2021). Elevated MeHg concentrations have also been also observed in settling particles in oligotroph lakes (Gallorini and Loizeau, 2022), upland forest soils (Obrist, 2012) and forest soils of contaminated sites (see Chapter 2). There is still not much known about potential risks involved with elevated MeHg concentrations in forest soils or not regularly flooded environments. But elevated MeHg concentration could directly affect local and regional wildlife, since it has been observed that elevated MeHg in soils have high bioaccumulation factors from soil to invertebrates (Rieder et al., 2011) and the terrestrial food chains may exhibit MeHg bioaccumulation/biomagnification comparable to aquatic food chains (Tsz-Ki Tsui et al., 2019).

To summarize, methylation potential has been observed in many environments and depending on the bioavailability of Hg and the microbial activities methylation rates may change. Especially, DOM may influence Hg methylation. DOM is a complex group of diverse organic compounds with a direct impact on Hg methylation in the environment. Nonetheless, it is likely to influence other mechanisms for Hg transformation, aside from de-/methylation. However, this influence is complex and may either promote or hinder methylation. Hence, when investigating de-/methylation in a specific area, it is advisable to understand and identify the source of organic matter present at the study site and characterize it not only for its total concentration (e.g., dissolved organic carbon, DOC) but also to assess its quality. Further, the investigation of Hg methylation in soils has been limited to periodically or constantly flooded soils such as wetland fluvisols, rice paddy soils, and peat soils. The geographical predominance of these soil types in boreal (peat soils) or subtropical climate regions (rice paddies) already suggest that methylation processes in floodplain soils of temperate regions, but also in upland soils - which are an important part of the Hg cycle (e.g. forest) - have not received sufficient attention in the context of Hg methylation (Graydon et al., 2008). The recently discovered pools in permafrost regions (Schuster et al., 2018) and the important role of plant cover in global Hg cycling (Obrist, 2012; Jiskra et al., 2018) have highlighted the significance of soils, especially due to the uncertainties associated with climate change. However, research on Hg methylation in these compartments has been scarce. Consequently, there is a significant knowledge gap in our understanding of methylation dynamics in different soils systems, which calls for more research to address this critical issue.

1.5. Analytical methods to quantify organo-mercury species in soils.

1.5.1. Extraction and Quantification

The analysis of organo-mercury species (e.g., MeHg, EtHg), in sediments and soils typically involves three stages: i) extraction, ii) optional purification, and iii) analysis by chromatographic methods. For MeHg there has been plenty extraction techniques suggested in the past decades. These involve acidic extractions using HCl, HNO_3, H_2SO_4 or alkaline extractions using KOH or Tetramethylammonium hydroxide (TMAH). Some extraction procedures also involve additives or complexing agents such as $CuSO_4$, NaCl, KCl (Jagtap and Maher, 2015). Successively, the analyte may be separated from the matrix by

extractions with organic solvents such as toluene or dichloromethane (DCM) and back extracted with an aqueous complexing agent (L-cysteine or thiosulfate) (Brombach et al., 2015; Hintelmann et al., 1997). Another option is to use a distillation under a N_2 together with an acid leaching using KCl and H_2SO_4. However, Hintelmann et al., 1997 discovered that this process may result in high false positives in sediment matrices. Chromatographic techniques are often used to further separate the extracted species (e.g. Hg^{2+}, MeHg, EtHg) including high-performance liquid chromatography (HPLC) or gas chromatography (GC) (US EPA, 2014). The most commonly employed detector systems are cold vapor atomic fluorescence detectors (CV-AFS) and Inductively Coupled Plasma Mass Spectrometry (ICP-MS), with the latter being particularly useful for methods involving isotopic spiking (Monperrus et al., 2003). Although, there are Environmental Protection Agency (EPA) methods for the analysis of MeHg in soils and sediments (US EPA, 2014), to date, there is no universally used standard technique for quantifying organo-Hg species (Hellmann et al., 2019). The applied techniques remain time and resource intensive to date, and trained lab personnel are required. Furthermore, there is still room for improvement regarding sample throughput and cost efficiency.

1.5.2. Analytical challenges

The MeHg concentrations typically range from few permilles to few percent point of the total Hg present in soils or sediments. Thus, final analytical result may be significantly affected by only small unintended transformations of the target species during sampling or sample preparation (Mesko et al., 2011). Transformation processes of Hg like Hg volatilization or Hg methylation and demethylation have been reported during sample storge, freezing/thawing cycles, and drying procedures (Kodamatani et al., 2017; Hojdová et al., 2015; Smeds et al., 2022). It is therefore key to apply least interfering sampling and preparation methods such as i.) direct freezing after sampling, ii.) freeze drying and iii.) avoid elevated temperatures while milling when preparing solid samples for organo Hg analyses.

The formation of artificial organo Hg species, especially MeHg, is a common issue during the extraction and analyses of soil or sediment (Hintelmann and Wilken, 1993; Hintelmann et al., 1997; Hellmann et al., 2019; Horvat et al., 1993). Despite attempts to address this problem dating back to the 1970s (Rogers, 1977; Falter, 1999a), there is currently no MeHg extraction technique that is completely free from artifact formation (Huang, 2005). Factors that can influence the formation of artificial MeHg include the organic matter content and quality of the sample matrix (Bloom et al., 1997; Nagase et al., 1984; Rogers, 1976; Rogers, 1977), concentration of inorganic Hg in the matrix (Hammerschmidt and Fitzgerald, 2001), pH (Nagase et al., 1984; Rogers, 1977), and the solvent used during extraction (Hintelmann et al., 1997). The rates of artificial methylation vary depending on the extraction method used and have been reported to range from 0.0003-0.046% (Qvarnström and Frech, 2002; Hintelmann et al., 1997; Huang, 2005).

While the rates of artificial methylation may result in insignificant amounts of MeHg formation in background soils and sediments, where MeHg typically makes up 0.5-1% of the total Hg pool, this issue becomes more significant in polluted soils and sediments. In these cases, the MeHg/Hg ratio is often <<0.1% (Gray et al., 2004; Xu et al., 2018; Gygax et al., 2019), and the high Hg concentrations can lead to false positives of MeHg formation greater than 100% of the initial concentration (Hellmann et al., 2019). Therefore, it is crucial to consider the potential for artifact formation when analyzing MeHg in polluted soils and sediments and to choose or develop appropriate extraction methods to minimize such artifact formation.

The double-spike isotope dilution (DSIDA) has been demonstrated to be effective in directly quantifying and correcting for the effects of artificial methylation and demethylation during the extraction of animal tissues (Monperrus et al., 2003). The method involves the addition of two isotopically labeled spikes (e.g., ^{201}Hg and ^{199}MeHg) to the sample prior to extraction. This allows for the back calculation of the ratio of the two spikes in the extracted sample is then used to calculate the proportion of artificially methylated or demethylated Hg present in the sample. The DSIDA method has been proven to be a useful tool and for the simultaneous analyses of MeHg and Hg. However in samples with high inorganic Hg concentrations and low MeHg/Hg ratios, it may not be an appropriate solution, due to increased uncertainty levels of unintentional artificial methylation (Monperrus et al., 2008; Monperrus et al., 2004).

Ethyl mercury is another form of organo Hg that has been found in industrial areas. It can be analyzed using the same measurement procedures as MeHg (e.g., HPLC). Compared to MeHg, artifact formation of EtHg is not as common. However, the analysis of EtHg can also be challenging, as it has been reported to decompose within hours under strong acidic condition in coexistence with Fe^{3+} (Han et al., 2003), or during extractions involving heating to 60° (Hight and Cheng, 2006). Additionally, it may have the same retention time as another Hg species (CH_3–S–Hg^+) during HPLC separation using separation using a acetonitrile–water eluent and 0.5 mmol L^{-1} sodium pyrrolidine dithiocarbamate as a complexing agent (Wilken et al., 2003).

In summary, the analyses of MeHg from soils and sediment is a procedure involving various sensitive steps sensitive such as i.) sampling and preservation, ii.) extraction and iii.) separation and analyses. Especially, the analyses of MeHg in highly contaminated soils with low MeHg/Hg ratios stays a challenge. It is essential to conduct a thorough evaluation of analytical methods, including those that are published and widely accepted, to evaluate the possibility of artificial formation or decomposition of the target analytes, specifically EtHg and MeHg, during the extraction process prior to their implementation in field studies. Although the above addressed issues are well known in the research community it is often not addressed.

Overall, the analysis of contaminated substrates with low MeHg/Hg ratios (< 1%) is a complex problem that requires careful consideration of numerous factors. Researchers need to carefully evaluate the analytical methods they use and conduct thorough validation studies to ensure that the method is suitable for the specific sample matrix and to minimize the risk of false positives or other analytical challenges. There should be more research effort to thoroughly evaluate substrate specific

methodologies. For example, assessing i.) the performance of substrate-specific analytical methods for detection and quantification of MeHg in contaminated substrates with low MeHg/Hg ratios or ii.) how these methods may be improved to minimize the risk of false positives.

1.6. Thesis outline

Currently, there are significant knowledge gaps regarding the impact of various land use types, anthropogenic disturbance or flooding on Hg methylation dynamics in soil systems, particularly in temperate climate regions. Despite reports of elevated MeHg concentrations in forest topsoils, there have been few studies aimed at reproducing these findings. Further, studies on the effects of soil amendments and flooding are often limited to rice paddy soils in subtropical climate regions and results on the application of organic fertilizers are often contradictory. Possible reasons for that are changes in DOC quality and Hg^{II} speciation. By conducting more detailed analyses of Hg in soil solution, such as through the characterization of colloidal Hg, one may be able to better explain the underlying effects of flooding and fertilization on mechanisms of Hg release and methylation at both a field and laboratory scale. Finally, analyzing MeHg in highly contaminated soils and sediments is complex due to the potential for false positives resulting from artificial Hg methylation. Although this process is known since many years, not all methods have been thoroughly tested and assess with respect to artificial Hg methylation.

As a result of the abovementioned knowledge gaps, this thesis aims to investigate how anthropogenic and natural factors, such as agricultural crop or forest cultivation, and regular flooding, affect the distribution, mobilization potential, and de-/methylation dynamics of Hg and MeHg in contaminated and uncontaminated soils. Further, we aimed to assess sources of organo-Hg species in highly contaminated soils of an alpine valley in Switzerland. To provide tools for this, we also sought to assess an existing method for extracting and analyzing MeHg by identifying potential false positive artifacts and developing tools to address them.

We addressed all these questions by studying soils from agricultural fields and grove sites in the region of Visp, Switzerland. This model site hosts both contaminated and uncontaminated fields and areas that are regularly subjected to flooding. In three chapters we aimed to characterize the field site in terms of Hg and organo Hg species, but also draw general conclusions on the fate of Hg in regularly flooded soil. The first chapter focuses on the background sites, where Hg concentrations are in the range of the global background for soils. In the absence of Hg contamination, we aimed to investigate how land use types impact the distribution of Hg and MeHg in the valley and if they may already have an impact on MeHg concentrations. Chapter two not only examines background sites but also heavily contaminated areas to gain a deeper understanding of the sources of Hg and, particularly, organo Hg species in the valley. The pollution at the site has a complex history. We aimed to answer if the present organo-Hg species (EtHg and MeHg) are a result of natural processes or anthropogenic deposition. Accurately measuring MeHg in these soils required to overcome analytical challenges like artificial methylation, which has been reported to be significant in highly polluted soil matrices. Chapter three examines the fate of Hg and MeHg in these contaminated fields in the context of regular soil flooding and agricultural practices, such as the application of manure. Organic carbon sources have the potential to enhance the activity of Hg methylating microorganisms, while also complexing and potentially inhibiting Hg bioavailability. In our study, we utilized a microcosm soil incubation approach to investigate the release, colloid formation,

and methylation of Hg in both soil and soil solution. Overall, the three chapters explore the dynamics and distribution of Hg and organo Hg species in anthropogenically disturbed soils by using microcosm experiments and field studies. The objectives of each individual chapter are summarized in the following paragraphs:

Chapter 1: Mercury distribution and contrasting net-mercury methylation among land use types in an alpine valley.

The first chapter focuses on the differences in Hg and MeHg distribution between tree groves and agricultural grasslands in background site of a historically contaminated valley close to Visp in Switzerland. The aims of this chapter are to:

- Find the distribution and levels of Hg and MeHg between different land uses in the valley.
- Evaluate and discuss the potential origin and sources for Hg and MeHg in the specific land use types.
- Assess and discuss the impact of tree groves on the bioavailability of Hg and MeHg to the terrestrial food chain in the valley.

Chapter 2: Organo-Mercury Species in a Polluted Agricultural Floodplain: Combining Speciation Methods and Polymerase Chain Reaction to Investigate Pathways of Contamination

The second chapter focuses on the characterization of organo mercury species in soil matrices and the origin of the organo mercury species in the contaminated soils alpine valley. Further, we discuss the analytical challenges of analyzing MeHg - namely artificially methylation - as well as the origin of organo mercury species in highly contaminated soils. Here we aim to:

- quantify and correct for the artificial methylation during specific extraction of MeHg in a soil matrix and correct for false positives.
- assess the origin of organic Hg species (MeHg, EtHg) and use signals of *hgcA* to distinguish between anthropogenic and natural sources.
- compare and discuss the advantages and disadvantages of two methods used to correct for artificial Hg methylation (simple iHg spiking and double-spike isotope dilution).Hg

Chapter 3: Mercury mobility, colloid formation, and methylation in a polluted Fluvisol as affected by manure application and flooding–draining cycle

The third chapter focuses on the influence of flooding and manure addition on the mobilization and methylation of Hg in an agriculturally used floodplain soil of the contaminated valley. Contaminated floodplain soils were artificially flooded and incubated in the lab over 42 days. The goals of this chapter are to:

- investigate the impact of flooding-draining cycles and manure addition, on the release and methylation of Hg in a contaminated Fluvisol.
- evaluate the hypothesis that the manure addition may accelerate the release of Hg and change its speciation towards Hg-NOM complexes and β-HgS(s) colloids.

2. Mercury distribution and contrasting net-mercury methylation among land use types in an alpine mountain valley.

This chapter is planned for publication as Gfeller, Lorenz; Caplette, Jaime N.; Deonarine, Amrika; Mestrot, Adrien: Mercury distribution and contrasting net-mercury methylation among land use types in an alpine mountain valley.

Author contributions:

Lorenz Gfeller: conceptualization, sampling, laboratory, visualizations, writing original draft, reviewing, and editing.

Jaime N. Caplette: sampling, laboratory.

Amrika Deonarine: conceptualization, sampling, laboratory, reviewing of the manuscript..

Adrien Mestrot: Supervision, conceptualization, reviewing and editing of the manuscript.

Abstract

Chlor-alkali and acetaldehyde producing companies are known anthropogenic point sources of mercury (Hg) to the environment. Often their legacy sites are ill characterized with respect to mercury methylation. This study focuses on the distribution of mercury (Hg) and methyl mercury (MeHg) in different land use types (grasslands, groves) in the vicinity of a former chlor-alkali and acetaldehyde producing chemical plant. We studied vertical distributions (profiles 0-50 cm) as well as small (5 m) and large (17 km) scale horizontal distribution of various chemical parameters. Agricultural grassland soils in this area did not show spatial gradients of Hg concentrations towards the chemical plants or in the preferential wind directions. However, we observed significant correlations between Hg and soil organic carbon (OC) in the topsoil (R^2 = 0.73, $p<0.05$). Further, the soils Hg enrichment factors were highest in the topsoils (0 to 10 cm) of both grassland ($EF_{Hg/Al}$: -36.2 to 1429 ; median = 323 ; n =38) and tree groves ($EF_{Hg/Al}$: : 599 to 3676 ; median = 1163 ; n =10). The correlation between Hg and OC as well as profiles of $EF_{Hg/Al}$ suggest the deposition Hg from the atmosphere as the main pathway. The absence of a spatial pattern might be caused by changing wind directions and seasonal temperature inversions in the valley. Although topsoils of grasslands and tree groves show similar levels of Hg, the latter express a significantly higher net-methylation potential (MeHg/Hg: 0.28 - 19.1 % ; median = 3.6 %; n =10) then grasslands (MeHg/Hg: 0.18 - 2.4 %, median = 0.53%, n = 40) suggesting higher input of easily available Hg, more bioavailable Hg and/or enhanced microbial activity. These elevated MeHg concentrations (up to 29.6 μg kg^{-1}) are in the range of global MeHg hotspots (e.g. Swedish peat soils) and underline the relevance of tree groves in areas of Hg point sources (e.g. chemical plants) since they provide a habitat for wildlife, including birds. This study emphasizes the importance of MeHg production and dynamics in temperate alpine environments and opens up the way for a whole ecosystem study in forest environments in this specific area.

2.1. Introduction

Mercury (Hg) is a highly toxic metal of global concern (UNEP and AMAP, 2019). As gaseous elemental mercury (GEM) it has a long residence time within the atmosphere (Obrist et al., 2018), which allows for a long range transport and a relatively homogenous distribution (Bank, 2012). In soils, sediments and waterbodies Hg maybe transformed to the neurotoxic monomethyl Hg (MeHg) by Hg methylating microorganisms in many different environments (Podar et al., 2015). Due to its lipophile properties MeHg is bioaccumulated across both terrestrial (Rimmer et al., 2010) and aquatic food chains (Atwell et al., 1998) and ultimately taken up by humans mainly through fish consumption (Sheehan et al., 2014). Despite political actions (UNEP, 2017) on a global scale Hg has been emitted through industrial activities (UNEP and AMAP, 2019).

Coal combustion, small-scale gold mining and the chemical industry are among the most important anthropogenic sources of Hg to the environment to date (Horowitz et al., 2014). Mercury emitted from chlor-alkali - and acetaldehyde plants was reported to be mainly in the form of Gaseous Elemental Mercury GEM and to smaller proportions gaseous oxidized mercury (GOM; mainly Hg^{2+}) or particulate bound Hg (HgP) to the atmosphere (Landis et al., 2004). Additionally, the remobilization of Hg from previously contaminated soils can have far-reaching consequences, as it can lead to an expansion of the affected area and the transport of Hg to niches with elevated Hg transformation potentials (e.g. Hg methylation in wetlands). Remobilization is attributed to a range of processes. Firstly, Hg may be remobilized in the form of GEM to the atmosphere through biological Hg reduction by microorganisms (carrying the *merA* gene) (Grégoire and Poulain, 2018), Hg reduction by UV light (Moore and Carpi, 2005), chemical Hg reduction by electron transfer from reduced DOM (Schlueter, 2000). Secondly, aerosol transport by dust dispersion from polluted areas may be an effective vector of Hg in the form of HgP, especially when the soils have low structural stability and are left barren for extended periods of time (Vos et al., 2022). And finally, Hg maybe remobilized into the water phase (e.g. soil pore water) as Hg^{2+}complexes (Gfeller et al., 2021; Kronberg et al., 2016; Poulin et al., 2016).

The Hg released to the atmosphere is subsequently deposited on by both dry and wet deposition. GEM which makes up 95% of the Hg in the atmosphere is mainly deposited by dry deposition in soils and plant material (Bishop et al., 2020). Recent studies suggest that the main uptake pathway of GEM into plants is through stomatal uptake (Zhou et al., 2021; Gustin et al., 2022). This is well observed that litterfall in forest environments represent a major Hg source in forest soils (Obrist et al., 2009). Field studies observed that latitude and soil organic matter (SOM) are good indicators for Hg concentrations in forest environments (Obrist et al., 2011). Colder climate conditions were demonstrated to more effectively retain deposited GEM due to slower decomposition of organic matter and reemission of Hg (Yu et al., 2014; Obrist et al., 2011). Compared to GEM, the forms of GOM and HgP have a lower residence time in the atmosphere and is mainly deposited by wet deposition (Bank, 2012). Although, ratios of GOM/GEM in emissions of chlor-alkali plants range only between 0.5-2% (Landis et al., 2004; Wängberg et al., 2003), the presence of ionized GOM can result in local gradients in soils around a point source (Biester et al.,

2002b; Guédron et al., 2013). As previously shown, local gradients of pollutants can be caused by temperature inversions in mountain valleys, which result in the accumulation of pollutants near their sources (Chazette et al., 2005).

The organo-mercury species methyl mercy (MeHg) is an environmentally relevant form of Hg with enhanced toxicity. It is mainly formed through microbial biotransformation of inorganic Hg^{2+}. Anaerobic iron and sulfate reducing bacteria as well as Archaea are thought to be the main Hg methylating microorganisms (Podar et al., 2015; Gilmour et al., 2013). Moreover, recent studies showed that bacteria expressing the gene pair essential for Hg methylation (*hgcAB*) are as well involved in nitrate reduction and denitrification processes (Vigneron et al., 2021). The net-methylation potential of a substrate (soil, sediment) can be expressed as a function of (i) the amount of bioavailable inorganic Hg^{2+}, (ii) the composition of the present microbial community and (iii) its activity. The bioavailability of Hg is coupled to its speciation and preferential binding forms. For example, particulate HgS(s) was shown to be less available for methylation compared to free Hg^{2+} (Zhang et al., 2014; Zhang et al., 2012). Thus, freshly deposited Hg is more likely to be transformed to MeHg as residual Hg bound to recalcitrant organic matter or sulfites (Bishop et al., 2020). Net-methylation is as well related to redox conditions and the availability of electron donors (SO_2^{4-}, labile organic matter etc.). Various studies underlined the influence of sulphate (Bergman et al., 2012; Mitchell et al., 2009; Åkerblom et al., 2020) and labile organic matter (Gygax et al., 2019; Achá et al., 2012) on the Hg net-methylation in environmental matrices. The abovementioned factors underline the large range of potential hotspots and niches for Hg methylation in terrestrial systems. Once formed in a soil MeHg might be bioaccumulated by invertebrates (e.g. earth worms) (Brantschen et al., 2020). Giving path for MeHg to move up the terrestrial food chain.

A substantial volume of research has been conducted on Hg in soils surrounding Hg point sources such as coal power-plants, chlor-alkali plants and acetaldehyde-producing industries (Biester et al., 2002b; Biester et al., 2002a; Grangeon et al., 2012; Guédron et al., 2013; Guney et al., 2020; Rodríguez Martín and Nanos, 2016). Moreover, the reemissions of GEM from these type of areas have been studied (McLagan et al., 2021; Osterwalder et al., 2019; Wängberg et al., 2003; Landis et al., 2004). In spite of this, the distribution of MeHg and the net-methylation potential in soils with respect to different land use types (forests, agricultural, urban) near these point sources have not been sufficiently characterized.

Here, we present the data of a field screening study conducted near an acetaldehyde and chlor-alkali chemical plant in a Swiss alpine region. We aimed i.) to assess the spatial patterns of Hg distribution and variations in net-methylation potential from soils in distinct landscape features (agricultural areas and tree groves) and ii.) to evaluate and discuss the potential origin and sources for Hg and MeHg in the specific land use types. This was done by analyzing the concentrations of MeHg, Hg, and additional soils parameters within a 7 km radius of the chemical plant. We hypothesized that: i) tree groves would have elevated methylation potential compared to agricultural sites, due to the increased input of labile carbon and newly deposited Hg from litterfall; and ii) there would be a Hg gradient around the chemical plant in the preferential wind directions, originating from the emission of RGM and PHg.

2.2. Methods and Materials

2.2.1. Sample collection

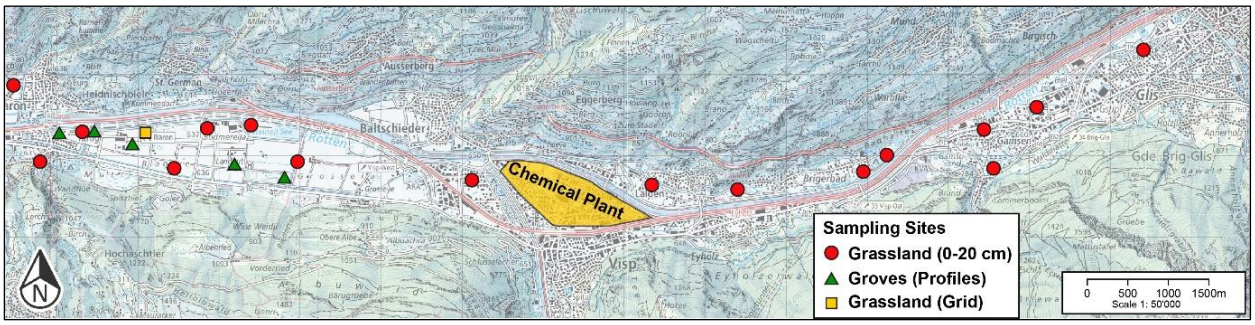

Figure 2 - 1 A map showing the locations of soil samples taken in 2016, including grassland soils (represented by red circles) and grove soil profiles (represented by green triangles). The grassland grid (represented by yellow squares) was sampled in 2017. The yellow-filled polygon marks the area where the local chemical plant released mercury between the 1930s and 2000s. The base map for this map was provided by the Federal Office of Topography swisstopo (map.geo.admin.ch).

The study area is situated in the Rhone Valley, Wallis, Switzerland and spans 14 km from Raron (46°18'10.66"N; 7°47'54.95"E) to Brig (46°18'49.33"N; 7°58'36.05"E (Fig. 2 - 1). The area includes an acetaldehyde producing chemical plant in the city of Visp. It used mercury from 1917 to 2013 in the production. Additionally, the plant applied Hg in the chlor-alkali process between 1944 and 1950. The facility was the source of historic Hg pollution which was released through the atmosphere as well as through a wastewater discharge canal between 1931 and 1976. The canals sediments were distributed on its bank and across the agricultural fields as fertilizer between the 1960s and 1980s (Glenz and Escher, 2011). Further, contaminated materials were historically used to fill pits and construct terrain modifications (Mudry, 2016). To the east, the area hosts the Gamsenried landfill which contains toxic waste from the chemical plant. The landfill holds an estimate of 33 tons of Hg. Other studies reported GEM emission from highly polluted soils in the urban areas, agricultural sites, and the

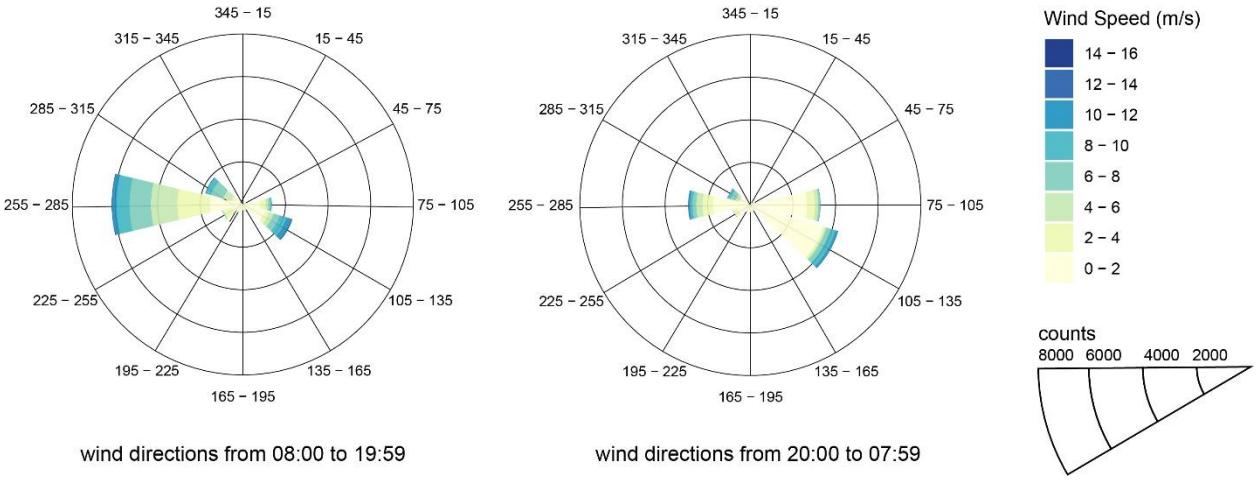

Figure 2 - 2 Windrose diagram showing the mean hourly wind direction and speed measurements at the MeteoSuisse Mid Valley Station in Visp, Switzerland (46°18′10.452″N 7°50′34.627″E) for the period from June 1, 2019, to August 30, 2022. The data is divided into daytime (8 AM to 8 PM, left) and night-time (8 PM to 8 AM, right) intervals. The colour represents the wind speed, and the thickness of the bars represents the number of measurements taken during the given time interval. Data source: IDAWEB MeteoSuisse

landfill (McLagan et al., 2021; Osterwalder et al., 2019). The valley is expresses strong westward wind preferentially during daytime (8 AM to 8 PM) and eastward wind mostly during night (8 PM to 8 AM) (Fig. 2-2).

Soils were sampled in two sampling schemes allowing for both (i) a screening of the area and (ii) a measure of Hg heterogeneity in the vertical direction at small scale. The first sampling was conducted on the 14th of October 2016. Sixteen sites on agricultural grassland fields were selected in areas where no soil Hg contamination had been reported earlier (Fig. 2-1), with roughly 50 % located upstream and the other 50% located downstream of the chemical plant. Surface soil samples were collected from the agricultural fields, a 10 m x 10 m grid was constructed and soil samples in alternating 1 m^2 squares were collected. Surface soil samples (top 20 cm) were obtained using a 25 cm gouge auger, pooled, and homogenized to obtain a composite sample. Additional 5 locations were situated within tree groves adjacent to the agricultural fields. These locations were randomly selected sites for comparison with the agricultural grassland field soils. At the tree grove sites, soil cores (0-50 cm) were collected using a gouge auger, and separated into 10 cm depth fractions (i.e., 0-10 cm, 10-20 cm, 20-30 cm, 30-40 cm, and 40-50 cm).

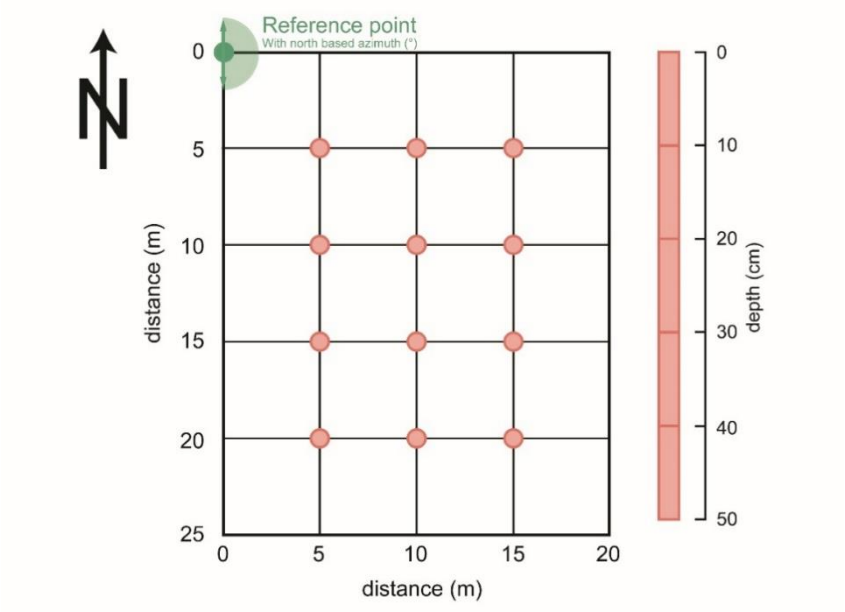

Figure 2 - 3 A map showing the sampling scheme for a small-scale sampling site, including the reference point for the grid (shown in green) and the sampling points and depth intervals (shown in rose). Sampling was conducted according to soil depth and may have crossed soil horizon boundaries. The orientation of the grid is determined by a north-based azimuth.

The second sampling campaign was conducted on the 10th of April 2017. One site on an unpolluted agricultural grassland field was chosen. Soils were sampled within a rectangle grid (25m x 20 m) divided into 5m x 5m squares. Following this scheme, a total number of 12 soil cores were taken per site (Fig. 2-3). Analogue to in the groves soil cores were taken using a 100 cm gouge auger with a target depth of 50 cm and divided into 10 cm intervals (Fig. 2-3). Generally sampling by depth was systematically preformed in 10 cm intervals and does not directly reflect distinct soil horizons.

Samples were double bagged using polyethylene (PE) bags. The bags were emptied from air, sealed, stored on ice immediately and frozen (-20°) at least 8 h hours after sampling. In the laboratory, samples were freeze-dried, sieved to <2mm grain size, and ground by hand using an agate mortar. The processed samples were double-bagged and stored at room temperature until analyses.

Materials and reagents

For the digestion and extractions, we used HPLC grade solvents (dichloromethane, methanol, Honeywell, Morristown, United States of America), ultra-pure water (MilliQ, >18.2 MΩ cm at 25 °C), Suprapure H_2O_2 (Sigma-Aldrich, St. Louis, United States of America) and acids (HNO_3, HCl) which were doubly distilled in our in-house clean lab. Glassware was cleaned by soaking in acid baths (both 10% (w/w) HNO_3 and 10% (w/w) HCl) for at least 24 h and rinsed with ultra-pure water. Corning® sterile polypropylene (PP) tubes were used to store digests for of total Hg and trace metal analyses. Borosilicate glassware was used for MeHg extractions and storage. Commercially available stock solutions for multi-element (ICP multi-element standard solution IV-ICPMS-71A, Inorganic Ventures, Christiansburg, United States of America) and total Hg (ICP inorganic Hg standard solution, TraceCERT®, Sigma-Aldrich, St. Louis, United States of America) analyses were used as standards. MeHg standards were prepared by dissolving MeHg chloride (Sigma-Aldrich, St. Louis, United States of America) in methanol (HPLC grade, Fisher Scientific, Reinach, Switzerland). All samples, standards and spikes were weighed with an analytical balance (ALJ 220-4, Kern & Sohn GmbH, Balingen, Germany) to a precision of 10^{-4} g. L-Cystein solutions were prepared from L-Cysteine hydrochloride monohydrate biochemistry grade and L-Cystein for biochemistry grade (both, Millipore, Merck, Darmstadt, Germany) salts.

2.2.2. Soil characterization

All soils were analyzed for CNS, organic carbon, MeHg, Hg and various metals (Fe, Mn, Al, As, Cr etc.). Soil Carbon (C), Nitrogen (N) and Sulfur (S) were measured with an elemental analyzer (vario El cube, Elementar Analysensysteme, Germany). Soil organic C (OC) was calculated by the difference in C concentration before and after a thermal loss on ignition (LOI) treatment at 550° C for 2h. Soil metals were leached by microwave assisted acid digestion (250 mg soil, 4ml 69 %, HNO_3, 2 ml 30 % H_2O_2). The leachates were analyzed for Hg (in 1% HNO_3, 0.5% HCl) and other metals (in 1% HNO_3) by Inductively Coupled Plasma Mass Spectrometry (ICP-MS; 7700x ICP-MS, Agilent Technologies, Santa Clara, United States of America). An internal standard of Indium (m/z 115) was continuously injected for trace metals and Hg calibration standards were measured repeatedly, during the run to check the stability of the system. The LOD for Hg in diluted leachates was <0.02µg kg^{-1} for all soil analyses. Soil digestions and extractions were verified using the certified reference materials SRM 2709a (San Joaquin Soil, National Institute of Standards and Technology, Gaithersburg, USA), PACS-3 (Marine sediment, National

Research Council of Canada, Ottawa, Canada) and ERM-CC580 (Estuary sediment, Institute for Reference Materials and Measurements, Geel, Belgium).

MeHg was quantified using a HCl-dichloromethane extraction. Details on the extraction procedure can be found elsewhere (Gfeller et al., 2022). Briefly, 250 mg of sample were leached in 10 mL 6 M HCl in ultrapure water, centrifuged, selectively extracted for MeHg with dichloromethane and back extracted to an aqueous solution of 0.1% L-cysteine. The extracts were stored in the dark at 4° C and analyzed within 48 hours. Then, MeHg was analyzed by coupling a High-Pressure Liquid Chromatograph (HPLC 1260 Series, Agilent Technologies, Santa Clara, United States of America) to ICP-MS (7700x ICP-MS, Agilent Technologies, Santa Clara, United States of America) (HPLC-ICP-MS) applying a method previously used in various media. We used a conventional reverse phase C18 column (Zorbax C-18, 4.6 x 50 mm, Agilent Technologies, Santa Clara, United States of America) and a mobile phase consisting of 0.1% L-Cysteine (98%) and Methanol (2%).

2.2.3. Enrichment factors

We calculated enrichment factors (EF) to assess the local enrichment in soils compared to their substrate. This was done by normalizing a target element's concentration (e.g. Hg) using rather refractory (immobile) element (e.g. Al, Ni) in soil. Although this approach is an object of discussion and might be biased by high heterogeneity soils substrate geochemistry (Reimann and Caritat, 2005), EF_X^Y has been widely applied to assess the relative enrichments of Hg in the vicinity of chlor-alkali plants (Hissler and Probst, 2006; Biester et al., 2002b; Guédron et al., 2013). An elements (X) enrichment factor (EF_X^Y) is defined using its relative abundance ($(X/Y)_{background}$) compared to a refractory element (Y) in the "geochemical background" and their relative abundance in the sample ($(X/Y)_{sample}$), as displayed in equation (1).

$$EF_{X/Y} = \left(\frac{\left(\frac{X}{Y}\right)_{Sample}}{\left(\frac{X}{Y}\right)_{Background}} - 1 \right) * 100 \qquad \text{(Eq. 2-1)}$$

The lowest point of the profiles (40 - 50 cm) was defined as background for each profile respectively. The mean $(Hg/Y)_{background}$ ratios of the grassland profiles at (40 - 50 cm) was used to calculate EF for the grassland soils of the wide screening campaign. We used the refractory elements Al and Ni as nominators in Eq.1. For samples where Hg was lower than the limit of detection (<0.02 mg kg^{-1}) we used half the limit of detection as Hg concentration.

2.2.4 Statistics

We applied an unpaired t-test (significance level: $\alpha = 0.05$) for variables that passed a Shapiro-Wilk-Test for normality in both groups (grasslands and groves). For variables that were not normally distributed, a Mann-Whitney U test (significance level: $\alpha = 0.05$) was used to compare the two environments (grassland and groves). For this comparison, the depth intervals (0 - 10 cm and 10 - 20 cm) of the grove profiles were averaged. For the linear regressions we always displayed the squared pearson's

correlation coefficient (r^2) and p values with a cut-off at ($p<0.05$). Assuming a not normally distributed population, we used spearman's rank correlations in environments (groves) with small sample size, with a cut-off at ($p<0.05$). For concentration data, mean concentrations are given with an uncertainty of one standard deviation for samples extracted in triplicates ($mean \pm 1*\sigma$). Alternatively, the uncertainty is calculated based on the relative standard deviation of samples in the same concentration quartile for the samples not extracted in triplicate.

2.3. Results

2.3.1. Horizontal distribution of Hg, MeHg OM and trace elements.

Mercury in topsoil (0 - 20 cm) ranged from <0.02 - 0.35 mg kg^{-1} in the grassland fields and from 0.06 - 0.56 mg kg^{-1} in the groves. On the small-scale screening site, Hg ranges were narrower (0.02 - 0.13 mg kg^{-1}) in topsoils (0 - 10 cm). The C/N ratios in the grassland soils (9.4 ± 0.4) and the grove's topsoil's (12.9 ± 1.4, 0 - 20 cm) did not show special variability. However, soil organic carbon (OC) ranged from 1.09 - 5.13 wt. % in the grassland fields and 2.34 - 13.1 wt. % in the grove's topsoil's (0 -20 cm). We observed a pronounced significant positive correlation between Hg and OC in grassland soils at small

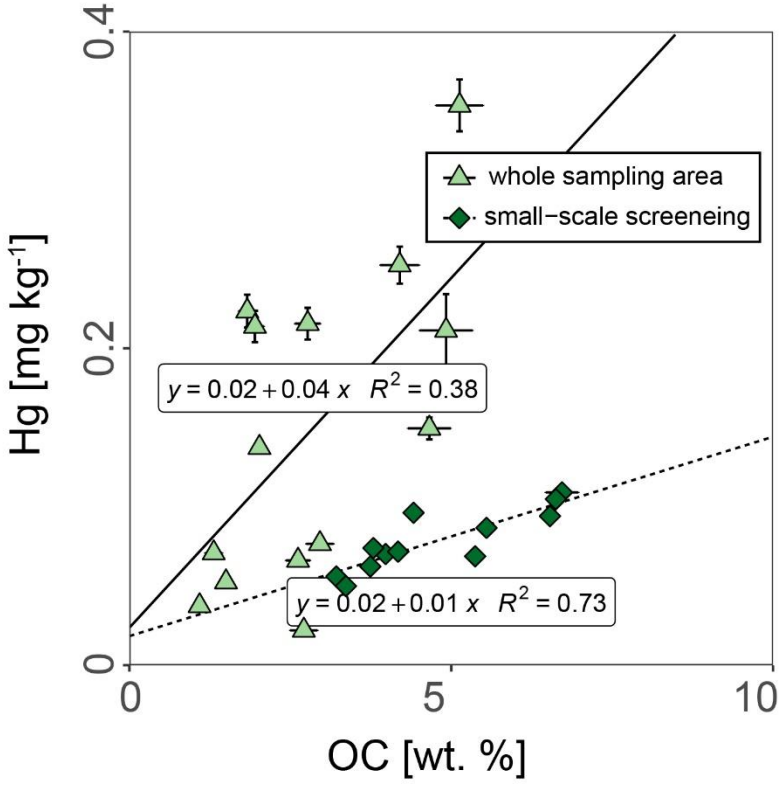

Figure 2 - 4 Scatter plots and linear regressions showing the relationship between organic carbon and Hg in the top 0-10 cm of soil at the small-scale screening site (shown in dark green) and across the entire sampling area (shown in light green).

scale (R^2 = 0.73, p<0.05) and a weaker relationship in grassland samples across the whole sampling area (R^2 = 0.38, p<0.05) (Fig. 2 - 4). MeHg concentrations ranged between 0.23 - 1.5 µg kg^{-1} with one outlier at 5.7 µg kg^{-1} in the grassland soils and 1.92 - 18.9 µg kg^{-1} in the groves in the averaged 0 - 20 cm depth. Compared to the grasslands (0.757 ± 1.02 µg kg^{-1}), groves (8.55 ± 6.60 µg kg^{-1}) showed significantly higher (p<0.01) MeHg concentrations (Fig. 2 - 5). Without considering outliers, grassland MeHg/Hg ratios ranged between 0.1-1.8 %. Grove environments show maximal MeHg/Hg ratios up to 19.1% underlining a high Hg net-methylation potential in these environments.

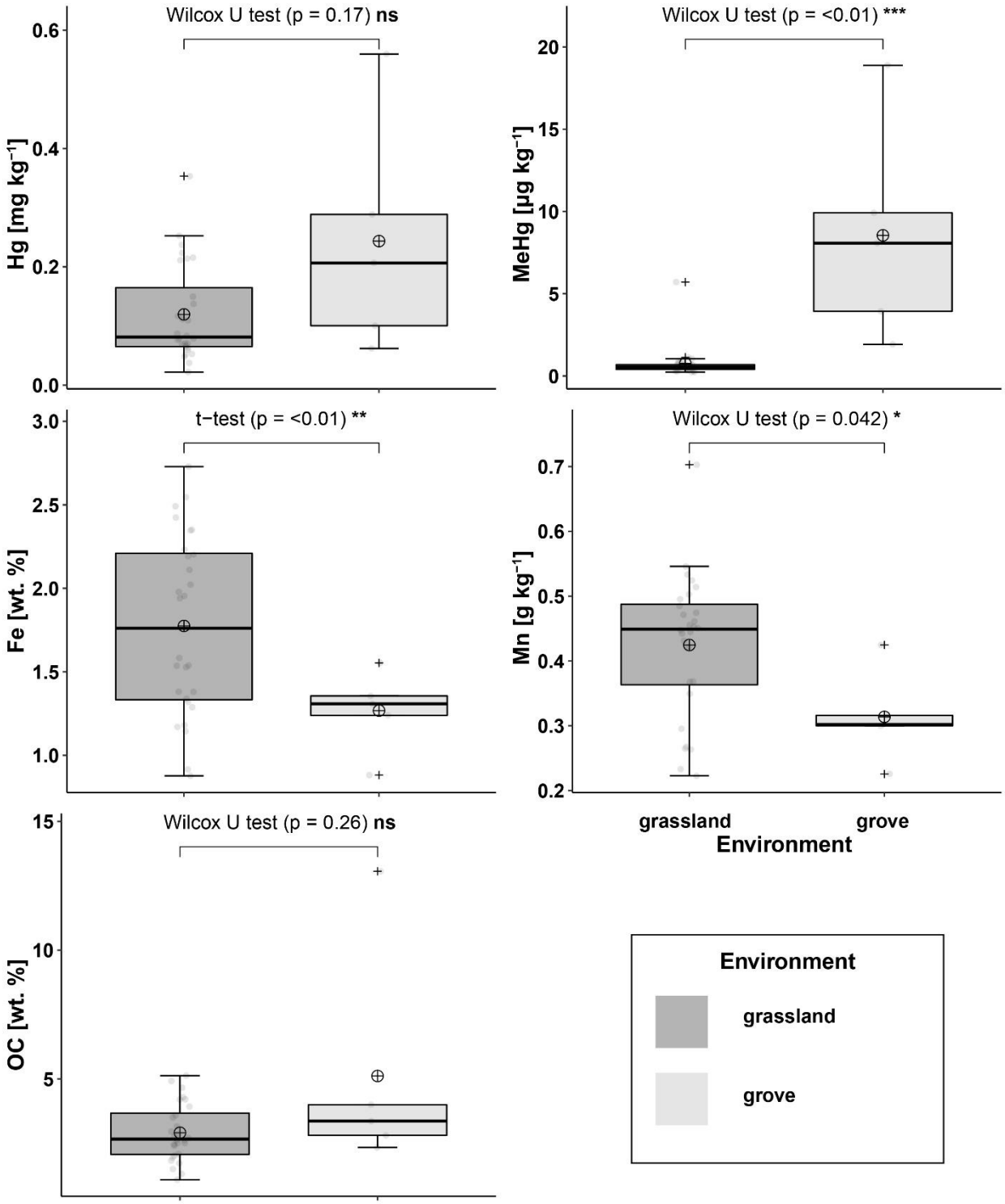

Figure 2 - 5 Box plots of Hg, MeHg, Fe, Mn, and organic carbon (OC). The data is grouped by landuse type (grassland, shown in dark gray, and groves, shown in light gray). The results of statistical tests (Wilcoxon U test or t-test) are shown above the corresponding box plots, along with their significance levels.

2.3.2. Vertical distribution of Hg, MeHg, OM and trace elements.

In profiles of the small-scale grassland site, OC concentrations vastly decreased from 4.8 ± 1.3 wt. % at 0 - 10 cm to 1.3 ± 0.5 wt. % between 10 - 20 cm and then continuously decreased to <0.5 wt.% in 40 - 50 cm depth. Mean Hg concentrations were relatively constant between 0 - 30 cm depth (0.07 ± 0.04 mg kg^{-1}) and then decreased to <0.02 mg kg^{-1} at 40 - 50 cm. Soil OC and Hg strongly correlated in the topsoil (0-10 cm depth, R^2 = 0.73, p<0.001) and less in depth of 10 to 30 cm (R^2 = 0.36, p<0.001) (Fig. 2 - 6). The Hg:OC slopes of the linear regressions between 10 and 30 cm depth (0.066) were similar to those observed in grassland samples collected across the entire sampling area. The topsoil layer between 0 and 10 cm had lower Hg:OC slopes (0.013) (Fig. 2 - 6). In addition, Hg had a negative correlation with certain oxide-forming metals that are relevant for Hg adsorption (such as Fe, Al, and Mn) in topsoils (0 - 10 cm), but a positive correlation at depths between 10 - 50 cm (as shown in Figs. A - 1, A - 2). Both Hg and Mn had a slight increase in concentration at depths of 20 - 30 cm at the grassland small-scale sampling site (as shown in Fig. 2 - 7). The pH in the grove profiles gradually increase with depth, from 6.7-7.4 in 0-10 cm depth to 8.0 - 8.8 in 40 - 50 cm depth. This indicates a carbonate buffered soil even in the Ah horizon.

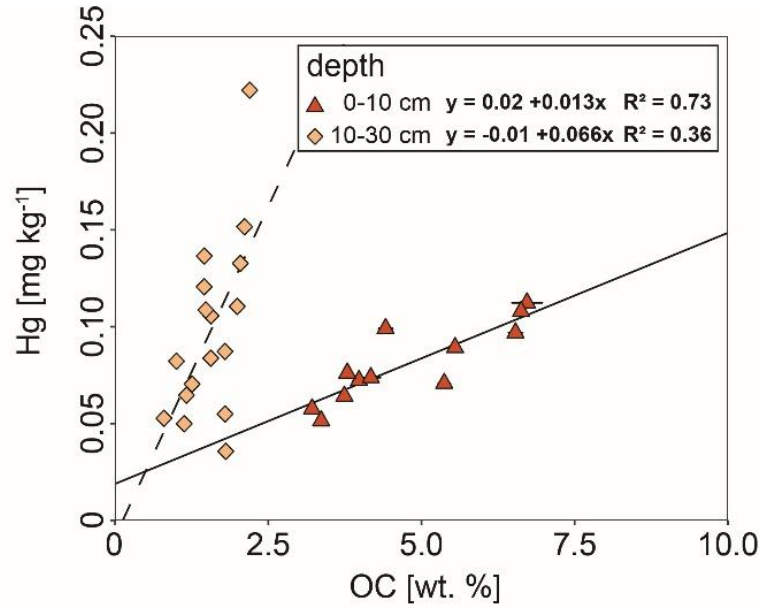

Figure 2 - 6 Scatter plots and linear regressions showing the relationship between Hg and organic carbon in grassland soils at the small-scale screening site. The solid line represents the regression for samples at a depth of 0-10 cm (shown as red triangles), and the dashed line represents the regression for samples at a depth of 10-30 cm (shown as orange diamonds).

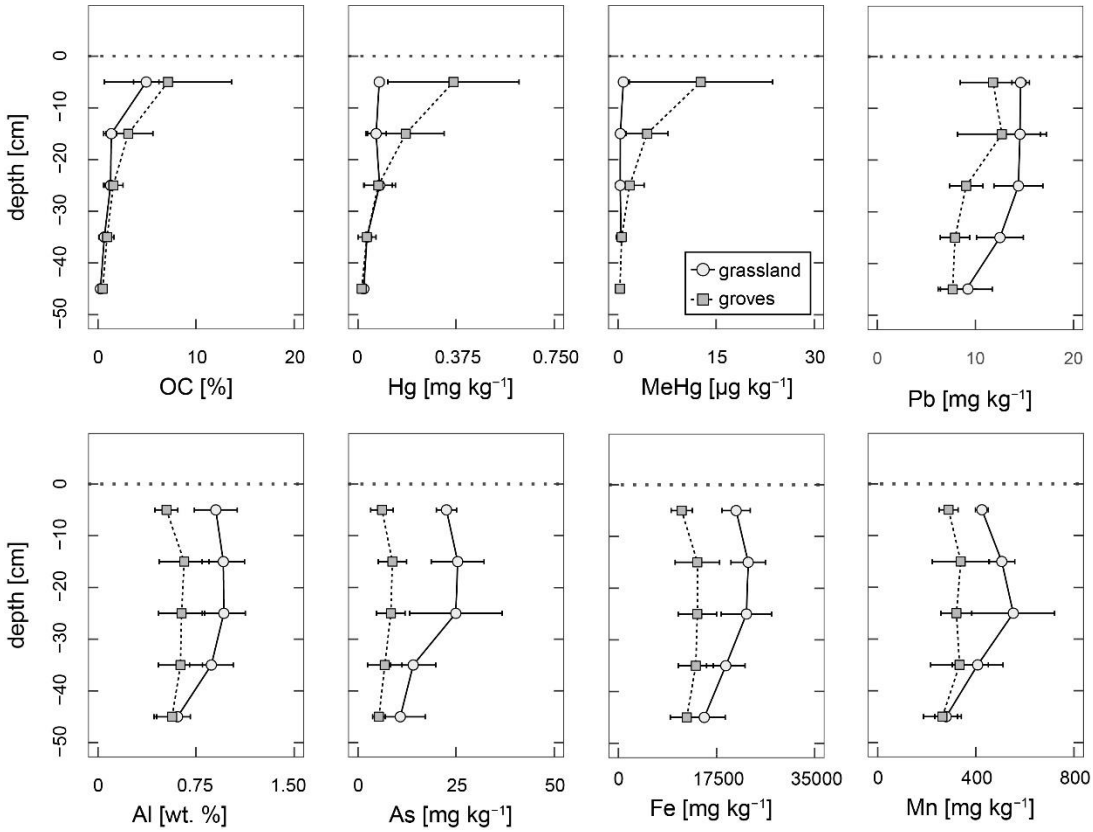

Figure 2 - 7 Depth profiles for organic carbon (OC), Hg, MeHg, Pb, Ni, Al, As, Fe and Mn. The points show the mean concentrations for groves (represented by grey squares) and grasslands (represented by white circles). Error bars show the 1σ standard deviation of all samples in each group. Sampling was conducted systematically in 10 cm intervals and does not correspond directly to distinct soil horizons.

Contrastingly, profiles in groves showed similar patterns for Hg, MeHg, and OC (Fig. 2 - 7) with Hg concentration highest in topsoils (0.37±0.25 mg kg^{-1}, at 0 - 10 cm) and a substantial decrease with depth (<0.02 mg kg^{-1}, at 40 - 50 cm). Soil Hg showed significant ranked correlations with OC (ρ = 0.85, $p<0.05$), Pb (ρ = 0.81, $p<0.05$), MeHg (ρ = 0.54, $p<0.05$) (Figs. 2 - 7, A - 3). Further, Hg, MeHg and OC concentrations showed negative ranked correlations with depth (Hg: ρ =-0.83, MeHg ρ =-0.79, OC: ρ = -0.86, $p<0.05$) (Fig. A - 3). In contrast, other trace (Ni, Cu, Co, Cr, Zn, V) or major (Al, Fe) metal concentrations were relatively constant with depth in profiles of both environments (Figs. 2 - 7, A - 4).

Patterns of both calculated enrichment factors $EF_{Hg/Al}$ and $EF_{Hg/Ni}$ were similar (Fig. 2 - 8). Thus, only $EF_{Hg/Al}$ will be addressed in the following paragraphs. Mean enrichment factors were higher than zero at all depths above 40 cm. This points towards a Hg enrichment in the topsoil of all soil profiles (grassland and groves). Groves showed significantly higher mercury concentrations and $EF_{Hg/Al}$ in the topsoils. There, $EF_{Hg/Al}$ gradually decreased from top (2400 ± 1262 %) to 40 cm depth (145 ± 117 %) and showed a similar pattern as OC, MeHg and Hg concentrations. In the grassland soils mean $EF_{Hg/Al}$ was constant between the top (415 ± 214 %) and 30 cm (339 ± 340 %) and then decreased between 30-40 cm depth (57.2 ± 214 %).

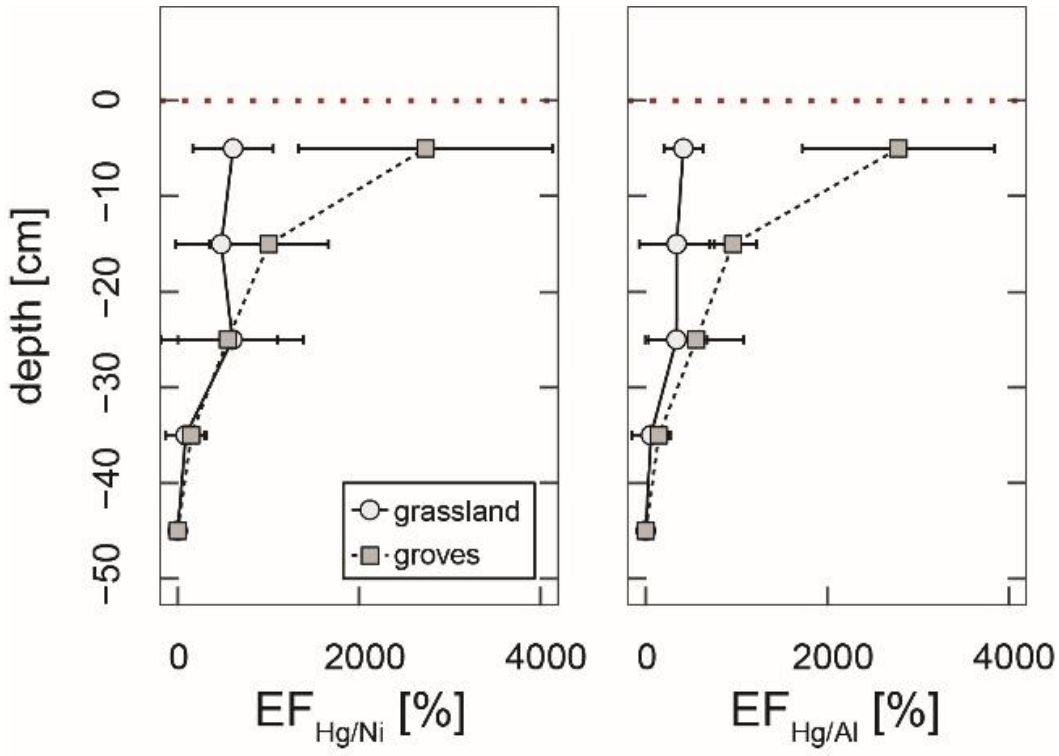

Figure 2 - 8 Depth profiles for enrichment factors calculated relative to Ni ($EF_{Hg/Ni}$) and Al ($EF_{Hg/Al}$). The points show the mean values for groves (represented by grey squares) and grasslands (represented by white circles). Error bars show the 1σ standard deviation of all samples in each group. Sampling was conducted systematically in 10 cm intervals.

MeHg concentrations in the grove profiles were highest in the topsoils (2.61 to 29.6 μg kg^{-1}) and gradually decreased to (<0.02 to 0.29 μg kg-1) (Fig. 2 - 8). The MeHg/Hg ratios were generally higher in groves compared to the grassland profiles. The maximal MeHg/Hg reached 19.1% reflecting a surprisingly high net-methylation potential of Hg in the grove soils. The soil MeHg concentrations between 0 and 20 cm were inversely proportional to Al, Fe and Mn concentrations (Fig. 2 - 9).

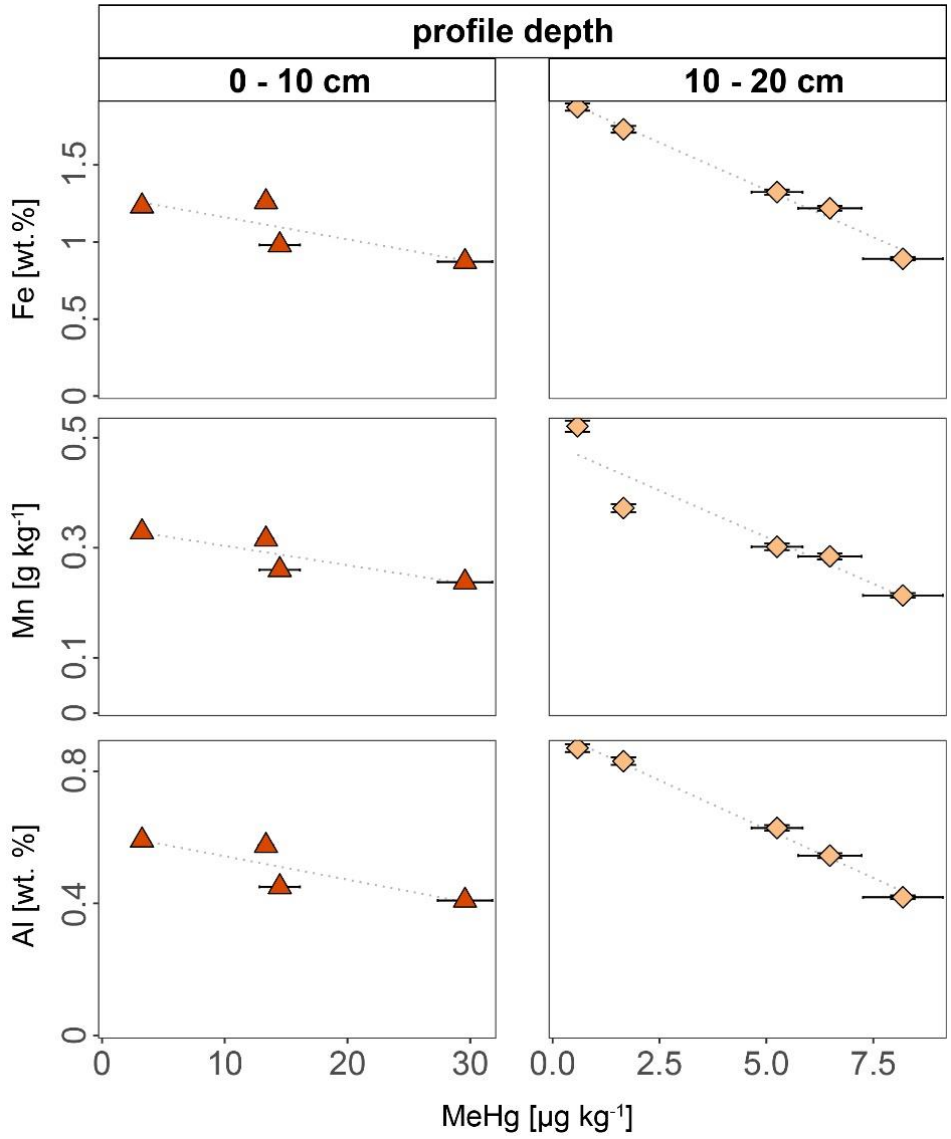

Figure 2 - 9 Scatter plots showing the relationships between MeHg and Mn, Fe, and Al in grove soils. The data was grouped by depth into intervals of 0-10 cm (shown as red triangles) and 10-20 cm (shown as light orange diamonds). The axis limits for MeHg are different between the two groups.

2.4. Discussion

2.4.1 Variability of soil parameters and origin of Hg in grassland.

We sampled soil samples across a mountain valley subjected to Hg pollution by a chemical plant. The industrial processes involving Hg were namely acetaldehyde production and the chlor-alkali process. Grassland soils concentrations were up to 3 magnitudes lower compared to soils affected by the deposition of Hg contaminated materials in the area (Mudry, 2016; Gfeller et al., 2021; Gygax et al., 2019) and in the range of European background (Panagos et al., 2021) and soils at Swiss Soil Monitoring sites (<0.1 mg/kg) (Gruber et al., 2015). However, the range of Hg concentrations (0.02 to 0.353 mg kg^{-1}) in the topsoil (0 - 20 cm) is still large, considering the small sampling area (17 km). Thus, an influence of the close by chemical plant or contaminated soils is apparent. Earlier studies in this area reported severely high Hg concentrations (470 mg kg^{-1}) where contaminated canal sediments were applied to agricultural land or where other solid contaminated materials were distributed (Mudry, 2016; Gfeller et al., 2022). It was shown that the chlor-alkali process might emit a significant proportion of GOM in which Hg is present as ionized Hg^{2+} (Landis et al., 2004), which has a lower residence time in the atmosphere compared to GEM and is deposited through wet deposition (Bishop et al., 2020). Spherical gradients of soil Hg concentrations up to 3 km around chlor-alkali plants were reported in previous studies, with forest soils being shown to have higher concentrations than grassland soils with similar proximities to the facilities (Biester et al., 2002b; Guédron et al., 2013). The authors suggested a rather fast deposition of GOM. However, we did not observe spherical spatial patterns of soils Hg concentrations e.g. (i) proximity to the Gamsenried landfill or the chemical plant or (ii) in the preferential wind directions (Fig. 2 - 2) in our study area. This finding is in line with the results of an extensive screening campaign in the study area conducted by the cantonal environmental agency (DUS, 2016). This screening reported spatial gradients in Hg concentrations only in the area 1 km around the facility. Further, the study reported that the highest Hg concentrations are unevenly distributed on the mostly in the residential areas and on agricultural fields. This is likely due to the translocation of contaminated material rather than atmospheric deposition. Additionally, temperature inversion in winter resulting in elevated air pollution and local deposition might have resulted in the narrow distribution of Hg (Chazette et al., 2005). However, the redistribution of contaminated material within the area (e.g. by dust dispersion) may not be ruled out. In this scope, the polluted fields in the area were observed to release GEM depending on their Hg concentration (Osterwalder et al., 2019).

At the small-scale grassland sampling site a ploughing horizon was visible at in 30 cm depth. This is further indicated by a decrease of $EF_{Al/Hg}$ and metal concentrations (e.g. As, Hg, Mn, Fe) in 30 - 40 cm depth (Figs. 2 - 7, 2 - 8). Since the last plowing event an Ah horizon already developed in the in the 0-10 cm sampling interval. Throughout our study area, grassland topsoil showed correlations between Hg and OC (Fig. 2 - 3). Highest correlations were found in the topsoil (0 - 10 cm) of agricultural grasslands at the small-scale sampling site (Fig. 2 - 3). There we observed a rather narrow and low Hg concentration when compared to lower depth. However, $EF_{Al/Hg}$ were positive and suggest an enrichment compared to the underlying parent

material. This underlines that the grassland topsoils, which formed since the most recent plowing event, already accumulated some Hg, presumably though the atmosphere. Together with correlations between Hg and OC in grasslands topsoils this suggest that (i) Hg concentrations in grassland topsoils are influenced by soil-atmosphere exchange, (ii) Hg is preferentially sorbed on soil organic matter, and (iii) Hg might be accumulated by uptake through plant material. Soil organic matter plays an important role in the accumulation of Hg in grassland topsoils. Atmospheric Hg^0 has been observed to be incorporated into organic material via plant uptake (Millhollen et al., 2006; Gustin et al., 2022). Further, it has been observed that Hg reduction and evaporation from a soil decreases with increasing organic matter, clay and oxide content. Likely due to the strong binding of Hg^{II} to solid organic matter, resulting in reduced Hg^0 fluxes (Schlueter, 2000). Nevertheless, it has been reported that Hg^{II} can be reduced by dissolved organic matter constituents (Schlueter, 2000).

Further, in the grassland soils Hg showed a negative correlation with metals that are relevant to Hg adsorption (e.g. Fe, Al, Mn) between 0 - 10 cm, yet a positive correlation at lower depths (10 - 50 cm) at the small-scale screening site (Figs. A - 1, A - 2). The lower depths expressed overall higher Hg concentrations. This indicates that the distribution of Hg in a soil profile is not solely dependent on atmospheric input. We suggest that Hg^{II} (e.g. Hg-NOM complexes) is transferred through the soil profile with percolating rainwater after atmospheric deposition of Hg or its uptake through plants. This is in line with Chen et al., 2022, who demonstrated the significance of soil formation processes, percolation of pore water, and binding to mineral particles in a Swiss podzol. At lower depth, Hg is less prone to relevant reemission processes (e.g. UV-reduction) and may accumulate through sorption on Fe- and Mn-oxyhydroxides (Gfeller et al., 2021) and/or transform to β-HgS (Manceau et al., 2015) even under oxic conditions. Soil organic matter and Mn-/Fe-(oxy-)hydroxides are important sorbent for Hg in soils. For example, Hg-OM complexes sorbed on Fe (oxy-)hydroxides were demonstrated to be dominant binding forms of freshly deposited Hg in paddy soil systems (Liu et al., 2022). In the soils of our area, studies have highlighted the significance of Mn-oxyhydroxides for Hg sorption (Gygax et al., 2019; Gfeller et al., 2021; Grigg et al., 2018). Although, Hg can be accumulated as described above, without sufficient evidence (e.g. from sequential extractions), we were unable to make a precise evaluation of total Hg storage and transport pathways in these soil profiles.

We found that ranges of Hg (0.02 mg kg^{-1} to 0.35), MeHg (0.23 to 1.14 µg kg^{-1}) concentrations and MeHg/Hg ratios (0.186 to 1.51 %) of the grassland soils were comparable to background paddy soils reported from a contaminated mining area in Wanshan China (Horvat et al., 2003; Qiu et al., 2005). But the grassland soils showed up to 15 times lower MeHg concentrations when compared to Swedish peatland soils with similar HgT concentrations (Åkerblom et al., 2020). Due to channeling, a wide area of the studied floodplain is not objected to regular flooding to date. In soils and sediments Hg methylation is thought to be mainly facilitated by iron and sulfate reducing conditions. The absence of regular water logging can explain the low MeHg concentrations in the grassland soils. However, Fluvisols contaminated with Hg along the constructed “Grossgrundkanal” canal have been reported to experience regular flooding, leading to the release of Hg and

elevated methylation potential. Under these conditions, concentrations of MeHg were found to reach up to 6.1 µg/kg (Gygax et al., 2019; Gfeller et al., 2021).

2.4.2. Vertical distribution and origin of Hg in grove environments.

The concentrations of mercury in Swiss soils have been decreasing since 1989 (Gruber et al., 2015). At a Swiss deciduous forest monitoring site, the concentrations of mercury in the topsoil decreased from roughly 0.22 mg kg^{-1} in 1989 to <0.1 mg kg^{-1} in 2019. At our site, the topsoil in the grove environments had observably higher Hg concentrations and surpassed the background levels of the Swiss monitoring site (Fig. 2 - 7). This points towards a higher net deposition of Hg in these environments as compared to grasslands. The highly elevated $EF_{Hg/Al}$ values compared to the lowest point in the profile suggest that Hg distribution originated rather from atmospheric deposition than from geological sources (Fig. 2 - 8). We suggest two possible pathways for Hg to enter the forest ecosystem: i) through the incorporation of mercury into leaves (litterfall) and/or ii) through the deposition of dust from polluted areas on the leave surfaces. The Hg dry deposition though the stomatal uptake of Hg by leaves and their subsequent deposition are an important pathway for Hg in forest systems (Wohlgemuth et al., 2021). Previous studies report relationships between the amount of Hg and organic carbon in forest soils across large spatial ranges (Obrist et al., 2011).

The $EF_{Hg/Al}$ profiles suggests that Hg input from the soils surface for example though atmospheric deposition (Fig. 2 - 8). At the grove sites, Hg is closely associated with organic matter. The strong correlation between OC and Hg (ρ =0.85, p>0.05) indicates that Hg-DOM is an important form in these soils, and that Hg deposition might be dominated by litterfall or that Hg transport is closely related to NOM rich material. The deposition of dust and subsequent deposition by throughfall represents another possible source for Hg in the groves. Guédron et al. 2013 showed that leaves from the vicinity of a chlor-alkali plant (Grenoble, France) can have up to 10 times higher Hg concentrations when not washed before analyses. Suggesting high HgP deposition on the leave surfaces. In our case, highly contaminated agricultural fields (up to 470 mg kg^{-1}) are situated in the vicinity of the grove patches (Mudry, 2016; Gfeller et al., 2021). These crop fields are regularly ploughed and lie fallow during parts of the year. The Hg containing dust particles are likely to be deposited on the leaves and incorporated on the soils by throughfall. However, Hg deposition by throughfall appears to be less pronounced, since reported correlations between Hg and trace metals (Cu, Zn, Ni) in highly contaminated soil of the area (Gfeller et al., 2022) could not be verified in the grove environments. In the groves, positive correlations between Hg and other trace metals were only verified for Pb (ρ =0.81, p>0.05). Further, the contaminated fields in the area were shown to emit GEM depending on their Hg concentration (Osterwalder et al., 2019). However, we did not observe a correlation between the levels of mercury and the proximity of those sites to the chemical plant or to highly contaminated soils. The limited sample size (5 profiles) and missing data on leaves, litter and precipitation did not allow for a mass balance calculation. An extended sampling of these pools is needed to establish

a quantitative Hg mass balance in these grove ecosystems to identify the predominant sources and annual fluxes (Chen et al., 2022).

2.4.3. Net-methylation and the potential impact of MeHg in grove environments.

We observed unexpectedly high MeHg levels (up to 29.6 μg kg^{-1}) and MeHg/Hg ratios (up to 18.8 %) in the groves top 10 cm of the grove soils (Ah and O horizons). This suggest that groves and forests in temperate alpine regions may express elevated net-Hg methylation, which is approximately 20 times larger than reported in forest soils from tropical and subtropical climate zones (Li et al., 2021a; Shanley et al., 2020) but similar to boreal peat soils (Åkerblom et al., 2020) or forest soils (Kronberg et al., 2016; Eklöf et al., 2018). Methylation potential in soils is a function of microbial taxonomy, microbial activity, and the availability of Hg to methylating microbes (Bishop et al., 2020; Beckers and Rinklebe, 2017). Topsoil horizons (0 - 10 cm) in the groves showed lower pH values (6.7 - 7.4) compared to the deeper profile (7.4 - 8.8) but were still carbonate buffered (>6.8 pH). It is common for the O an Ah horizons to express lower pH due to the elevated concentrations of organic acids and higher amounts of labile carbon, which may increase microbial activity. Bioreporter experiments showed that Hg uptake by bacteria increased in towards lower pH (5-6) ranges compared to pH common of carbonate buffered systems (pH 7-8) (Kelly et al., 2003; Golding et al., 2008). The here presented comparably high MeHg concentrations in the lower pH topsoils are in line with these observations. Further, MeHg concentrations correlate negatively with Fe, Mn, Al (Fig. 2 - 9), in the grove profiles. Under oxic conditions, these metals are commonly present as oxides or hydroxides with high specific surface areas and large sorption potential. Thus, topsoils that express higher sesquioxide and hydroxide forming metals were lower in MeHg concentrations. We suggested that MeHg de-/methylation in these soils is influenced by of the amount of Mn-, Fe- and/or Al-oxides in these soils. Due to the high sorption Hg capacity of Mn, Fe and Al (oxy-) hydroxide phases, these metals are also thought to be a influencing factor for net-Hg methylation (Beckers and Rinklebe, 2017). Although they reduce bioavailability of Hg, it has been demonstrated that Hg bound to hydroxide phases (Zhang et al., 2019) and complexed with dissolved organic matter (Zhao et al., 2017) can be methylated. The identification of predominant binding forms of Hg by e.g. single or sequential extraction (Bloom et al., 2003; Ticknor et al., 2015) or thermal desorption (Biester et al., 2002a) might provide further insights into the availability of Hg. However, both of these methods require elevated Hg levels and are typically used in areas of high Hg contamination (Grigg et al., 2018; McLagan et al., 2022; Biester et al., 2002a).

The tree groves on agricultural land that have been sampled in this study are more than isolated patches. They can be considered ecological compensation areas which are a central part of the Swiss agri-environmental scheme. The importance of ecological compensation areas has been proven and they increase biodiversity and the abundance of organisms such as invertebrates (Pfiffner and Luka, 2000) and birds (Birrer et al., 2007). Further, in temperate climate regions, it has been shown that terrestrial forest food webs are bioaccumulating Hg similar to aquatic food webs (Tsz-Ki Tsui et al., 2019). The authors explained the

unexpectedly high MeHg in terrestrial invertebrates by the relevance of food webs that are based on detritus, or dead plant material, in the forest floor. Earthworms in our sampling region have been found to bioaccumulate mercury (Hg) and methylmercury (MeHg) to up to 32 and 27 times higher than the levels found in respective soils (Brantschen et al., 2020). As mentioned above, the here presented MeHg concentration in the tree grove soils are comparably high. Although we have no data on wildlife in the region, the high MeHg concentration suggests that these tree groves may serve as a source of Hg and MeHg to the terrestrial food chain. Further, research is needed to assess the processes of Hg methylation in forest of temperate alpine climate zones and their effects on the bioaccumulation in the terrestrial food chain.

2.5. Conclusions and Outlook

This study examined the levels of Hg and net-methylation potential (MeHg/Hg) in both groves and grasslands located near a chemical plant which had been releasing mercury into the environment. Soil samples were taken from each land use type and analyzed to compare the concentrations of Hg and the potential for net-methylation between the two. The aim was to determine (i) the distribution of Hg, (ii) potential Hg pathways and the extent of net-methylation potential present in these two distinct land use types.

We show that Hg in topsoil of grassland environments is likely a result of constant exchange of GEM between soils and atmosphere. This becomes evident from (i) a very narrow Hg concentration range in topsoil, (ii) a significant correlation between Hg and OC in topsoil and (iii) no spatial trends towards the chemical plant indicating only minor influence of GOM from the atmosphere.

Grove environments showed a higher Hg content and surprisingly high MeHg concentrations in the top 0-10 cm. This indicates an increased Hg deposition, elevated net-methylation of Hg in these groves and opens further questions about the fate and pools of Hg in these soils. Mercury methylation is a dynamic process and the result of Hg methylation and MeHg demethylation rates in the soil environment. Although Hg is generally methylated under anerobic conditions; many environments have been identified as possible Hg methylation hot spots. The groves are not a priori anerobic environments. However, steep redox gradients on surfaces (e.g. soil aggregates) may also serve as potential Hg methylation hotspots. To identify regions of high net-methylation potential further studies are needed. We suggest a systematic sampling of the soil by horizons and an assessment of net-methylation potential (e.g. using specie specific isotopic tracers in batch experiments).

The surprisingly high MeHg concentrations in the groves were comparable to global MeHg hotspots (e.g. Swedish peat soils). We revealed the importance of forest environments in temperate climates as a source for MeHg to wildlife.

Our study design featured (i) a systematic sampling of soil profiles in 10 cm intervals and (ii) the measurement of Hg, MeHg and common soil parameters. This did not allow for a complete assessment of methylation rates, Hg mobility and deposition pathways. Further studies are needed to assess (i) the Hg fluxes pathways in grove environments, (ii) differences in Hg methylation potential between environments (iii) the mobility and speciation of Hg in these soils and (iv) potential risks of the high MeHg levels to the wildlife.

3. Organo-mercury species in a polluted agricultural flood plain: combining speciation methods and polymerase chain reaction to investigate contaminant pathways.

This chapter was published as Gfeller, Lorenz; Caplette, Jaime N.; Frossard, Aline; Mestrot, Adrien (2022):

Organo-mercury species in a polluted agricultural flood plain: combining speciation methods and polymerase chain reaction to investigate contaminant pathways. In *Environmental Pollution* 311 (2022) 119854.

DOI: https://doi.org/10.1016/j.envpol.2022.119854

Author contributions:

Lorenz Gfeller: conceptualization, sampling, laboratory, visualizations, writing original draft, reviewing, and editing.

Jaime N. Caplette: sampling, laboratory.

Aline Frossard: laboratory, qPCR expertise , reviewing of the manuscript..

Adrien Mestrot: Supervision, conceptualization, reviewing and editing of the manuscript.

Abstract

The analysis of organic mercury (Hg) species in polluted soils is a necessary tool to assess the environmental risk(s) of mercury in contaminated legacy sites. The artificial formation of monomethylmercury (MeHg) during soil extraction and/or analysis is a well-known limitation and is especially relevant in highly polluted areas where MeHg/Hg ratios are notoriously low. Although this has been known for almost 30 years, the thorough characterization of artificial formation rates is rarely a part of the method development in scientific literature. Here we present the application of two separate procedures (inorganic Hg (iHg) spiking and double-spike isotope dilution analyses (DSIDA)) to determine and correct for artificial Hg methylation in MeHg-selective acid-leaching/organic solvent extraction procedure. Subsequently, we combined corrected MeHg and ethyl mercury (EtHg) measurements with PCR amplification of hgcA genes to distinguish between naturally formed MeHg from primary deposited MeHg in soils from a legacy site in a Swiss mountain valley. We found the DSIDA procedure incompatible with the organomercury selective extraction method due to the quantitative removal of iHg. Methylation factors from iHg spiking were in the range of (0.0075 ± 0.0001%) and were consistent across soils and sediment matrices. Further, we suggest that MeHg was deposited and not formed *in-situ* in two out of three studied locations. Our line of evidence consists of 1) the concomitant detection of EtHg, 2) the elevated MeHg concentrations (up to 4.84 µg kg^{-1}), and 3) the absence of hgcA genes at these locations. The combination of Hg speciation and methylation gene (hgcA) abundance analyses are tools suited to assess Hg pollution pathways at Hg legacy sites.

3.1. Introduction

Mercury (Hg) is a pollutant of global concern due to its high toxicity and its biogeochemical cycle which spans all environmental compartments (atmosphere, oceans, soils) (UNEP, 2019). Relevant anthropogenic Hg sources are small scale artisanal gold mining, fuel combustion as well as the chemical industry (Horowitz et al., 2014). Sediments and soils are major Hg pools with relatively long Hg residence times (Amos et al., 2013; Driscoll et al., 2013). Legacy Hg from industrial sites (e.g. chlor-alkali plants or mining areas) retained in soils is a key source for present-day gaseous elemental mercury (GEM) in the atmosphere and a threat to downstream ecosystems due to the formation and bioaccumulation of toxic monomethylmercury (MeHg) in both aquatic and terrestrial food chains (Singer et al., 2016; Bigham et al., 2017). Fuel combustion, small-scale artisanal gold mining activities and Hg ore smelters are mainly emitting Hg as GEM. In the case of chemical plants, the speciation of the emitted Hg may often vary with the applied processes and consist of GEM, inorganic Hg (iHg) (Glenz and Escher, 2011), MeHg (Matsumoto et al., 1965), and ethyl mercury (EtHg). However, the reconstruction of Hg emissions is often difficult due to the lack of publicly available information on the pollution history. Therefore, speciation of Hg in soils may be an important tool to better understand and assess the pollution history of legacy sites.

There are many published techniques to extract and quantify organic Hg species in soils and sediments. Generally, they involve 1) an extraction step (acid, alkaline or distillation), 2) a purification (derivatization or solvent extraction) and 3) chromatographic separation and analysis (HPLC-ICP-MS or GC-CVAFS). To date, there is no standardized technique for the quantification of organic Hg species (Hellmann et al., 2019; Jagtap and Maher, 2015).

Artificial formation of organic Hg species is one of the major problems during their extraction from soil or sediment. The formation of MeHg occurs in many extraction techniques (Hellmann et al., 2019). The first report of artificial MeHg formation dates back to the 1970s (Rogers, 1977; Rogers, 1976). Although this problem preoccupied the Hg community already in the last century (Quenvauviller and Horvat, 1999; Falter, 1999b, 1999a; Hintelmann et al., 1997), no MeHg extraction technique for soil and sediment matrices has yet been proven to be free from artifact formation (Hellmann et al., 2019). The relative amounts of MeHg artifacts depend on the sample matrix (soil, sediment etc..) (Falter, 1999b; Rogers, 1977; Nagase et al., 1984; Bloom et al., 1997), the amount of leached iHg (Hammerschmidt and Fitzgerald, 2001), the pH (Rogers, 1977; Nagase et al., 1984) and the extraction solvent and method used. Published ratios of MeHg artifact formation from iHg range from 0.0003 to 0.28% in soil and sediment matrices (Bloom et al., 1997; Hintelmann et al., 1997; Huang, 2005) and from 0 to 11.5% in fish tissues (Hintelmann et al., 1997; Qvarnström and Frech, 2002). Table 3-1 summarizes the existing Hg extraction methods and their respective MeHg artifact formation. Since MeHg accounts for around 0.5 - 1% of the total Hg pool in background soils and sediments, these ratios result in negligible amounts of artificial MeHg formed. Polluted soils and sediments usually have very low MeHg/Hg ratios (<<0.1%) (Gray et al., 2004; Gygax et al., 2019; Xu et al., 2018) which may result in significant false positives of MeHg in polluted soils and sediments that often lead to misinterpretations (Hellmann et

al., 2019). Double-spike isotope dilution analysis (DSIDA) has been successfully applied to directly quantify and correct for artificial methylation and demethylation during Hg extraction from animal tissues; however, this state-of-the-art method has shown limitations when extracting Hg from non-biological samples with high iHg concentrations (Monperrus et al., 2004; Monperrus et al., 2008). Ethyl mercury is another organic Hg species previously observed in industrial areas (Tomiyasu et al., 2017). Although, artifact formation of EtHg has rarely been reported (Huang, 2005), the detection of EtHg is not straight forward. For example, EtHg can decompose to iHg within hours under strong acidic conditions in coexistence with Fe^{3+} (Han et al., 2003), or if extracted at 60°C in 0.1% L-Cysteine (Hight and Cheng, 2006). Further, Wilken et al., 2003 found that EtHg may have the same retention time as a certain mercury sulfur polymers (e.g. CH_3–S–Hg^+) during liquid chromatographic separation. For all the reasons stated above, it is crucial to thoroughly evaluate the analytical methods, even published and established ones, for the potential artificial formation or decomposition of the target analytes during extraction (i.e., EtHg and MeHg), before application in the field. If that cannot be avoided, a suitable and transparent method for correction must be established.

Table 3 - 1 Methylation rates taken from the literature for various extraction methods for soils, sediments and fish tissues.

Extraction technique	Matrix	Measurement	Study	Methylation rates (%)	Reference
Distillation	sediment	GC-CV-AFS	Hg^{2+} spiking	0.036 ± 0.038	Bloom et al. 1997
KOH/Methanol	sediment	GC-CV-AFS	Hg^{2+} spiking	0.046	
Formic Acid	sediment	GC-CV-AFS	Hg^{2+} spiking	<0.0003	
10 % HCl	sediment	GC-CV-AFS	Hg^{2+} spiking	<0.002	
KOH/CH_2Cl_2	sediment	GC-CV-AFS	Hg^{2+} spiking	0.022 ± 0.021	
KBr/H_2SO_4/$CuSO_4$	sediment	GC-CV-AFS	Hg^{2+} spiking	0.0025 ± 0.0013	
TMAH	fish tissue	HPLC-ICP-MS	SS-ID	0.1 - 11.5	Qvarnström et al. 2002
TMAH/Ethylation	sediment	GC-ICP-MS	SS-ID	0.03	Hintelmann et al. 1997
5M HCL/Toluene	sediment	HPLC-ICP-MS	SS-ID	0.005	
TMAH/Ethylation	fish tissue	GC-ICP-MS	SS-ID	4.3	
Distillation	fish tissue	HPLC-ICP-MS	SS-ID	no MeHg formation	
$CaCl_2$/Tropolene/Acetic acid/Propylation	soil	GC-ICP-MS	Hg^{2+} spiking	0.03-0.28	Huang et al. 2005

The natural formation of MeHg from iHg is mainly driven by microbial (de)methylation processes. Environments with redox oscillation (e.g., floodplains, estuaries) represent hot spots for Hg methylation (Marvin-DiPasquale et al., 2014; Windham-Myers et al., 2014; Bigham et al., 2017; Driscoll et al., 2013). Common Hg methylators are anaerobic microorganisms such as sulfate reducing bacteria (SRB), iron reducing bacteria (FeRB), archaea and some firmicutes (Podar et al., 2015). It is commonly accepted that a two-gene cluster (*hgcAB*) is responsible and essential for Hg biomethylation (Parks et al., 2013; Poulain and Barkay, 2013).

The potential for a soil net MeHg production depends on the physicochemical soil properties and Hg bioavailability (Zhang et al., 2018; Wang et al., 2021b). The binding of Hg in the soil matrix has a major influence on its bioavailability and methylation. Hg in bulk sulfide particles is generally less available for methylation than if bound to sulfide nanoparticles or dissolved

organic matter (DOM) (meta-cinnabar<cinnabar<Hg-DOM<Hg^{2+}) (Zhang et al., 2014; Jonsson et al., 2012). In solution, DOM promotes the dissolution and affects the crystallinity of HgS(s) phases, as well as decelerates the aggregation and growth of HgS(s) colloids. The size and structure of ß-HgS(s) and HgSe(s) particulates are hypothesized to be reciprocal to Hg bioavailability to MeHg-producing microorganisms. Further, amendments of organic matter in form of organic fertilizers enhance the net MeHg production in soils (Gygax et al., 2019).

Hg demethylation, however, is comparably less studied/understood. The most prominent pathways for MeHg decomposition are UV-light and reductive chemotrophic demethylation. For the latter, the *merB* gene was found to be essential (Parks et al., 2009). This gene is part of the mer-operon, which comprises genes encoding for Hg transport and detoxification pathways. It is also responsible for Hg reduction by the *merA* gene (Grégoire and Poulain, 2018). The abundance of *merA* linearly increases with Hg concentration in industrially contaminated soils (Osterwalder et al., 2019).

Other sources of MeHg to soil and sediments are the direct inputs of industrially contaminated materials (Matsumoto et al., 1965; Hintelmann et al., 1995). In that case, we hypothesize that Hg compounds such as EtHg could be emitted alongside MeHg. The presence of EtHg in soils and sediments has been reported in different environments: remote wetlands (Mao et al., 2010), industrial areas (Tomiyasu et al., 2017; Hintelmann et al., 1995), or close to volcanic activity (Tomiyasu et al., 2017). The detection of EtHg in soil from the Everglades suggests that non-anthropogenic Hg ethylation might be possible (Mao et al., 2010). However, direct, or indirect anthropogenic emissions should not be excluded. Unfortunately, no systematic studies about pathways for natural Hg-ethylation exist.

Industrially Hg polluted areas are often extensively studied in terms of contamination levels and spatial pollution extent. However, more information on the speciation of Hg could further the understanding of soil processes that cope with Hg pollution and the risks to groundwater and downstream ecosystems. Furthermore, information on Hg speciation, coupled with microbial DNA analyses, may serve as tools to determine whether organic Hg species are formed *in-situ* or directly deposited from industrial activities, and thus retrace the history of pollution in the area. We hypothesize that the absence of *hgcA* in a soil sample with a high MeHg concentration would suggest that this MeHg was deposited and not formed *in-situ*, since the *hgcAB* gene cluster is essential for the biomethylation of Hg. This hypothesis can be further strengthened by the presence or absence of other organic Hg species such as EtHg.

In this study, we tested, improved, and applied a previously published high-throughput extraction method for organo-Hg species (MeHg and EtHg) and analysis by high performance liquid chromatography-inductively coupled plasma-mass spectrometry (HPLC-ICP-MS) in less than 7 min (Brombach et al., 2015; Sannac et al., 2017; Gygax, 2015). We analyzed 163 samples from polluted agricultural floodplain in an alpine mountain region. We aimed to precisely quantify the artificial methylation of Hg during extraction to correct for false positives using two different methods (iHg spiking and DSIDA). We

successfully corrected for artificial Hg methylation and discussed the advantages and disadvantages of the two methods tested. Subsequently, we characterized the soils from the legacy site and assessed its pollution history.

3.2. Methods and Materials

3.2.1. Sample location, sample collection, sample processing

Soil samples were collected between April and May 2017 from an agriculturally used floodplain between Visp (N 46°17′58.780″; E 7°51′06.369″) and Niedergesteln (N 46°18′46.464″; E 7°46′54.455″), Wallis, Switzerland (Fig. B - 1). The site is situated downstream from an acetaldehyde and chlor-alkali chemical plant and is historically affected by Hg pollution. The Hg was released from the plant through a wastewater discharge canal between 1931 and 1976. The canal sediments were used as fertilizer on the canal's bank and across the agricultural fields between the 1960s and 1980s. Further contaminated materials were used to fill pits and construct terrain modifications in the floodplain (Mudry, 2016). The reported Hg concentrations in the soils from this area range from 0.5 to 470 mg kg^{-1} (Mudry, 2016; Gilli et al., 2018; Gygax et al., 2019) and atmospheric emissions of GEM have been documented at this site (Osterwalder et al., 2019; Glenz and Escher, 2011 and references there in). For this study, three sites with elevated Hg levels were chosen based on a preliminary Hg-screening campaign (Dienststelle für Umwelt, 2016). Soils were sampled within a rectangular grid (25 × 20 m) divided into 25 m^2 squares. Following this scheme, a total of 12 soil cores were taken using a Pürckhauer corer with a target depth of 50 cm and divided into 10 cm intervals (Fig. B - 2). Sites were named Canal Site, Landfill and Hotspot after their geographical location (Table B - 1) or previously measured Hg concentrations.

Samples were double bagged in polyethylene (PE) bags. The sample bags were stored on ice immediately then frozen (−20°C) at most 8 h after sampling. A selection of fresh samples for DNA extraction was kept in at −20°C in extraction buffer using the DNeasy® PowerSoil® Kit (QIAGEN, Venlo, NL) until DNA extraction. In the laboratory, the remaining material was freeze-dried, sieved to <2mm grain size, and ground using an agate mortar. In soil and sediment matrices, freeze drying was demonstrated to affect Hg concentration and speciation the least when compared to oven drying (Hojdová et al., 2015). The processed samples were stored at room temperature until analysis.

3.2.2. Materials and reagents

HPLC grade solvents and ultra-pure water (MilliQ, >18.2 MΩ*cm at 25 °C) were used. Acids (HNO_3, HCl) were doubly distilled in our in-house clean lab. Glassware was cleaned by soaking in acid baths (both 10% (w/w) HNO_3 and 10% (w/w) HCl) for at least 24 h and rinsed with ultra-pure water. Corning® sterile polypropylene (PP) tubes were used to store digests for of total Hg and trace metal analyses. Borosilicate glassware was used for MeHg extractions and storage. Commercially available stock solutions for multi-element (ICP multi-element standard solution IV-ICPMS-71A, Inorganic Ventures, Christiansburg, United States of America) and total Hg (ICP inorganic Hg standard solution, TraceCERT®, Sigma-Aldrich, St. Louis, United States of America) analyses were used as standards. MeHg standards were prepared by dissolving MeHg chloride (Sigma-Aldrich, St. Louis, United States of America) in methanol (HPLC grade, Fisher Scientific, Reinach,

Switzerland). The EtHg standard solution was kindly provided by Prof. Milena Horvat (Laboratory of the Department of Environmental Sciences, Jožef Stefan Institute Ljubljana, Slovenia). Commercially available isotopically enriched standards of ^{199}iHg and ^{201}MeHg (Enriched Standards, ISC Science, Oviedo, Spain) were used for DSIDA. Working solutions for analyses were prepared daily by gravimetric dilution using the analyte-specific solvents. All samples, standards and spikes were weighed with an analytical balance (ALJ 220-4, Kern & Sohn GmbH, Balingen, Germany) to a precision of 10^{-4} g.

3.2.3 Standard soil parameters

All soils were analyzed for pH, carbon (C), nitrogen (N), sulfur (S), soil organic carbon (SOC) and the metals relevant for Hg cycling in soil (i.e., Fe, Cu and Mn). Soil pH was measured in an equilibrated 0.01 mol L^{-1} $CaCl_2$ solution (1:5 soil:liquid ratio) using a pH probe (SenTix® 41, WTW, Weilheim, Germany). Soil CNS was measured with an elemental analyzer (vario El cube, Elementar Analysensysteme, Germany). SOC was calculated by the difference in C concentration before and after a thermal loss on ignition (LOI) treatment at 550°C for 2 h. Soil metals were leached by microwave-assisted acid digestion (250 mg soil, 4 mL 69 % (w/w) HNO_3, 2 mL 30% (v/v) H_2O_2). The soils trace and major metals (in 1% HNO_3) and Hg (in 1% HNO_3, 0.5% HCl) concentrations were quantified by inductively coupled plasma-mass spectrometry (ICP-MS; 7700x ICP-MS, Agilent Technologies, Santa Clara, United States of America). An internal standard of indium (m/z 115) was continuously injected through the peristaltic pump using a T-piece. The ICP-MS operating conditions for multi-element and Hg analyses are shown in Table B - 2. The rinsing protocol shown in Table B - 3 was used during HgT analyses to avoid memory effects. The limit of detection (LoD) for Hg in soil solution was < 0.02 µg kg^{-1} for all soil analyses. Soil digestions and extractions were verified using the certified reference materials (CRMs) SRM 2709a (San Joaquin Soil, National Institute of Standards and Technology, Gaithersburg, USA), PACS-3 (Marine sediment, National Research Council of Canada, Ottawa, Canada) and ERM-CC580 (Estuary sediment, Institute for Reference Materials and Measurements, Geel, Belgium). The recoveries of multi-element, Hg and MeHg of CRMs are shown in Table B - 4. For a selected set of samples soil grain size distribution was analyzed. Samples (sieved <2mm) were treated with 30% (v/v) hydrogen peroxide (H_2O_2, Sigma-Aldrich, St. Louis, United States of America) to remove SOM and dispersed in a solution of 22 mM sodium carbonate and 18 mM sodium hexametaphosphate. Particle-size composition was measured using a MasterSizer 2000 (Malvern Panalytical Ltd., UK).

3.2.4. Organo Hg speciation analyses

We modified a published method for high sample throughput (up to 64 samples per extraction batch) in 8 h for the extraction of organic Hg species (Gygax et al., 2019; Brombach et al., 2015). Briefly, 0.25 g of sample was suspended with 10 mL of a 6 mol L^{-1} HCl solution in a 20 mL borosilicate glass vial (Fig. B - 3). After 30 min of overhead shaking, the vial was centrifuged for 3 min at 680 × g and the supernatant was decanted. Then, 5 mL of CH_2Cl_2 (dichloromethane or DCM, Fisher Scientific, Reinach, Switzerland) was added to the extract, shaken for 60 min to extract organic Hg species and transferred to a borosilicate

glass vial. Then, 2 mL of a 0.1% (w/v) L-cysteine aqueous solution were added. For the back-extraction, the organic solvent was evaporated with a constant flow of N_2 at 50°C. The amount of L-cysteine solution was weighed at every step to account for loss by evaporation. The extracts were stored in the dark at 4°C and analyzed within 48 h. To assess MeHg extraction efficiency, we used a CRM ERM CC-580 (68 ± 2 µg kg^{-1}, recovery = 90.8%, n = 39, Table B - 4) for MeHg recoveries. To date, there is no suitable CRM available for EtHg for validation of EtHg extractions. Measured EtHg concentrations were interpreted as minimum concentrations in a sample, due to reported degradation of EtHg to Hg during acidic extractions using HCl (Duan et al., 2016) or extractions involving heating at 60°C in 0.1% (w/v) L-cysteine (Hight and Cheng, 2006). Degradation of EtHg was not reported to produce interference with MeHg for the speciation analysis method used (Hight and Cheng, 2006).

After extraction, Hg species were separated and analyzed using a previously published method (Sannac et al., 2009; Gygax et al., 2019; Sannac et al., 2017) by coupling a high performance liquid chromatograph (HPLC 1260 Series, Agilent Technologies, Santa Clara, United States of America) to the ICP-MS (HPLC-ICP-MS). We used a reversed phase C18 column (Zorbax C-18, 4.6 × 50 mm, Agilent Technologies, Santa Clara, United States of America) and a mobile phase consisting of 0.1% (w/v) L-cysteine (98% v/v) and methanol (2% v/v). The detailed HPLC operation conditions are given in Table S5. The LoD was calculated from the daily calibration curve and was < 0.14 µg kg^{-1} in soil samples. Three Hg species (Hg^{2+}, $MeHg^{+}$ and $EtHg^{+}$) were separated within 7 min under isocratic conditions (Fig. B - 4).

Two approaches were chosen to quantify the formation of artificial MeHg during the extraction of organic Hg species.

As a first approach, we used a double-spike isotope dilution analysis (DSIDA) (Monperrus et al., 2008). Briefly, 0.25 g of sample were weighted into the glass vial and spiked with both isotopically enriched ^{199}MeHg and ^{201}iHg to achieve isotope ratios ($^{199}Hg/^{202}Hg$ for MeHg and $^{201}Hg/^{202}Hg$ for iHg) in the range of 0.8 - 1.5. The spike and the samples were mixed for 30 min by overhead shaking. Then, the soils were extracted according to the method in section 3.2.3. This procedure did not compensate for non-quantitative extraction or speciation changes during the acid leaching step by HCl due to the relatively short equilibration time between solid and spike. However, it reduced the risk of speciation changes of the spiked material prior to the extraction. The samples were then analyzed by HPLC-ICP-MS. A Tl internal standard solution was continuously introduced through the peristaltic pump using a T-piece. Mass bias was corrected with $^{203}Tl/^{205}Tl$ ratios during each measurement. The instrument setup used for isotope dilution analysis by HPLC-ICP-MS can be found in Table B - 6. The analyzed isotopic ratios ($R^{202/201}_{MeHg}$, $R^{202/199}_{MeHg}$) allowed for the quantification of MeHg using the classic isotope dilution approach (Eq.1) (Monperrus et al., 2004 and references cited therein):

$$c = \frac{c' w' A_r (RY' - X')}{w A'_r (X - RY)} \qquad \text{(Eq.3.1)}$$

Where c = concentration of sample; w = mass of sample; A_r= relative atomic mass of the element (or species) being determined; X = isotopic abundance (atom-%) Hg^{202}; and Y = isotope abundance (atom-%) Hg^{199}. Correspondingly for the spike, c' =

concentration of the spike; w' = mass of the spike; A_r'= relative atomic mass of the element (or species) in the spike; X' = isotopic abundance (atom-%) Hg^{202}; and Y' = isotope abundance (atom-%) Hg^{199}. The parameters analyzed by HPLC-ICP-MS are therefore R (here $R^{202/199}{}_{MeHg}$). The other parameters are constants or masses weighed with analytical balances to a precision of 10^{-4} g.

The enriched ^{201}iHg spike was used to quantify the methylation factor ($F_{methylation}$). It was calculated with the equation (Eq.3.2) developed by Monperrus et al., 2008. The authors used ^{201}MeHg and ^{199}iHg spikes. We adopted these equations to our ^{199}MeHg and ^{201}iHg spikes (Enriched Standards, ISC Science, Oviedo, Spain).

$$F_{methlyation} = \frac{N_{sp}^{MeHg}}{N_{sp}^{IHg}} \times \frac{\left[\frac{(At_{sp,MeHg}^{202} - R_{MeHg,m}^{202/199} At_{sp,MeHg}^{199})}{(R_{MeHg,m}^{202/199} At_{S}^{199} - At_{S}^{202})} - \frac{(At_{sp,MeHg}^{202} - R_{MeHg,m}^{202/201} At_{sp,MeHg}^{201})}{(R_{MeHg,m}^{202/201} At_{S}^{201} - At_{S}^{202})}\right]}{\left[\frac{(At_{sp,IHg}^{202} - R_{MeHg,m}^{202/201} At_{sp,MeHg}^{201})}{(R_{MeHg,m}^{202/201} At_{S}^{201} - At_{S}^{202})} - \frac{(At_{sp,IHg}^{202} - R_{MeHg,m}^{202/199} At_{sp,MeHg}^{199})}{(R_{MeHg,m}^{202/199} At_{S}^{199} - At_{S}^{202})}\right]} \quad \text{(Eq.3.2)}$$

The selective extraction of organic Hg species did not allow for the complete correction proposed by Monperrus et al., 2008. The authors used $R^{202/201}{}_{iHg}$ and $R^{202/199}{}_{iHg}$ to correct for MeHg demethylation during the experiments. However, iHg was not consistently detected using our selective extraction procedure.

The second approach was spiking soil samples with a standard of iHg as 1000 mg Hg L^{-1} before extraction (see Sect. 3.2.2). This was done at three different spike levels to meet ratios of 2:1,1:1,1:2 with respect to the amount of Hg leached by HCl. The experiment was conducted using two paddy soil samples from our sample bank, a contaminated sediment standard material (ERM-CC 580), and a blank without a soil or sediment matrix. In the blank samples, we spiked four different levels in the range of 6.4 to 51 µg. After extraction, the samples were analyzed by HPLC-ICP-MS. The measured MeHg concentrations were compared to MeHg concentrations recovered without addition of iHg spikes. Here the methylation factor ($F_{methylation}$) was calculated as the slope of the linear model between $MeHg_{measured} \sim (Hg_{spiked} + Hg_{ambient})$. This linear model is shown in Eq. 3.3

$$MeHg_{present} = MeHg_{measured} - F_{methylation} * (Hg_{spiked} + Hg_{ambient}) \quad \text{(Eq.3.3)}$$

Calculated values of $Hg_{ambient}$ were used to correct for the artificially produced MeHg (see Sect 3.3.1). This was done by HCl leaching, which directly corresponds to the first step of the organo-Hg extraction procedure. The HCl extracts were measured for total Hg using ICP-MS by a set of standards calibrations. Corrections for both experimental approaches were done using Eq. 3.4.

$$MeHg_{corrected} = MeHg_{measured} - F_{methylation} * Hg_{HCl-leached} \quad \text{(Eq.3.4)}$$

3.2.7 Microbial DNA extraction and hgcA gene amplification

Total genomic DNA was extracted from 0.25 g of fresh soil sieved at 2 mm using the DNeasy® PowerSoil® Kit (QIAGEN, Venlo, NL) and following manufacturer recommended protocol. DNA concentrations were determined using PicoGreen

(Molecular Probes, Eugene, OR, USA). Polymerase chain reaction (PCR) of the hgcA gene was performed using the primers hgcA_262F and hgcA_941R as described in (Liu et al., 2018). The presence or absence of the amplified hgcA gene in the soil samples was visually verified by the absence or presence of a specific band corresponding to the amplification length (315 bp) on the gel.

3.2.8 Statistics

Plotting, data treatment, calculations and statistical analyses (linear regressions and correlation coefficients) were conducted with R Studio (RStudio Team, 2020) using the packages “tidyverse”, “HMisc” and “corrplot”. Mean concentrations and percentual recoveries are given with an uncertainty of one standard deviation for samples extracted in triplicates (mean ± 1*σ). For the linear regressions we give the squared Pearson’s correlation coefficient (r^2) and p values with a cut-off at ($p < 0.05$). Correlation matrices of all assessed parameters, aggregated by site are given in Figures B -.5, B -.6 and B -.7.

3.3 Results and Discussion

3.3.1 Soil properties and distribution of contaminants.

During the field campaign, we sampled soil from three sites in a contaminated agricultural area in the canton of Wallis, Switzerland. The canal site was situated on an agricultural field cultivated with corn for the past three years. The soil at this site was classified as *fluvi gleyic anthrosol* (IUSS Working Group WRB, 2015), and showed a clear ploughing horizon (Ap) at a depth of 30 cm with very few soil aggregates with no meso- or macrofauna spotted during sampling. The Ap horizon is followed by a horizon with gleyic properties between 30 - 50 cm depth featured by red and black redoximorphic features (interpreted as Fe and Mn oxides) and a layered sandy texture that indicates fluviatile influence (Fig. B - 8). Chemical and physical soil parameters are given in Table B - 6. According to public records, Hg contaminated canal sediments heavily affected the pollution of soils at the borders of the discharging canal (Grossgrundkanal) (Glenz and Escher, 2011). At this site, Hg concentrations show both a horizontal gradient perpendicular to the canal as well as a sharp decrease at a depth of 30 cm (ploughing horizon). The horizontal gradient indicates a continuous physical transport of the contaminated material from the

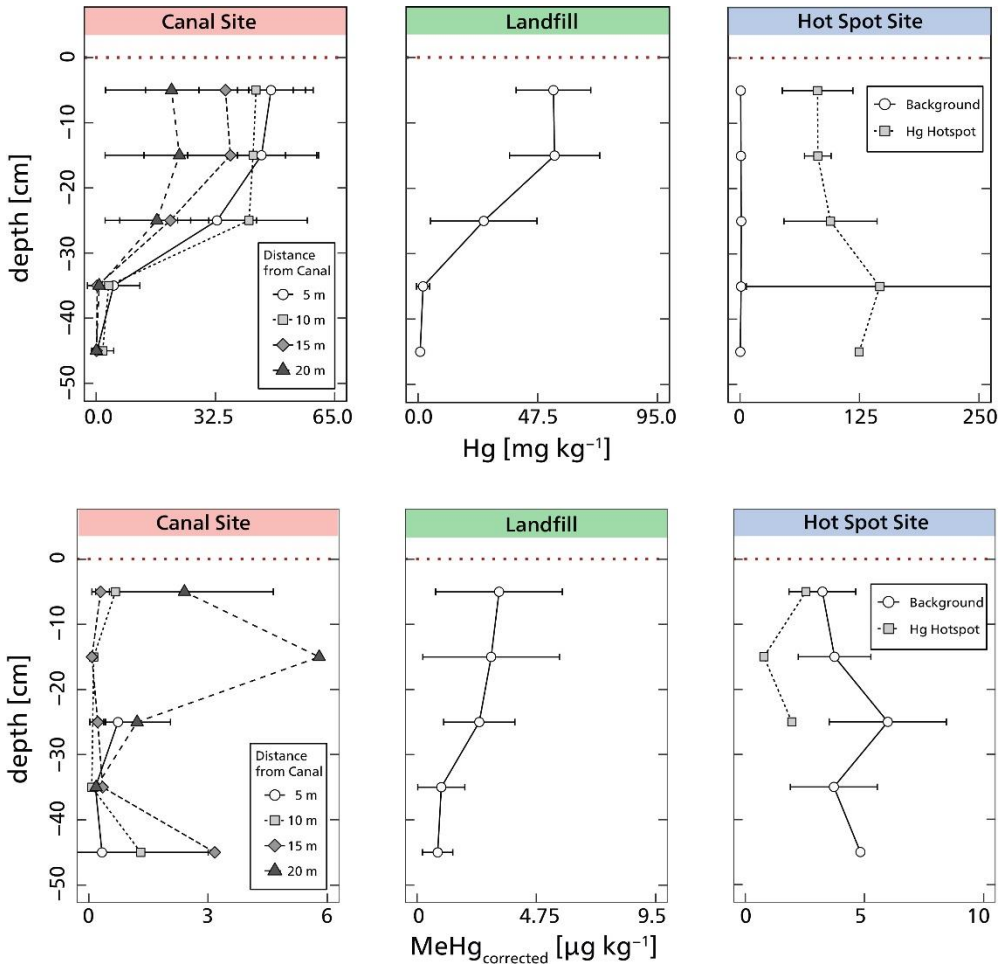

Figure 3 - 1 HgT and corrected MeHg concentrations of the soil profiles at each site. Points represent the mean; error bars represent one standard deviation of soil HgT concentrations. For the canal site the data was aggregated to the distance from the canal bank of the Grossgrundkanal. For the Hot Spot Site data was aggregated according to cores within the Hg hotspot and cores outside of the Hg hotspot.

initially contaminated bank to the agriculturally used field. For the sampled soil, Hg correlates with the clay grain size (R^2 = 0.7, $p < 0.001$), which was described earlier at the same legacy site (Gygax et al., 2019). A sharp vertical decrease in Hg coincides with a change in the grain size distribution between 30 - 40 cm (Fig. 3 - 1). This textural change is clearly visible in the sampled cores and marks the Ap horizon of the agricultural field (Fig. B - 8). These observations suggest that the bulk Hg pool is mainly transported by anthropogenic processes (e.g., ploughing). However, Hg was shown to be mobilized and transported in the aqueous phase (e.g., thought reductive dissolution of Mn oxides associated with Hg) and advective transport (Gfeller et al., 2021; Gilli et al., 2018; Frossard et al., 2018; Gygax, 2015).

0

At the canal site, soil Hg concentrations positively correlate with other chalcophile metals such as Cu (R^2 = 0.54, $p < 0.001$), Zn (R^2 = 0.88, $p < 0.001$) and Pb (R^2 = 0.79, $p < 0.001$) (Fig. 3- 2). Co-occurrence of Hg with higher levels of Zn and Cu has been documented earlier in industrial legacy floodplain soils (Lazareva et al., 2019). This suggests that the canal sediment is a common source of these metals in the contaminated soil, although they get there through different pathways. Among others,

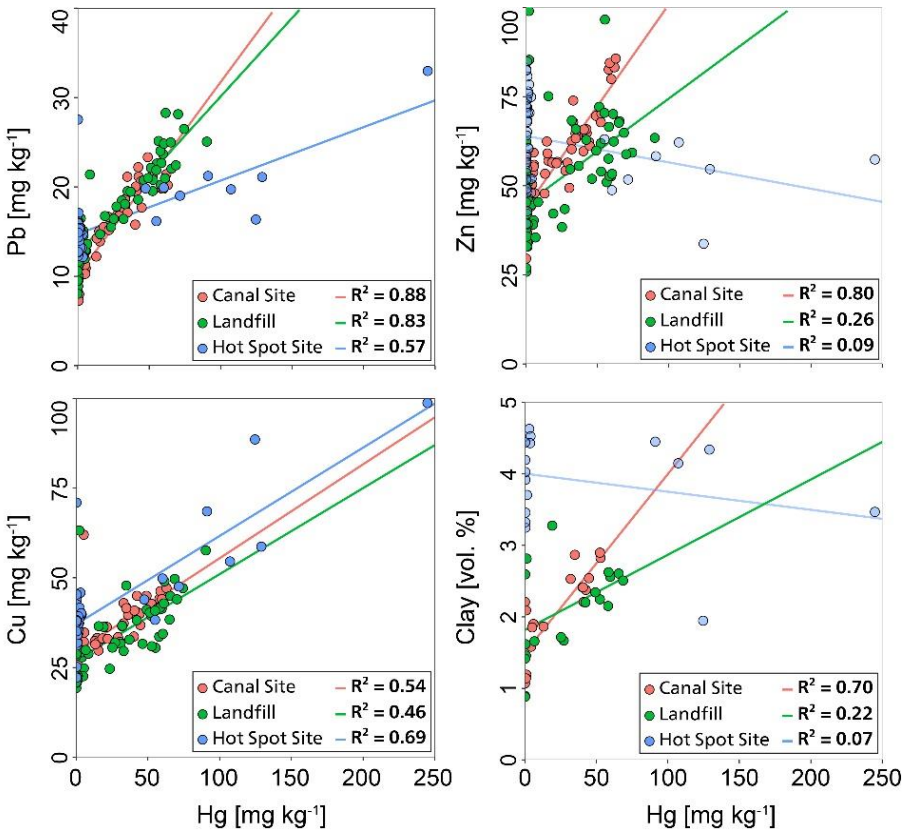

Figure 3 - 2 Scatterplot displaying relationships between soil HgT and Pb, Cu, Zn concentrations and clay percentage for the canal site (red), landfill site (green), and hot spot site (blue). Lines show the fitted linear regression models at each site.

inputs of Zn and Cu in agricultural soils come from the application of organic fertilizers (Imseng et al., 2019; Mantovi et al., 2003) or fungicides. Further, Pb is immobile under high pH conditions and originates from tire abrasion, mining or shooting activities. We suggest that the historically polluted canal sediments (Glenz and Escher, 2011) represent the source of Hg, Zn, Cu and Pb in the soil at this site given the shared special gradient (distance from canal) and the good correlation between them.

More data along the canal site is needed to further evaluate Pb, Cu, and Zn as proxies for Hg levels at this specific site. Earlier studies reported that Hg was mainly present as HgS in the recalcitrant fraction of sequential extractions and less as bound to Mn oxyhydroxides and NOM in contaminated soils of the area (Grigg et al., 2018). Also, Hg bound to Mn oxyhydroxides were reported as relevant pools for remobilization of soil bound Hg to the aqueous phase (Gilli et al., 2018; Gfeller et al., 2021). In summary, we show indications that the bulk Hg pool is mainly present in a fine grain size fraction together with other metals often bound to sulfides (e.g., Cu, Zn and Pb).

The landfill site situated on the agricultural area is around 500 m away from the discharging canal (Fig. B - 1). High Hg levels were already measured earlier at this site (Dienststelle für Umwelt, 2016). However, the source and history of pollution at this site is not completely documented (Glenz and Escher, 2011). The soil was classified as a *toxic Technosol* (IUSS Working Group WRB, 2015) consisting of a single Au horizon (0 – 50 cm) (Fig. B - 1) with a silty sand texture consistent with depth. SOC decreases from 2.1 ± 0.3 % to 0.9 ± 0.8 % and the pH varied between 8.17 and 7.30 without horizontal trends. During the sampling, we did not spot macrofauna. At increasing depth, Hg gradually decreases from approximately 50 mg kg^{-1} to 25 mg kg^{-1} between 0 - 30 cm and to < 5 mg kg^{-1} below 30 cm (Fig. 3 - 1). As for the canal site, Hg concentrations positively correlates with Cu ($R^2 = 0.46$, $p < 0.001$) and Pb ($R^2 = 0.83$, $p < 0.001$), although that correlation was weaker for Zn and Hg ($R^2 = 0.26$, $p < 0.001$) (Fig. 3 - 2).

The hot spot site is situated in the vicinity of a farm on a pasture field. High Hg concentrations (> 20 mg kg^{-1}) were reported earlier at this site (Dienststelle für Umwelt, 2016). The soils parental material was heterogenous within the sampled grid. Due to detected artificial objects and the high Hg concentration the soil at this site was also classified as a *toxic Technosol* (IUSS Working Group WRB, 2015). We observed variations from high amounts of soil skeleton to its complete absence (⌀ > 2 mm, gravel and angular rock pieces). Cores could not be fully retrieved (0 - 30 cm) in profiles with high amounts of gravel. Some profiles showed sharp changes between gravel-rich material and sandy material. Anthropogenic artifacts (e.g., metal shavings) were identified in some cores. The fine soil (⌀ < 2 mm) showed a silty sand texture consistent with depth. All profiles expressed a thin A-horizon (approximately/c.a. 5 cm) indicative for a recent onset of soil development. SOC decreases sharply between 0 - 10 cm (from 4 ± 1 to 3.0 ± 0.7 wt. %) and then gradually without distinct horizontal trends to 1.0 ± 0.6 wt. % at 50 cm depth. Soil pH was in the neutral range (6.51 to 7.87) and showed no spatial gradients. The heterogeneity of the soil skeleton is indicative of glacial fluvial or anthropogenic deposition of the parent material. The placement of the sampling grid did not allow for the full coverage of the previously reported hot spot by a sampling campaign of the local authorities (Dienststelle für Umwelt, 2016). We detected high Hg concentrations (47.5 to 244.8 mg kg^{-1}) in two soil cores at the NE edge of the grid, which represents a Hg hotspot (Fig. 3 - 1). The cores around the hot spot still showed elevated Hg concentrations (0.02 to 3.92 mg kg^{-1}) when compared to the European background of 0.023 mg kg^{-1} (Panagos et al., 2021). Similarly to the other two sites, Hg concentrations positively correlated with Cu ($R^2 = 0.69$, $p < 0.05$) and Pb ($R^2 = 0.57$, $p < 0.05$); but there was no relationship

between Zn and Hg (Fig. 3 - 2). There is an indication for a common source of the contaminated material at all studied sites given by the common linear relationships between relatively immobile trace elements (Cu, Pb, Hg). However, analysis of organic Hg species could help to better understand the history and the source material of these contaminated sites as well as processes involved in the formation of these species in soil. For that we tested and validated an analytical method for the determination of organic Hg species in soil.

3.3.2 Methylmercury extraction method development

Validated high throughput MeHg extraction methods are needed to monitor MeHg and study (de)methylation processes in highly contaminated areas. Here, we optimized the HCl- Cl_2CH_2 extraction procedure by Brombach et al., 2015 to extract 64 samples per day. This method was chosen since it allows for selective extraction of MeHg, which is important in soils where most of the Hg is iHg. Also, the extracts can be directly measured by HPLC-ICP-MS. Further, we tested the method for net artificial MeHg production in blanks and soil matrices. This was especially important in the scope of earlier studies using HCl extractions reporting insufficient quantitative leaching (Horvat et al., 1993), MeHg decomposition above 4 mol L^{-1} HCl (Horvat et al., 1993) or the artificial methylation of iHg (Hintelmann et al., 1997) in sediment and soil matrices. To our knowledge, no such tests have yet been published for this specific soil and sediment extraction procedure. During the test phase, we did not observe MeHg when directly injecting 10 µg L^{-1} iHg into the HPLC-ICP-MS and conclude that no significant amounts of MeHg are produced during the actual analysis. Thus, the extraction procedure accounts for any artificial MeHg formation observed in the following tests.

Experiment A - artificial methylation: Species specific isotope dilution approach

For the isotopic dilution experiment, we analyzed one top-soil sample in triplicate (0 to 10 cm) from each site (canal, landfill and hot spot) as well as the CRM ERM CC-580 in triplicate. During the selective extraction, iHg was highly variable in the analyzed extract since it was mainly partitioning in the HCl (Fig. B -10). Therefore, Hg^{2+} could not be analyzed for target isotopes (^{199}Hg, ^{201}Hg, ^{202}Hg).and demethylation of MeHg ($F_{demethylation}$) was not quantified by DSIDA equations due to the low

Table 3 - 2 Experimentally determined methylation factors from species specific double spike isotope dilution (Experiment A) and corrected concentrations for isotope dilution analyses.

Sample	Experiment	Quantification Method	Hg_{HNO3} (µg/g)	Hg_{HCl} (µg/g)	$MeHg_{analyzed}$ (ng/g)	$MeHg_{corrected}$ (ng/g)	MeHg formation			
							$F_{methylation}$ (%)	MeHg (ng/g)	formed (%)	Resulting error
ERM CC580	Acid leaching	Set of Standards		78.1 ± 2.9						
	Isotope dilution	IDA			99 ± 1	73±2	0.033 ± 0.001	26 ± 1.2	35	
	Extraction	Set of Standards			68 ± 2					
	Certified Value		132±3		75 ± 4					
Canal Site (one sample)	Acid leaching	Set of Standards	41 ± 2	32 ± 2						
	Isotope dilution	IDA			2.75 ± 0.07	1.20 ± 0.02	0.0048 ± 0.0003	1.56 ± 0.08	130	
	Extraction	Set of Standards			1.9 ± 0.1					
Landfill Site (one sample)	Acid leaching	Set of Standards	60 ± 3	53 ± 1						
	Isotope dilution	IDA			16.9 ± 0.4	13.1 ± 0.5	0.0072 ± 0.0006	3.8 ± 0.3	29	
	Extraction	Set of Standards			11.2 ± 0.5					
Hot Spot Site (one sample)	Acid leaching	Set of Standards	0.72 ± 0.04	0.72 ± 0.03						
	Isotope dilution	IDA			2.9 ± 0.1	2.7 ± 0.1	0.03 ± 0.02	0.23 ± 0.17	9	
	Extraction	Set of Standards			2.2 ± 0.1	2.2 ± 0.1				

iHg signals. However, Monperrus et al., 2008 reported issues with the quantification of $F_{demethylation}$ due to the overestimation of the demethylation of ^{199}MeHg to ^{199}iHg in the presence of high natural iHg levels during the acid-leaching derivatization procedure. Therefore, MeHg concentrations were calculated with the classical isotope dilution equation (IDA) (Eq.1). Independently, methylation factors ($F_{methylation}$) were calculated according to Eq. 2. Then, separately analyzed iHg concentrations were used to calculate the corrected MeHg concentrations according to Eq. 4. The resulting concentrations, methylation factors ($F_{methylation}$), and corrections are displayed in Table 2. As a comparison, the MeHg concentrations measured with a classical set of standards methods are displayed. Generally, the MeHg concentrations from isotopic dilution analyses (IDA) were higher when compared to the set of standard method or certified values. This shows that MeHg is overestimated during IDA experiment as previously reported (Monperrus et al., 2008). Methylation factors ($F_{methylation}$) ranged between 0.0072 - 0.033%, were sample specific, and were similar to other published $F_{methylation}$ using acid-leaching organic solvent extraction procedures (Hintelmann et al., 1997). However, these corrections only account for the methylation of iHg and do not cover the net MeHg production including the potential demethylation. The results of MeHg concentrations from DSIDA were generally higher than the results from the set of standards calibrations (Table 2) but were in the same range after correction according to Eq.4.

Experiment B - artificial methylation: Spiking of iHg^{2+}.

In experiment B, blanks, two soil samples from our inhouse sample bank and the CRM ERM CC-580 were spiked with iHg. We observed linear relationships between the amount of iHg in HCl and that of MeHg present after extraction (Fig. 3 - 3), where the slope for each linear model (Eq.3) represents the factor of MeHg produced from iHg. Table 3 shows the methylation factors and regression coefficients for the linear regressions of all experimental runs. Methylation factors are consistent within the

tested natural soil and sediment matrices (0.0075%) and are within the same order of magnitude as that using 5 mol L^{-1} HCl and toluene as extraction solvent (0.005%) from Hintelmann et al., 1997. This contrasts with the results from IDA where $F_{methylation}$ was sample-specific. However, Hg^{2+} spiking allowed for an evaluation of net MeHg production for Hg^{2+} in the extract. The $F_{methylation}$ of the Hg^{2+} spiking experiments represents net MeHg production during sample extraction. The data further suggests that $F_{methylation}$ is sample-independent.

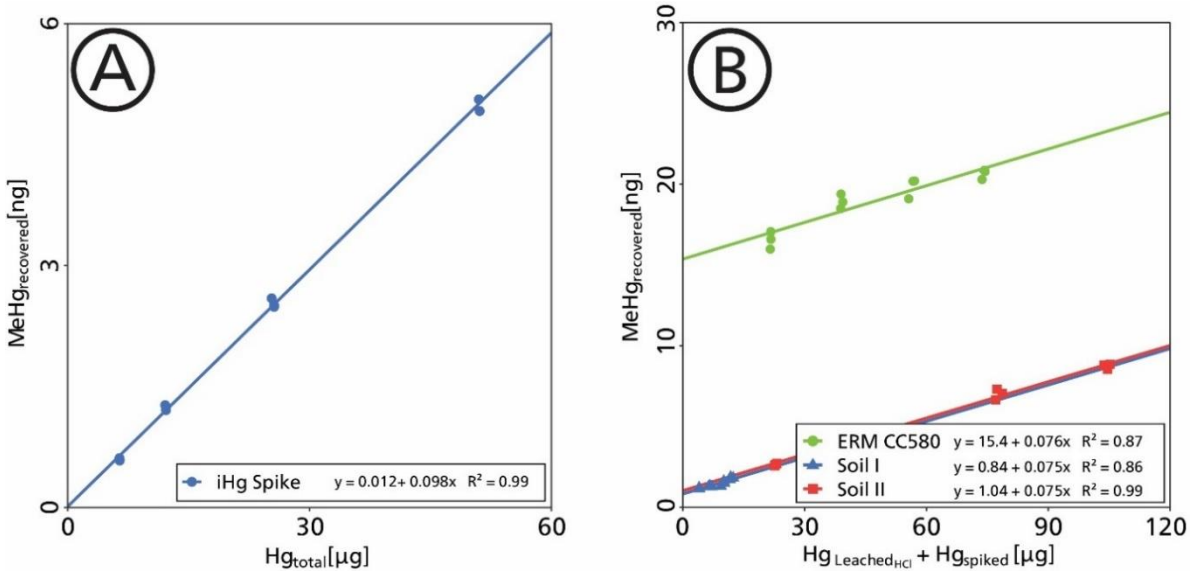

Figure 3 - 3 Amount of MeHg [ng] recovered from HCl/CH_2Cl_2 extraction as a function of A) spiked iHg [µg] to a blank sample B) spiked iHg and HCl leached Hg [µg] of 250 mg sample material. Functions displayed show linear regressions of the specific runs. Experimental replicates (n=3) are displayed as individual points.

Table 3 - 3 Experimentally determined methylation factors (Fmethylation) calculated from spiking of iHg (Experiment B)

Sample Type	Name	Hg µg g^{-1}	$Hg_{leached(HCl)}$ µg g^{-1}	MeHg ng g^{-1}	$F_{methylation}$ %	Artificial MeHg ng g^{-1}	Resulting error %
iHg spike	-	10	10	-	0.00980	9.8	100
Sediment	ERM-CC580	132 ± 3*	86 ± 2	75 ± 4	0.00756	6.5	9
Soil	Soil I	21 ± 1	15.8 ± 0.2	4.99 ± 0.09	0.00749	1.2	24
Soil	Soil II	193 ± 2	91 ±3	11.4 ± 0.2	0.00748	7	60

The highest factors of MeHg produced from iHg were observed in the experiments where blanks were only spiked with iHg^{2+} (Table B - 7; Fig. 3 - 3). This suggests that CH_2Cl_2 acts as the source of C for iHg methylation during the extraction procedure. Based on earlier studies, we assumed that an iHg spike behaves similar to ambient Hg during acid extraction (Liang et al., 2004). Our results are in disagreement with Hintelmann et al., 1997 who observed methylation only during the HCl leaching step, but none during the extraction step with the organic solvent (toluene). They concluded that mainly soil and sediment constituents were responsible for the artificial formation of MeHg. Here, we show evidence that the abiotic methylation of iHg took place with CH_2Cl_2 as the C source. In the future, this information should be considered during the development of MeHg

* Certified concentrations taken from the certificate of the respective CRM.

extraction procedures. The presence of MeHg in the added iHg standard can be ruled out as this high purity standard is backtraced to a metallic Hg standard by the producer and kept in 12% HNO_3. Further, the lower $F_{methylation}$ for soil matrices suggests that the constituents of sediments and soils may passivate iHg^{2+} (e.g., by complexing) and make it less prone to artificial methylation during the HCl-CH_2Cl_2 extraction.

In any case, soil samples from contaminated sites are often reported to have MeHg/Hg ratios << 0.01%. It cannot be emphasized enough that even a small percentage of artificial methylation (< 0.01%) may result in false positives that account for > 60% of the MeHg concentration in a sample (Table 3 - 3). Thus, reports of uncommonly high MeHg concentrations in polluted areas should always be interpreted with caution if MeHg was extracted by acid-leaching and organic solvents (Gray et al., 2004; Kodamatani et al., 2022). Our results call for the correction of artificially formed MeHg in samples with elevated Hg concentrations by using Eq.4. The requirements for this approximation include an analysis of 1) concentrations of extracted MeHg, 2) Hg leached by HCl (1st step of the extraction procedure) and 3) calculating $F_{methlyation}$ for a specific extraction procedure. Although the correction is straight forward, the correction factors still must be interpreted with caution since the exact reactions or mechanisms of the artificial methylation are still unclear.

For the CRM ERM CC-580 the correction resulted in a concentration of 62 ± 2 µg kg^{-1} (n = 39) representing a recovery of 82 ± 3% compared to the certified concentration. The uncorrected recovery was 91 ± 3% and does not reflect the actual performance of the applied method. This CRM is one of few materials certified for MeHg (Leermakers et al., 2003). Its properties differ in many aspects (e.g. organic matter or carbonate content) from our target sample matrix. The use of a dissimilar CRM may be deceptive when assessing the effectiveness of an extraction procedure since artificial MeHg formation might 1) result as a misinterpretation of the performance and 2) be sample-specific and not comparable to the study's target sample matrices. MeHg artifact formation was often reported to depend on substrate properties (e.g., organic matter, pH or Hg speciation) (Bloom et al., 1997; Hammerschmidt and Fitzgerald, 2001; Falter, 1999b; Hintelmann et al., 1997). It is therefore crucial to increase the availability of new soil CRMs with high Hg and certified MeHg concentrations to help in the development of suitable methods for MeHg determination in soils. Producers of these materials emphasize the diversity of substrate properties (pH, organic matter or Hg speciation etc.).

3.3.3 Distribution of organic Hg species in the sites.

For the sampled soils of the field campaign, uncorrected MeHg concentrations significantly correlate to HgT in both canal (R^2 = 0.5, $p < 0.05$) and landfill (R^2 = 0.66, $p < 0.05$) sites (Fig. B - 9). This indicates that the MeHg analyses were affected by MeHg artifact formation since, in contaminated soils (> 2 mg kg^{-1} Hg), MeHg/Hg ratios were generally < 0.1%. Thus, we applied the mean $F_{methylation}$ of ERM CC-580, Soil 1, and Soil 2 (0.0075%) and Eq. 4 to correct the MeHg concentrations in the field study. The site-specific HCl-leachable percentage was measured by ICP-MS on a selection of samples per site (Fig. B -

10). For each sampling site, the specific HCl-leachable percentages were multiplied by the HgT concentration to obtain an estimate of HCl-leachable Hg. The corrections resulted in 27 out of 163 samples with negative MeHg concentrations indicating an overestimation of HCl leachable Hg or the $F_{methylation}$. For the rest of the manuscript, they are treated as samples < LoD (0.16 µg kg^{-1}).

The $MeHg_{corrected}$ values in the different soil profiles are displayed in Fig. 3 - 1. At the canal site, MeHg had no distinct spatial

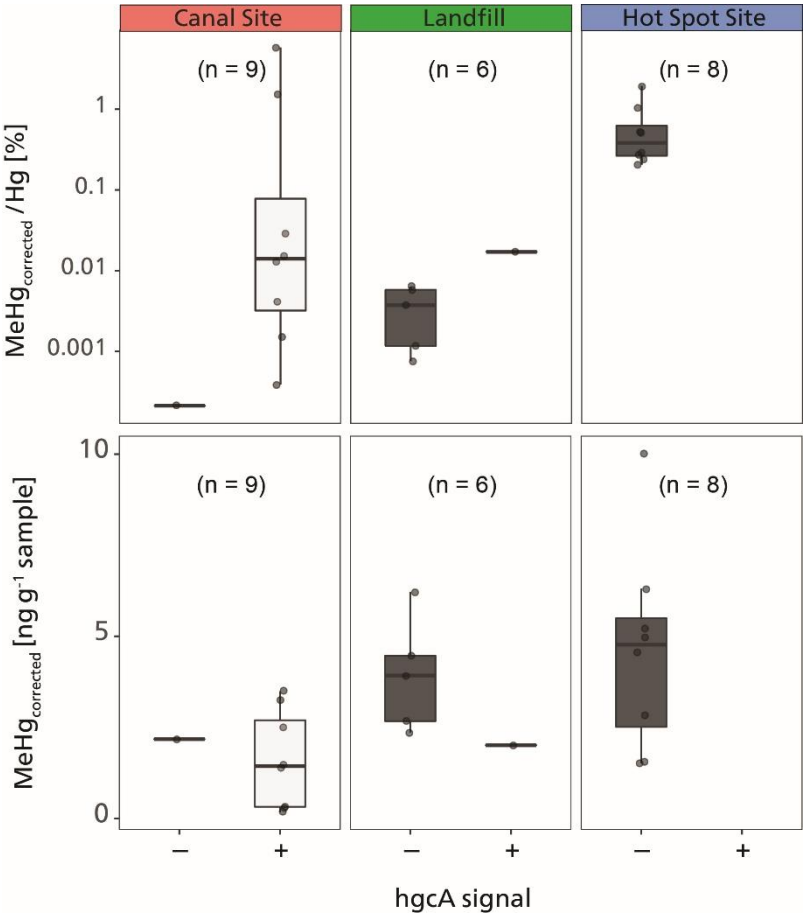

Figure 3 - 4 Boxplots displaying concentration and MeHg/Hg ratios for the samples analyzed for hgcA at each sampling sites. Data is aggregated by hgcA positive resp. negative signals.

trend. The highest concentrations (5.8 µg kg^{-1}) were detected at a 20 m distance from the canal (Fig. 3 - 1). No EtHg was detected at this site. The mean $MeHg_{corrected}$ values continuously decrease with soil depth with no horizontal trends at the landfill site. At the hotspot site, $MeHg_{corrected}$ concentrations range from 0.8 to 9.8 µg kg^{-1}. High $MeHg_{corrected}$ concentrations do not necessarily correlate to high Hg concentrations.

The uncorrected MeHg concentration is the only parameter showing a positive correlation (R^2>0.75, p<0.05) to the $MeHg_{corrected}$ concentrations (Fig. B - 9). This suggests that neither textural nor chemical soil properties were governing MeHg concentrations in the sampled soils. Different factors may be more important including changing redox conditions (Gfeller et al., 2021), the presence of Hg methylating or demethylating microorganisms (carrying *hgcAB complex* or *merA/B* genes, respectively), or an external source of MeHg.

The presence of the *hgcA* gene was detected after PCR amplification in 8 out of 9 samples of the regularly flooded canal site (Fig. 3 - 4). The elevated rate of *hgcA* gene presence in addition to the observed regular redox oscillations (Gfeller et al., 2021) indicates that soils at the canal site have a high potential for Hg biomethylation (Fig. 3 - 4). We suggest that MeHg is mainly produced *in situ* at this site, which is in line with our previous work (Gygax et al., 2019 and Gfeller et al., 2021) where we demonstrated a positive net methylation potential of these soils in microcosm experiments. However, the abundance of the *hgcA* gene does not imply higher MeHg concentrations (Liu et al., 2018; Christensen et al., 2019). This is not surprising since Hg biomethylation is a dynamic process governed by 1) the soil chemistry, 2) the activity and expression of the two-gene cluster (*hgcAB*) and 3) site-specific redox dynamics. Landfill and hot spot sites only showed positive signals for *hgcA* in 1 out of a total of 14 samples (Fig. 3 - 4). We hypothesize that the absence of *hgcA* is an indication of low to no biomethylation processes in the soil, which, combined with elevated MeHg levels, suggests an anthropogenic source of MeHg.

EtHg was detected in 11 samples at the landfill site and 5 samples at the hotspot site but was not detected at the canal site. At the hotspot site, EtHg was only detected in the core with the highest Hg concentrations (91 to 245 mg kg^{-1}). No spatial pattern was found in the landfill site. In the samples where EtHg was detected, the concentrations were between 0.14 to 0.47 µg kg^{-1}. EtHg concentrations should be interpreted as minima since EtHg degrades relatively fast under our extraction conditions (Han et al., 2003; Hight and Cheng, 2006). EtHg concentrations were 2-fold lower than the EtHg concentrations measured in a smelter site in Slovenia (Tomiyasu et al., 2017), but were within the range of EtHg measured in a remote area in the Everglades in Florida (Mao et al., 2010). To our knowledge, no systematic studies showed that EtHg is formed quantitively in the environment and EtHg formation pathway(s) remain unstudied in soils or sediments. It appears more likely that EtHg in soils comes from an anthropogenic source when detected close to industrial legacy sites. Elevated levels of EtHg at chlor-alkali and acetaldehyde producing legacy sites have been attributed to side products of the chemical industry (Tomiyasu et al., 2017; Hintelmann et al., 1995).

The pollution history in our study area remains complex since contaminated soils and sediments were reportedly transported and redistributed (e.g., as fill material) and no exhaustive documentation exists on these events (Glenz and Escher, 2011; Mudry, 2016). We suggest that organic Hg species in both hotspot and landfill sites were directly emitted from the chemical plant, and not produced post-deposition. The line of evidence consists of 1) the detection of EtHg, 2) the elevated MeHg concentrations (up to 4.84 µg kg^{-1}), and 3) the absence of the *hgcA* gene. We suggest that the directly deposited MeHg is as well demethylated through time. This hypothesis is supported by Osterwalder et al., 2019, who found that the abundance of the *mer*-operon in soil DNA linearly increased with Hg concentrations in our study area and the missing correlation between MeHg and Hg at our study sites. At the canal site, Hg contamination is well documented and mainly originates from the canal sediments deposited on the canal's bank (Glenz and Escher, 2011). There, soil MeHg may not be fully attributed to either

anthropogenic emissions or biological activity. These soils are subjected to regular redox oscillations, show net methylation potential (Gfeller et al., 2021; Gygax et al., 2019) and present *hgcA* genes.

3.4. Conclusions

We sampled soil from three sites in a contaminated agricultural floodplain in the canton of Valais, Switzerland. The soils in all three sites showed high concentrations of Hg correlating with those of Cu and Pb, indicating a common contamination source. The pollution history was only well documented for one site (canal), while missing for the other two (landfill and hotspot). We used and improved organic Hg speciation method to further understand the local pollution at these sites.

Our results agree with earlier studies reporting artificial MeHg formation during MeHg extraction with HCl-Cl_2CH_2 and we observed consistent methylation rates ($F_{methylation}$ = (0.0075 ± 0.0001%) throughout different sample types. These rates were consistent with previously published acid-leaching solvent extraction procedures. Although small, the the fractions of artificial methylation were demonstrated to be relevant for Hg polluted soil or sediment samples with low MeHg/Hg ratios resulting in false positives of > 60% of the analyte concentration (Table 3 - 3). We are not aware of neither an artifact-free extraction method nor suitable soil CRM to overcome these limitations in the study of MeHg dynamics in highly Hg polluted soils. Therefore, it is of utmost importance for the scientific community to develop suitable extraction methods and reference materials.

We used the determined methylation factor to correct for false positives in the above-mentioned field campaign. The detection of MeHg and EtHg, as well as the absence of the *hgcA* genes, served as evidence to conclude that these organic Hg species were directly emitted by the chemical plant. Although, these circumstances are rather coincidental since the change in environmental conditions (e.g., flooding of soils) might ultimately result in a change of microbial communities and consequently blur the grounds for our conclusions. Organic Hg speciation and methylation gene (*hgcA*) abundance analyses are strongly complementing classic methods (e.g., literature research and interviews with stakeholders) when assessing the pollution history of a legacy site.

4. Mercury mobility, colloid formation, and methylation in a polluted fluvisol as affected by manure application and flooding-draining cycle.

This chapter was published as Gfeller, Lorenz; Weber, Andrea; Worms, Isabelle; Slaveykova, Vera I.; Mestrot, Adrien (2021):

Mercury mobility, colloid formation and methylation in a polluted Fluvisol as affected by manure application and flooding–draining cycle. In *Biogeosciences* 18 (11), pp. 3445–3465.

DOI: 10.5194/bg-18-3445-2021.

Author contributions:

Lorenz Gfeller: conceptualization, sampling, laboratory, visualizations, writing original draft, reviewing, and editing.

Andrea Weber: sampling, laboratory.

Isabelle Worms: laboratory, AF4 expertise, reviewing of the manuscript.

Vera I. Slaveykova: reviewing of the manuscript.

Adrien Mestrot: Supervision, conceptualization, reviewing and editing of the manuscript.

Abstract

Floodplain soils polluted with high levels of mercury (Hg) are potential point sources to downstream ecosystems. Repeated flooding (e.g. redox cycling) and agricultural activities (e.g. organic matter addition) may influence the fate and speciation of Hg in these soil systems. The formation and aggregation of colloids and particles influences both Hg mobility and its bioavailability to methylmercury (MeHg) forming microbes. In this study, we conducted a microcosm flooding-draining experiment on Hg polluted floodplain soils originating from an agriculturally used area situated in the Rhone Valley (Valais, Switzerland). The experiment comprised two 14 days flooding periods separated by one 14 days draining period. The effect of freshly added natural organic matter on Hg dynamics was assessed by adding liquid cow manure (+MNR) to two soils characterized by different Hg (47.3 ± 0.5 mg kg^{-1} or 2.38 ± 0.01 mg kg^{-1}) and organic carbon (OC: 1.92 wt. % or 3.45 wt. %) contents. During the experiment, the release, colloid formation of Hg in soil solution and the net MeHg production in the soil were monitored. Upon manure addition in the highly polluted soil (lower OC), an accelerated release of Hg to the soil solution could be linked to a fast reductive dissolution of Mn oxides. The manure treatments showed a fast sequestration of Hg and a higher percentage of particulate (0.02 – 10 µm) bound Hg. As well, analyses of soil solutions by asymmetrical flow field-flow fractionation coupled with inductively coupled plasma mass spectrometry (AF4–ICP–MS) revealed a relative increase of colloidal Hg bound to dissolved organic matter (Hg-DOM) and inorganic colloidal Hg (70 - 100 %) upon manure addition. Our experiment shows a net MeHg production the first flooding and draining period and a subsequent decrease in absolute MeHg concentrations after the second flooding period. Manure addition did not change net MeHg production significantly in the incubated soils. The results of this study suggest that manure addition may promote Hg sequestration by Hg complexation on large organic matter components and the formation and aggregation of inorganic $HgS_{(s)}$ colloids in Hg polluted fluvisols with low levels of natural organic matter.

4.1 Introduction

Mercury (Hg) is a pollutant of global concern due to its high toxicity and to its global biogeochemical cycle which spans all environmental compartments (atmosphere, oceans, soils etc.) (UNEP and AMAP, 2019; Beckers and Rinklebe, 2017). Sediments and soils are major Hg pools with relatively long residence times (Amos et al., 2013; Driscoll et al., 2013). Legacy Hg from industrial sites (e.g. chlor-alkali plants or mining areas) retained in soils are a key source for present day atmospheric Hg (Amos et al., 2013). However, this retained Hg pool can also be remobilized by landscape alteration, land use (e.g. fertilization, manure addition) or climate induced changes such as drought-flood-drought cycles of soils (Singer et al., 2016). These inputs are a threat to downstream ecosystems and human health due to release of inorganic Hg and the formation and bioaccumulation of toxic monomethylmercury (MeHg) in both aquatic and terrestrial food chains (Bigham et al., 2017).

Mercury is redox sensitive and occurs mainly as elemental Hg^0, inorganic Hg^{2+} or in the form of MeHg in soils. In general, Hg speciation in soils depends on the biogeochemical conditions. For example, in natural organic matter (NOM) rich boreal peatlands and forest soils, Hg is primarily bound to thiol-groups of NOM (NOM–Hg), associated with $FeS_{(s)}$ or found as cinnabar ($HgS_{(s)}$) or meta-cinnabar (ß-$HgS_{(s)}$).These species are the thermodynamically most favored forms of Hg in these environments (Skyllberg et al., 2006; Skyllberg and Drott, 2010; Biester et al., 2002a). However, Hg sorbed on the surfaces of manganese (Mn), iron (Fe) and aluminum (Al) oxy-hydroxides may also represent important Hg-pools in soils with low amounts of NOM (Guedron et al., 2009).

The fate of Hg in soils is still not well characterized, and its mobilization and sequestration in soil depends on a variety of factors and mechanisms. The release of Hg to the soil solution and its further transport has been associated with the mobilization of NOM (Kronberg et al., 2016; Eklöf et al., 2018; Åkerblom et al., 2008), copper (Cu) nanoparticles (Hofacker et al., 2013) or the reductive dissolution of Fe/Mn-oxyhydroxides (Frohne et al., 2012; Gygax et al., 2019; Poulin et al., 2016). Earlier studies reported a relatively rapid decrease of dissolved Hg after its release upon flooding in various riparian settings (Hofacker et al., 2013; Poulin et al., 2016; Gygax et al., 2019). Possible pathways for this decrease are Hg^{2+} reduction to Hg^0, sorption to recalcitrant NOM, formation of meta-cinnabar ß-$HgS_{(s)}$ or co-precipitation of Hg in sulfides (e.g. $FeS_{(s)}$) or metallic particles.

Metallic colloids in soil may be formed by biomineralization during soil reduction or precipitation in the root zone and potentially incorporate toxic trace elements like Hg (Weber et al., 2009; Manceau et al., 2008). These colloids may increase the mobility and persistence of toxic trace metals in soil solution if they do not aggregate to bigger particles. During a flooding incubation experiment, Hofacker et al. (2013) observed the incorporation of Hg in Cu nano-particles, which were shown to be formed by fermetive bacteria species (Hofacker et al., 2015). Colloidal ß-$HgS_{(s)}$ has been reported to form abiotically in soils under oxic conditions directly by interaction with thiol-groups of NOM (Manceau et al., 2015). In solution, Dissolved Organic Matter (DOM) has a major influence in the formation and aggregation of metallic colloids and particles. It may promote the

dissolution of $HgS_{(s)}$ phases, decelerate the aggregation and growth of $HgS_{(s)}$ colloids as well as affect the crystallinity of $HgS_{(s)}$ phases (Miller et al., 2007; Ravichandran et al., 1998; Gerbig et al., 2011; Poulin et al., 2017; Pham et al., 2014). Same effects were also observed for other metal sulfide-, oxide- or carbonate colloids (Aiken et al., 2011; Deonarine et al., 2011). In case of Hg, inhibition of ß-$HgS_{(s)}$ formation may in turn increase its mobility and bioavailability to MeHg producing microorganisms (Deonarine and Hsu-Kim, 2009; Ravichandran et al., 1999; Aiken et al., 2011; Graham et al., 2012). Chelation of Hg with higher molecular weight NOM may as well inhibit the microbial availability of Hg (Bravo et al., 2017). Within Hg–NOM, hydrophobic, thiol rich NOM with higher molecular weight contain a higher density of strong sorption sites (thiol groups) (Haitzer et al., 2002). However, different ligand exchange reactions (e.g. carboxyl-groups to thiol groups) kinetically control this sorption and thus the bioavailability of dissolved Hg in aqueous systems (Miller et al., 2007; Miller et al., 2009; Liang et al., 2019). The partly contradicting statements above illustrate the complex role of NOM and DOM on the Hg cycle and Hg bioavailability and the need for more research in this field.

The formation of MeHg from inorganic Hg^{2+} has been shown to be primarily microbially driven. Environments of redox oscillation (e.g. floodplains, estuaries) represent hot spots for Hg methylation (Marvin-DiPasquale et al., 2014; Bigham et al., 2017). Mercury methylators are usually anaerobe microbial species such as sulfate reducers (SRB), Fe reducers (FeRB), archaea and some firmicutes (Gilmour et al., 2013). Generally, Hg is bioavailable to methylators in the form of dissolved Hg^{2+}, Hg complexed by labile DOM, Hg bearing inorganic nanoparticles (e.g. $FeS_{(s)}$, $HgS_{(s)}$) but is less available when complexed by particulate organic matter (Hg–POM) or larger inorganic particles (Chiasson-Gould et al., 2014; Graham et al., 2013; Rivera et al., 2019; Zhang et al., 2012; Jonsson et al., 2012). Further, DOM is a main driver of Hg methylation as it influences both bioavailability and microbial activity. The role of DOM as electron donor may enhance the microbial activity and thus the cellular uptake. The composition and origin of DOM were reported to change Hg methylation rates (Bravo et al., 2017; Drott et al., 2007). For example, (Bravo et al., 2017) showed that in lake sediments, terrestrial derived DOM led to slower methylation rates than phytoplankton derived DOM. The addition of DOM in form of organic amendments (e.g. manure, rice straw, biochar) has been reported to have both an enhancing (Gygax et al., 2019; Liu et al., 2016; Wang et al., 2019; Eckley et al., 2021; Wang et al., 2020) or no effect (Zhu et al., 2016; Liu et al., 2016) on the net MeHg production in soils. Further, organic amendments were reported to shift microbial communities. Both the enhancement of Hg demethylators, Hg reducers (Hu et al., 2019) as well as the enhancement Hg methylators upon organic amendments were reported (Tang et al., 2019; Wang et al., 2020). Environments of elevated Hg methylation (riparian zone, estuary) are also places of elevated NOM degradation and mineralization due to temporal changes in redox conditions. The degradation of large NOM to more bioavailable low molecular weight (LMW) compounds promoted by microbial Mn oxidation, especially in systems with neutral pH (Jones et al., 2018; Ma et al., 2020; Sunda and Kieber, 1994), is also hypothesized to increase bioavailability of Hg–NOM. However,

amendments of Mn oxides were also shown to inhibit Fe, SO_4^{2-} reducing conditions and thus MeHg formation in sediments (Vlassopoulos et al., 2018).

Hg methylation and mobilization is intensively studied in paddy field soils and peat soils due to their relevance in food production or the Hg global cycle (Wang et al., 2019; Tang et al., 2018; Liu et al., 2016; Hu et al., 2019; Wang et al., 2016b; Zhao et al., 2018; Zhu et al., 2016; Kronberg et al., 2016; Skyllberg, 2008; Skyllberg et al., 2006). However, only few studies focused on Hg methylation and mobility in temperate floodplain soils (Frohne et al., 2012; Hofacker et al., 2013; Gilli et al., 2018; Poulin et al., 2016; Lazareva et al., 2019; Wang et al., 2020; Beckers et al., 2019). As well, few studies have examined the effect of flooding and/or land use (NOM addition in the form of animal manure) in polluted soils with respect to Hg release and methylation potential (Tang et al., 2018; Gygax et al., 2019; Zhang et al., 2018; Hofacker et al., 2013; Frohne et al., 2012). Furthermore, most of these studies were focusing on soils with rather high OC levels (5 – 10 wt. %) and only few researchers have addressed the decrease of Hg in soil solution of flooded soils over time, including the fate of colloidal Hg.

This work focused on the effect of the agricultural practices on the Hg mobility and methylation in a real-world contaminated fluvisol with specific emphasis on the flooding-draining cycle and manure addition. By conducting microcosm experiments, we studied the effect of these cycles and manure addition on 1.) the release and sequestration of Hg, 2.) the methylation of Hg and 3.) the evolution of colloidal and particulate Hg in soil solution. The latter was studied by analyzing different soil solution filter fractions (0.02 and 10 µm) as well as analyzing selected samples by asymmetric flow field flow fractionation coupled to a UV_{vis} detector, a fluorescence detector and an ICP–MS (AF4–ICP–MS). Based on the presented state of knowledge, we hypothesize that the manure addition would accelerate the release of Hg by accelerated reductive dissolution of Mn-oxyhydroxides in these soils and eventually change Hg speciation in the system towards Hg-NOM complexes and ß-$HgS_{(s)}$ colloids.

4.2. Methods and Materials

4.2.1 Sample collection

We sampled soil from agriculturally used fields in the alpine Rhone Valley in Wallis, Switzerland on September 30th, 2019. The fields are situated in a former floodplain next to the artificial “Grossgrundkanal” canal. This canal was built in the 1900s to drain the floodplain and as a buffer for the wastewater releases of a chemical plant upstream historically using Hg in different processes (chlor-alkali electrolysis, acetaldehyde- and vinyl chloride production). The soils on the floodplain were subjected to Hg pollution from this plant between the 1930s and the 1970s, mostly through the removal and dispersion of the canal sediments onto the agricultural fields (Glenz and Escher, 2011). After heavy rain events, the fields are subjected to draining-flooding cycles (Fig. C - 1) and have been identified as potential hotspots for Hg methylation and release (Gygax et al., 2019). For this study, soil was sampled from a cornfield and a pasture field next to the canal. A map and the coordinates of the

sampling locations is provided in the supplement (Fig. C - 1, Table C - 1). At each site, a composite sample of approx. 10 kg of soil was sampled between 0 – 20 cm depth from ten points on the fields. The soil samples were named after their relative pollution and organic carbon levels (High Mercury, Low Carbon (HMLC) and Low Mercury, High Carbon (LMHC), see Part 4.3 below for details on the soils. After sampling, roots were removed, and the fresh soil was sieved to < 2 mm grain size, further homogenized, split in two parts and stored on ice in airtight PE Bags for transport to the laboratory. Additionally, approx. 2 L of liquid cow manure was sampled from a close-by cattle farm. One aliquot of the samples was stored at - 20° C until further processing. The remaining part was used for the incubation experiment within 12 h after sampling. A detailed description of the site and sampling procedures is given in the supplement (Sect. C.1.).

4.2.2 Microcosm experiments

An initial incubation was conducted in 10 L HDPE containers in the dark for seven days in an atmosphere of 22 °C and 60 % relative humidity (RH) in order to equilibrate the soils and to prevent a peak of microbial respiration induced by the soil sieving before the onset of the experiment (Fig. 4 - 1). After the initial incubation period soils were used in the flooding and draining experiments, which were conducted in 1 L borosilicate glass aspirator bottles (Fig. C - 2). The environment created through soil flooding in these bottles will be called microcosm (MC) in the following text. Microcosm experiments were performed in experimental triplicate and named after the relative Hg- and organic carbon levels of the used soil (HMLC and LMHC) and the treatment with or without manure addition (added +MNR). The microcosms were equipped with an acid washed suction cup with a pore size of < 10 µm (model: 4313.7/ETH, ecoTech Umwelt-Meßsysteme GmbH, Bonn, Germany). In the following sequence, 700 g of artificial rainwater (NH_4NO_3 11.6 mg L^{-1}/ K_2SO_4 7.85 mg L^{-1}/ Na_2SO_4 1.11 mg L^{-1}/ $MgSO_4 \cdot 7H_2O$ 1.31 mg L^{-1}/ $CaCl_2$ 4.32 mg L^{-1}) was added to the microcosms. For the manure treatment, 0.6 % (w/w) (3 g) of liquid cow manure was added to the microcosms corresponding to one application of liquid manure on a cornfield following the principles of fertilization of agricultural crops in Switzerland (Richner and Sinaj, 2017) and finally fresh soil was added with a $soil_{dry}$:water ratio of 1:1.4 (w/w). Then, the microcosms were gently shaken for at least one minute to remove any remaining air bubbles in the soil and pore space. An additional mixture of fresh soil artificial rainwater (1:1.4 (w/w)) was shaken for 6 h to assess the equilibration of the solid and liquid phase during the experiment. The microcosms were covered with Parafilm®, transferred to the incubation chamber (APT.line™ KBWF, Binder, Tuttlingen, Germany) and incubated in the dark for 14 days in atmosphere of 22 °C and 60 % RH. The incubation temperature was chosen to be close to the daily mean soil temperature in 10 cm depth during summer months between 2015–2019 (21.4 °C) at the closest soil temperature monitoring station (Sion, VS, provided by MeteoSwiss) situated downstream. After the first flooding period, the supernatant water was pipetted off, and remaining water was sampled through the suction cups to drain the microcosms. They were weighted before and after water removal. Then, approximately 25 g of moist soil was sampled by two to three scoops though the whole soils column using a

disposable lab spoon. The microcosms were kept drained in an atmosphere of 22 °C and 10 % RH for 14 days. For the second flooding period, the microcosms were again flooded with 500 g of artificial rainwater and incubated for another 14 days in an atmosphere of 22 °C and 60 % RH (Fig. 4 - 1). After the incubation, the suction cups were removed, the soils were homogenized and then transferred from the MC to a PE bag and stored at -20 °C until further processing.

4.2.3 Soil and manure characterization

Frozen soil and manure samples were freeze dried to avoid a loss of Hg prior to analyses (Hojdová et al., 2015), ground using an automatic ball mill (MM400, Retsch, Haan, Germany) and analyzed for the following chemical parameters. Carbon (C), nitrogen (N) and sulfur (S) were measured with an elemental analyzer (vario EL cube, Elementar Analysensysteme, Langenselbold, Germany). Organic Carbon (OC) was calculated by subtracting the C concentration of a loss on ignition sample (550 °C for 2 h) from the original C concentration. pH was measured in an equilibrated 0.01 M $CaCl_2$ solution (1:5 soil:liquid ratio). Mineral composition was measured by X-ray diffraction (XRD, CubiX^3, Malvern Panalytical, Malvern, United Kingdom). Trace and major metals (e.g. Fe, Mn, Cu) and Hg were extracted from soils using a 15.8 M nitric acid microwave digestion and measured using an Inductively Coupled Plasma - Mass Spectrometer (ICP–MS, 7700x, Agilent Technologies, Santa Clara, United States of America). Methylmercury was selectively extracted with HCl and dichloromethane (DCM) using an adapted method described elsewhere (Gygax et al., 2019). We modified this method to achieve high throughput (64 Samples per run) and measurements by High Pressure Liquid Chromatography (HPLC, 1200 Series, Agilent Technologies, Santa Clara, United States of America) coupled to the ICP–MS. Details on laboratory materials, extractions, analytical methods and instrumentation are provided in the supplement (Sects. C.2., C.3.). The change in MeHg concentration in the microcosms were likely a result of the simultaneous production and degradation of MeHg. Thus, the term “net MeHg production” was used to represent these processes. We calculated the relative net MeHg production during the incubation as the relative difference of MeHg/Hg ratios between two time points (t) using Eq. 4 - 1.

$$net\ MeHg\ production\ (\%) = \frac{\left(\frac{MeHg}{Hg}_{t_{i-1}} - \frac{MeHg}{Hg}_{t_i}\right)}{\frac{MeHg}{Hg}_{t_{i-1}}} \times 100 \qquad \text{(Eq. 4 - 1)}$$

4.2.4 Soil description

Both soils were identified as *Fluvisols gleyic.* They have a silt loam texture, the same mineral composition but differing Hg and organic carbon (C_{org}) concentrations (Table 4 - 1). For elements relevant for Hg cycling, Hg molar ratios (Hg:Cu, Hg:C_{org}, Hg:Mn) differ between samples and soils used in similar incubation experiments (Hofacker et al., 2013; Poulin et al., 2016). We note that the $[C_{org}/Mn]_{molar}$ was 30 % higher in the LMHC soil compared to HMLC. X-Ray diffractograms of both soils are shown in Fig. A-4. The soils diffractograms are overlapping each other and the qualitative analyses of the diffractograms

show that the soils parental material is composed of the same five main mineral phases, quartz, albite, orthoclase, illite/muskovite, calcite.

Table 4 - 1: List of soil parameters for the two incubated soils (HMLC and LMHC) and manure (MNR). Uncertainties are given as 1σ standard deviation of triplicate experiments (method triplicates).

Parameter		Cornfield (HMLC)		Pasture field (LMHC)		Cow Manure (MNR)	
Land use		Corn field		Pasture		-	
Depth		0 - 20 cm		0 - 20 cm		-	
Soil Type (WRB)		Fluvisol Gleyic		Fluvisol Gleyic		-	
pH		8.16		7.84		-	
Water content	(wt. %)	13.8		8.5		90.3	
	Unit (dry.wt.)	Concentration	SD	Concentration	SD	Concentration	SD
C_{org}	wt. %	1.92	0.01	3.45	0.01	45.22	0.09
N_{tot}	wt. %	0.181	0.001	0.372	0.002	3.68	0.08
C_{org}/N_{tot}	-	10.61	-	9.29	-	-	-
S	g kg^{-1}	0.63	0.05	0.77	0.05	3.7	0.1
Hg	mg kg^{-1}	47.3	0.5	2.4	0.3	0.045	0.001
MeHg	µg/kg	26.9	0.2	6.4	0.2	<0.02	-
MeHg/Hg	%	0.06	-	0.28	-	-	-
Al	wt. %	0.91	0.05	1.05	0.04	0.0106	0.0003
Fe		1.95	0.07	2.38	0.05	0.0336	0.0009
Mg		1.25	0.07	1.39	0.05	0.49	0.03
Mn	mg kg^{-1}	493	21	672	38	53	1
P		1169	80	1044	85	8245	232
Cr		56	4	64	5	0.68	0.01
Co		10.75	0.06	11.22	0.43	0.4	0.2
Ni		81.7	0.8	78.3	2.9	2.3	0.1
Cu		40.1	1.2	28.0	0.7	13.1	0.6
Zn		61.8	0.5	47.3	2.0	81	3
As		11.74	0.07	16.04	0.72	0.8	0.4
Cd		0.21	0.04	0.17	0.01	0.042	0.004
Pb		20.8	0.5	18.34	0.5	-	-
V		17.2	0.4	20.99	1.1	0.31	0.01
Sr		137	2	202	6	45.9	1.6
Cs		1.99	0.02	1.52	0.04	-	-
Ba		60.2	1.1	76.9	1.6	9.1	0.5
Ce		7.0	0.4	8.6	0.6	-	-
Gd		0.94	0.03	1.00	0.05	0.021	0.001
U		1.74	0.08	1.29	0.01	0.19	0.01
Hg/Cu molar	‰	366.3	-	25.73	-	-	-
Hg/Mn molar		25.758	-	0.926	-	-	-
Hg/C_{org} molar		0.147	-	0.004	-	-	-
Mn/C_{org} molar		0.0056	-	0.0042	-	-	-

4.2.5 Soil solution sampling and analyses

Soil solution was sampled 0.25, 1, 2, 3, 4, 5, 7, 9, 11, 14 days after the onset of each flooding period respectively (Fig. 4 - 1, Fig. C - 5). It was sampled though the tubing connected to the suction cup (< 10 µm pre size). The first 2 ml were sampled with a syringe and discarded to prime the system and condition the tubing. After, 4 ml were drawn through an airtight flow-through system to measure the redox potential (Hg/HgCl ORP electrode) and pH. Then, approximately 35 ml of soil solution were sampled using a self-made syringe pump system allowing for a regular flow and minimal remobilization of fine particles. Like this, 4-6 % of the added artificial rainwater volume was sampled at each sampling point (Fig. C - 3). Throughout the experiment the soils remained entirely submerged. At each sampling time, sample splits were preserved without further filtration (<10 µm) and filtered at 0.02 µm (Whatman® Anodisc 0.02 µm, Sigma-Aldrich, St. Louis, United States of America). Additionally, at 2,5 and 9 days an additional sample split was filtered at 0.45 µm (Polytetrafluoroethylene Hydrophilic, BGB,

Boeckten, Switzerland) for colloid characterization. Incubation experiment blanks were taken by sampling MilliQ water through from an empty 1 L borosilicate aspirator bottle 3 times throughout the experiment. Subsequently, the samples were subdivided and treated for different analyses. They were preserved in 1 % HNO_3 for multi elemental analysis (Mn, Fe, Cu, As) and in 1 % HNO_3 and 0.5 % HCl for Hg analysis and analyzed by ICP–MS. For major anion (Cl^-, NO_3^-, SO_4^{2-}) and cation (K^+, Na^+, Mg^{2+}, Ca^{2+}) measurements, samples were diluted 1:4 in ultra-pure water and analyzed by Ion Chromatography (Dionex Aquion™, Thermo Fisher Scientific Inc., Waltham, United States of America). Samples for Dissolved Organic Carbon (DOC), Particulate Organic Carbon POC and Total Nitrogen Bound (TN_b) were diluted 1:5 and stabilized using 10 µl of 10 % HCl and measured using an Elemental Analyzer (vario TOC cube, Elementar Analysensysteme, Langenselbold, Germany).

Table 4 - 2: Description of the symbols and terms used for different filter fractions in the publication. The particulate fraction is calculated as the difference of the 20 nm and the 10µm filtrate concentrations.

Filter Type	Filter size	Symbol (e.g. HgT_x)	Description
Suction Cup	10 µm	$HgT_{<10µm}$	Soil solution sampled directly from the suction cup contains a variety of particles (clay minerals, bacteria, Mn-/Fe-hydroxides, POM aggregates etc.). We refer to this fraction by adding the subscripts <10µm to the analyte symbol.
Syringe Filter	0.02 µm	$HgT_{<0.02µm}$	Soil solution <0.02µm is a cutoff size that may still carry colloids. We refer to this fraction by adding the subscripts <0.02µm to the analyte symbol.
-	-	P-HgT	Particulate Hg is calculated as: $PHg = Hg_{<10µm} - Hg_{<0.02µm}$
-	-	$P\text{-}HgT_{rel.}$	Relative particulate Hg is calculated as: $PHg_{rel.} = (Hg_{<10µm} - Hg_{<0.02µm})/Hg_{<10µm}$
AF4 membrane	1 kDa	$HgT_{<1kDa}$	Molecules in solution under this cutoff size are not expected to have colloidal properties. Therefore, this range is referred to as "truly dissolved" in the text.

Incubation experiment blanks were below 4.75 mg L^{-1} and 22.4 µg L^{-1} for DOC and TN_b, respectively. These relatively high blank values might originate from either the syringes or the suction cups (Siemens and Kaupenjohann, 2003). Uncertainties of soil solution parameters are displayed as 1SD of the triplicate incubation experiments throughout the manuscript. HCO_3^- concentrations were estimated based on the ionic charge balance of the soil solution using VisMinteq (https://vminteq.lwr.kth.se/). A detailed schedule and list of analyses is provided in Figure 4 - 1. Concentrations of specific filtered fractions are labelled with subscripts (e.g. $HgT_{<0.02µm}$) for all measured metals. Particulate concentrations (0.02 µm < X < 10 µm) (e.g. P-Fe) and its proportion to the total (e.g. $P\text{-}Mn_{rel}$) were determined as the difference between unfiltered and filtered concentration (Table 4 - 2).

4.2.6 Characterization of Colloids (AF4)

An aliquot of the soil solution was used for characterization of colloids in one out of three replicate microcosms (Rep1) of each treatment on days 2, 5, 9 days after the onset of each flooding period respectively. Right after sampling, the aliquots were transferred to a N_2 atmosphere in a glove box. There, the samples were filtered to <0.45 µm and preserved in airtight

borosilicate headspace vials at 4 °C. Colloidal size fractions and elemental concentrations of the filtrates were analyzed by Asymmetrical Flow Field-Flow Fractionation (AF4, AF2000, Postnova analytic, Landsberg am Lech, Germany) coupled to a UV_{254nm} absorbance detector (UV, SPD-M20A, Shimazu, Reinach, Switzerland), a Fluorescence detector (FLD, RF-20A, Shimazu, Reinach, Switzerland) and an ICP–MS (7700x, Agilent Technologies, Santa Clara, United States of America) within 14 days after sampling. Colloids contained in 1 mL of samples were separated in a channel made of a trapezoidal spacer of 350 µm thickness and a regenerated cellulose membrane with a nominal cut-off of 1 kDa used as accumulation wall. The mobile phase used for AF4 elution was 10 mM NH_4NO_3 at pH 7 and was degassed prior entering the channel by argon flowing. A linear decrease of crossflow from 2 to 0 mL min^{-1} over 20 min was used after injecting the samples at an initial crossflow of 2.7 mL min^{-1}. At the end of a run, the crossflow was kept at 0 mL min^{-1} for 5 min in order to elute non-fractionated particles. Retention times were transformed into hydrodynamic diameters (d_h) by an external calibration using Hemocyanin Type VIII from Limulus polyphemus hemolymph (monomer d_h = 7 nm, Sigma-Aldrich) and ultra-uniform gold nanoparticles (Nanocomposix) of known d_h (19 nm and 39 nm). Additionally, the elution of the smallest retention times (d_h < 10 nm) were converted into molecular masses (Mw) using PSS standards (Postnova analytic, Landsberg am Lech, Germany) with Mw ranging from 1.1 to 64 kDa (Fig. A-6), using AF4-UVD_{254nm}.

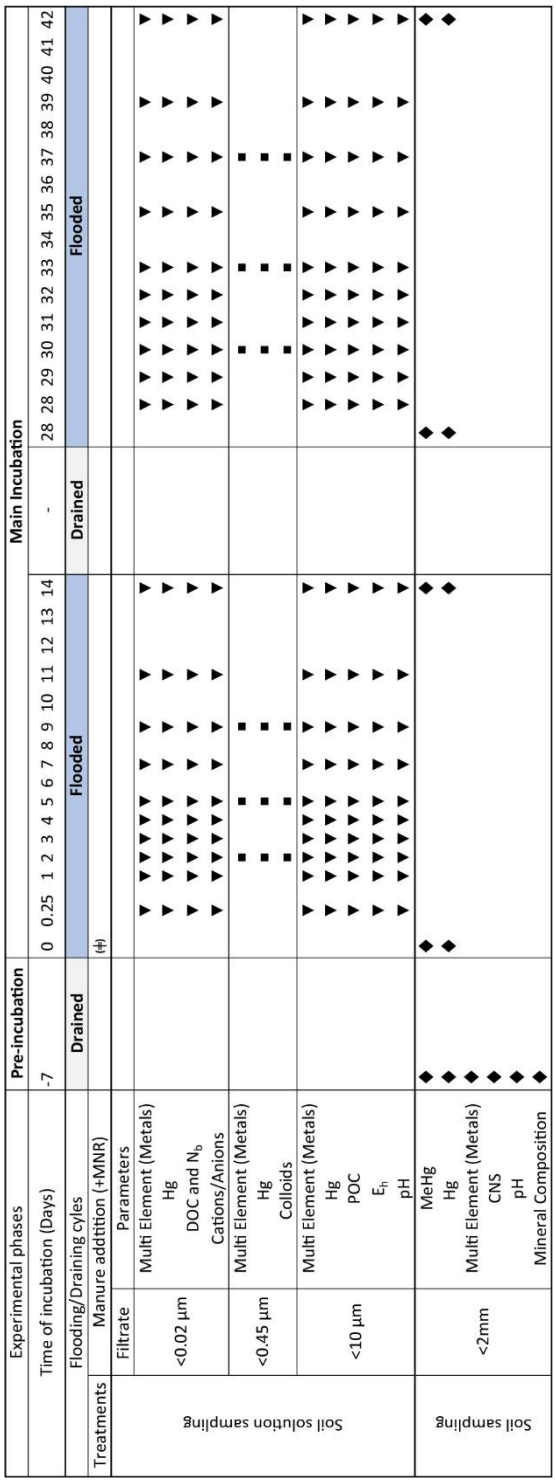

Figure 4 - 1 Schedule of preformed incubation experiment, samplings, and measurements: blue bars indicate soil flooding periods. Gray bars represent drained periods. The width of the columns is not proportional to the time of incubation. In the treatments row the (╪) symbol indicates the addition of liquid manure to the microcosms specifically treated with manure (+MNR). Triangles represent regular soil solution sampling points. Rectangles represent soil solution sampling for colloid analyses. Diamonds represent time points for soil sampling. At -7 days, soil was sampled from the pooled soil directly before the pre-incubation.

Fractograms obtained in Counts Per Seconds (CPS) from Time Resolved Analysis (TRA) acquisition were converted to µg L^{-1} using external calibrations made from a multi-element standard solution (ICP multi-element standard solution VI, Merk, Darmstadt, Germany) diluted in 1 % HNO_3 or a Hg standard (ICP inorganic Hg standard solution, TraceCERT®, Sigma-Aldrich, St. Louis, United States of America) diluted in 1.0 % HNO_3 and 0.5 % HCl. The different size fractions were obtained by multiple extreme-shaped peak fitting, using OriginPro 2018 software (OriginLab Corporation). The peaks obtained were then integrated individually, after conversion of elution time to elution volume, to provide the quantity of Hg in each size fractions (Dublet et al., 2019). The analytes passing the 1 kDa membrane are considered as the (< 1 kDa) truly dissolved fraction. It was calculated by subtracting the concentrations of colloidal HgT recovered by AF4–ICP–MS (total integration of the Hg signals) to the total dissolved HgT concentrations measured separately by ICP–MS in corresponding acidified samples. The concentration of truly dissolved Hg is displayed as $HgT_{<1kDa}$ for the rest of the article (Table 4 - 1). AF4–ICP–MS, UV_{254nm} and fluorescence signals were used to further characterize Hg bearing colloids, after hydrodynamic size separation by AF4. The UV_{254nm} light absorption is widely used to detect organic compounds but it should be noted that part of the UV_{254nm} light signal can as well originate from Fe(II) or Fe hydroxides (Dublet et al., 2019). This was not the case in this study since UV_{254nm} signals co-eluted with C signals recorded by ICP–MS and matched the fractograms obtained by the FLD detector tuned at the wavelengths specific for humic-like fluorophores. It is therefore assumed that UV_{254nm} signal represents organic compounds throughout the manuscript.

4.3. Results

4.3.1 Soil solution chemistry and Hg dynamics

In the HMLC microcosms, the pH of the soil solutions remained in a neutral to alkaline range of 8.0 to 8.4 during the incubation experiment (Fig. C - 7). Soil solution conditions and concentrations of constituents support a continuous reduction of soils with increased flooding time (Fig. 4 - 2a). Soil solution NO_3^- depletion was observed during the first 7 days of incubation (Fig. 4 - 2 b). Nitrate was under detection limit for the second flooding phase. At day 7, Mn concentrations increased together with a marginal increase of Fe (Fig. 4 - 2c-f). This was coincided with a decrease of the relative particulate fraction ($P\text{-}Mn_{rel.}$ and $P\text{-}Fe_{rel.}$) of these

metals. Release of Mn and Fe were assumed to mark the onset of reductive dissolution of Mn- and Fe-oxyhydroxides. The decrease in sulfate (SO_4^{2-}) concentration could not be used to assess the onset of sulfate reduction. This is due to a chemical gradient between supernatant water and soils solution demonstrated by the continuous decrease in concentration of conservative ions (Cl^-, Na^+, K^+) (Sect. 4.4.4).

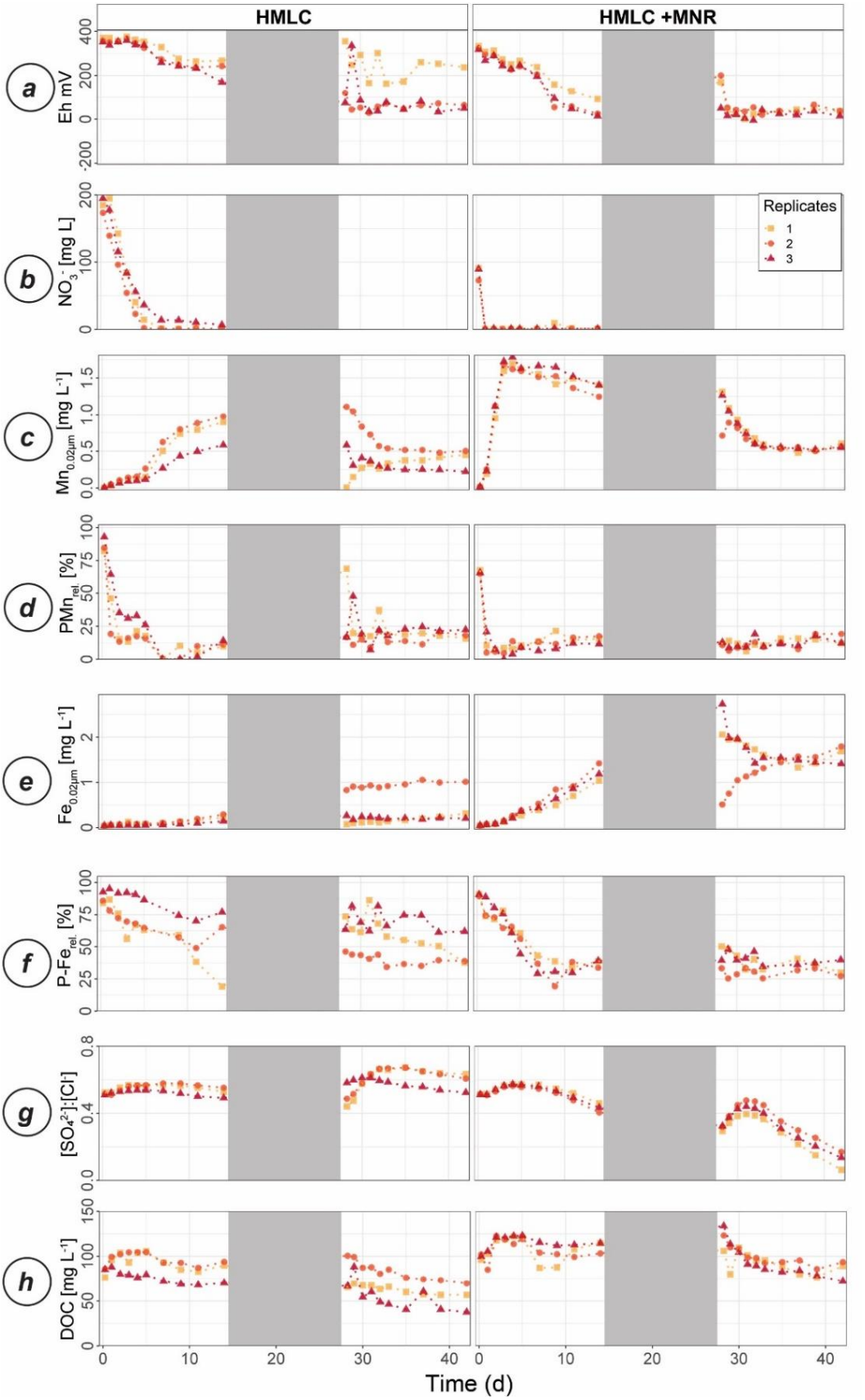

Figure 4 - 2 Soil solution dynamics in cornfield soil (HMLC) incubations for redox potential (a), redox reactive elements (Mn, PMn, Fe, P-Fe, $[SO_4^{2-}]$:$[Cl^-]$) (b-f) and dissolved organic carbon (h). Lines between points were plotted to improve readability. The gray area indicates the drained period.

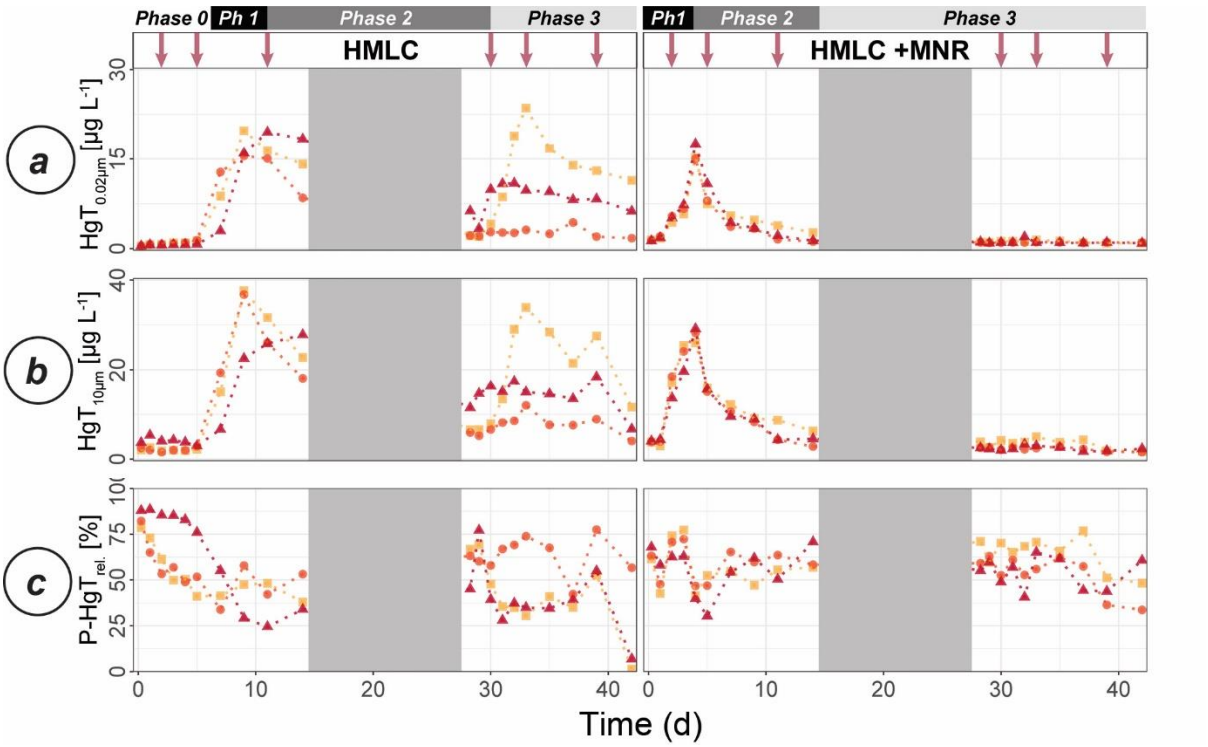

Figure 4 - 3 Soil solution dynamics in cornfield soil (HMLC) incubations for Hg (a-c) subdivided in phases (0-3). Lines between points were plotted to improve readability. The gray area indicates the drained period. Red ar-rows indicate sampling days for AF4-ICP-MS analyses.

To monitor sulfate reduction, we use the molar ratios of SO_4^{2-} to Cl^- (Fig. 4 - 2g). Sulfate to chloride ratios stood constant during the first flooding and slightly increased at the onset of second flooding phase. This suggests that no sulfate reduction took place in the HMLC microcosms during the whole experiment. The DOC concentration ranged between 37.5 and 106 mg L^{-1} (Fig. 4 - 2 h). Both $HgT_{<0.02µm}$ and $HgT_{<10µm}$ concentrations remained low between day 0-5 (Phase 0), then increased together with the Mn release between days 5-11 (Phase 1) and decreased between 14-29 (Phase 2) during the draining period (Fig. 4 - 3 a). The relative fraction of particulate HgT ($P\text{-}HgT_{rel.}$), gradually decreased from a maximum of 88 % to a minimum of 25 % during phase 0 and phase 1 but increased again to 60-77 % during phase 2 (Fig. 2 - 3b-c). $Cu_{<0.02µm}$ concentrations increased up to 88.2 ± 17.5µg L^{-1} within the first 4 days and then gradually decreased to 30.6 ± 3.54 µg L^{-1} at day 14 (Fig. 4 - 4a). Arsenic concentrations simultaneously increased with the release of Fe during the whole incubation (Fig. 2 - 4b).

During the second flooding period, individual microcosms behaved differently in the HMLC run. The differences of soil solution E_h and redox sensitive metals (e.g. Mn, Fe, Hg, Cu) were apparent from the start of the second flooding (Figs. 4 – 2c-f, 4 - 3a-c, 4 - 4a). Contrastingly, DOC concentrations and pH remained similar between incubators (Figs. 4 - 2h, C - 7). One replicate (Rep1) showed a pronounced increase of redox potential after the draining period (Fig. 4 - 2a). The E_h remained high (150 to 300 mV) for the whole second flooding period. A depletion and subsequent release of Mn in soil solution was observed, indicating the formation and redissolution of Mn oxyhydroxide minerals (Fig. 4 - 2c-d). Subsequently, $Mn_{<0.02\mu m}$ increased and peaked at 448 µg L^{-1} by the end of the experiment in Rep1. The E_h of Rep2 was lower (between 28 and 120 mV), Mn concentrations did not decrease during the draining phase, and a release of Fe was observed during the second flooding phase indicating the reduction of Fe oxyhydroxides. Rep3 had a E_h in the range of Rep2 but neither a rerelease of Mn nor a release of Fe was observed during the second flooding phase. Also, HgT behaved differently within incubators during the second flooding period. Between days 29-42 (Phase 3), $HgT_{<0.02\mu m}$ and $HgT_{<10\mu m}$ concentrations increased or remained at higher levels for Rep1 and Rep3. During this phase P-HgT_{rel} vastly decreased and was at a minimum of 1-7 % by the end of the incubation. Contrastingly, $HgT_{<0.02\mu m}$ and $HgT_{<10\mu m}$ stayed constantly low for Rep2 during phase 3 and P-HgT_{rel} remained overall above 50%. The Rep1 was the only MC that showed an increase in Cu concentrations during the draining phase (Fig. 4 - 4a).

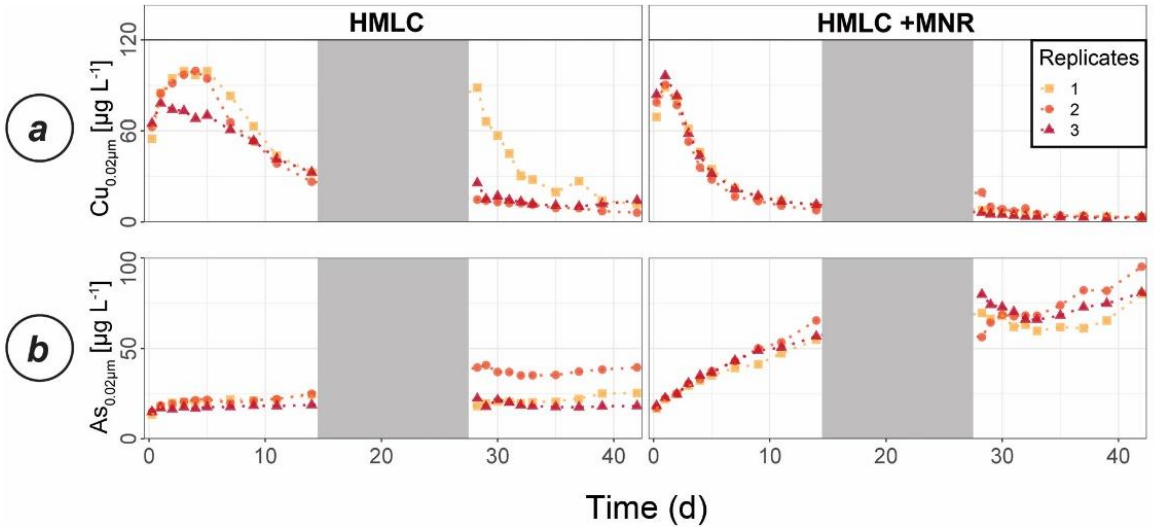

Figure 4 - 4 Soil solution dynamics in cornfield soil (HMLC) incubations for Cu (a) and As (b). Lines between points were plotted to improve readability. The gray area indicates the drained period.

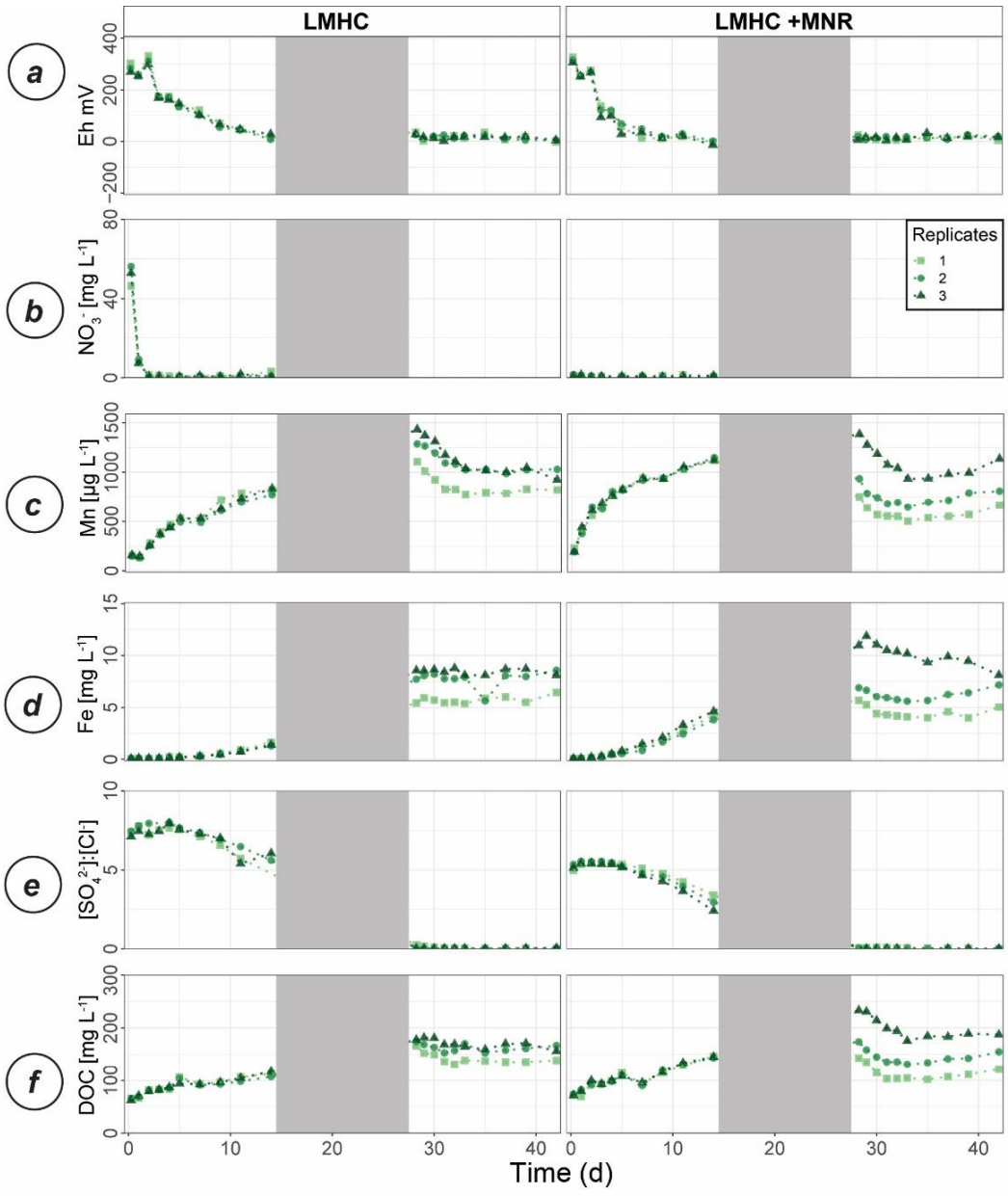

Figure 4 - 5 Soil solution dynamics in pasture field soil (LMHC) incubations for redox potential (a), redox reactive elements (Mn, PMn, Fe, P-Fe, [SO42-]:[Cl-]) (b-f) and dissolved organic carbon (h). Lines between points were plotted to improve readability. The gray area indicates the drained period.

In the HMLC +MNR microcosms, pH remained in the range of 8 to 8.35 with minor fluctuations over both flooding periods (Fig. C - 7). The redox potential decreased rapidly from approx. E_h 300 mV to 5.27 ± 14.4 mV within the first 14 days and remained constant at 14.3 ± 8.12 mV during the second flooding period. Depletion of NO_3^- was observed within the first day of incubation and was under detection limit during the second flooding period (Fig. 4 – 2b). A rapid release of Mn started at day 2 and a slow release of Fe started at day 3 of first flooding period (Fig. 4 - 2c-f). The $[SO_4^{2-}]$:$[Cl^-]$ ratios decreased from 0.57 ± 0.01 to 0.37 ± 0.02 between day 4-29. During the second flooding period $[SO_4^{2-}]$:$[Cl^-]$ ratios initially increased slightly between day 29-31 and then decreased to a minimum (0.12 ± 0.05) by the end of the incubation (Fig. 4 - 2g). DOC concentrations were between 72.2 and 134 mg L^{-1} (Fig. 4 - 2h). This was significantly higher (3 to 43 mg L^{-1}) than in HMLC without manure. In these microcosms $HgT_{<0.02µm}$ and $HgT_{<10µm}$ concentrations instantly increased together with the Mn release

between days 0-4 (Phase 1) decreased during the days 5-14 (Phase 2) and remained low between day 14-42 (Phase 3) (Fig. 4 - 3 a-c). The particulate HgT (P-$HgT_{rel.}$) decreased to 30-52.5 % in phase 1 and remained overall above 50 % for the rest of the incubation. At the onset of phase 2 black precipitates were visually observed in the HMLC +MNR microcosms (Fig. C - 13). Cu concentrations decreased gradually during the course of the incubation experiment (Fig. 4 - 4a). Arsenic concentrations simultaneously increased with the release of Fe during the whole incubation (Fig. 4 - 4b).

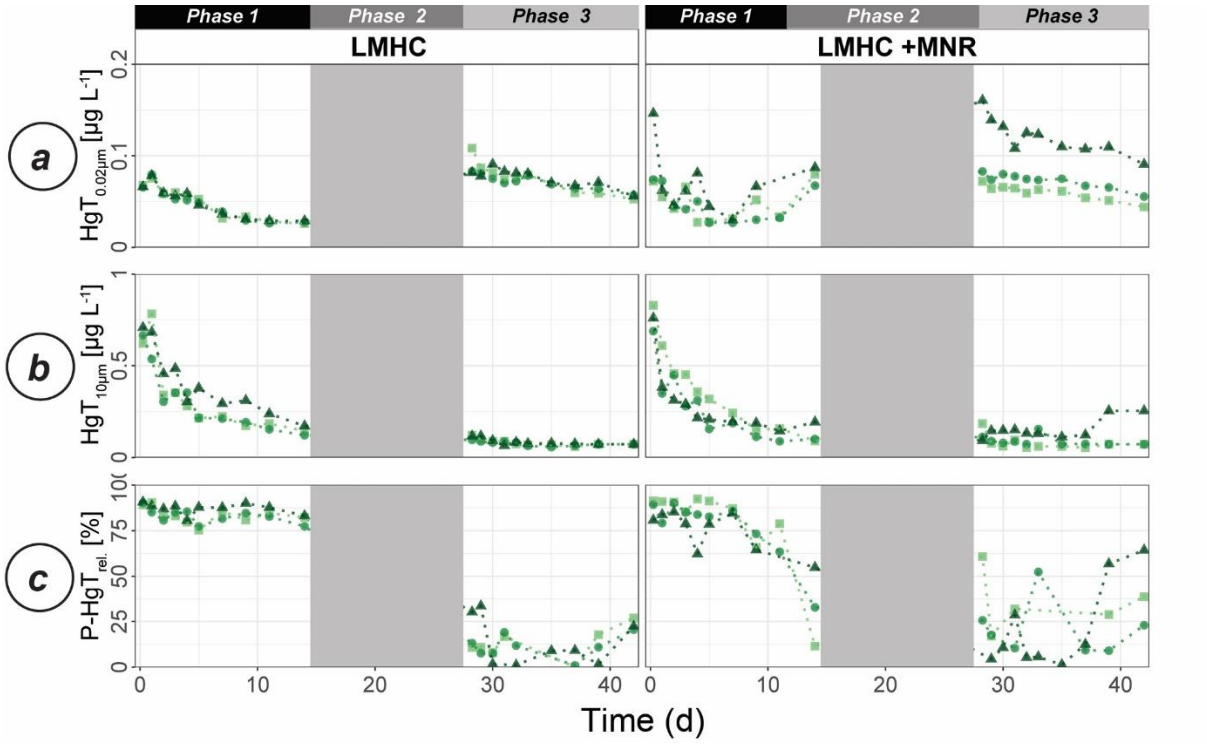

Figure 4 - 6 Soil solution dynamics in pasture field soil (LMHC) incubations for Hg (a-c) subdivided in phases (1-3). Lines between points were plotted to improve readability. The gray area indicates the drained period.

LMHC differed from HMLC in soil solution chemistry. In both treatments (LMHC and LMHC +MNR), pH remained neutral but gradually decreased from 8.2 to 7.5 during the incubation (Fig. C - 7). Soil reduction progressed rapidly from a max of 332 mV at day 3 to -14.3 mV at day 14 (Fig. 4 - 5a). During the second flooding E_h stayed in the range of - 2.3 to 34.5 mV. Nitrate was exhausted within the first day of incubation and marked the onset of Mn release. Mn as well as DOC concentrations gradually increased during the first flooding period (Fig. 4 - 5b-c). Fe release started on day 4 and day 6 in LMHC and LMHC +MNR respectively (Fig. 4 - 5d). A decrease in $[SO_4^{2-}]$:$[Cl^-]$ ratio was observed after day 5 and remained stable at 0.03 ± 0.04 during the second flooding period. This is indicative for sulfate reduction during the draining phase and the second flooding phase (Fig. 4 - 5e). Soil solution $HgT_{<0.02\mu m}$ concentration (25 – 160 ng L^{-1}) were two orders of magnitude lower than in the HMLC runs (Fig. 4 - 3a, 4 - 6a). Dissolved $HgT_{<0.02\mu m}$ degreased during the first flooding period (phase 1), increased during the draining period (phase 2) and gradually decreased again during the second flooding period (phase 3) (Fig. 4 - 6a-c). No other soil solution parameter followed the trend of $HgT_{<0.02\mu m}$. Particulate $HgT_{<10\mu m}$ decreased during phase 1 and remained low during phase 2 and 3. In the LMHC microcosms P-$HgT_{rel.}$ changed drastically between phase 1 (> 65 %) and

phase 3 (<< 50 %) (Fig. 4 - 3c). In the LMHC +MNR microcosms the P-$HgT_{rel.}$ was high during the phase 1 (> 65 %) and fluctuated between phase 3 (<< 50 %) (Fig. 4 - 3c). Cu concentrations gradually decreased during the course of the experiment (Fig 4 - 7a). Arsenic concentrations simultaneously increased with the release of Fe during the whole incubation (Fig 4 - 7b).

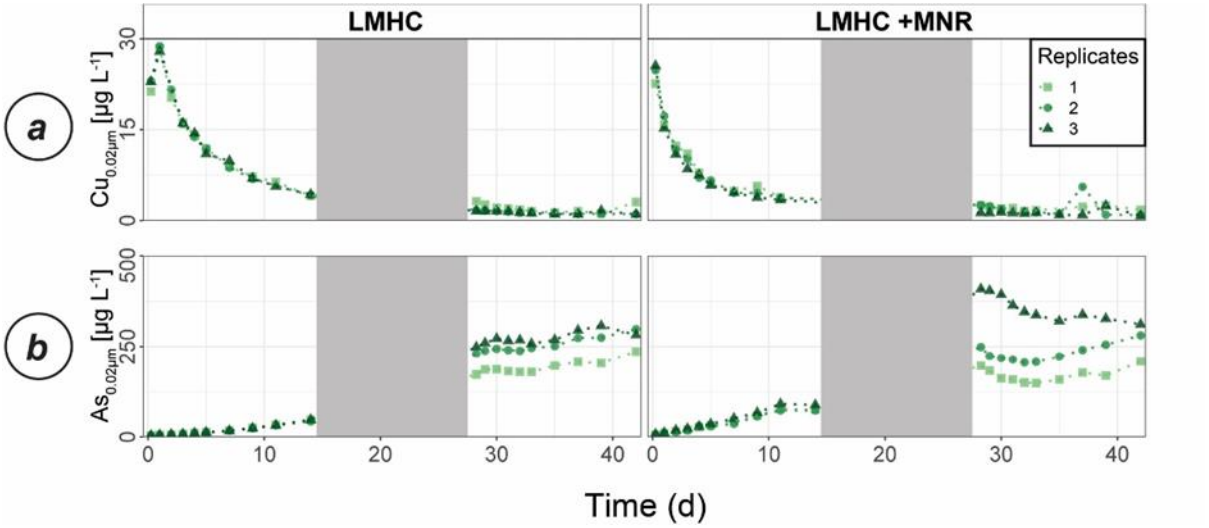

Figure 4 - 7 Soil solution dynamics in pasture field soil (LMHC) incubations for Cu (a) and As (b). Lines between points were plotted to improve readability. The gray area indicates the drained period.

4.3.2 Colloidal Hg (AF4)

Hg bearing colloids were detected in all soil solution samples of HMLC incubations. Due to low signal to noise ratios (< 3) we did not detect colloidal Hg in samples of the LMHC incubations. Figure 4 - 8 shows the evolution of concentrations and relative proportions of HgT size fractions. Generally, changes in proportions were apparent during phases of Hg release and decrease in soil solution, but little change was observed during when Hg concentrations were stagnant (HMLC +MNR, Phase 3). The proportion of truly dissolved $HgT_{<1kDa}$ varied between 0 % and 67 % in the HMLC experiment and was high during Hg release to soil solution (phases 1 and 3) (Fig. 4 - 8). In the HMLC +MNR treatment, $HgT_{<1kDa}$ were lower and ranged between 0 % and 29 %. The colloidal Hg can be divided into 3 main fractions (Fig. 4 - 9). The first Hg colloidal fraction showed a main peak ranging between 1 – 40 kDa (d_h < 6 nm) and was associated with UV_{254nm}-absorbing compounds and various metals (Mn, Fe, Cu, Ni, Zn). This fraction was interpreted as humic substance type Hg–NOM. The proportion of this colloidal Hg fraction varied with no specific trends from 11.5 to 23.3 % in HMLC and 13.6 to 38.6 % in HMLC +MNR throughout the course of the experiment. A second fraction of Hg colloids ranged between 6 nm and 20 nm. This well-defined size fraction was eluting in the tail of the first fraction for other metals (e.g. Fe, Mn, Cu) but did not overlap with UV_{254nm} and fluorescence signals (Fig. 4 - 9). This fraction could not be chemically defined but is hypothesized to consist of ß-$HgS_{(s)}$ colloids. In the HMLC run, we observed a decrease in the proportion of these inorganic colloids from 28 % in phase 0 to 15.3 % at the end phase 3 (Fig. 4 - 9). In the HMLC +MNR treatment, the proportion of this fraction ranged

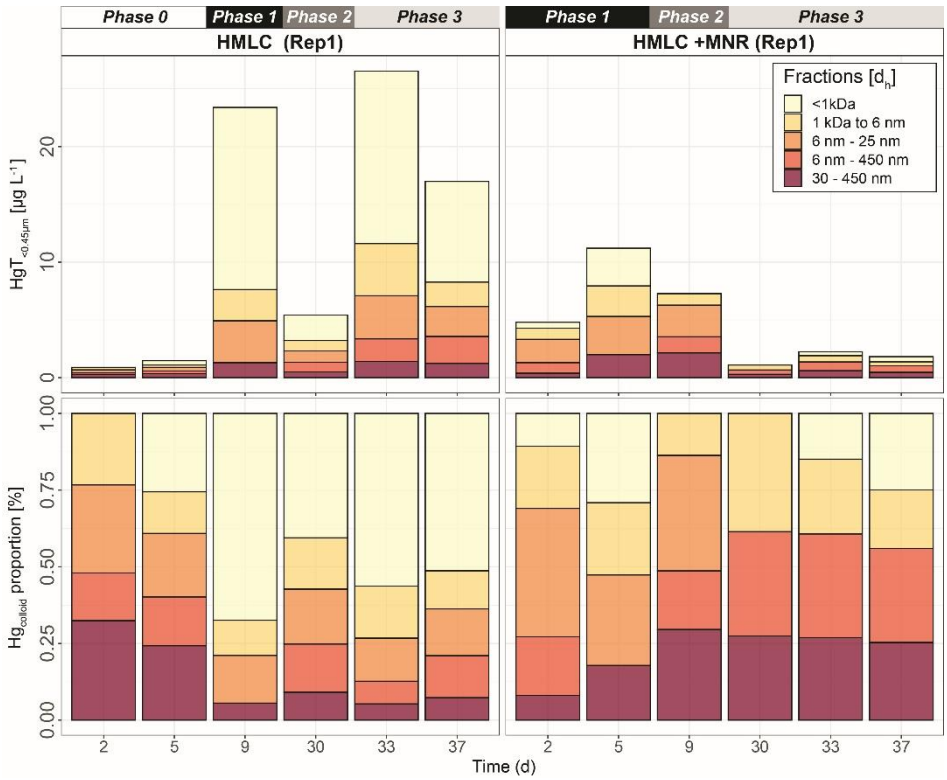

Figure 4 - 8 Size distribution of Hg estimated after AF4 fractogram deconvolution for Rep1 of cornfield soil incubation (HMLC and HMLC +MNR) subdivided in phases (0-3). The concentration of HgT in size fractions was calculated using an external calibration of the ICP–MS directly after the AF4 run. The concentration of HgT in "< 1kDa" was calculated by subtracting the sum of the fractions from the HgT concentration in the same sample measured separately by ICP–MS. The fractograms of all analysed time points are shown in the supplement (Figs. C - 9 to C - 12).

between 29.5 % and 41.9 % during the phases 1 and 2 and could not be detected during the phase 3. Further, we observed a third colloidal fraction that continued to elute after the stop of the AF4 crossflow and it included colloids in the range of 30 – 450 nm (effective cut-off of the filter used for the sample preparation). In some cases, this fraction was better fitted using two overlapping populations (Fig. 4 - 9, Figs. C 9 to C 12). In all the cases, HgT signal was associated with those of other metals and a slight bump of the UV_{254nm} signal but more specifically an increase of fluorescence signal associated to protein-like fluorophores. This fraction decreased continuously in the HMLC runs during the incubation from 32.4 % in phase 2 , to 5.6 % in phase 2 and stood under 9.1 % during phase 3. By contrast, the HMLC +MNR showed an increase in the proportion of this fraction from 7.3 % in phase 1 to 25.3 % by the end of phase 3 (Fig. 4 - 8). The deconvolution of the fractograms included an intermediate fraction of Hg bearing colloids ranging between d_h = 6 nm and d_h = 450 nm depending on the sample. This fraction was added to refine the fractogram fittings but could not directly be associated to another measured metal. This indicates that this population represents a polydispersed Hg particle population although in some cases the presence of small Hg particles dominates. This broad fraction was not detected in HMLC +MRN treatments during phases 1 and 2 but made up > 30 % during phase 3.

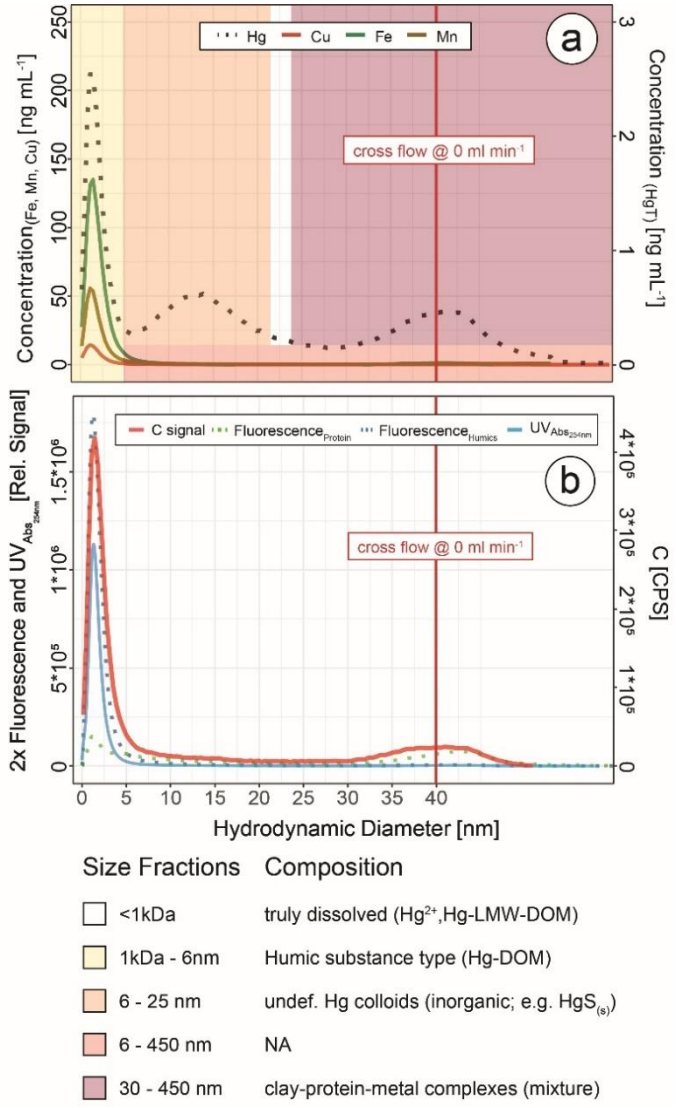

Figure 4 - 9 Hg, Cu, Mn and Fe concentrations (a) and C signals (ICP–MS), UV254nm absorbance and fluorescence signals (b) in colloids as a function of hydrodynamic diameter (related to retention times on AF4) in a sample from HMLC at day 9 after flooding. These fractograms were obtained at linearly decreasing crossflow from 2 to 0 mL min-1 over 20 min. The red line indicates the time point where the crossflow reached 0 ml min^{-1}. Areas (yellow to red colour) indicate size fraction ranges assigned during deconvolution.

4.3.3. Net MeHg production in soil.

Soil MeHg levels fluctuated over the course of the incubation experiment (Fig. 4 - 10 and Table 4 - 3). Highest net MeHg production was observed during the first flooding period for the treatments with manure (up to + 81 %) and during the draining phase for the treatments without manure (up to + 73.1 %). We observed a significant decrease of MeHg/HgT and absolute MeHg concentrations in all incubators during the second flooding period (Fig. 4 - 10). In all microcosms, MeHg/HgT increased by a factor of 1.18 to 1.36 throughout the incubation (Table 4 - 2).

4.4. Discussion

4.4.1. Mercury release and sequestration.

Cornfield soil (HMLC) and pasture field soil (LMHC) behaved differently in this incubation experiment and will be discussed separately. In the cornfield soil (HMLC) Hg and Mn releases were simultaneous and started when soil solution E_h entered the field of Mn reduction below approx. 300mV (Figs. 4 - 2c,4 - 3a), strongly suggesting that this Hg pool was released by reductive dissolution of Mn-oxyhydroxides. During all experiments, low Hg:DOM ratios (<<1 nmol Hg (mg DOM)$^{-1}$) suggest that strong binding sites of DOM were never saturated with respect to mercury, assuming a binding site [RS_2^{2-}] density of 5 nmol Hg (mg DOM)$^{-1}$ and that DOC is 50 % the DOM (Haitzer et al., 2002). The low Hg:DOM ratio suggests that Hg is mainly present as complexed with DOM given reported strong interaction with thiol sites of DOM. However, these assumptions might not reflect the actual composition of DOM which might drastically differ in amended soils (Li et al., 2019). Reductive dissolution of Mn-oxyhydroxides drives both 1.) the release of labile Hg-NOM complexes and Hg^{2+} sorbed on the oxide's surfaces and/or 2.) enhanced the degradation and mineralization of unsubtle NOM binding Hg in soils (Jones et al., 2018). After Hg release (phase 1), Hg concentrations remained high, and the relative particulate Hg fraction was low throughout the experiment. This illustrates that the released Hg-pool mainly originated from

Mn-oxyhydroxides or degradation of suspended POM during Mn reduction. However, the released Hg-pool is relatively small compared the HgT levels of the soil. We estimate that about 12.8 ± 4.2 µg kg^{-1} Hg (0.02 % of HgT_{soil}) was evacuated by sampling during the experiment. In this fluvisol, Hg mobilization is thus mainly driven by reductive dissolution of Mn oxyhydroxides. Direct mobilization of DOM was reported to govern Hg levels in peat soils, Histosols or Podsols in boreal environments (Åkerblom et al., 2008; Kronberg et al., 2016; Jiskra et al., 2017) or floodplain soils with higher OC levels (Beckers et al., 2019; Wang et al., 2021a) in temperate soils.

Table 4 - 3: Soil MeHg concentrations and net-methylation (MeHg/Hg) over the time of the experiment.

Treatment	day	n	Mean MeHg (µg kg^{-1})	SD MeHg (µg kg^{-1})	Range MeHg (µg kg^{-1})	MeHg/Hg (‰)	net MeHg production (%)
HMLC	0	1	26.9	-	26.9 - 26.9	0.57	-
	14	3	30.14	2.19	28.04 - 32.42	0.64	12.0
	28	3	52.04	10.65	39.74 - 58.25	1.1	73.1
	42	3	30.03	5.05	26.93 - 35.86	0.75	-32.4
HMLC +MNR	0	1	26.9	-	26.9 - 26.9	0.57	-
	14	3	43.41	1.99	42 - 44.81	1.03	81.1
	28	3	57.79	13.79	41.88 - 66.41	1.24	20.7
	42	3	30.94	3.43	28.85 - 34.9	0.67	-45.9
LMHC	0	1	6.4	-	6.4 - 6.4	2.72	-
	14	3	8.11	1.09	7.33 - 9.36	2.99	10.0
	28	3	12.07	1.1	10.81 - 12.87	4.11	37.2
	42	3	7.95	0.35	7.73 - 8.36	3.42	-16.7
LMHC +MNR	0	1	6.4	-	6.4 - 6.4	2.69	-
	14	3	10.86	1.86	8.76 - 12.32	3.72	38.1
	28	3	14.31	0.17	14.12 - 14.43	4.7	26.6
	42	3	8.4	0.09	8.33 - 8.5	3.67	-22.0

Further, Hg mobilization was not simultaneous to Cu release. This was reported for polluted soils with high Cu levels (Hofacker et al., 2013) and comparably low Hg/Cu_{molar} ratio in the soil matrix. In neighboring soils, the main Hg pool was previously reported as $HgS_{(s)}$ and Hg complexed by recalcitrant NOM (Grigg et al., 2018). Earlier studies assumed that 0.1 to 0.6 % (w/w) of NOM was reduced sulfur with high affinity to Hg (Grigg et al., 2018; Ravichandran, 2004). Following this assumption, reduced sulfur groups of the cornfield soils NOM could sorb between 11.9 to 71.9 mg kg^{-1} of Hg. The soils high Hg concentration (47.3 ± 0.5 mg kg^{-1}) suggests that soil NOM thiol sites are likely saturated in terms of Hg. Therefore, saturated NOM sorption sites are not competing with Mn-oxyhydroxide sorption sites, resulting in a substantial Mn-oxyhydroxide bound Hg-pool. This leads to a higher mobility of Hg upon reductive dissolution of Mn-oxyhydroxide compared to fluvisols used in other incubation studies (Hofacker et al., 2013; Poulin et al., 2016; Beckers et al., 2019).

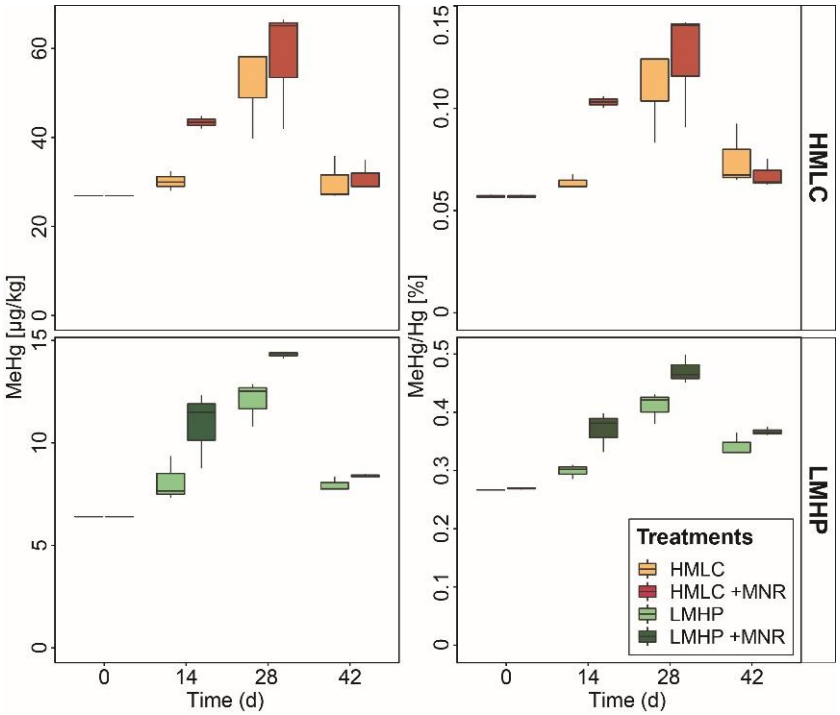

Figure 4 - 10 Soil MeHg concentrations and MeHg/Hg ratios over the course of the experiment for corn field soils (HMLC, yellow/red) and pasture field soils (LMHC, lime/green). Highest net methylation was observed during first flooding for +MNR treatments and during the draining period for microcosms without manure addition. A significant decrease of MeHg/Hg was observed during the second flooding for all treatments.

During the second flooding phase, the cornfield soil (HMLC) runs showed a higher variability in redox sensitive soil solution parameters (Fig. 4 - 2). This might be explained as 1.) a shift in microbial communities, 2.) disturbance of the soil column by invasive soil sampling in between the flooding periods or 3.) uneven draining of the pore space after the first flooding. It can also reflect how redox cycle can be easily affected *in situ*. We suggest that the second release of Mn and Hg in Rep1 is due to Mn re-oxidation during the draining period and a second reductive dissolution of Mn oxyhydroxides upon reflooding. This is supported by the elevated E_h at the onset of the second flooding. Further, Mn reduction oxidation and reduction cycles were shown to enhance the degradation of NOM to more labile forms (Jones et al., 2018) which might contribute to the degradation/mineralization of recalcitrant Hg-NOM. The HMLC Rep3 showed a second release of Hg without a remobilization of Mn. Changing redox conditions have been shown to enhance microbial respiration and therefore NOM degradation (Sunda and Kieber, 1994). Thus, we interpret the second Hg release in Rep 3 as a degradation/mineralization of NOM that bound Hg.

The carbon amendments were reported to decrease total Hg release in polluted floodplain soils (Beckers et al., 2019) but may have a mobilizing effect in NOM depleted environments (Eckley et al., 2021). The addition of manure accelerated the release of Hg through reductive dissolution of Mn oxyhydroxides in the cornfield soil (HMLC). Mercury was released 4 day earlier, as result of additional labile carbon of the liquid manure 1.) acting as electron donor enhancing microbial soil reduction (Liu et al., 2020), 2.) act directly as reductant of the Mn oxyhydroxides (Remucal and Ginder-Vogel, 2014). In the manure treatment, we observed a fast decrease of Hg concentration and a constantly high proportion of particulate P-$HgT_{rel.}$ even after the plateau of Mn concentration in soil solution and the relative decrease of particulate Mn. The addition of manure a source of POM (manure was sieved to < 500 µm) and increased DOC approximately by 20 mg L^{-1}. Sorption of Hg is directed towards thiol rich high molecular weight NOM (Liang et al., 2019) following different ligand exchange reactions (e.g. carboxyl-groups to thiol groups) which happen within days (Miller et al., 2009; Chiasson-Gould et al., 2014). The constant of P-Hg_{rel} proportion is suggested to be partly caused by the complexation of dissolved Hg with the added POM of the manure.

In addition, we visually observed black precipitates (Fig. C - 13) and the decrease of $[SO_4^{2-}]$:$[Cl^-]$ ratios (Fig. 4 - 2g) at the onset of Hg decrease (phase 2) in the microcosms with manure addition. This indicates the precipitation of sulfide mineral particles. Although, redox potential measurements did not indicate sulfate reduction, the monitoring of E_h in soil solution provides only a qualitative measure in a complex soil system. We suggest that formation and aggregation of ß-$HgS_{(s)}$ explains the faster decrease in the manure amended experiment. Furthermore, formation of metacinnabar ß-$HgS_{(s)}$ was observed under oxic conditions by conversion of thiol bound $Hg(SR)_2$ (Manceau et al., 2015). The formation and aggregation of ß-$HgS_{(s)}$ is further supported by AF4 results (Sect. 4.4.2).

Hofacker et al. (2013) reported a quantitatively relevant incorporation of Hg into metallic Cu^0 particles. However, we do not consider this a relevant pathway, due to the relatively high Hg/Cu_{molar} ratio in our soil compared to Hofacker et al. (2013). Although the simultaneous decrease of Hg and Cu may be interpreted as the immobilization of Hg though incorporation into metallic Cu particles, i) we did not observe the formation of colloidal Cu associated with Hg (Sect. 4.4.2) and ii) relatively high Hg/Cu molar ratios indicate that the decrease of Hg in the soil solution cannot be solely explained by this mechanism as Hg would be marginally incorporated metallic Cu^0 particles.

As well, Hg in soil solutions is volatilized by reduction of Hg^{2+} to Hg^0 (Hindersmann et al., 2014; Poulin et al., 2016; Li et al., 2021b). Our experimental design did not allow for quantification of gaseous Hg^0 and it may have exited the microcosms since they were only sealed with parafilm. Reduction of Hg^{2+} may happen both biotically (Grégoire and Poulain, 2018) and abiotically under UV-light and in the dark (Allard and Arsenie, 1991). Biotic reduction is a detoxication mechanism of bacteria carrying *merA* genes in Hg polluted environments. Biotic volatilization has been observed in neighboring soils of our sampling site (Frossard et al., 2018). Organic amendments and high Hg levels have been shown to increase the abundance of Hg reducing bacteria (Hu et al., 2019). Further, dark abiotic reduction of Hg^{2+} complexed to functional groups of DOM in soils has been

demonstrated (Jiang et al., 2015). However, it is unlikely that Hg reduction can solely explain the decrease of Hg in the soil solution in our microcosms. We therefore interpret the decrease in Hg concentration to be due to a combination of manure NOM complexation and sequestration together with the formation of $HgS_{(s)}$ during flooding. Our data shows that manure addition may have an immobilizing effect on Hg in flooded soils. By contrast, carbon amendments may increase Hg mobility and methylation in NOM depleted and cinnabar rich mountain soils (Eckley et al., 2021).

In the pasture field soil (LMHC), soil solution Hg concentrations remained at low levels (< 0.16 µg L^{-1} $Hg_{<0.02µm}$) during the whole experiment in both treatments (Fig. 4 - 6a). Unlike in the cornfield soil (HMLC), we did not observe a simultaneous release of Hg upon Mn reduction (Fig. 4 - 5c). We explain this with the not completely Hg saturated NOM in this soil, if we assume that 0.1 – 0.6 % (w/w) of NOM was reduced S with high affinity to Hg (Grigg et al., 2018; Ravichandran, 2004; Skyllberg, 2008). Thus, the pasture field soil has a rather limited pool of labile Hg compared to the cornfield soil. Both $Hg_{<0.02µm}$ and $Hg_{<10µm}$ negatively correlate with the sum of sampled soil solution (R^2 = -0.841, p= <0.001) during both flooding periods and decreased fast. This suggests that the concentration gradient between supernatant artificial rainwater and the soil solution contributed to the fast exhaustion of the small labile Hg pool in pasture field soil. The presence of this concentration gradient in our incubation setup is confirmed by the continuously decreasing concentrations of conservative ions (Cl^-, Na^+, K^+) in soil solutions of the HMLC runs (Sect. C 5.2, Figs. C - 7, C - 8). The relatively high proportion of particulate Hg vastly decreased during the draining period (Fig. 2-3b,c) and we speculate that this change is a result of the mobilization of the POM–Hg pool by mineralization/degradation of NOM which sorbed Hg during the draining period (Jones et al., 2018). In summary, flooding of the pasture field soils did mobilize only a small pool of particulate bound Hg which was exhausted within the first flooding period.

4.4.2. Colloidal Hg

For runs without manure, AF4 results show that the Hg released from Mn-oxyhydroxides (Sect. 4.4.1, Fig. 4 - 2) was dominated by dissolved Hg (Hg^{2+} or LMW–NOM–Hg, Fig. 4 - 8). The high Cl^- concentrations (up to 800 mg L^{-1}, Fig. C - 13) likely influenced the Hg speciation in the soil solution, as chloride is a main complexant for Hg^{2+} (Li et al., 2020; Gilli et al., 2018). During Hg release, the proportions of larger Hg colloids (> 25 nm) decreased. The stable proportion of humic substances bound Hg and inorganic Hg colloids between 6 nm and 25 nm indicates that once released no major adsorption or aggregation of truly dissolved Hg and larger colloidal Hg occurs. Additional complexation of Hg by DOM can be excluded if we assume the saturation state of thiol-sites of the NOM pool in the soil (Sect. 4.4.1). These observations illustrates the remarkably high Hg mobility and potentially increased bioavailability (proportion of truly dissolved Hg) to Hg metabolizing microorganisms compared to other studies (Hofacker et al., 2013; Poulin et al., 2016). These authors did either not observe Hg in truly dissolved form or a decrease to low levels within the first days of incubation. Overall, the released Hg from cornfield soil (HMLC) shows

a high mobility and might represent a possible threat to downstream ecosystems and a source for Hg methylating bacteria. However, the total Hg released and sampled from soil solution represents a rather small pool (12.8 ± 4.2 µg HgT kg^{-1} soil) of the total Hg (47.3 ± 0.5 mg kg^{-1}). Further work would be needed to establish a Hg flux model to better understand *in situ* soil Hg mobility in these soils.

The manure addition had a key effect on the proportions of colloidal fractions in soil solution, and overall led to a low proportion of truly dissolved fraction (Fig. 4 - 8). We suggest that the distinct fraction of colloids with d_h = 6 – 25 nm represents metacinnabar like $HgS_{(s)}$ colloids (Gerbig et al., 2011). This is supported by the onset of sulfate reduction in phase 2 (Rivera et al., 2019; Poulin et al., 2016) and reported Hg-NOM interactions that may cause the precipitation of Hg bearing sulfide phases ($FeS_{(s)}$, ß-$HgS_{(s)}$) (Manceau et al., 2015). The size of ß-$HgS_{(s)}$ nano particles formed from free sulfide is dependent in the sulfide concentration as well as on the Hg:DOM ratio (Poulin et al., 2017). The formation of a distinct size fraction of HgS(s) has experimentally observed at comparable Hg:DOM ratios (Gerbig et al., 2011). The Hg colloidal distribution was dominated by the presence of large fractions (d_h = 30 - 450 nm). Larger organic acids with high aromaticity usually contain higher proportions of thiols groups than smaller molecules and selectively complex Hg (Haitzer et al., 2002). This suggests that Hg complexation is kinetically driven and it can shifts from LMW–DOM to larger NOM and larger aggregates of POM as supported by earlier incubation experiments (Poulin et al., 2016). We therefore interpret that the relative increase of Hg colloids with d_h = 30 – 450 nm (Fig. 4 - 8) is caused by 1.) complexation of the released dissolved $Hg_{<1kDa}$ by strong binding sites of thiol rich NOM in larger clay-organo-metal complexes and 2.) the aggregation of $HgS_{(s)}$ colloids during the experiment. Although the presence of e.g. humic substances and larger NOM was shown to narrow the size range of $HgS_{(s)}$ nanoparticles precipitating from solution (Aiken et al., 2011) , through time, these colloids may grow, aggregate and form clusters in a wide size distribution (Deonarine and Hsu-Kim, 2009; Poulin et al., 2017). Thus, their aggregation during the draining period may explain the decrease in monodisperse Hg bearing colloids, also leading to sequestration of Hg in the soil matrix, without remobilization during the second flooding. Our data suggests meta cinnabar formation (ß-$HgS_{(s)}$) in a distinct size fraction (d_h = 6 – 25) and their aggregation to large fractions (d_h = 30 – 450 nm) at environmental conditions in real-world samples.

4.4.3. Net MeHg production in soil.

The studied soils show uncommonly high initial MeHg levels (6.4 – 26.9 µg kg^{-1}) when compared to other highly polluted mining or industrial legacy sites (Horvat et al., 2003; Neculita et al., 2005; Qiu et al., 2005; Fernández-Martínez et al., 2015), supposedly as a result of a flooding event prior to sampling resulting in a net MeHg production. Still, we observed significant net MeHg production during the first 28 days of the incubation resulting in even higher MeHg concentrations of up to 44.81 µg kg^{-1} (Table 4 - 3; Fig. 4 - 10). Soils treated with manure showed a faster net MeHg production with highest increase of MeHg during the first flooding period. Controls showed highest net MeHg production during the draining period and reached

similar levels of MeHg at the start of the second flooding on day 28 (Fig. 4 - 10). For cornfield soil (HMLC), both treatments show a high concentration of bioavailable Hg^{2+} or Hg associated with labile NOM ($HgT_{<0.02\mu m}$ > 15µg L^{-1}) in soil solution during the first flooding. Net MeHg production is therefore rather limited by cellular uptake of Hg or the microbial activity of methylating microorganisms than bioavailability. Thus, we interpreted the addition of labile carbon in the form of manure to result in a higher microbial activity and net MeHg production during the first flooding period. However, we did neither assess the activity nor the abundance of Hg methylating bacteria such as sulfate reducers (SRB), Fe reducers (FeRB), archaea or firmicutes (Gilmour et al., 2013). In the runs without manure addition, a substantial part of Hg was methylated during the draining period. This indicates that even if low concentrations of Hg is released (LMHC microcosms day 14: $HgT_{.<0.02\mu m}$ < 50 ng L^{-1}) a substantial amount of Hg can be methylated. Micro- and mesopore spaces with steep redox gradients act as ideal environments for microbial methylation even in drained and generally aerobic system (e.g. HMLC without manure during the draining period).

Further, we observed a decrease in absolute MeHg concentrations in all microcosms during the second flooding period. Oscillating net de-/methylation in environments characterized by flood-drought-flood cycles have been reported earlier (Marvin-DiPasquale et al., 2014). Degradation of MeHg was reported to happen either abiotically by photodegradation or biotically by chemotrophic reductive or oxidative demethylation by microorganisms carrying the *mer*-operon (Grégoire and Poulain, 2018). Photodegradation of MeHg can be excluded as the experiment was conducted in the dark. However, demethylation could have happened as biotic reductive demethylation. A possible explanation is a MeHg detoxification reaction by microorganisms carrying the *mer*-operon (*merB*) (Hu et al., 2019; Frossard et al., 2018; Dash and Das, 2012). However, we can only hypothesize about demethylation mechanisms, as neither communities (DNA) nor gene expression (mRNA) dynamics in the soils were analyzed during the experiment.

4.4.4. Experimental limitations

Incubation experiments on a laboratory scale are a common way to study the changes in mobility of trace elements in floodplain soils (Gilli et al., 2018; Frohne et al., 2011; Poulin et al., 2016; Abgottspon et al., 2015). These study designs allow for controlled conditions and replicable results. However, controlled experiments usually fail to cover the complexity of a real floodplain soil system (Ponting et al., 2020). Our study design did not involve temperature gradients, realistic hydrological flow conditions or intact soil structure. In this study, the artificial rainwater and the soil were equilibrated by shaking for a few minutes. However, the equilibration appeared to be incomplete with respect to highly soluble chloride bearing minerals for the experiment with cornfield soil (Fig. C - 14). The incomplete equilibration is indicated by the temporal patterns of conservative ions (Cl^-, K^+ and Na^+) in soil solution (Figs. C - 7,C - 8) and the difference in Cl^- concentration between the soil solutions at t = 6 h and the same water-soil mixture shaken for 6 h (Fig. C - 14). These patterns are a result of a concentration gradient

between supernatant water and the solution in the soil pore space. They only became visible, due to high levels of conservative ions to start with, which most likely stem from a fertilization event prior to sampling the soil. Infiltration of supernatant water was facilitated by the sampling of 4 - 6 % of the total added water at each time point. This resulted in a dilution of the soil solution. Consequently, the continuous decrease in sulfate was not directly indicative for sulfate reduction, but the result of this dilution effect. However, this effect did not directly affect the release of soil bound elements (e.g. Hg, Mn, Fe, As) by e.g. reductive dissolution (Figs. 4 - 2,4 - 3,4 - 4). It should also be noted that high initial Cl^- concentrations in the soil solution, may influence Hg solubility since Cl^- is a complexant for Hg^{2+} (Li et al., 2020) and this warrants further studies on the role of inorganic fertilization on Hg mobility.

4.5. Conclusions

We studied the effect of manure addition on the mobility of Hg in soil during a flooding-draining experiment. We observed formation and size distribution changes of Hg colloids (ß-$HgS_{(s)}$, Hg-NOM) at environmental conditions in soil solution by AF4–ICP–MS. The results of this study show that manure addition 1.) diminished HgT mobility, 2.) facilitated Hg complexation with fresh NOM and formation of ß-$HgS_{(s)}$ and 3.) had only limited effect on net MeHg production in polluted and periodically flooded soils.

Mercury was mobilized upon reductive dissolution of Mn oxyhydroxides in highly Hg polluted (47.3 ± 0.5 mg kg^{-1}) and NOM poor soils. The application of manure accelerated the release of Hg, facilitated the formation of colloidal Hg and exhausted the mobile Hg pool within the first 7 days of flooding. This prevented Hg remobilization during the second flooding period. Contrastingly, Hg was mainly released as particulate bound Hg in soils with moderate Hg pollution (2.4 ± 0.3 mg kg^{-1}) and high NOM levels. Presumably, due to its higher soil organic carbon content. This relatively small pool of particulate Hg was exhausted within the first flooding period. In both soils, soil reduction enhanced net MeHg production of a substantial part of the Hg pool as confirmed by MeHg formation upon flooding-draining cycles. However, MeHg was either subsequently removed from the soil by advective transport of dissolved MeHg in the soil column or transformed by reductive demethylation. We suggest that the temporal changes in net MeHg production are limited by microbial activity of Hg methylators, given the similar net MeHg production in treatments and soils with variable dissolved Hg levels. Microbial activity is likely to be stimulated by manure addition.

The release of Hg from polluted soils to downstream ecosystems does depend on both biogeochemical conditions as well as on hydrological transport. Our experiment shows that redox oscillations (flooding-draining-flooding cycles) of a polluted floodplain soil are likely to induce pulses of both Hg and MeHg to the downstream ecosystems. This is supported with earlier studies (Poulin et al., 2016; Frohne et al., 2012; Hofacker et al., 2013). In contrast to NOM rich soil systems, we show that the Mn dynamics may govern the release of Hg in highly polluted soil systems low in NOM. Further, the application of additional

NOM in form of manure facilitates soil reduction, contributed to the transformation of Hg towards less mobile species reduced the Hg mobilization. However, effects of carbon amendments (organic amendments or biochar) are contrasting between enhancing (Li et al., 2019; Eckley et al., 2021) and diminishing (Beckers et al., 2019; Wang et al., 2020; Wang et al., 2021a) Hg mobility. We therefor stress the need for characterization of soil properties and especially NOM in future studies focusing on Hg mobility upon organic amendments (Li et al., 2019). We further emphasize the need of field trials integrating biogeochemical processes, hydrological transport and Hg soil-air exchange in order to establish Hg flux models to better understand *in situ* soil Hg mobility.

5. General conclusions and outlook

In this thesis we investigated how the influence of agricultural practices (manure addition), forest land use, and regular flooding, affect the distribution, mobilization potential, and de-/methylation dynamics of Hg in contaminated and uncontaminated soils. Further, we developed tools to trace sources of organo-Hg species in highly contaminated soils of an alpine valley in Switzerland. This was done by testing an existing method for extracting and analyzing MeHg, identifying false positive artifacts and establishing a correction factor to correct for them.

Elevated MeHg concentrations in tree groves

In chapter 2 we observed that tree groves in alpine valley may express high MeHg concentrations comparable to peat soils in boreal environments. Further, we suggest that the main source of Hg in the topsoil of agricultural grasslands close to a legacy site is likely dry deposition of atmospheric Hg with no special relation towards the point source.

Tree groves in agricultural land in the agri-environmental scheme of Switzerland are considered ecological compensation areas and have been found to be important for increasing biodiversity and supporting the abundance of organisms such as invertebrates and birds. Elevated levels of MeHg in tree grove soils suggest that these groves may serve as a source of Hg and MeHg in the terrestrial food chain in temperate alpine climate regions. However, although we observed significant differences in MeHg concentrations between groves and agricultural grassland, our dataset does not allow for a clear interpretation about the actual processes of Hg deposition and methylation in the groves and grasslands.

We suggest building up on the results of this study by establishing a Hg mass balance for both groves and grasslands. This should be done by assessing the Hg fluxes, possible Hg sources and the current Hg pools in these environments (Chen et al., 2022; Zhou et al., 2021). Exemplary for the grove environments, possible sources cover GEM deposited by leave uptake, litterfall and subsequent decomposition (dry deposition), the deposition of ionized RGM and particulate Hg (Hg_p) contaminated fields on the surface of leaves and subsequent deposition by throughfall. On the other hand, Hg may also be emitted though microbial reduction of ionized Hg in the soil column, or evacuation of dissolved Hg or Hg bound to dissolved DOM by water infiltration.

A follow up study should cover systematic collection of inputs such as i.) precipitation inside (throughfall) and outside (rainfall) of the forests, ii.) collection of litter fall and measurements of both washed (dry deposition) and unwashed leaves (deposited Hg_p) (Guédron et al., 2013) as well as iii.) assessing Hg pools in the soil profiles. For the latter, different pools should be divided into soil horizons rather than depth intervals since soil horizons are the result and location of distinct biogeochemical processes and reactions. Soil density measurements should be conducted for each horizon separately to properly assess Hg pools in these soils. Besides the Hg inputs, outputs should be assessed by regular sampling of soil porewater at the bottom of a soil profile (C-Horizon) and measurement of GEM fluxes soil atmosphere fluxes by deployment of a dynamic flux chamber e.g. as described in Osterwalder et al., 2018.

Mercury methylation is a dynamic process and Hg is constantly methylated and demethylated in the soil environment. Mercury is generally methylated under anerobic conditions; however, many environments have been identified as possible Hg methylation hot spots (Gilmour et al., 2013; Podar et al., 2015). Although the groves are not a priori anerobic environments, steep redox gradients on surfaces (e.g. soil aggregates) may also serve as potential Hg methylation hotspots. Obrist, 2012 observed distinct differences in MeHg concentrations between soil horizons in 14 US forest environments with Oa horizons expressing the highest MeHg concentrations . Thus, we suggest a systematic sampling of the soil by horizons and an assessment of horizon specific methylation rates to identify hot spots of high net-methylation potential within a soil system.

The elevated concentrations of MeHg in the groves are similar to those found in global MeHg hotspots, such as Swedish peat soils. This highlights the significance of forest environments in temperate climates as a MeHg source for wildlife. Therefore, it is necessary to conduct biochemical studies alongside studies focusing on bioaccumulation and biomagnification in terrestrial food webs. These studies will help determine the implications of increased MeHg concentrations in alpine forest environments and the impact of Hg sources like the legacy site in the Rhone valley in Visp.

Implications and suggestions for solving analytical challenges for MeHg in soils and sediments.

Numerous techniques have been applied for the analysis of MeHg and other organomercury species in solid matrices (Jagtap and Maher, 2015; Hellmann et al., 2019). Species-specific extraction is a preferred technique for analyzing organomercury species in heavily contaminated substrates such as soils and sediments. One of the reasons is the resolved issue of Hg^{2+} and $MeHg^{+}$ overlaps during chromatographic separation. We show in Chapter 3 that the extraction of MeHg using HCl and dichloromethane suggested by Brombach et al., 2015 produces small (0.0075 %) fractions of artificial MeHg. These MeHg artifact fractions are still relevant when analyzing MeHg in soils with very high Hg levels. The correction factor remained constant over different soil and sediment matrices and can be used to correct for MeHg artifacts in highly contaminated matrices. Furthermore, it is crucial to determine the total HCl leachable Hg fraction to effectively correct for artificial methylation, as this fraction potentially methylated fraction is a function of the speciation of Hg in the solid sample.

Although the here established methylation factor remained constant across different sample matrices, it can vary depending on the extraction technique used. Further previous research has suggested that the formation of MeHg artifacts may also be influenced by substrate properties such as organic matter, pH, and Hg speciation. Hence, it is of high importance to validate a method using matrices that resemble the investigated sample type when establishing an analytical method for a larger set of samples. The use of dissimilar CRMs can be misleading when evaluating their effectiveness and is to date still an issue in MeHg analytics. We call for a wider range of soil CRMs available, containing various high Hg concentrations and certified MeHg levels, to aid in the development of suitable methods for MeHg determination in soils. The producers of these materials are also urged to incorporate diverse substrate specific properties such as pH, organic matter content, and Hg speciation.

The possibilities and limitations of PCR and speciation techniques to assess Hg pollution pathways at Hg legacy sites.

In chapter 3 we combined PCR and organo mercury speciation in highly contaminated soils to draw conclusions about the pollution pathways of organo mercury species. The direct emission of organic mercury species by the chemical plant was inferred based on the detection of MeHg and EtHg, along with the absence of *hgcA* genes in two of the three polluted sites. When evaluating the pollution history of a legacy site, the analysis of organo mercury species and the abundance of methylation gene pair (*hgcAB*) provide valuable insights in combination with traditional methods such as literature research and stakeholder interviews.

It must be noted that there is no consistent evidence of a direct relationship between the concentration of MeHg and the abundance or concentration of *hgcAB* genes across different real-world settings. The transformation of Hg to MeHg still is a function of the expression of the *hgcAB* genome and the activity of microorganisms carrying it. Environmental factors such as periodic redox changes or the input of labile NOM can influence the microbial activity. In our study, the absence (or undetectably low concentration) of *hgcA* genes, coupled with the presence of EtHg - which has rarely been observed in remote areas - and elevated levels of MeHg, led us to conclude that the observed organic mercury species are of anthropogenic origin. In soils where the presence of *hgcAB* genes is detected, the established lines of evidence mentioned earlier may not be valid or sufficient to differentiate between anthropogenic MeHg and naturally formed MeHg.

Mercury release and methylation in NOM poor fluvisols.

In chapter 4, we showed that Hg sorbed to manganese oxides represent a relevant fraction in soils with comparably low natural organic matter content. This fraction expresses fast release to soil solution upon flooding and is therefore likely available for Hg methylation. By including an incubation scenario with the addition of manure we also highlighted, the relevance of highly labile and available organic matter in a soil. The organic fertilizer addition observably enhanced the formation and size distribution changes and formation of Hg colloids (β-HgS(s), Hg–NOM) during wet-dry cycles in soils. Further, we show that organic fertilizer additions can accelerated the release of Hg and facilitated the formation of colloidal Hg but also facilitate resorption of the dissolved Hg to the solid soil pool. Finally, we confirmed the hypothesis that flooding and agricultural practices do facilitate the methylation of Hg in a contaminated fluvisol. To improve our understanding of the processes responsible for Hg release and methylation, further field and microcosm studies should be conducted. Four approaches are suggested.

The application of isotopically enriched species specific Hg and MeHg isotopes is a frequently applied tool that not only provides information about net-methylation but also allows for the assessment of substrate specific methylation rates. In most studies that used enriched isotopes, Hg and MeHg were applied as either nitrate or chloride complexes, which are known to express relatively high bioavailability to Hg methylating microorganisms. To account for this bias the application of multiple Hg species with individual Hg isotopic signatures (e.g. ^{202}HgS(s), ^{201}Hg-NOM etc..) have been successfully used to draw

conclusions about the specific methylation rates of inorganic species in real world samples (Jonsson et al., 2012). Although these experimental setups are challenging and require a high level of mathematical and analytical skills, they might provide a more representative picture of the role of the different inorganic Hg binding forms (e.g. Mn-oxyhydroxides).

Pore water analyses by asymmetrical flow field-flow fractionation coupled with inductively coupled plasma mass spectrometry (AF4–ICP–MS) provided an insight into the present colloidal fractions present in the soil pore water. However, with the used setup we were not able the monitor sulfur signals due to the use of 10 mM NH_4NO_3 as eluent and the known polyatomic interferences of ^{32}S and ^{34}S with various O and N polyatomic species. In a follow up study, the use of a triple quadrupole ICP-MS in O_2 mass shift mode might provide sulfur signals when coupling AF4 to ICP–MS. For studies focusing on trace elements with affinity for sulfur (e.g. Hg or Sb) this setup might provide further insights.

As mentioned above, our results suggested that the reduction and oxidation cycle of Mn resulted in an elevated release of DOC during wet-dry cycles. This is in line with earlier studies highlighting NOM decomposition upon Mn redox cycling (Sunda and Kieber, 1994; Jones et al., 2018). Thus, in the scope of Hg methylation and Hg transport. Future studies should therefore also focus on decomposition mechanisms of NOM in systems with elevated recalcitrant NOM concentrations (e.g. forests or wetlands).

The microcosm experiments conducted in Chapter 4 did allow to investigate the release and methylation upon flooding of contaminated soils. However, further studies on laboratory and field scale are required to get an estimate about the actual transport of the released Hg in surface and groundwater. A mass balance might be established using column or soil percolation experiments with metered flow-though and coupled to a fraction collection of the soil pore water. In the field a more representative dataset might be achieved through the sampling of pore water through in situ suction plates in contaminated soil and systematic sampling of drainage water after flooding events.

A. Supplement to Chapter 2: Mercury distribution and contrasting net-mercury methylation among land use types in an alpine mountain valley.

A.1. Profiles and Correlation matrices

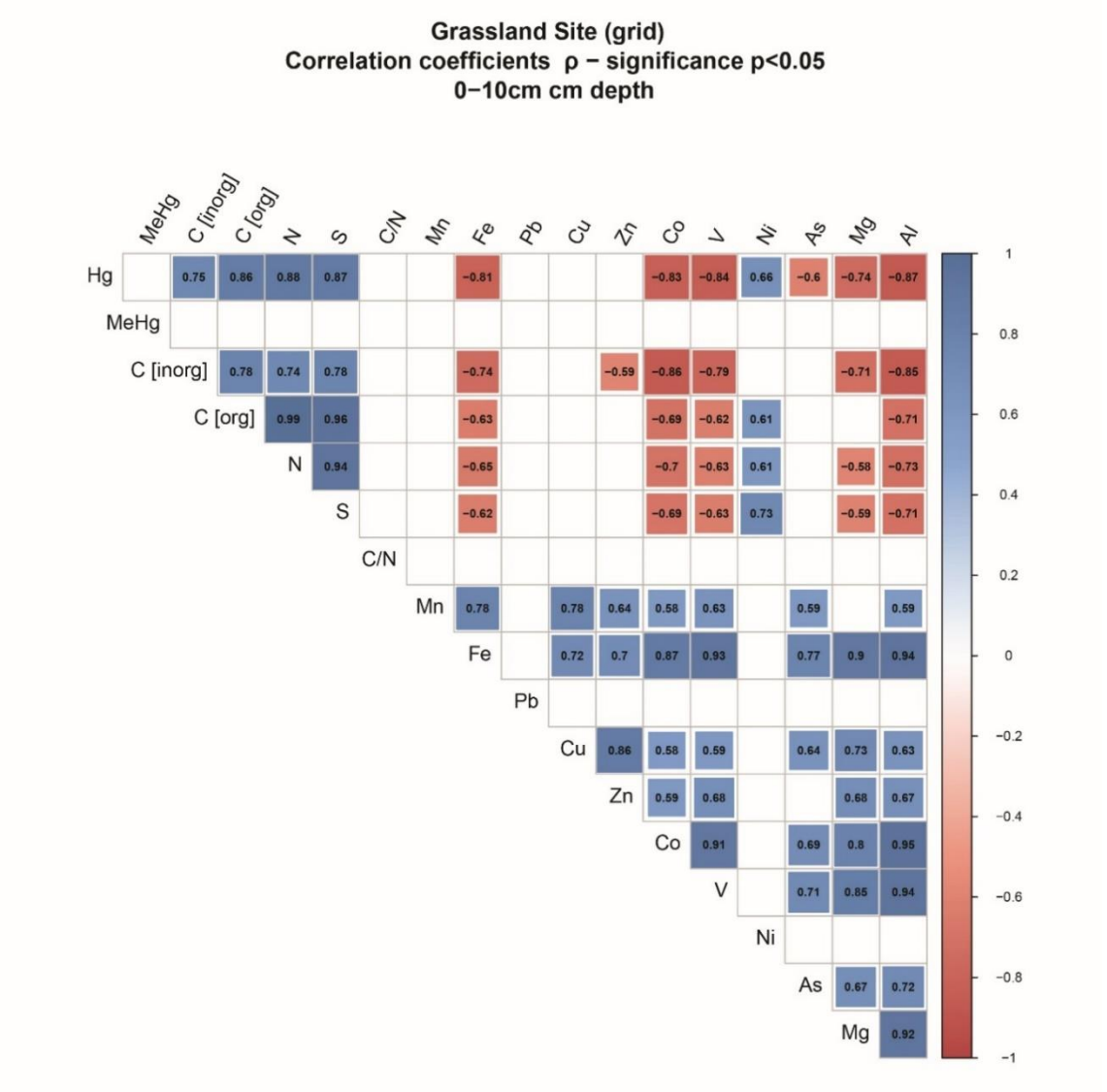

Figure A - 1 Spearman correlation matrix for soil parameters measured in grassland samples within the 0-10 cm depth interval. The continuous colour scale represents the level of correlation, with red indicating negative correlation, white indicating no correlation, and blue indicating positive correlation. Only correlations with a p-value less than 0.05 are displayed.

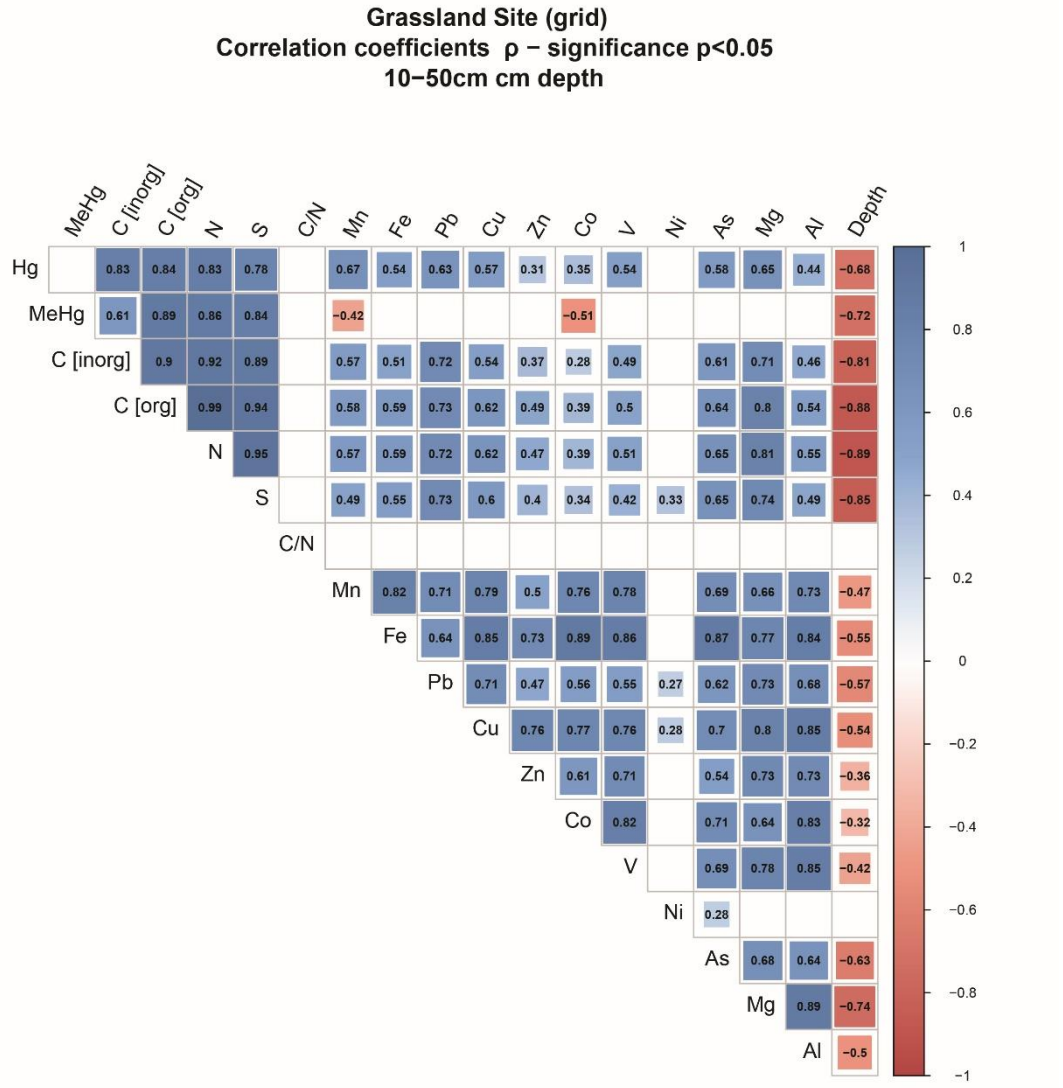

Figure A - 2 Spearman correlation matrix for soil parameters measured in grassland samples within the 10 - 50 cm depth interval. The continuous colour scale represents the level of correlation, with red indicating negative correlation, white indicating no correlation, and blue indicating positive correlation. Only correlations with a p-value less than 0.05 are displayed.

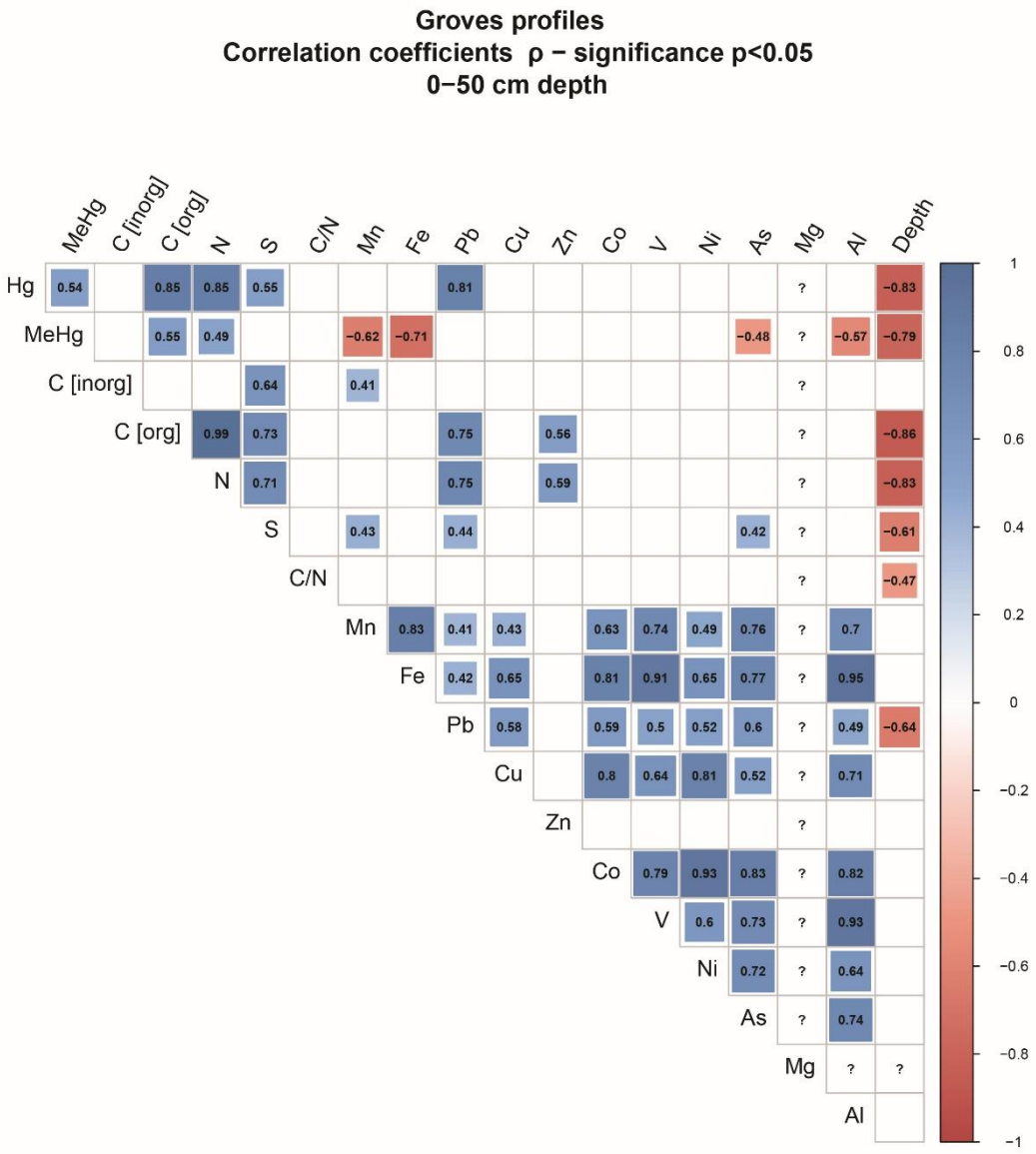

Figure A - 3 Spearman correlation matrix for soil parameters measured in grove samples within the 0-50 cm depth interval. The continuous colour scale represents the level of correlation, with red indicating negative correlation, white indicating no correlation, and blue indicating positive correlation. Only correlations with a p-value less than 0.05 are displayed.

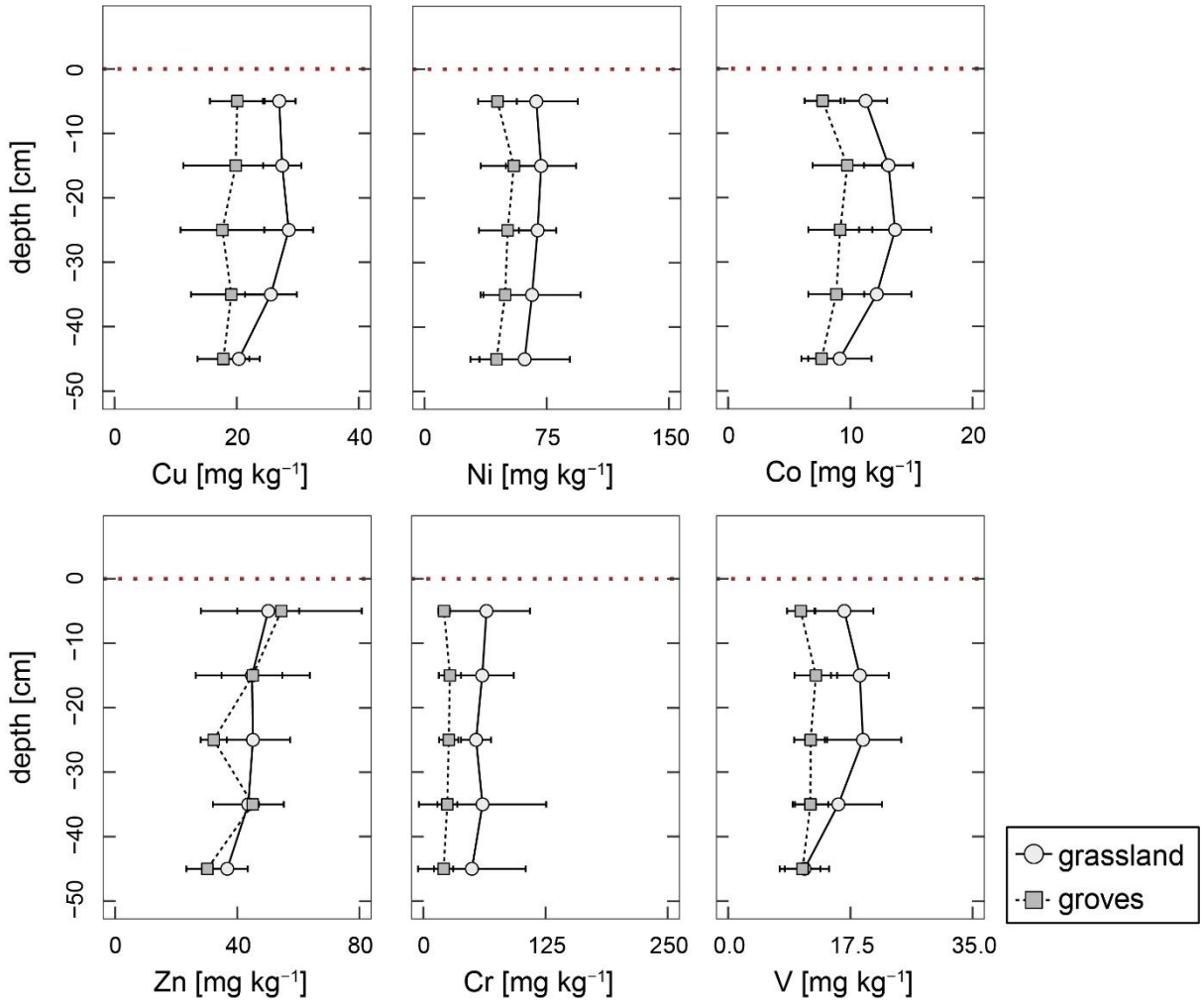

Figure A- 4 Depth profiles of Cu, Ni, Co, Zn, Cr and V concentrations in groves (grey squares) and grasslands (white cycles). Error bars represent the standard deviation of all samples within each group. Sampling was conducted at 10 cm intervals and does not necessarily correspond to distinct soil horizons.

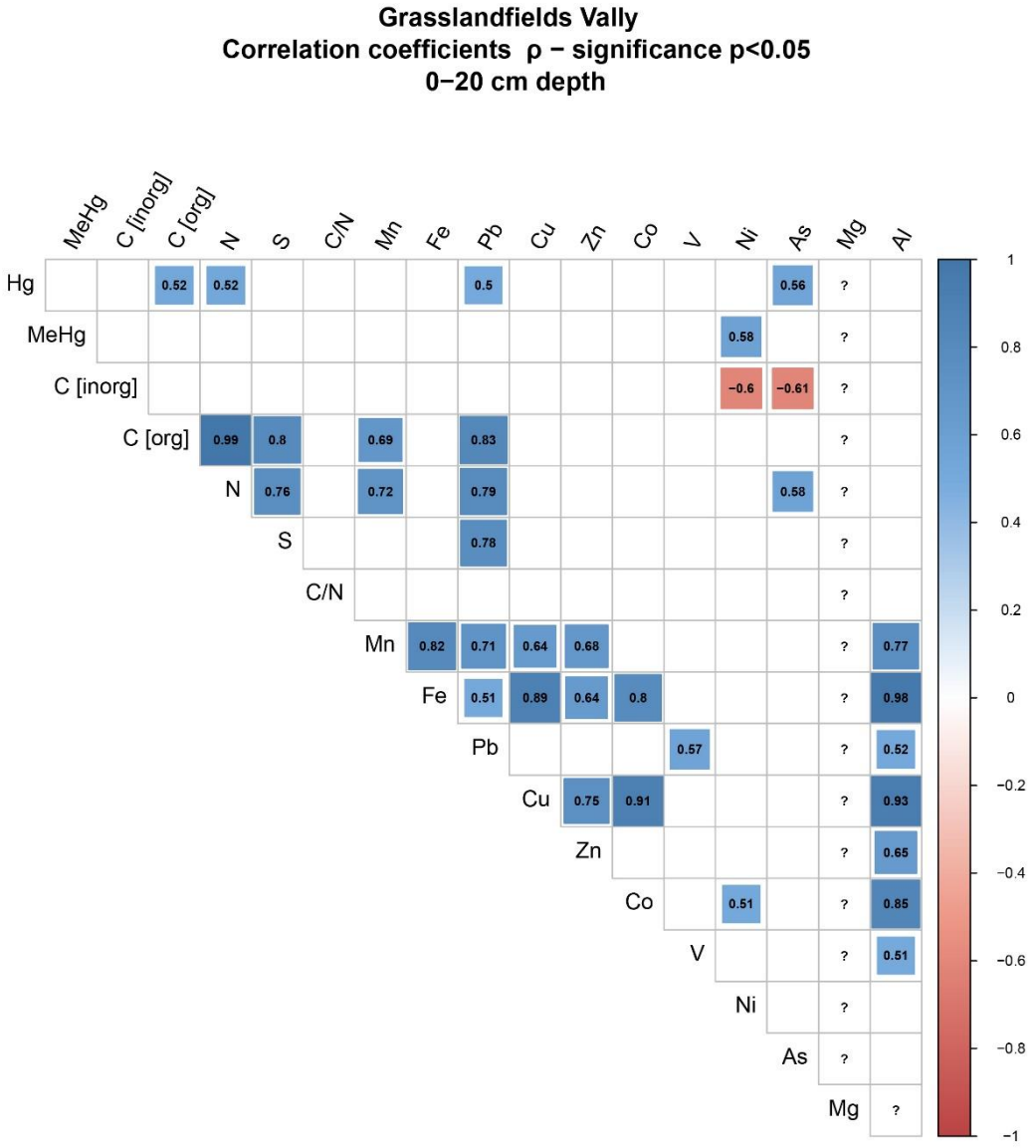

Figure A- 5 Spearman correlation matrix for soil parameters measured grassland samples of the whole sampling area. The continuous colour scale represents the level of correlation, with red indicating negative correlation, white indicating no correlation, and blue indicating positive correlation. Only correlations with a p-value less than 0.05 are displayed.

B. Supplement to Chapter 3: Organo-mercury species in a polluted agricultural flood plain: combining speciation methods and polymerase chain reaction to investigate contaminant pathways.

B.1. Sample location, sample collection, sample processing

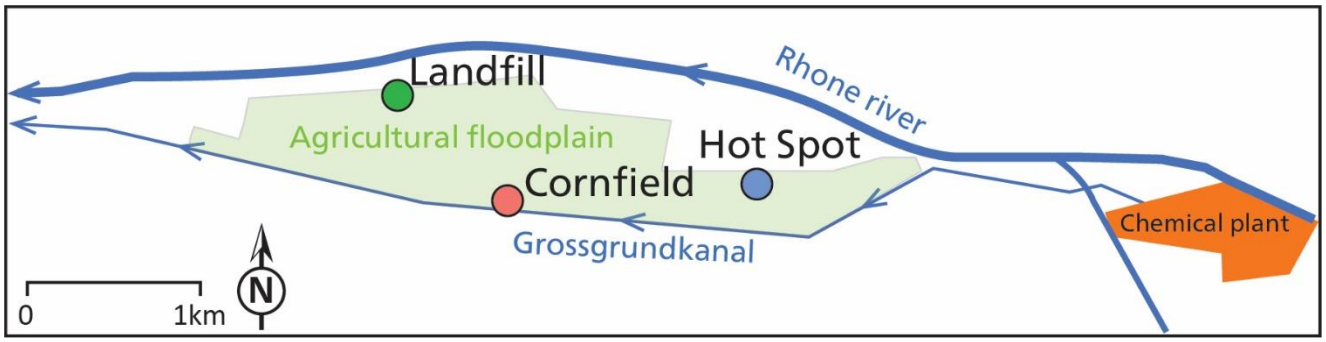

Figure B - 1 Map of the study site. Filled circles mark the sampling sites: Canal Site (red), Hot Spot Site (blue) and Landfill (green). The Grossgrundkanal (blue line) was subjected to Hg pollution between 1931 and 1976. The soils had not been remediated at the sampling date.

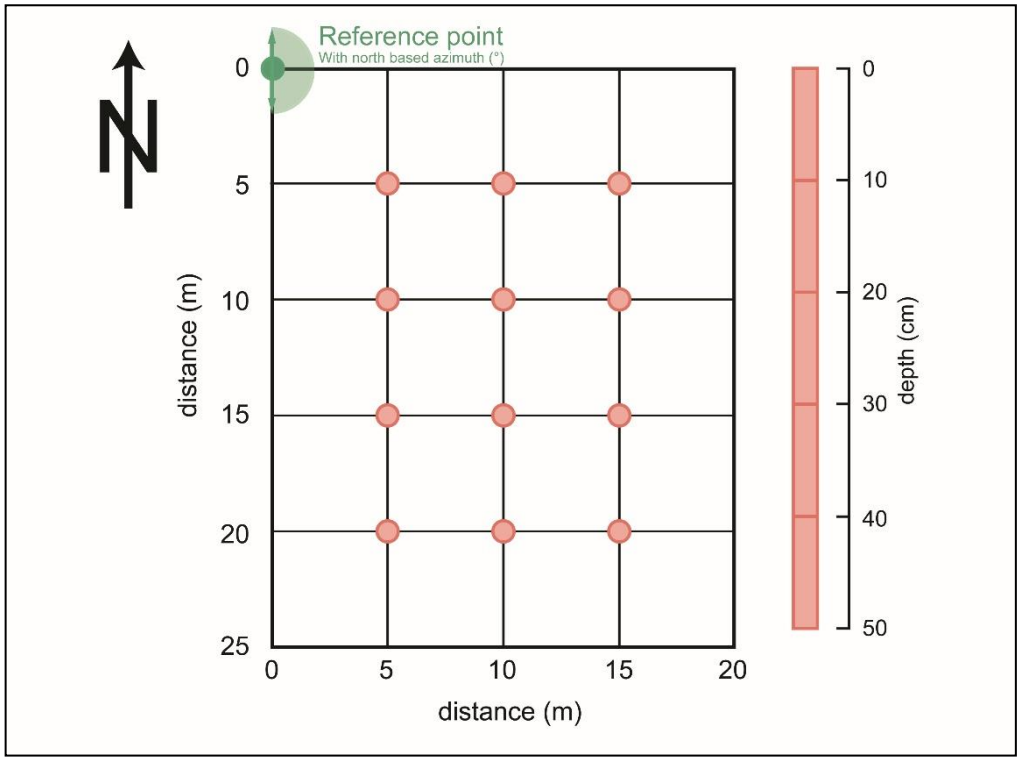

Figure B - 2 Sampling scheme for soil sampling, with reference point for the sampling grid (green) sampling points and depth intervals (rose). Sampling was conducted based on soil depth and may cut with soil horizons boundaries. Orientation of the grid is defined by a north-based azimuth.

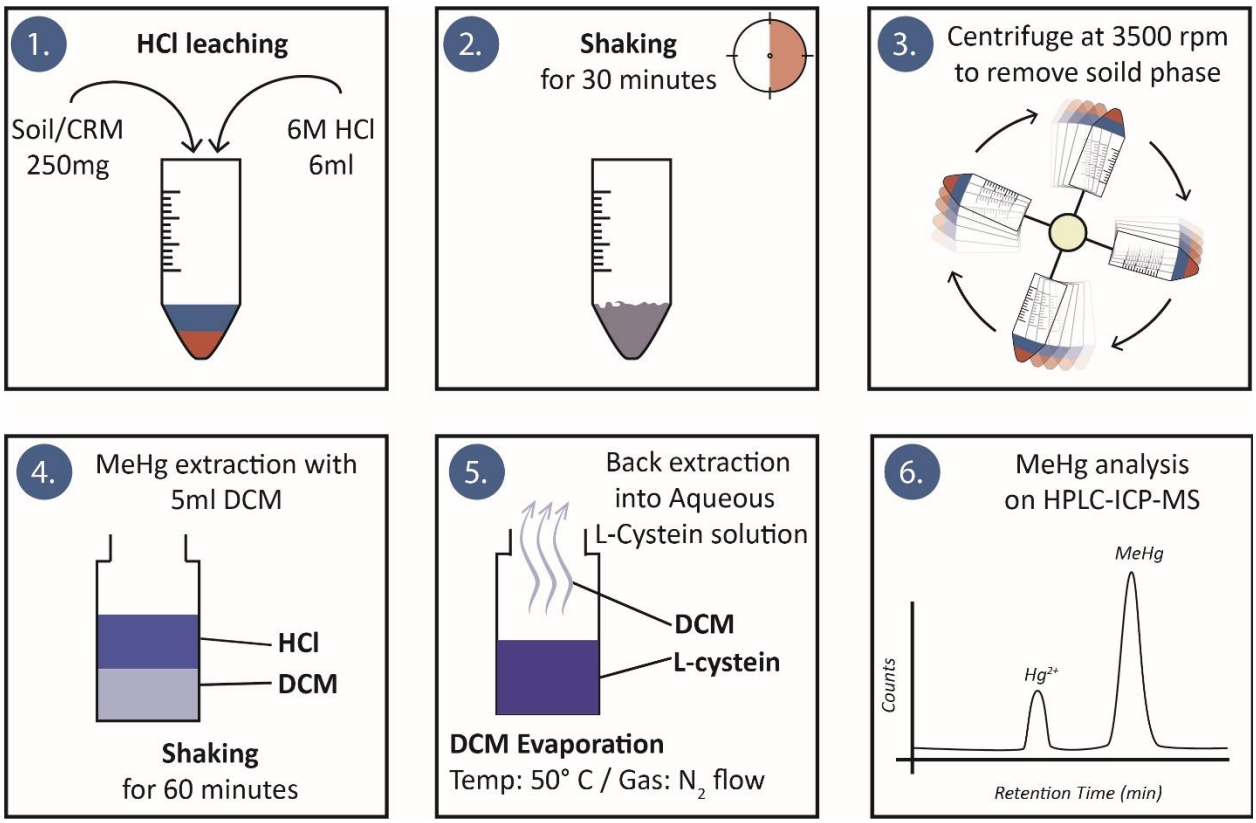

Figure B - 3 Schematic illustration of the HCl-DCM Extraction procedure used here. This extraction is based on earlier work by Brombach et al., 2015 and Gygax et al., 2019.

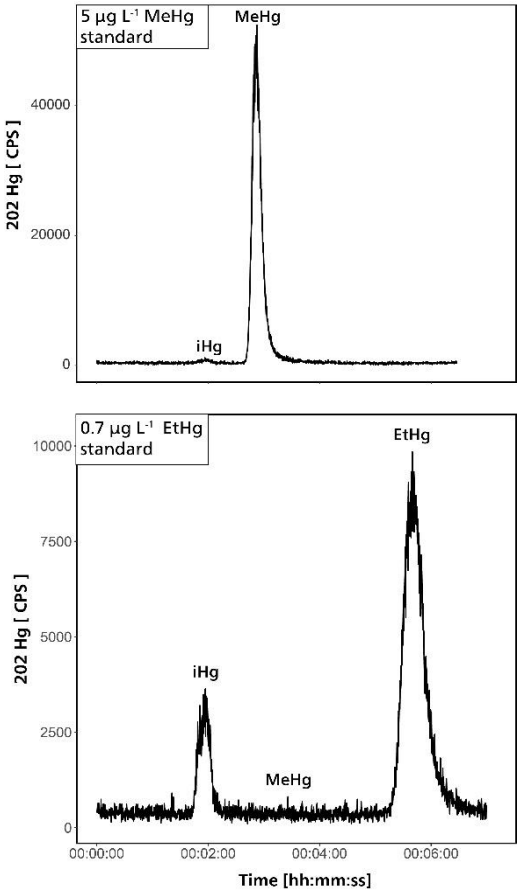

Figure B - 4 HPLC-ICP-MS Chromatogram shows counts on ICP-MS of 202Hg for a) MeHg (5 µg mL-1) and b) EtHg (0.7775 µg mL-1) standards. Both species were eluted within 7 minutes. Both standards contained traces of iHg.

Table B - 1 Coordinates of the reference point for the sampling sites and the present soil types. Coordinates are given both in the LV03 and the WGS 84 system. Uncertainties of the LV03 coordinates are ± 3 and the north-based azimuths may deviate by ± 5°.

Site	Abr.	Azimuth	Y (LV03+)	X (LV03+)	Latitude (WGS 84)	Longitude (WGS 84)	Soil Type	Land use
Canal Site	CS	5°	630062	127710	46.30012396	7.828809308	Fluvi Glayic Anthrosol	Crops (Maize)
Landfill	LF	1°	629450	128372	46.30610607	7.820908188	Toxic Technosol	Landfill
Hot Spot Site	HS	10°	631664	127757	46.3004732	7.849604341	Toxic Technosol	Pasture

B.2. Laboratory materials and Instrument methods

Table B - 2 ICP MS operating conditions for Hg and Multi-Elements (set of standards).

ICP MS Parameters		
Torch box		
RF Forward Power	1550 W	
Sample Depth	8 mm	
Gas flow rate		
Nebulizer	1.2 L min^{-1}	
Makeup	-	
Auxiliary	0.9 L min^{-1}	
Plasma	15 L min^{-1}	
Spray Chamber		
Temperature	2° C	
Collision Cell		
Helium flow (He-Mode)	4.3 mL min^{-1}	
Quadrupole		
Quantification	*Set of standards*	
	Mass	Dwell time
Multi Element	div.	diverse
ISTD (In/Rh)	103,115	90 ms

Table B - 3 Rinsing protocol for HgT analyses by ICP–MS

Solution	Contents	Rinsing time
Matrix for all samples	1 % HNO3 + 0.5 % HCl	-
Washing solution 1	Ultrapure water	5 s
Washing solution 2	0.6% v/v NH_4OH 0.8% v/v H_2O_2 0.01% v/v Triton X100 0.1% w/v EDTA Diluted 1:10 before use.	40 s
Washing solution 3	5 % HNO3 + 5 % HCl	30 s
Washing solution 4	1 % HNO3 + 0.5 % HCl	40 s

Table B - 4 Recoveries of Multi-Element, Hg, and MeHg for certified reference materials.

Standard Reference Material	Analyte	Recovery (%)	Concentration	Unit	n
ERM CC-580	*MeHg*	*90.8*	*68.1 ± 2.3*	*µg kg^{-1}*	*39*
	MeHg$_{correctecd}$	*82.1*	*61.6 ± 2.3*	*µg kg^{-1}*	*39*
PACS-3	*Hg*	*104*	*3.09 ± 0.05*	*mg kg^{-1}*	*3*
SRM 2709a - San Joaquin	*Hg*	*87.89*	*0.791 ± 0.04*	*mg kg^{-1}*	*38*
	Mn	92.99	491 ± 37	mg kg^{-1}	36
	Co	88.04	11 ± 1	mg kg^{-1}	48
	Cu	86.7	29.3 ± 1.9	mg kg^{-1}	45
	Cd	85.48	0.317 ± 0.023	mg kg^{-1}	12
	Gd	82.23	2.46 ± 0.51	mg kg^{-1}	30
	Ni	80.62	68 ± 19	mg kg^{-1}	42
	Mg	80.35	11731 ± 989	mg kg^{-1}	33
	Fe	77.32	25979 ± 2006	mg kg^{-1}	36
	Zn	77.29	79.6 ± 7.8	mg kg^{-1}	39
	As	74.43	7.81 ± 0.79	mg kg^{-1}	36
	Ce	71.14	29 ± 2	mg kg^{-1}	36
	Pb	60.51	10.4 ± 0.8	mg kg^{-1}	42
	U	48.8	1.537 ± 0.097	mg kg^{-1}	24
	Cr	43.2	56.1 ± 6.9	mg kg^{-1}	39
	V	42.79	47 ± 5	mg kg^{-1}	39
	Sr	42.42	101 ± 8	mg kg^{-1}	15
	Ba	41.22	403 ± 19	mg kg^{-1}	30
	Tl	33.51	0.194 ± 0.028	mg kg^{-1}	18
	Al	21.29	15693 ± 1412	mg kg^{-1}	33

Table B - 5 HPLC-ICP-MS operating conditions for speciation (set of standards).

HPLC Parameters		
Column	Zorbax SB-C18 4.6 x 150 mm, 5 µm	
Injection volume	100 µL	
Column temperature	20°C	
Mobile phase		
Composition	*98 % A (0.1 % w/v L-cysteine·HCl·H2O at pH = 2.3)*	
	2 % B (Methanol)	
Flow rate	*1 mL min^{-1}*	
ICP MS Parameters		
Torch box		
RF Forward Power	1600 W	
Sample Depth	7 mm	
Gas flow rate		
Nebulizer	0.9 L min^{-1}	
Makeup	0.3 L min^{-1}	
Auxiliary	0.9 L min^{-1}	
Plasma	15 L min^{-1}	
Spray Chamber		
Temperature	-5° C	
Quadrupole		
Quantification	*Set of standards*	
	Mass	Dwell time
Hg	200,201,202	50 ms
ISTD (Tl)	203,205	8 ms

Table B - 6 HPLC-ICP-MS operating conditions for speciation (isotopic dilution).

HPLC Parameters		
Column	Zorbax SB-C18 4.6 x 150 mm, 5 µm	
Injection volume	100 µL	
Column temperature	20°C	
Mobile phase		
Composition	*98 % A (0.1 % w/v L-cysteine·HCl·H2O at pH = 2.3)*	
	2 % B (Methanol)	
Flow rate	*1 mL min^{-1}*	
ICP MS Parameters		
Torch box		
RF Forward Power	1600 W	
Sample Depth	7 mm	
Gas flow rate		
Nebulizer	0.9 L min^{-1}	
Makeup	0.3 L min^{-1}	
Auxiliary	0.9 L min^{-1}	
Plasma	15 L min^{-1}	
Spray Chamber		
Temperature	-5° C	
Quadrupole		
Spike Characterization		
	Mass	Dwell time
Hg	196,198,199,200,201,202,204	30 ms
ISTD (Tl)	203,205	8 ms
Isotope Dilution		
	Mass	Dwell time
Hg	199,201,202	30 ms
ISTD (Tl)	203,205	8 ms

B.3. Soil characterization

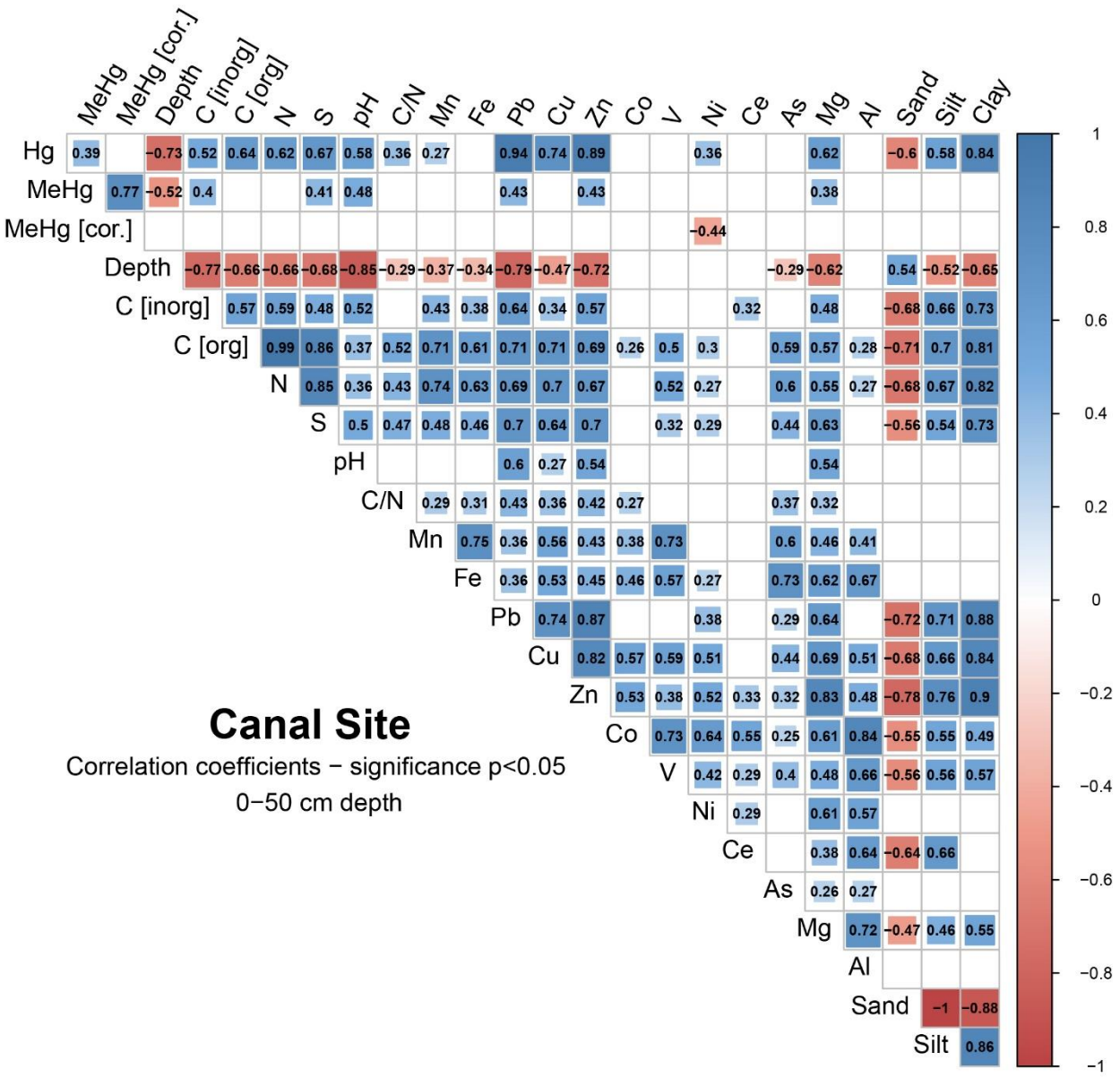

Figure B - 5 Correlation matrix for parameters measured soil samples of the Canal Site. The continuous color scale marks the level of correlation coefficients (red = -1, white = 0, blue = 1)

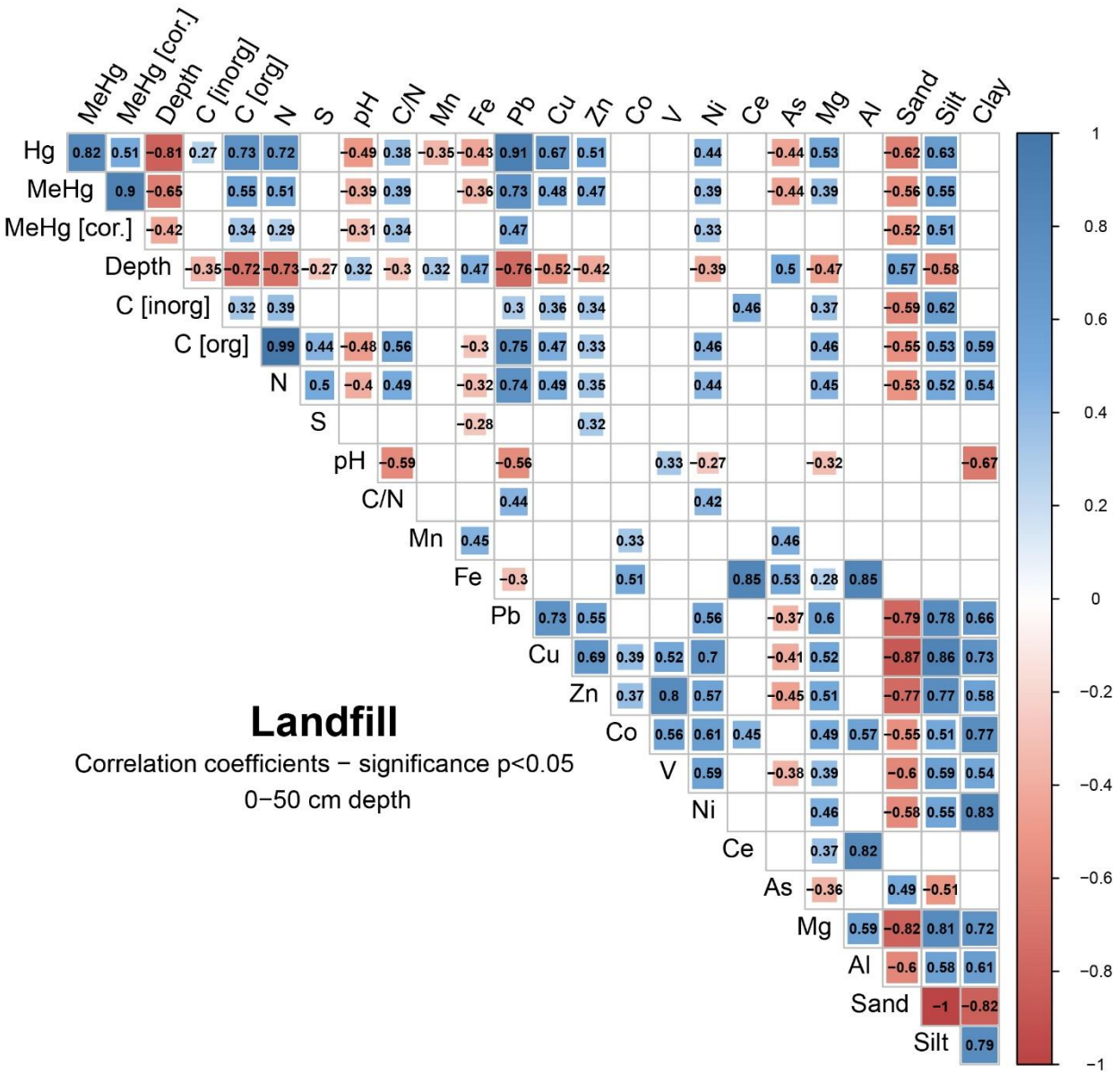

Figure B - 6 Correlation matrix for parameters measured soil samples of the Landfill. The continuous color scale marks the level of correlation coefficients (red = -1, white = 0, blue = 1)

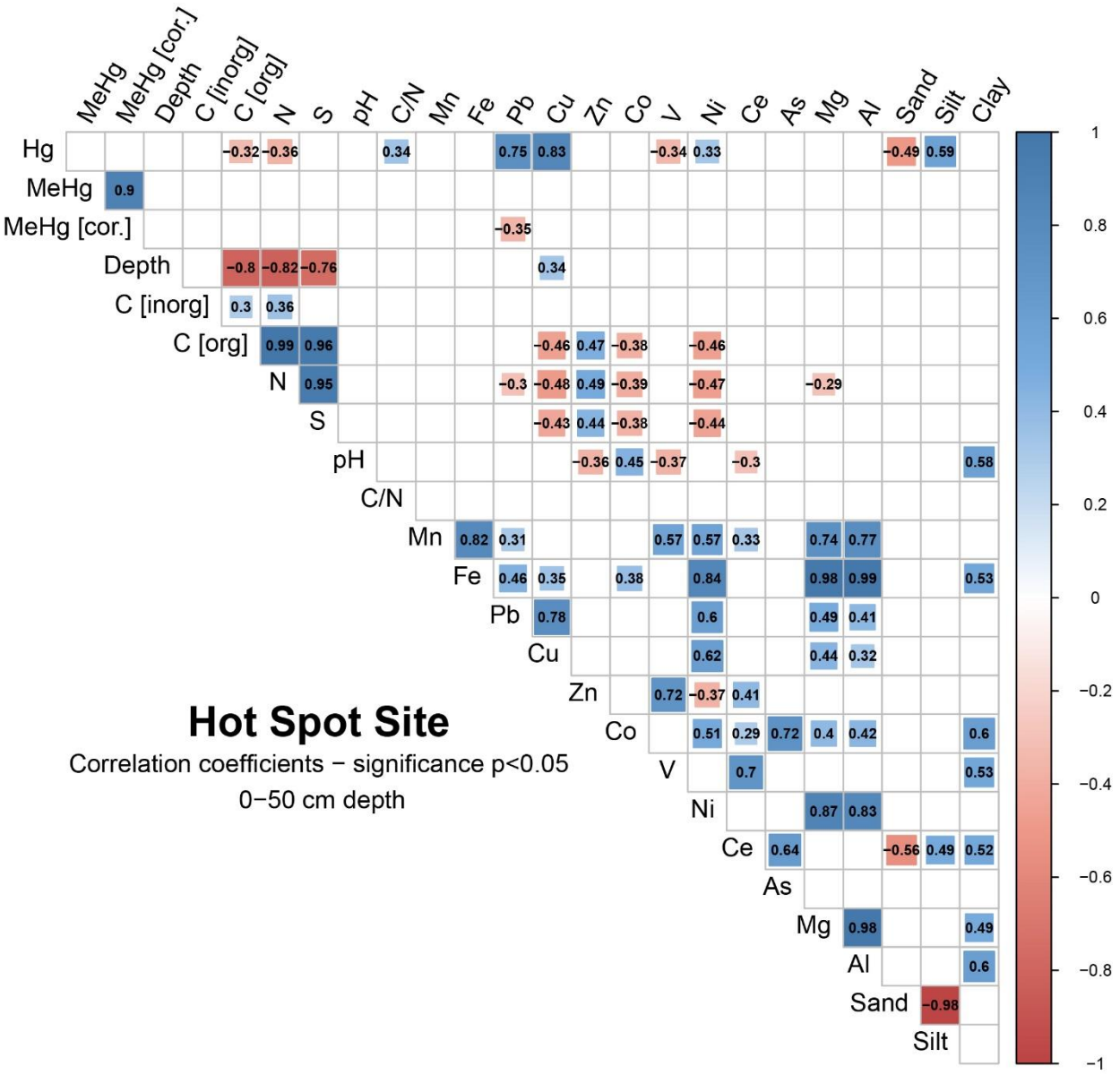

Figure B - 7 Correlation matrix for parameters measured soil samples of the Hot Spot Site. The continuous color scale marks the level of correlation coefficients (red = -1, white = 0, blue = 1)

Table B - 7 Summary statistics of soil properties of the study sites aggregeted by depth.

Site	Depth to edge [cm]	n	Hg [mg kg^{-1}]	MeHg [µg kg^{-1}]	OC wt. %	pH min	pH max	Fe wt. %	Mn [mg kg^{-1}]	Cu [mg kg^{-1}]	Pb [mg kg^{-1}]	Zn [mg kg^{-1}]	Clay [mg kg^{-1}]	Silt [mg kg^{-1}]	Sand [mg kg^{-1}]
Canal Site (CS)	0	12	36.75 ± 17.69	1.26 ± 1.69	1.78 ± 0.32	8.05	8.45	1.899 ± 0.005	507.2 ± 50.9	38.52 ± 5.79	18.7 ± 3.36	66.45 ± 10.65	2.3 ± 0.4	63.4 ± 2.6	34.2 ± 2.9
	10	12	36.76 ± 17.99	2 ± 3.29	1.72 ± 0.26	7.74	8.09	1.918 ± 0.006	508.1 ± 59.6	37.8 ± 6.15	17.86 ± 3.07	64.47 ± 10.23	2.4 ± 0.4	63.4 ± 2	34.1 ± 2.4
	20	12	27.84 ± 15.73	0.81 ± 0.73	1.67 ± 0.48	7.42	7.85	1.975 ± 0.012	583.5 ± 117.5	37.22 ± 4.71	16.97 ± 3.24	60.24 ± 8.56	2.3 ± 0.5	63.6 ± 3.2	34.1 ± 3.7
	30	12	2.33 ± 3.71	0.19 ± 0.1	0.86 ± 0.57	7.33	7.73	1.83 ± 0.014	451.4 ± 144.2	29.57 ± 3.74	10.24 ± 1.39	43.85 ± 5.72	1.6 ± 0.4	56.1 ± 10.6	42.2 ± 10.9
	40	12	0.55 ± 1.5	1.53 ± 1.54	0.56 ± 0.72	7.13	7.78	1.687 ± 0.018	412.2 ± 181	30.09 ± 10.61	9.51 ± 1.61	43.98 ± 8.87	1.3 ± 0.6	52.2 ± 12.3	46.5 ± 12.8
Landfill (LF)	0	12	53.73 ± 14.82	3.27 ± 2.52	2.1 ± 0.28	7.30	7.82	1.549 ± 0.004	377 ± 39.3	39.3 ± 6.24	22.55 ± 3.84	63.07 ± 13.06	2.3 ± 0.4	56.1 ± 4.5	41.7 ± 4.9
	10	12	54.18 ± 17.91	2.95 ± 2.72	2.05 ± 0.29	7.40	7.97	1.535 ± 0.006	375.7 ± 57.1	40.57 ± 8.16	21.87 ± 2.87	58.41 ± 9.48	2.2 ± 0.4	55.9 ± 4.4	41.8 ± 4.9
	20	12	26.09 ± 21.11	2.48 ± 1.42	1.49 ± 0.53	7.50	8.17	1.675 ± 0.014	455.4 ± 143.8	32 ± 6.92	16.4 ± 3.7	51.9 ± 14.4	2.4 ± 0.7	54.6 ± 1.8	43 ± 2.2
	30	12	2.01 ± 2.6	0.97 ± 0.94	0.96 ± 0.48	7.45	8.08	1.877 ± 0.064	766.5 ± 642.8	29.57 ± 12	13.42 ± 3.63	44.69 ± 15.68	1.9 ± 0.9	50 ± 8.3	48 ± 9.1
	40	8	0.86 ± 0.68	0.82 ± 0.6	0.87 ± 0.8	7.48	7.86	1.875 ± 0.026	544.9 ± 262.7	26.19 ± 6.53	12.36 ± 1.85	47.21 ± 22.83	1.5 ± 0.1	44.5 ± 5.9	54 ± 6
Hot Spot Site (HS)	0	12	14.18 ± 33.2	3.18 ± 1.35	4.59 ± 1.01	6.68	7.87	1.662 ± 0.003	446.2 ± 30.9	37.02 ± 7.08	14.86 ± 2	64.75 ± 9.51	3.8 ± 0.4	56.7 ± 2.3	39.5 ± 2.7
	10	12	14.43 ± 31.56	3.48 ± 1.69	3.01 ± 0.67	6.51	7.27	1.75 ± 0.003	457.3 ± 32.2	41.92 ± 9.43	15.81 ± 2.37	65.26 ± 10.96	4.1 ± 0.5	60.8 ± 4	35 ± 4.5
	20	11	18.33 ± 40.77	5.58 ± 2.64	2.64 ± 0.52	6.51	7.35	1.742 ± 0.003	439.6 ± 33	40.42 ± 7.56	15.68 ± 2.68	61.4 ± 11.13	4.1 ± 0.5	60.2 ± 4.8	35.7 ± 5.2
	30	9	33.38 ± 80.77	3.73 ± 1.84	2.01 ± 0.49	6.58	7.70	1.887 ± 0.015	453 ± 145.5	46.54 ± 23.65	18.2 ± 7.3	61.63 ± 16.59	4.1 ± 0.6	59.2 ± 3.2	36.7 ± 2.7
	40	2	62.51 ± 87.86	4.84	0.97 ± 0.63	6.71	7.83	1.679 ± 0.011	327.9 ± 109.2	66.25 ± 31.56	15.54 ± 1.15	40.9 ± 10.16	3.5 ± 2.2	57.6 ± 3	39 ± 0.8

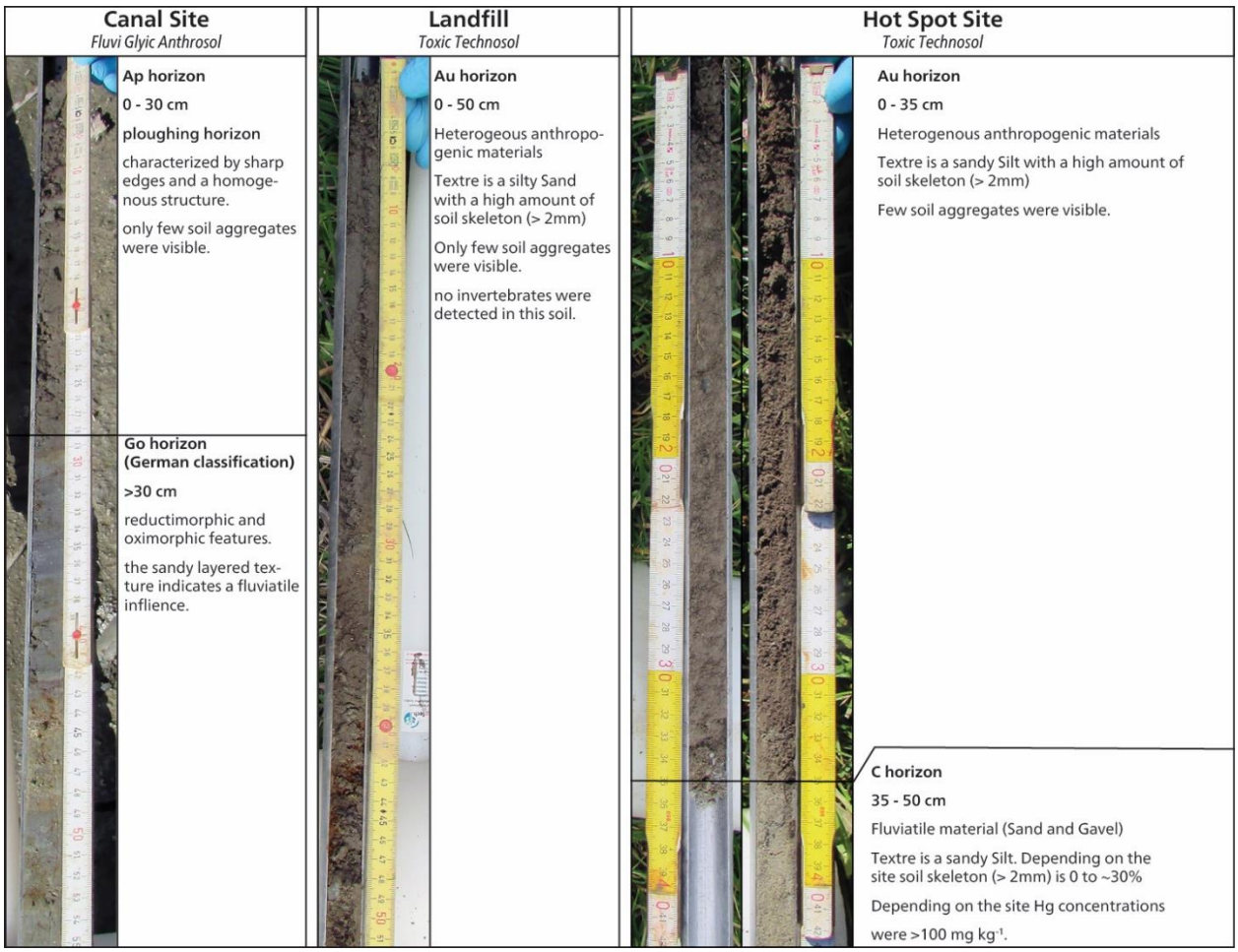

Figure B - 8 Soil descriptions for the soils at the sampling sites. Pictures show representative cores for all cores taken at each site (n=12).

Table B - 8 Results of iHg spiking (Experiment B) in blank samples. The Hg^{2+} spike was added prior to the addition of HCl.

iHg_{spiked} ng	$MeHg_{recovered}$ ng	n
-	<0.016	3
6.5 ± 0.02	0.6 ± 0.01	3
12.2 ± 0.06	1.24 ± 0.03	3
25.5 ± 0.17	2.53 ± 0.06	3
51.1 ± 0.1	4.99 ± 0.1	3

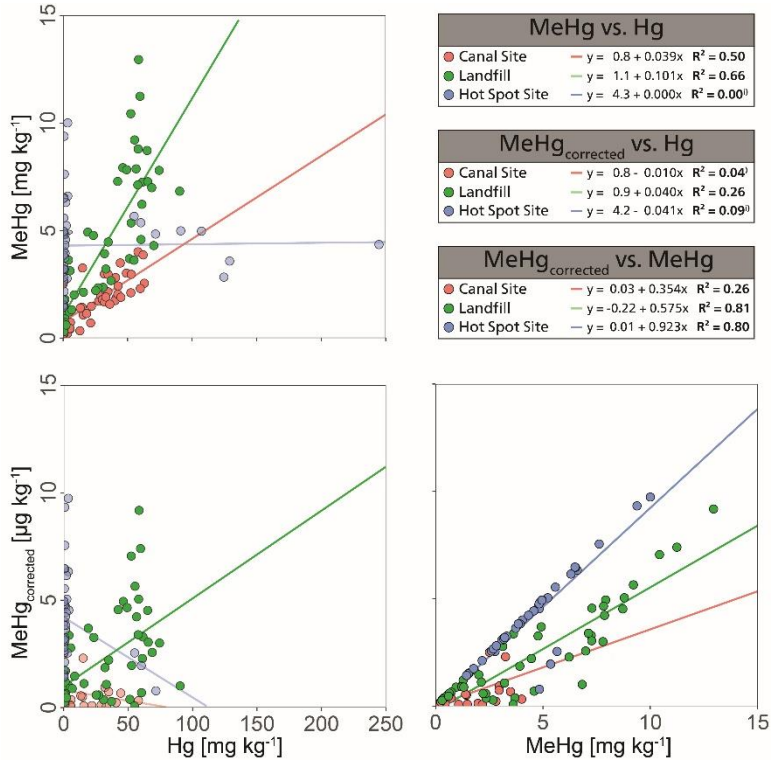

Figure B - 9 Scatterplot displaying relationships between soil HgT, MeHg, and corrected MeHg concentrations for the canal site (red), landfill site (green), and hot spot site (blue). Lines show the fitted linear regression models at each site. Linear models are displayed in the boxes

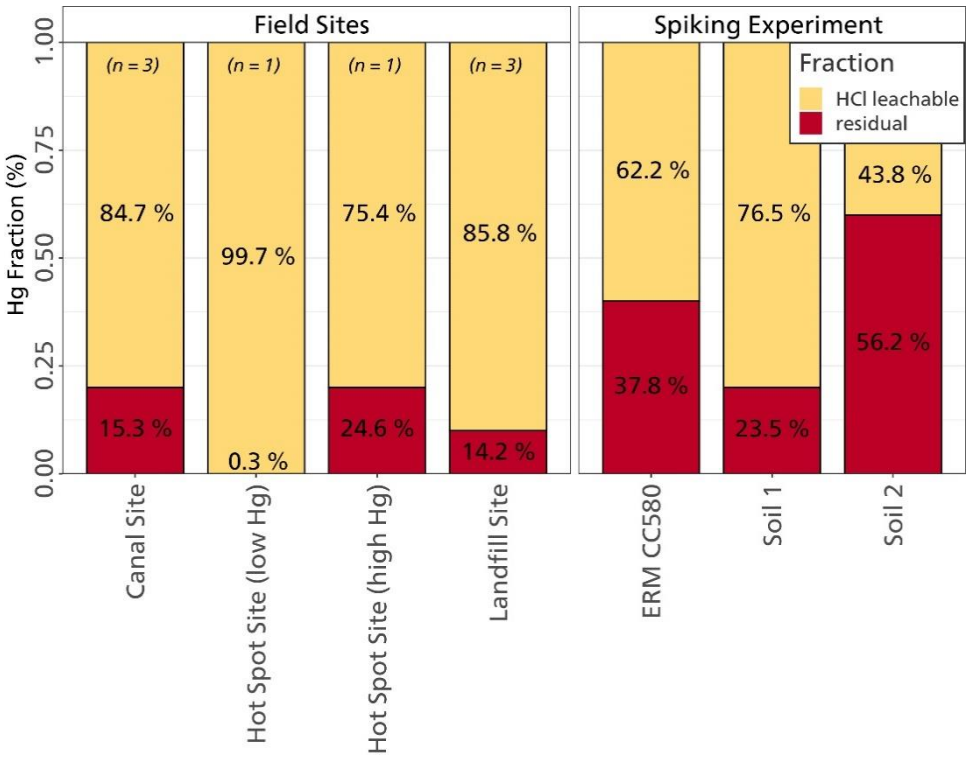

Figure B - 10 Relative amounts of the HCl leachable Hg (yellow) and the HNO_3 leachable residual (red) fractions. HCl leachable fraction are used for correction of MeHg concentrations with Eq.3.4.

C. Supplement to Chapter 4: Mercury mobility, colloid formation, and methylation in a polluted fluvisol as affected by manure application and flooding-draining cycle.

C.1. Sampling site and soil sampling

Soils were sampled from agriculturally used fields situated between Visp and Raron in the Rhone Valley Wallis, Switzerland. The sampling location is situated next to a wastewater discharge channel 5 km downstream from a chemical plant historically using Hg in different processes (chlor-alkali electrolysis, acetaldehyde- and vinyl chloride production). Into this canal the company released their untreated effluents form the 1930's to the 1970's , when a new water treatment plant was installed. There, the fields were subject to Hg pollution by Hg contaminated canal sediments (Grossgrundkanal) which were used for fertilization of the nearby fields until the 1980s Ever since the polluted soils have been ploughed and turned over. Pollution decreases gradually with distance from the canal and the soil marks a sharp decrease at the plowing horizon at ca. 30 cm depth (Gygax et al., 2019; Glenz and Escher, 2011). Further, an artificial dam separates the channel from the fields inhibiting fast drainage of the fields after heavy rain events.

Samples were taken on 30th of September 2019 along a Hg gradient on a cornfield and a pasture field. Exact coordinates are given in Table S1 a map of the area is shown in Fig. A-1. A composite sample of approximately 10 kg of soil was sampled from 10 points along the Hg gradient. After sampling, roots were removed and the samples were pulled in a HDPE bucket, well homogenized, filled in PE zip bags and stored on ice for transportation. In the laboratory, one part of the fresh soil was sieved to <2 mm, further homogenized and used for the incubation. The other part was stored at -20° C.

Fresh liquid manure was sampled from a slurry pit of a cattle farm close to the sampling site. This manure is frequently used to fertilize the soils in the area. Two liters of sample were taken after homogenizing the manure in the slurry pit with an agitator for more than 10 minutes. The samples were kept on ice in HDPE bottles for transportation. In the laboratory, the manure was sieved to <0.5 mm and homogenized. The sample was divided in 2 aliquots and kept for storage at -20° C for characterization and 4° C for addition to the incubation.

C.2. Laboratory materials

Trace metal grade acids, HPLC grade solvents, and ultra-pure water (>18.2 MΩ*cm at 25 °C, Milli-Q® IQ 7000, Merck, Darmstadt, Germany) were used in this study. Glassware was cleaned by soaking in acid baths (both 10% HNO_3 and 10% HCl) for at least 24 h and rinsing three times with ultra-pure water. Further, jars used for the incubation were sterilized in an autoclave for a minimum of 30 min at 120°C. Soil solution samples were stored in Corning® sterile PP tubes for trace metal, DOC and ion chromatography (IC) analyses. Borosilicate glass vials with PTFE caps (Wheaton®, DWK Life Sciences GmbH, Wertheim/Main, Germany) were used for storage of Hg soil solution samples.

C.3. Chemical characterization of soil and soil solution

All solid samples were freeze dried to avoid a loss of Hg prior to analyses (Hojdová et al., 2015). After drying, the samples were milled and homogenized using an automatic ball mill (MM400, Retsch, Haan, Germany) with stainless steel beakers and balls. In between samples, the beakers were cleaned using phosphate free detergent (RBS™), deionized water and ethanol.

Pre-incubation was conducted in 10 L HDPE buckets in the dark for 7 days at 22 °C and 60% relative humidity (RH) in order to prevent high microbial respiration at the onset the experiment. Microbial respiration is likely to be increased by sieving the soil. After pre-incubation, 50 g of each soil were sampled, and oven dried in order to determine moisture content or soil dry weight.

Soil Hg concentrations were measured by thermal desorption atomic fluorescence spectroscopy (DMA-80 evo, Milestone Srl, Sorisole) with a limit of detection of <0.01 ng Hg. Soils were analyzed in a working range of 300 - 800 ng Hg. Blank background levels after a 500 ng Hg standard were <1 ng Hg. After every 10^{th} sample, two liquid standards (300 ng and 500 ng Hg from a 1 mg L^{-1} Hg standard solution (ICP inorganic Hg standard solution, TraceCERT®, Sigma-Aldrich, St. Louis, United States of America) were measured to check the instruments stability and to calculate correction factors. Recovery of liquid standards was within the range of 95 to 105 %.

Soil metals were leached by microwave assisted acid digestion (250 mg soil, 4ml 69 %, HNO_3, 2 ml H_2O_2). The leachate and soil solution trace and major metal concentrations (in 1% HNO_3) as well as soil solution HgT (in 1% HNO3, 0.5% HCl) concentrations were quantified by Inductively Coupled Plasma Mass Spectrometry (ICP-MS; 7700x ICP-MS, Agilent Technologies, Santa Clara, United States of America). Calibration curves were prepared fresh from both a multi element and a Hg standard solution (TraceCERT®, Sigma-Aldrich, St. Louis, United States of America). An internal standard of Indium (m/z 115) or Thallium (m/z 205) was continuously injected for trace metals and Hg, respectively. Calibration standards were measured repeatedly, during the run to check the stability of the system. The rinsing protocol shown in Table S2 was used during HgT analyses in order to avoid memory effects. The LOD for Hg in soil solution was <0.01µg L^{-1} for all soil solution analyses.

A selective HCl - dichloromethane (DCM) extraction described elsewhere was optimized for high throughput (64 Samples per run) to extract soil methylmercury (MeHg) (Brombach et al., 2015; Gygax et al., 2019). Briefly, 250 mg of sample was suspended in 5 mL of 35% HCl and 5 mL ultrapure water in a 20 mL borosilicate glass vial (Wheaton, Milleville, NJ, UK). After 30 min overhead shaking, the vial was centrifuged for 15 min at 680 g (3500 rpm) and the supernatant transferred to a second 20ml vial. Then, the lipophilic organic Hg was extracted by addition of 5mL DCM and overhead shaking for 60 min. The DCM solution was pipetted of in a third 20 mL borosilicate glass vial. For aqueous back extraction 2 mL of 0.1% L-Cysteine were added to the DCM extract and the DCM was evaporated with a constant flow of N_2 on a heating bloc at 50°C. The samples where weighted using an analytical balance after each extraction step to correct for sample losses upon pipetting

or evaporation. Detailed validation of this method can be found in Gygax et al., 2019. The final extracts were stored at 4°C and analyzed within 48 hours. They were analyzed by coupling a High-Pressure Liquid Chromatograph (HPLC 1200 Series, Agilent Technologies, Santa Clara, United States of America) to the ICP-MS (HPLC-ICP-MS). The mobile phase consisted of 0.1% L-Cysteine (98%) and Methanol (2%). The detailed HPLC method is given in Table S3. Table S4 contains certified reference material (CRM) concentrations and recoveries of Hg and MeHg. Limit of detection (LOD) was calculated from the daily calibration curves. The LOD was <0.02 µg L^{-1} for the HPLC-ICP-MS method and <0.16 µg kg^{-1} in soil samples.

Soil Carbon (C), Nitrogen (N) and Sulfur (S) were measured with an Elementar® vario EL analyzer. After every 15^{th} sample, standards of sulfanilic acid and glutamic acid were measured to assure the instruments stability and to calculate correction factors. SOM was determined by loss on ignition (LOI) (550°C for 2h). Organic Carbon (OC) was calculated by subtracting the C concentration of the LOI sample from the original C concentration.

Soil pH was measured in an equilibrated 0.01M $CaCl_2$ solution (1:5 soil:liquid ratio) using a pH-probe (SenTix® 41, WTW, Weilheim, Germany). The probe was calibrated using a two-point calibration using standard solutions (ROTI® Calipure, ROTH, Arlesheim, Switzerland) of pH 7 and 9. During the incubation, pH probes for soil solution pH were calibrated on each sampling day. Oxidation reduction potential (ORP) was measured using a ($Hg/HgCl_2$) ORP probe (Lazar Research Laboratories, Los Angeles, United States of America) and checked with a 200mV ORP standard solution (Hach Company, Loveland, United States of America) on each sampling day.

Soil solution major inorganic ions were analyzed by Ion Chromatography using a Dionex Aquion™ conductivity detector system (Thermo Fisher Scientific Inc., Waltham, United States of America). Details on instrument specifics are given in Table S5.

X-ray diffraction analyses (XRD) was performed on both soils (HMLC and LMHC). XRD powder patterns were measured with a Panalytical $CubiX^3$ diffractometer using a Cu tube (Kα-radiation: λ=1.54Å at 45kV/40 mA), secondary monochromator and automatic divergence slits. 2 theta diffractograms were processed using PANalytical X'Pert HighScore Plus.

Colloidal size fractions and elemental concentrations of the filtrates were analyzed by Asymmetrical Flow Field-Flow Fractionation (AF4, AF2000, Postnova analytic, Landsberg am Lech, Germany) coupled to a UV_{254nm} absorbance detector, a Fluorescence detector (RF-20A, Shimazu, Reinach, Switzerland) and an ICP-MS (7700x, Agilent Technologies, Santa Clara, United States of America). The hydrodynamic size and small colloids molecular mass were calibrated externally. The relationship between molecular mass and hydrodynamic diameter is also given in Fig. A-6e. Hydrodynamic diameter calibration was obtained using Hc3 (d_h = 7 nm) and ultra-uniform gold nanoparticles (d_h = 19 ; 39 ; 59 nm). The bigger nanoparticles elute after the end of fractionation when the crossflow is turned off (xf0, red vertical lines at retention time of 20.8 min), while using a linear decrease in crossflow starting at 2 mL min^{-1} over 20 minutes (xf2grad). In this case, the upper size limit of fractionation was evaluated at d_h = 45 nm (Fig. A-6a). In the case of a linear decrease of crossflow starting at 1

mL min^{-1} (xf1grad, B), this upper limit rose to d_h =80 nm, and most of the colloidal Hg is eluted before the end of elution. As shown in Fig. A-6c, the size of small Hg-particles (indicated with a *) is identical while using one or the other program. Based on the effective cut-off of the filter use for preservation (450 nm), the upper size of colloids was surprisingly low, but suggest artefactual removal of higher size colloids. The recovery of those was shown to be more effective using selective centrifugation and filtration with 5 µm cut-off and the use of lower ionic strength mobile phase (µM) than the one used (mM) may probably have increased the interaction of larger inorganic colloids, if present, with the AF4 membrane. For the sample (HMLC +MNR, day 2) shown in Fig A-6, it must be noted however that the Hg recovery was of 70% and 74% for xf2grad and xf1grad respectively, suggesting that the loss of bigger colloids has little influence on Hg behavior. For the xf2grad program, the elution of smaller colloidal Hg was related to molecular mass (Mw) using separate injections of PSS (Fig. A-6d) and related to hydrodynamic size elution (Fig. A-6e).

To further characterize the colloids, we collected fractions of soil solution during AF4 runs by using a T-piece. Factory new, borosilicate headspace GC-vials were used for fraction collection. During the manual fraction collection vials were constantly flushed with argon. After fraction collection the samples were kept stable in 0.01M NH_4NO_3 in air-tight GC vials at 4°C in the dark until further analyses (> 240 days). The collected fraction were studied by Continuous Flow Analysis Inductively Coupled Plasma Time-Of-Flight Mass Spectrometry (ICP-TOF-MS). The ICP-TOF-MS used in this study is the commercially available icpTOF (TOFWERK AG, Thun, Switzerland). The instrument uses the ICP generation, ion-optics, and the collision/reaction cell (Q-Cell) of an iCAP-RQ instrument (Thermo Scientific, Bremen, Germany). In the icpTOF, the original quadrupole mass analyzer of the iCAP-RQ is replaced by a quadrupole notch filter and TOF mass analyzer, both built and integrated by TOFWERK. Further information about the instrumentation can be found elsewhere (Erhardt et al., 2019). Rh in 1% HNO_3 was introduced as an internal standard using a T-piece directly before the nebulizer.

C.4. Incubation and sampling setup

One application of liquid manure (0.6 % (w/w)) represented the recommended minimal application of 0.67 t km^{-2} following the principles of fertilization of agricultural crops in Switzerland (Richner and Sinaj, 2017). We assumed an affected soil depth of 10 cm and soil bulk density of 1.2 g cm^{-3}. This value is in the range of bulk density of soils from this area previously measured in our lab.

Scheme of the incubation setup is shown in Fig. A-2. During the incubation, the MCs were covered with parafilm which could not fully prevent exchange with the ambient air. A list as well as a flow chart of sample preparations and aliquots for the specific analyses is given in Table S6 and Fig A-5. Approximately, 4-6 % of the added water was sampled during each sampling step. The evolution of absolute and relative sampling volumes is given in Fig. A-3.

C.5. Complementary statements about colloidal fraction and nanoparticulate formation.

We visually observed black precipitates (Fig. A-8 in MCs (HMLC +MNR)) suggesting the precipitation of sulphide minerals and potentially HgS(s). However, we did not observe any sulfur nor Hg signals during the continuous flow ICP–TOF–MS run. This is presumably due to the long storage time and unideal conditions during sample preservation until analyses (> 240 days).

C.6. Tables

Table C - 1 GPS coordinates of the sampling locations.

Sample	Latitude	Longitude
Corn field (HMLC)	46°17′59.900″N	7°49′43.124″E
Pasture field (LMHC)	46°18′04.825″N	7°49′00.229″E
Slurry pit manure (MNR)	46°18′10.435″N	7°49′56.082″E

Table C - 2 Rinsing protocol for HgT analyses by ICP–MS

Solution	Contents	Rinsing time
Matrix for all samples	1 % HNO3 + 0.5 % HCl	-
Washing solution 1	Ultrapure water	5 s
Washing solution 2	0.6% v/v NH_4OH 0.8% v/v H_2O_2 0.01% v/v Triton X100 0.1% w/v EDTA Diluted 1:10 before use.	40 s
Washing solution 3	5 % HNO3 + 5 % HCl	30 s
Washing solution 4	1 % HNO3 + 0.5 % HCl	40 s

Table C - 3 HPLC method details for MeHg analyses

Parameter	HPLC-ICP-MS
HPLC Column	Zorbax SB-C18 4.6 x 150 mm, 5 µm
Injection volume	100 µL
Column temperature	20°C
Mobile phase flow rate	1 ml min^{-1}
Mobile phase composition	2 % MeOH 98 % of 0.1 % w/v L-cysteine & 0.1 % L-cysteine·HCl·H_2O pH = 2.3

Table C - 4 Measured CRM concentrations and recoveries for MeHg and Hg. MeHg was measured by HCl-DCM extraction HPLC–ICP–MS. Hg was analyzed by thermal desorption AFS using a DMA-80 evo.

CRM	Type	MeHg (µg kg^{-1})	$MeHg_{recovery}$ (%)	n	Hg (µg kg^{-1})	$Hg_{recovery}$ (%)	n
ERM® - CC580	Estuarine sediment	77.3 ± 3.3	103.1	3	-	-	-
SRM® 2709a	Agricultural soil	-	-	-	906 ± 57	100.7	9
NRC® PACS-3	Marine sediment	-	-	-	3155 ± 149	105.8	3

Table C - 5 Ion Chromatography method.

Analytes	Pre column	Column	Suppressor	Eluent	Flow rate
Cations	Dionex™ IonPac™ CG12A 4x50 mm	Dionex™ IonPac™ CS12A 4x250 mm	Dionex™ CSRS™ 300	20mM Methanesulfonic Acid (MSA)	1 ml min^{-1}
Anions	Dionex™ IonPac™ AS12A 4x50 mm	Dionex™ IonPac™ AS12A 4x200mm	Dionex™ AERS™ 500	2.7mM Na_2CO_3 0.3mM $NaHCO_3$	1 ml min^{-1}

Table C - 6 List of sample preparations and aliquots for the specific soil solution analyses performed during the incubation.

Analyses	Filter size	Sample volume (ml)	Treatment
Rinse	10 µm	2	-
pH and Eh, $Hg/HgCl_2$	10 µm	4	-
Trace metals	0.02 µm	2	8 ml 1 % HNO_3
Trace metals	10 µm	2	8 ml 1 % HNO_3
Hg	0.02 µm	3	5 ml (1 % HNO3 + 0.5 % HCl)
Hg	10 µm	3	5 ml (1 % HNO3 + 0.5 % HCl)
Dissolved organic carbon	0.02 µm	3	5 ml MilliQ + 50 uL 10% HCl
Particulate organic carbon	10 µm	3	5 ml MilliQ + 50 uL 10% HCl
Ion chromatography	0.02 µm	1.5	4.5 ml MilliQ
On days 2, 5, 9 after each flooding.			
AF4	0.45 µm	5	Glovebox under N_2 atmosphere.
Trace metals and Hg	0.45 µm	3	5ml (HNO_3 1%, HCl 0.5%)

C.7. Figures

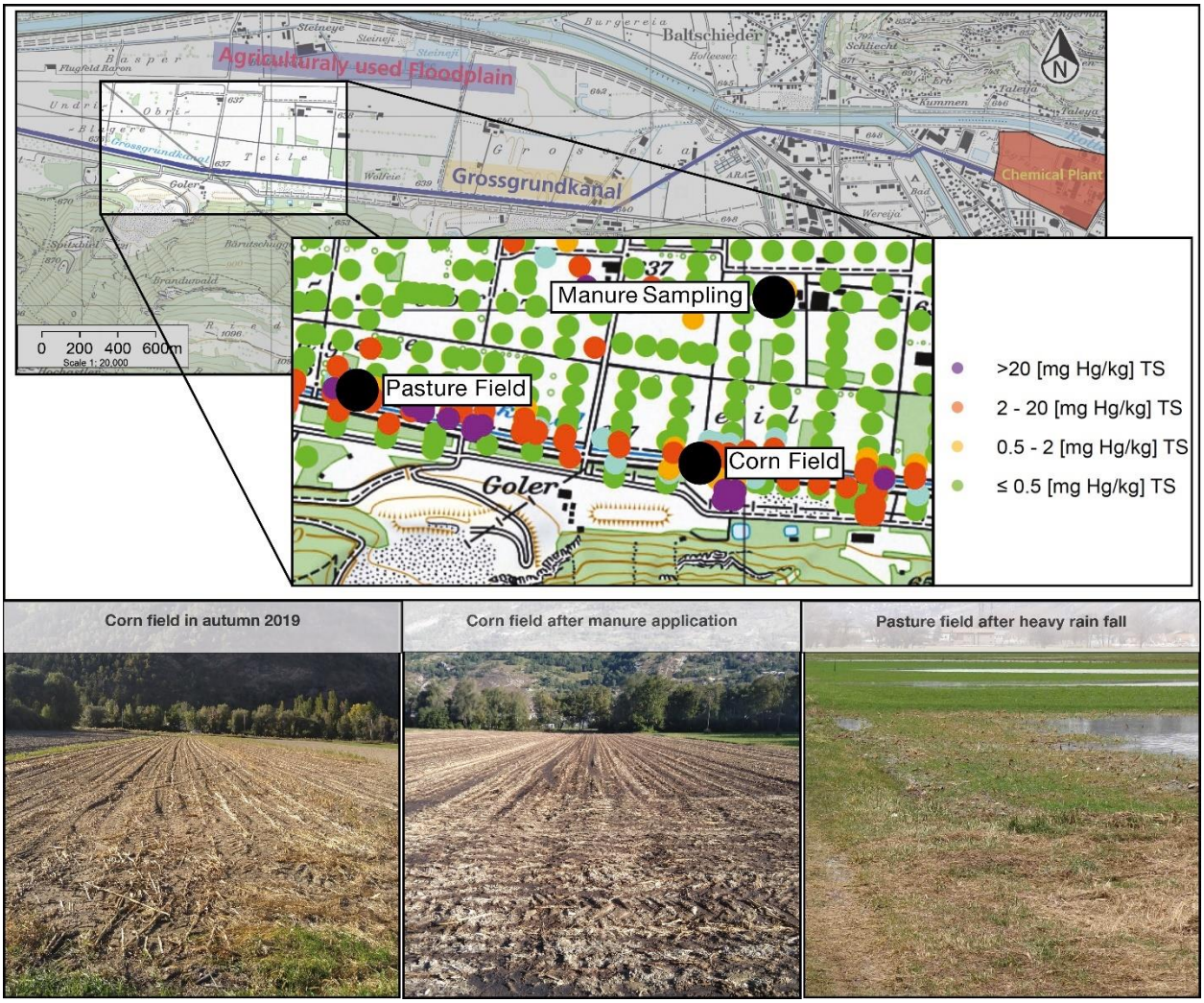

Figure C - 1: Map and pictures of the sampling location. The high-resolution Hg concentration data was collected, and the map was generated by the regional environmental office ("Dienststelle für Umweltschutz") using a map of the Bundesamt für Landestopografie swisstopo (geo.admin.ch).

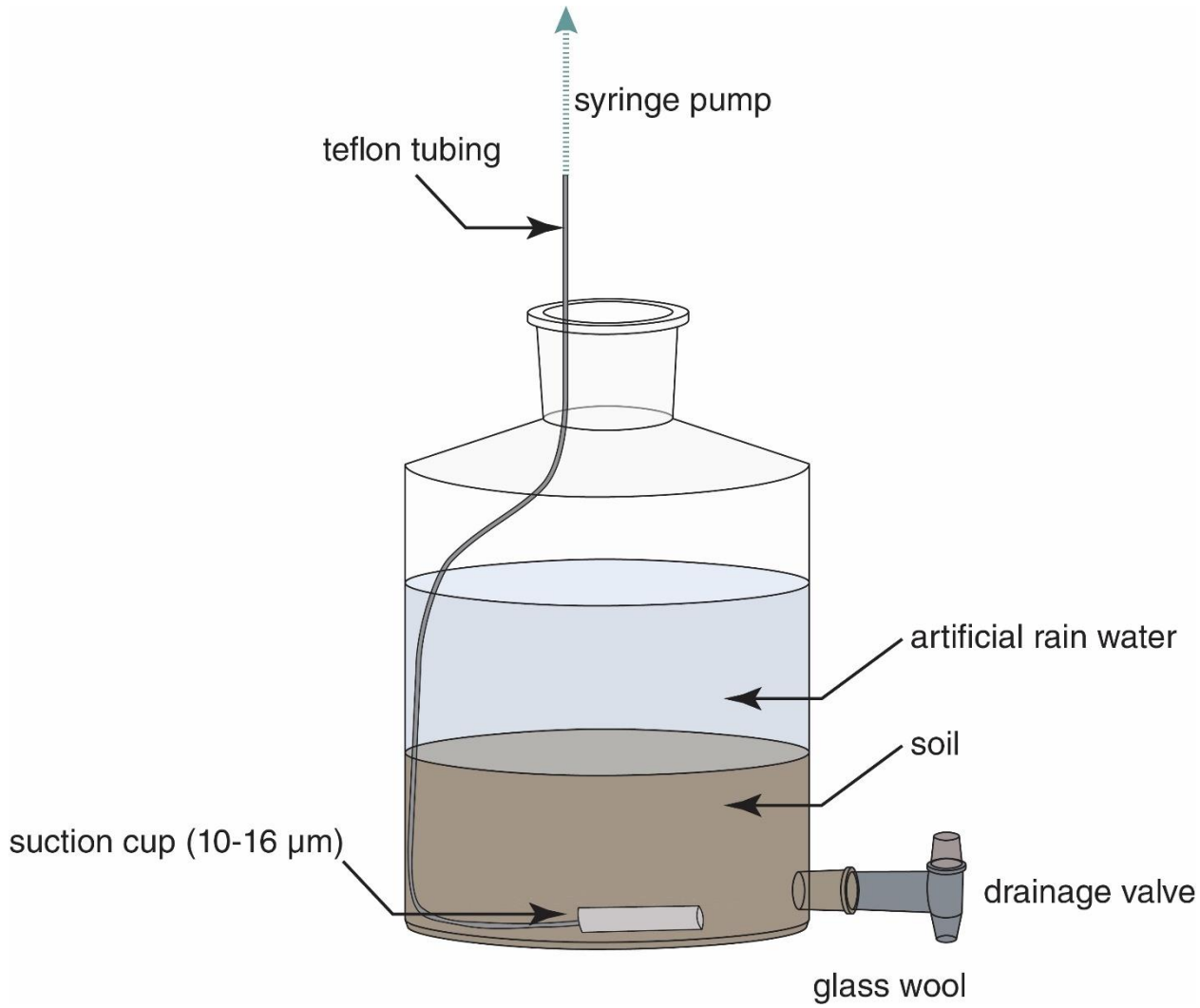

Figure C - 2 Scheme of the incubation setup. During the incubation the system was covered with parafilm.

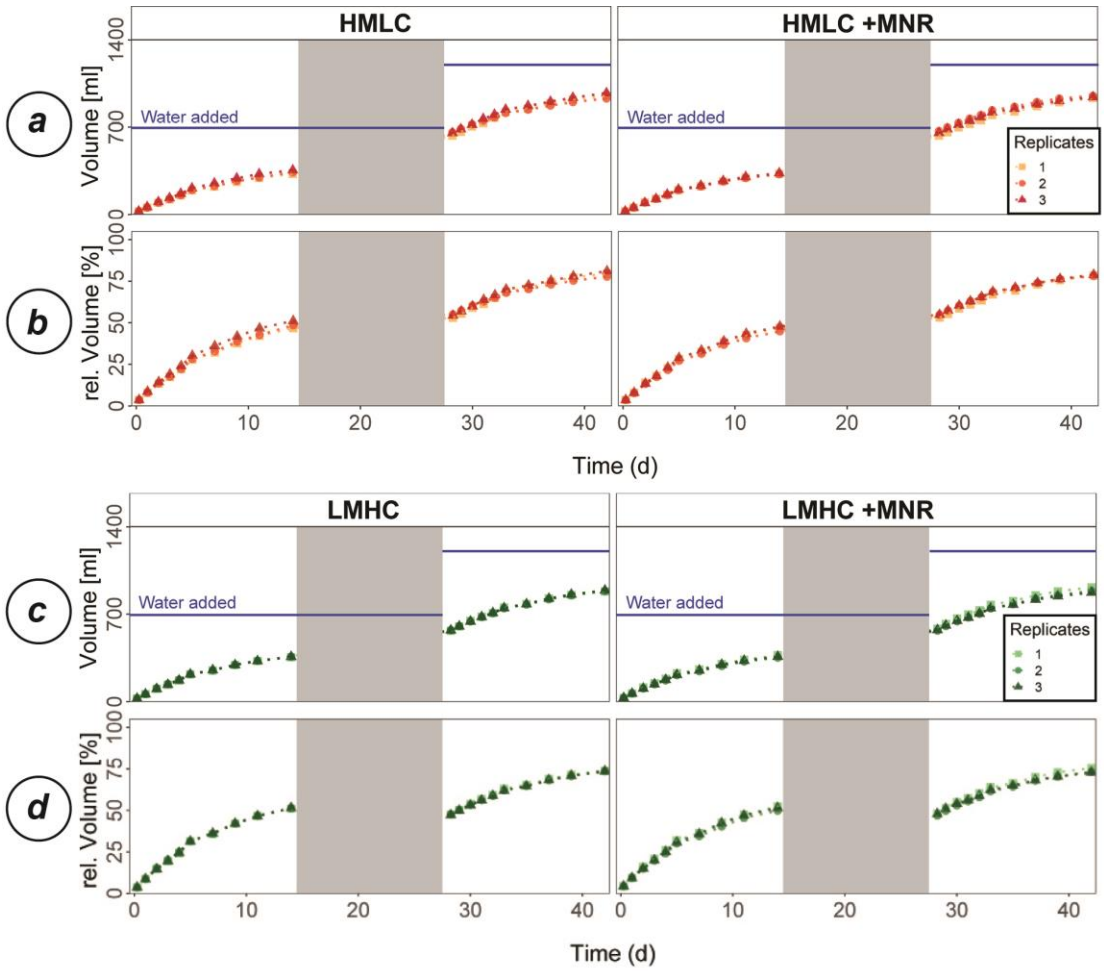

Figure C - 3 The evolution of sampled solution. a.) and c.) display the sum of sampled solution during the incubation experiment for the HMLC and LMHC soil respectively. b.) and d.) display the relative volume of previously sampled solution with respect to added artificial rainwater. Blue lines mark the sum of water added during the experiment. The gray area indicates the drained period. The three shades of green/orange distinguish the 3 replicate incubators.

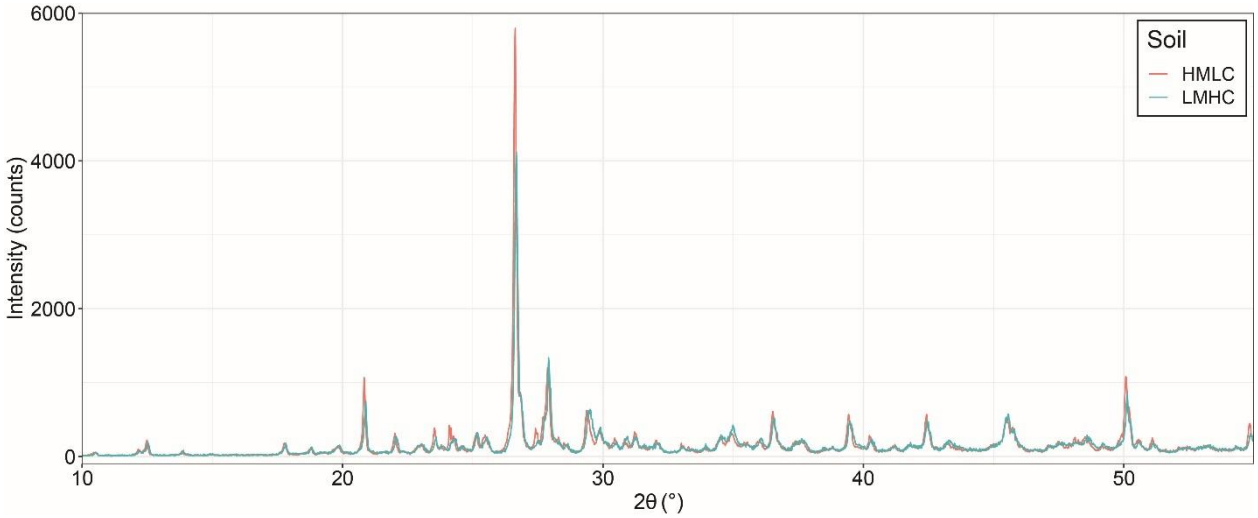

Figure C - 4 XRD diffractograms of both soil samples used for the incubation (HMLC, LMHC). The overlapping spectra suggest the common origin of parental material of the two soils.

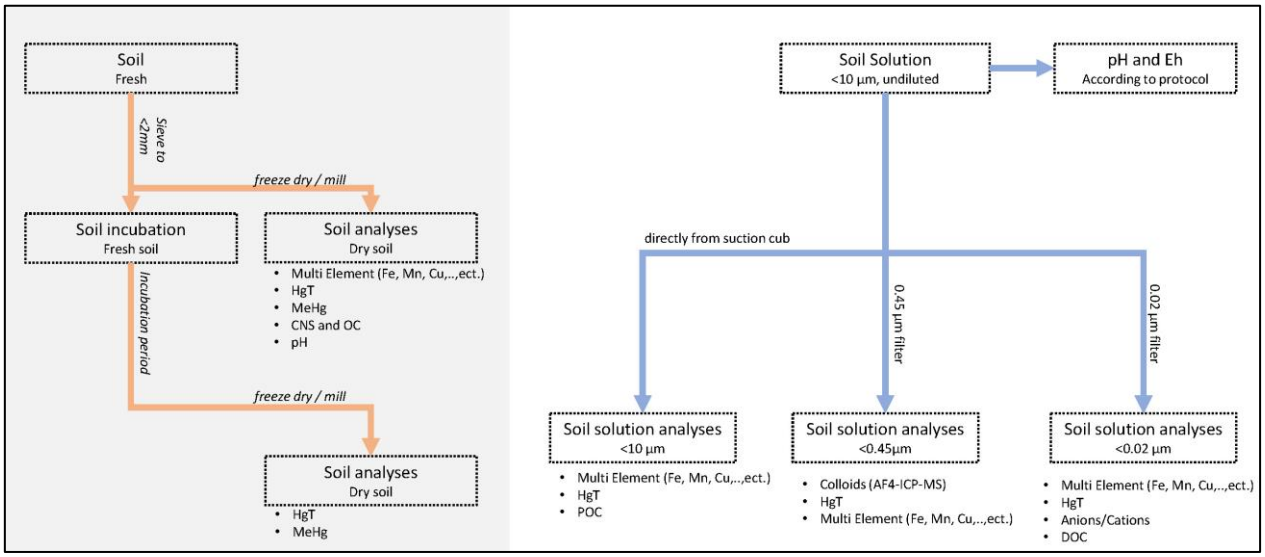

Figure C - 5 Flow chart of sampling procedure and analyses of soils and soil solution samples.

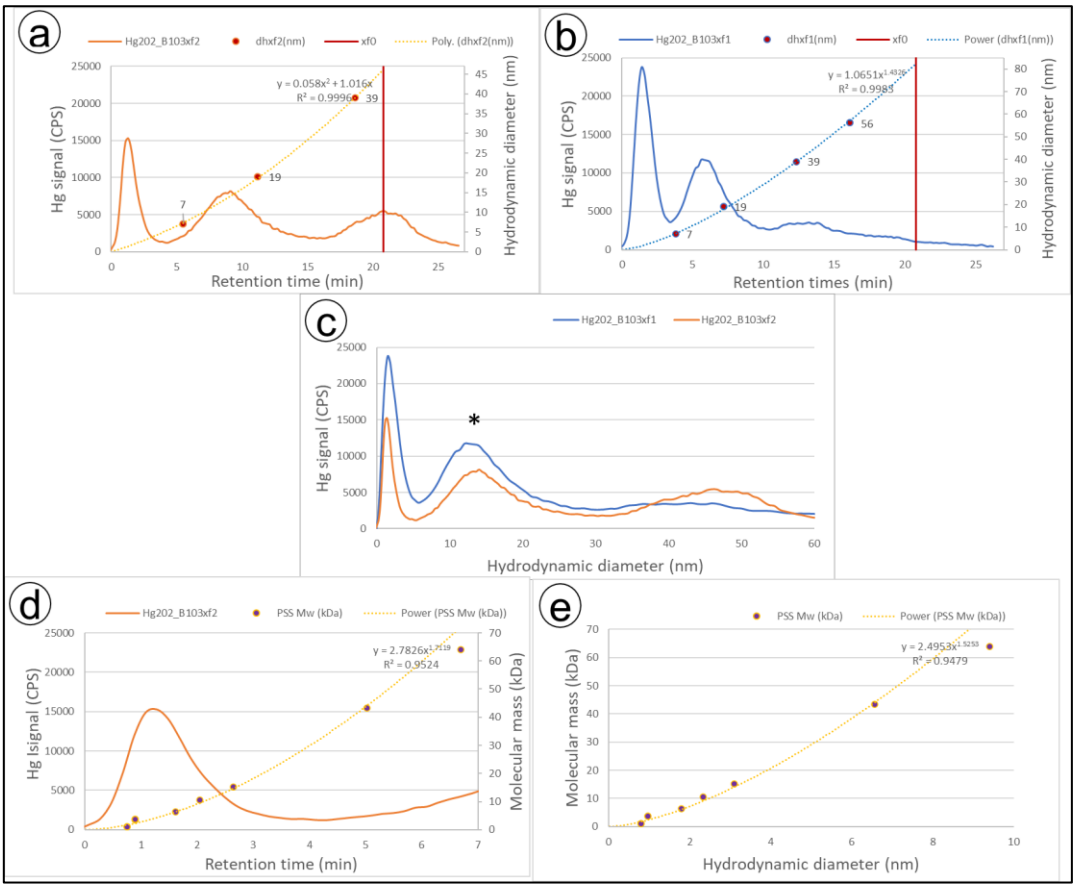

Figure C - 6 Hydrodynamic size (a, b, c) and small colloids molecular mass (d) calibrations of the elution. The relationship between molecular mass and hydrodynamic diameter is also given in e. Hydrodynamic diameter calibration was obtained using Hc3 (d_h = 7 nm) and ultra-uniform gold nanoparticles (d_h = 19 ; 39 ; 59 nm).

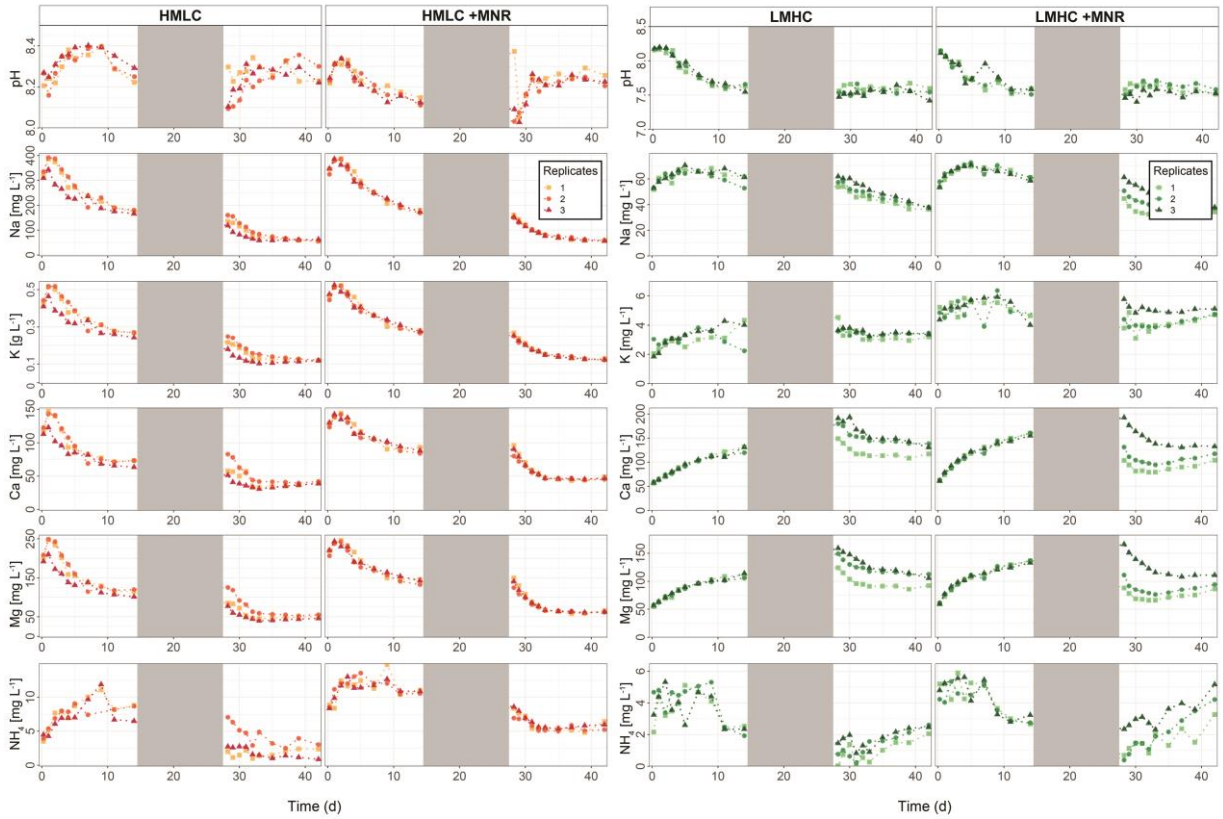

Figure C - 7 Soil solution time series for pH and major cation concentration of both cornfield (HMLC) in orange and pasture field (LMHC) in green. The gray areas mark the drained period.

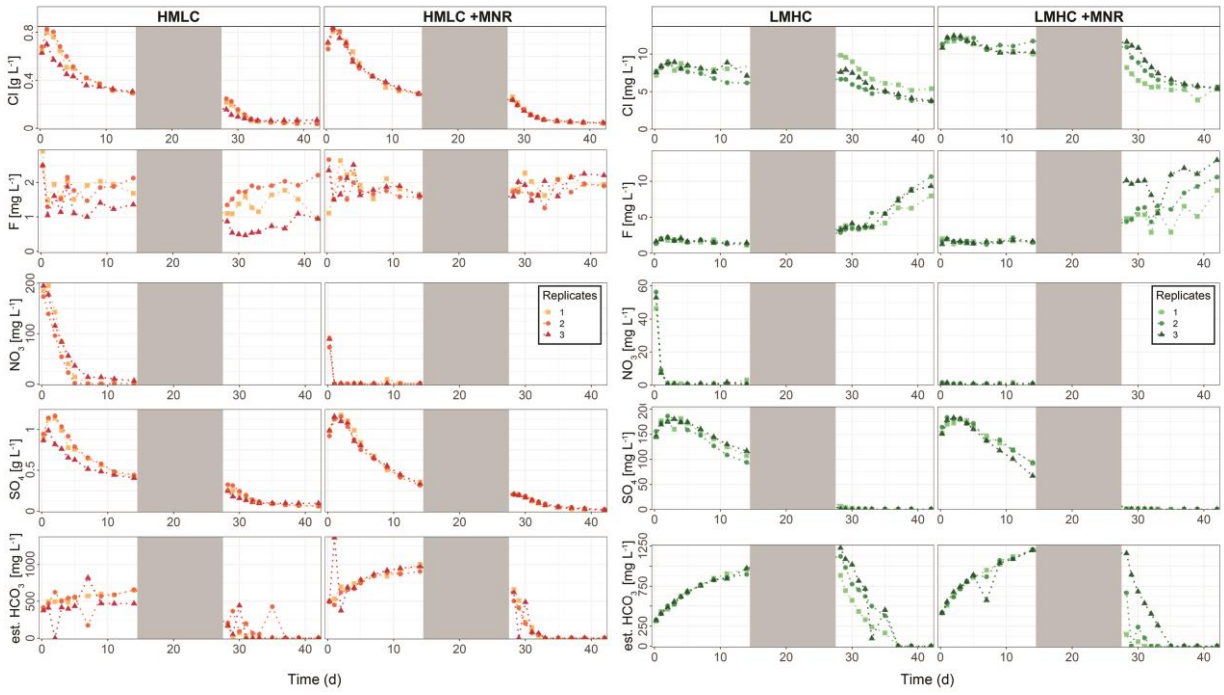

Figure C - 8 Soil solution time series for major anion concentrations in soil solution of both cornfield (HMLC) in orange and pasture field (LMHC) in green. The gray areas mark the drained period.

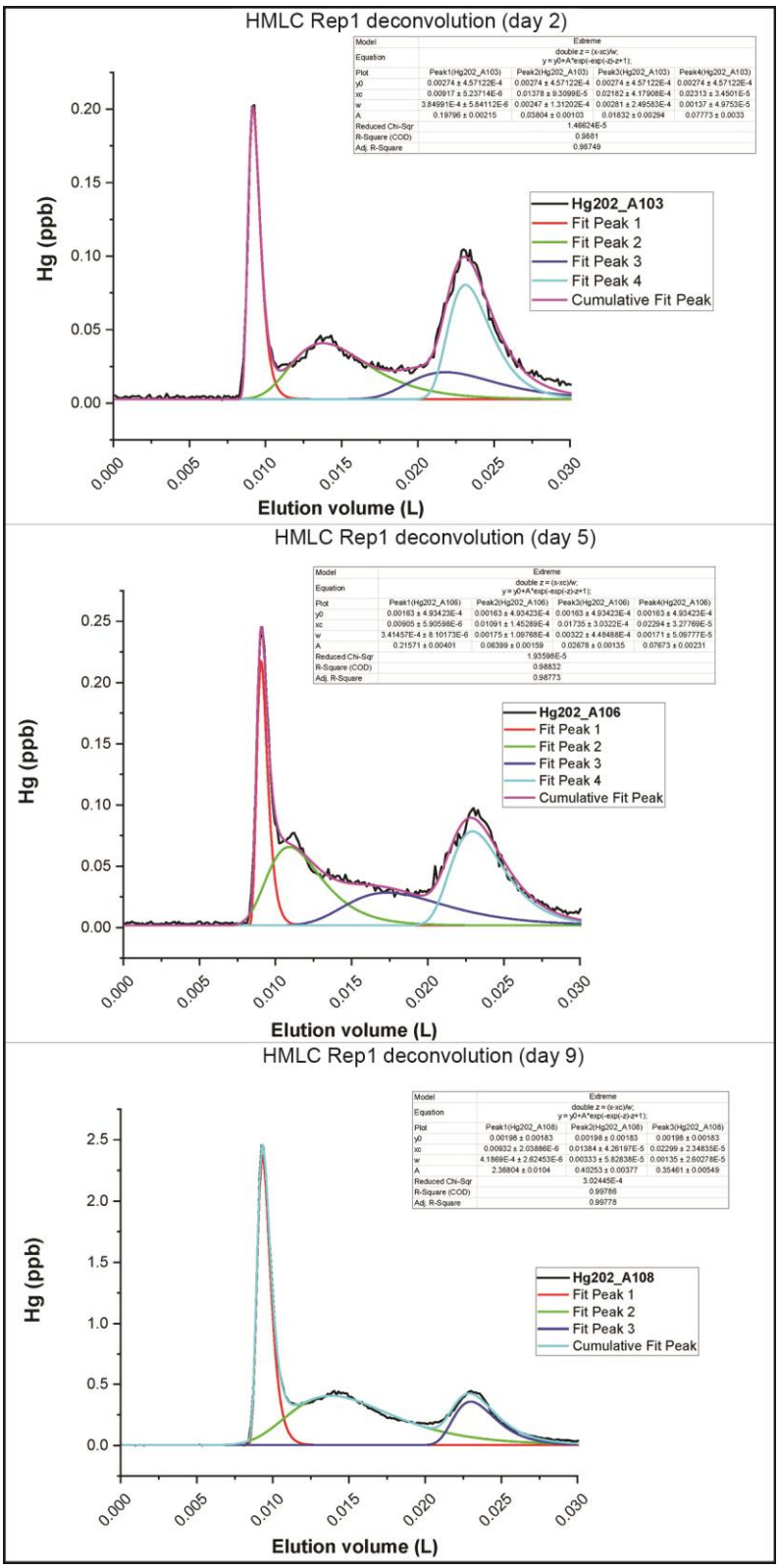

Figure C - 9 Fractograms and deconvolution for the soil solution samples of HMLC (Rep1) during the first flooding period.

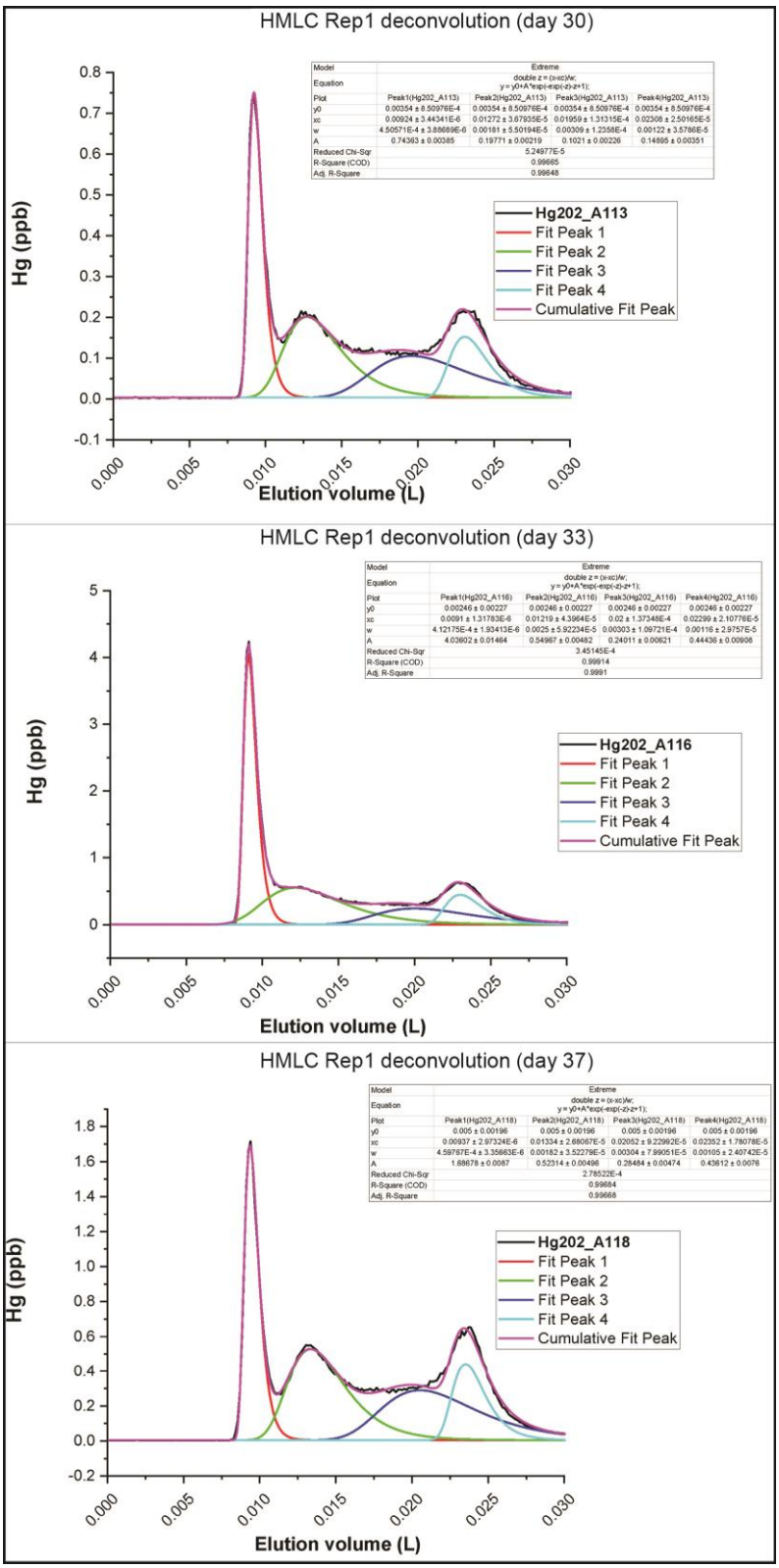

Figure C - 10 Fractograms and deconvolution for the soil solution samples of HMLC (Rep1) during second flooding period.

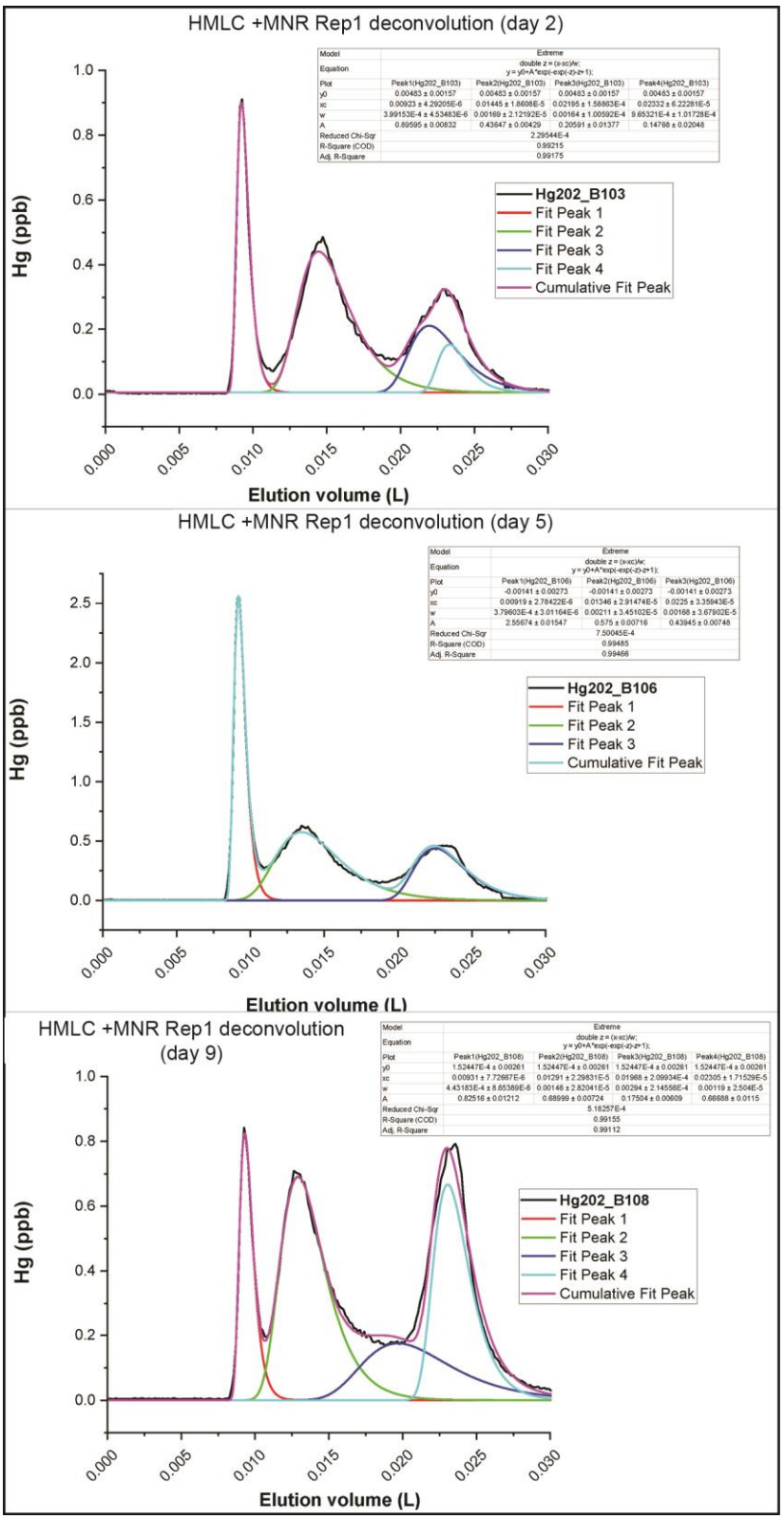

Figure C - 11 Fractograms and deconvolution for the soil solution samples of HMLC +MNR (Rep1) during the first flooding period.

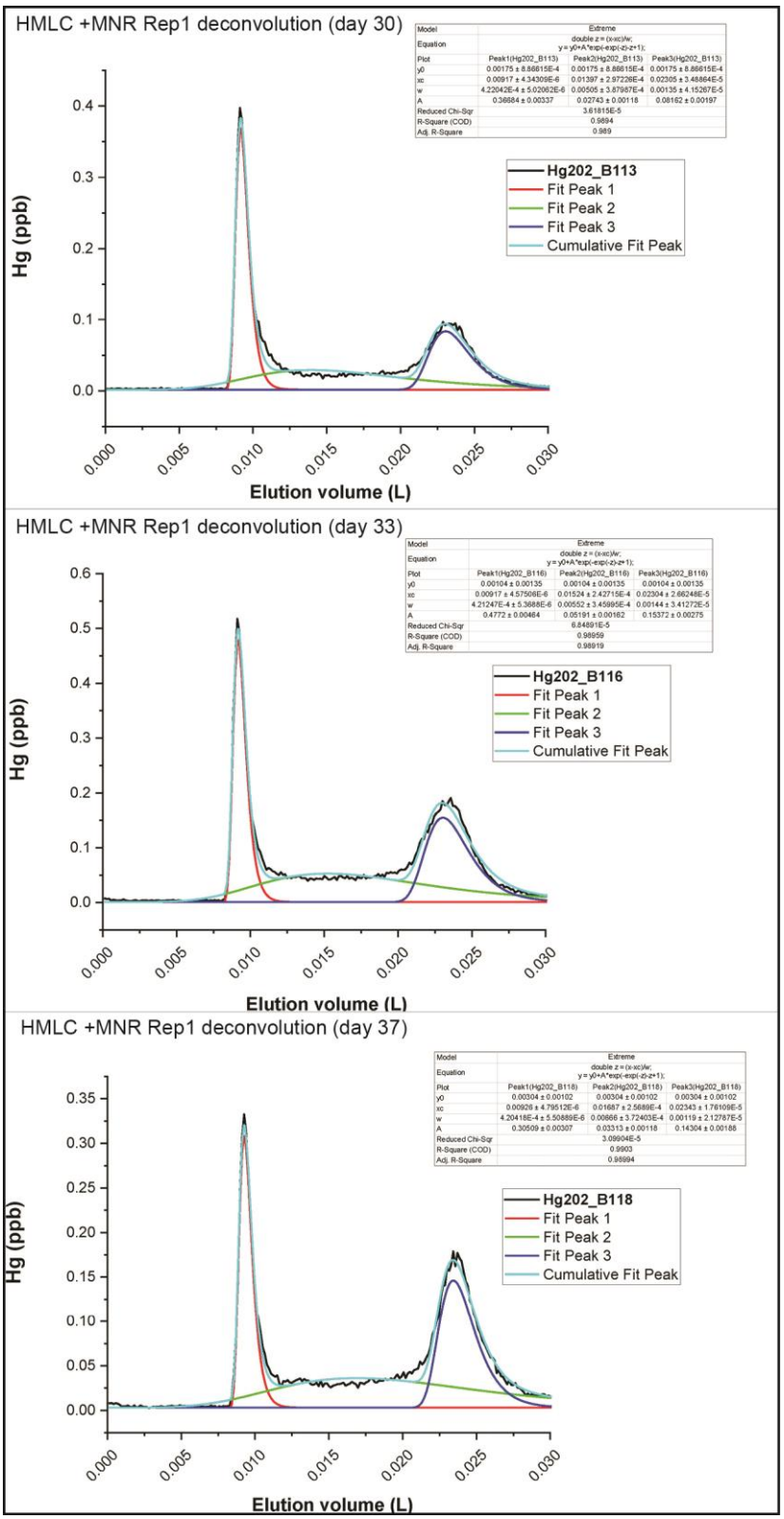

Figure C - 12 Fractograms and deconvolution for the soil solution samples of HMLC +MNR (Rep1) during the second flooding period.

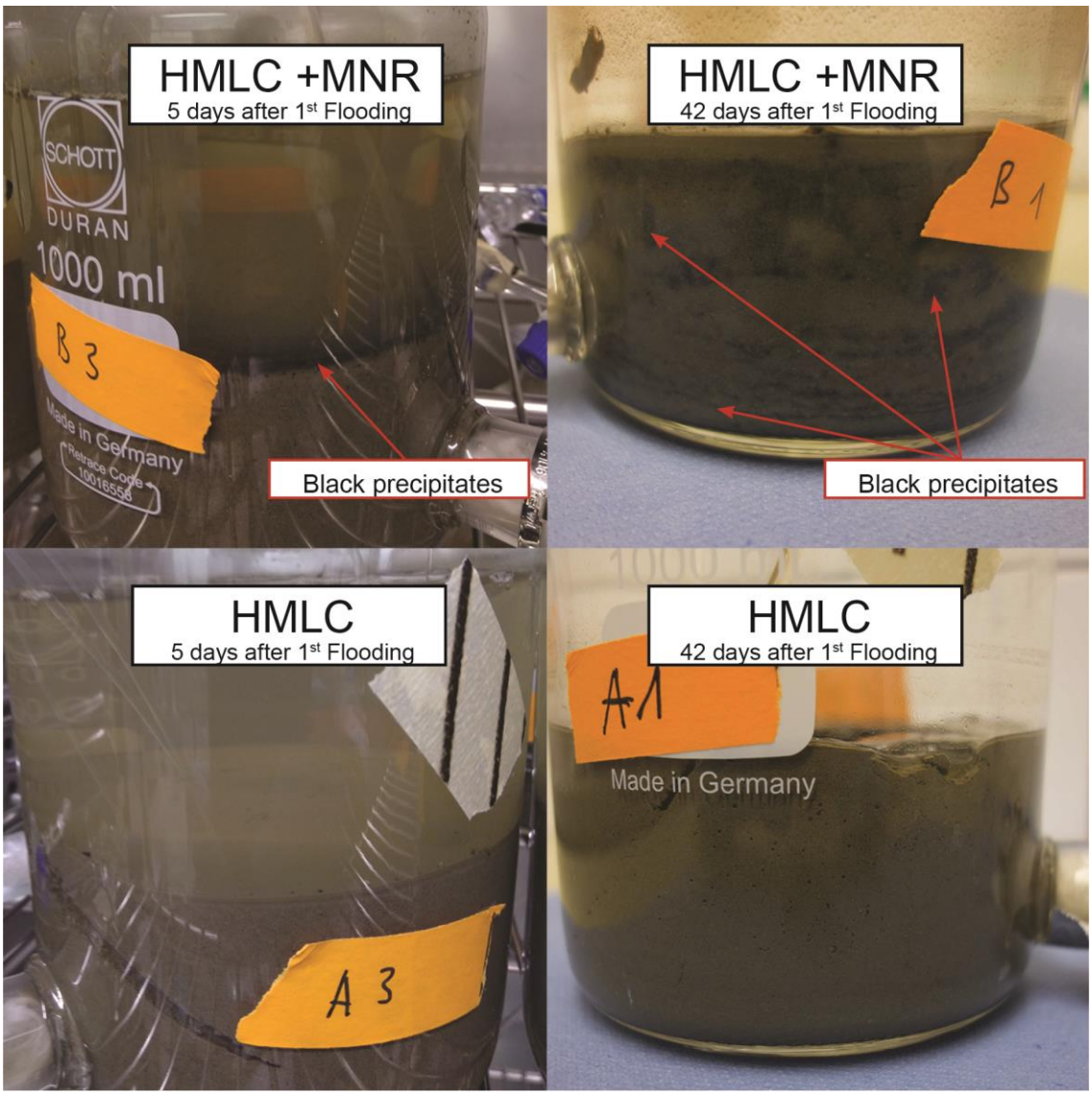

Figure C - 13 Photographs of MC (HMLC and HMLC +MNR) after 5 days (left) and 42 days (right) of incubation. In the MCs treated with MNR black precipitates become visible already after 5 days on the top of the soil column and are present in the whole soil column at the end of the incubation experiment.

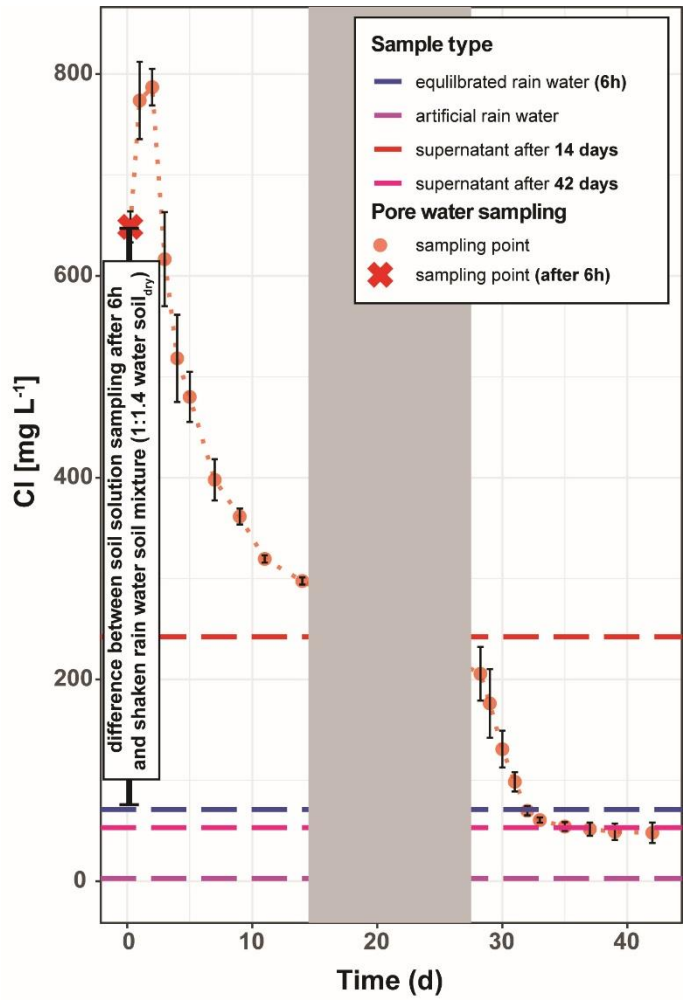

Figure C - 14 Soil solution chloride concentrations time series of microcosm "HMLC" (orange), the supernatants at the end of the flooding period (red: 14 days, pink: 42 days), artificial rainwater (purple) and equilibrated (6h) rainwater-soil mixture (blue). Gray bar indicates the drained phase during the main incubation. Difference between the sampled soil solution and the equilibrated rainwater-soil mixture are >500 mg L-1 suggesting that solid and liquid phase were not equilibrated with respect to highly soluble minerals at the onset of the incubation.

References

Abell, A. B., Willis, K. L., and Da Lange: Mercury Intrusion Porosimetry and Image Analysis of Cement-Based Materials, Journal of Colloid and Interface Science, 211, 39–44, doi:10.1006/jcis.1998.5986, 1999.

Abgottspon, F., Bigalke, M., and Wilcke, W.: Fast colloidal and dissolved release of trace elements in a carbonatic soil after experimental flooding, Geoderma, 259-260, 156–163, doi:10.1016/j.geoderma.2015.06.005, 2015.

Achá, D., Hintelmann, H., and Pabón, C. A.: Sulfate-reducing Bacteria and Mercury Methylation in the Water Column of the Lake 658 of the Experimental Lake Area, GEOMICROBIOLOGY JOURNAL, 29, 667–674, doi:10.1080/01490451.2011.606289, 2012.

Aiken, G. R., Hsu-Kim, H., and Ryan, J. N.: Influence of dissolved organic matter on the environmental fate of metals, nanoparticles, and colloids, Environ. Sci. Technol., 45, 3196–3201, doi:10.1021/es103992s, 2011.

Åkerblom, S., Meili, M., Bringmark, L., Johansson, K., Kleja, D. B., and Bergkvist, B.: Partitioning of Hg Between Solid and Dissolved Organic Matter in the Humus Layer of Boreal Forests, Water Air Soil Pollut, 189, 239–252, doi:10.1007/s11270-007-9571-1, 2008.

Åkerblom, S., Nilsson, M. B., Skyllberg, U., Björn, E., Jonsson, S., Ranneby, B., and Bishop, K.: Formation and mobilization of methylmercury across natural and experimental sulfur deposition gradients, Environmental pollution (Barking, Essex 1987), 263, 114398, doi:10.1016/j.envpol.2020.114398, 2020.

Allard, B. and Arsenie, I.: Abiotic reduction of mercury by humic substances in aquatic system.: An important process for the mercury cycle, Water Air Soil Pollut, 457–464, 1991.

Amos, H. M., Jacob, D. J., Streets, D. G., and Sunderland, E. M.: Legacy impacts of all-time anthropogenic emissions on the global mercury cycle, Global Biogeochem. Cycles, 27, 410–421, doi:10.1002/gbc.20040, 2013.

Atwell, L., Hobson, K. A., and Welch, H. E.: Biomagnification and bioaccumulation of mercury in an arctic marine food web: insights from stable nitrogen isotope analysis, Can. J. Fish. Aquat. Sci., 55, 1114–1121, doi:10.1139/cjfas-55-5-1114, 1998.

Bank, M. S.: Mercury in the Environment: Pattern and Process, 1st ed., University of California Press, 2012.

Beckers, F., Mothes, S., Abrigata, J., Zhao, J., Gao, Y., and Rinklebe, J.: Mobilization of mercury species under dynamic laboratory redox conditions in a contaminated floodplain soil as affected by biochar and sugar beet factory lime, The Science of the total environment, 672, 604–617, doi:10.1016/j.scitotenv.2019.03.401, 2019.

Beckers, F. and Rinklebe, J.: Cycling of mercury in the environment: Sources, fate, and human health implications: A review, Critical Reviews in Environmental Science and Technology, 47, 693–794, doi:10.1080/10643389.2017.1326277, 2017.

Benoit, J. M., Gilmour, C. C., Mason, R. P., and Heyes, A.: Sulfide Controls on Mercury Speciation and Bioavailability to Methylating Bacteria in Sediment Pore Waters, Environ. Sci. Technol., 33, 951–957, doi:10.1021/es9808200, 1999.

Bergman, I., Bishop, K., Tu, Q., Frech, W., Åkerblom, S., and Nilsson, M.: The influence of sulphate deposition on the seasonal variation of peat pore water methyl Hg in a boreal mire, PloS one, 7, e45547, doi:10.1371/journal.pone.0045547, 2012.

Biester, H., Müller, G., and Schöler, H.: Binding and mobility of mercury in soils contaminated by emissions from chlor-alkali plants, Science of The Total Environment, 284, 191–203, doi:10.1016/S0048-9697(01)00885-3, 2002a.

Biester, H., Müller, G., and Schöler, H. F.: Estimating distribution and retention of mercury in three different soils contaminated by emissions from chlor-alkali plants: part I, Science of The Total Environment, 284, 177–189, doi:10.1016/S0048-9697(01)00884-1, 2002b.

Biester, H. and Scholz, C.: Determination of Mercury Binding Forms in Contaminated Soils: Mercury Pyrolysis versus Sequential Extractions, Environ. Sci. Technol., 31, 233–239, doi:10.1021/es960369h, 1997.

Bigham, G. N., Murray, K. J., Masue-Slowey, Y., and Henry, E. A.: Biogeochemical controls on methylmercury in soils and sediments: Implications for site management, Integrated environmental assessment and management, 13, 249–263, doi:10.1002/ieam.1822, 2017.

Birrer, S., Kohli, L., and Spiess, M.: Haben ökologische Ausgleichsflächen einen Einfluss auf die Bestandsentwicklung von Kulturland-Vogelarten im Mittelland?, Der Ornithologische Beobachter, 104, 189–208, 2007.

Bishop, K., Shanley, J. B., Riscassi, A., Wit, H. A. de, Eklöf, K., Meng, B., Mitchell, C., Osterwalder, S., Schuster, P. F., Webster, J., and Zhu, W.: Recent advances in understanding and measurement of mercury in the environment: Terrestrial Hg cycling, The Science of the total environment, 721, 137647, doi:10.1016/j.scitotenv.2020.137647, 2020.

Bloom, N. S., Colman, J. A., and Barber, L.: Artifact formation of methyl mercury during aqueous distillation and alternative techniques for the extraction of methyl mercury from environmental samples, Fresenius Journal of Analytical Chemistry, 371–377, 1997.

Bloom, N. S., Preus, E., Katon, J., and Hiltner, M.: Selective extractions to assess the biogeochemically relevant fractionation of inorganic mercury in sediments and soils, ANALYTICA CHIMICA ACTA, 479, 233–248, doi:10.1016/S0003-2670(02)01550-7, 2003.

Bouchet, S., Goñi-Urriza, M., Monperrus, M., Guyoneaud, R., Fernandez, P., Heredia, C., Tessier, E., Gassie, C., Point, D., Guédron, S., Achá, D., and Amouroux, D.: Linking Microbial Activities and Low-Molecular-Weight Thiols to Hg Methylation in Biofilms and Periphyton from High-Altitude Tropical Lakes in the Bolivian Altiplano, Environ. Sci. Technol., 52, 9758–9767, doi:10.1021/acs.est.8b01885, 2018.

Brantschen, J., Gygax, S., Mestrot, A., and Frossard, A.: Soil Hg Contamination Impact on Earthworms' Gut Microbiome, Applied Sciences, 10, 2565, doi:10.3390/app10072565, 2020.

Bravo, A. G., Bouchet, S., Tolu, J., Björn, E., Mateos-Rivera, A., and Bertilsson, S.: Molecular composition of organic matter controls methylmercury formation in boreal lakes, Nature communications, 8, 14255, doi:10.1038/ncomms14255, 2017.

Brombach, C.-C., Gajdosechova, Z., Chen, B., Brownlow, A., Corns, W. T., Feldmann, J., and Krupp, E. M.: Direct online HPLC-CV-AFS method for traces of methylmercury without derivatisation: a matrix-independent method for urine, sediment and biological tissue samples, Analytical and bioanalytical chemistry, 407, 973–981, doi:10.1007/s00216-014-8254-1, 2015.

Canil, D., Crockford, P. W., Rossin, R., and Telmer, K.: Mercury in some arc crustal rocks and mantle peridotites and relevance to the moderately volatile element budget of the Earth, Chemical Geology, 396, 134–142, doi:10.1016/j.chemgeo.2014.12.029, 2015.

Capo, E., Broman, E., Bonaglia, S., Bravo, A. G., Bertilsson, S., Soerensen, A. L., Pinhassi, J., Lundin, D., Buck, M., Hall, P. O. J., Nascimento, F. J. A., and Björn, E.: Oxygen-deficient water zones in the Baltic Sea promote uncharacterized Hg methylating microorganisms in underlying sediments, Limnology & Oceanography, 67, 135–146, doi:10.1002/lno.11981, 2022a.

Capo, E., Feng, C., Bravo, A. G., Bertilsson, S., Soerensen, A. L., Pinhassi, J., Buck, M., Karlsson, C., Hawkes, J., and Björn, E.: Expression Levels of hgcAB Genes and Mercury Availability Jointly Explain Methylmercury Formation in Stratified Brackish Waters, Environ. Sci. Technol., 56, 13119–13130, doi:10.1021/acs.est.2c03784, 2022b.

Chazette, P., Couvert, P., Randriamiarisoa, H., Sanak, J., Bonsang, B., Moral, P., Berthier, S., Salanave, S., and Toussaint, F.: Three-dimensional survey of pollution during winter in French Alps valleys, Atmospheric Environment, 39, 1035–1047, doi:10.1016/j.atmosenv.2004.10.014, 2005.

Chen, C., Amirbahman, A., Fisher, N., Harding, G., Lamborg, C., Nacci, D., and Taylor, D.: Methylmercury in marine ecosystems: spatial patterns and processes of production, bioaccumulation, and biomagnification, EcoHealth, 5, 399–408, doi:10.1007/s10393-008-0201-1, 2008.

Chen, C., Huang, J.-H., Meusburger, K., Li, K., Fu, X., Rinklebe, J., Alewell, C., and Feng, X.: The interplay between atmospheric deposition and soil dynamics of mercury in Swiss and Chinese boreal forests: A comparison study, Environmental pollution (Barking, Essex 1987), 307, 119483, doi:10.1016/j.envpol.2022.119483, 2022.

Chiasson-Gould, S. A., Blais, J. M., and Poulain, A. J.: Dissolved organic matter kinetically controls mercury bioavailability to bacteria, Environmental science & technology, 48, 3153–3161, doi:10.1021/es4038484, 2014.

Christensen, G. A., Gionfriddo, C. M., King, A. J., Moberly, J. G., Miller, C. L., Somenahally, A. C., Callister, S. J., Brewer, H., Podar, M., Brown, S. D., Palumbo, A. V., Brandt, C. C., Wymore, A. M., Brooks, S. C., Hwang, C., Fields, M. W., Wall, J. D., Gilmour, C. C., and Elias, D. A.: Determining the Reliability of Measuring Mercury Cycling Gene Abundance with Correlations with Mercury and Methylmercury Concentrations, Environmental science & technology, 53, 8649–8663, doi:10.1021/acs.est.8b06389, 2019.

Deonarine, A. and Hsu-Kim, H.: Precipitation of Mercuric Sulfide Nanoparticles in NOM-Containing Water: Implications for the Natural Environment, Environ. Sci. Technol., 43, 2368–2373, doi:10.1021/es803130h, 2009.

Deonarine, A., Lau, B. L. T., Aiken, G. R., Ryan, J. N., and Hsu-Kim, H.: Effects of humic substances on precipitation and aggregation of zinc sulfide nanoparticles, Environmental science & technology, 45, 3217–3223, doi:10.1021/es1029798, 2011.

Díez, E. G., Graham, N. D., and Loizeau, J.-L.: Total and methyl-mercury seasonal particulate fluxes in the water column of a large lake (Lake Geneva, Switzerland), Environmental science and pollution research international, doi:10.1007/s11356-018-2252-3, 2018.

Driscoll, C. T., Mason, R. P., Chan, H. M., Jacob, D. J., and Pirrone, N.: Mercury as a global pollutant: Sources, pathways, and effects, Environmental science & technology, 47, 4967–4983, doi:10.1021/es305071v, 2013.

Drott, A., Lambertsson, L., Björn, E., and Skyllberg, U.: Importance of dissolved neutral mercury sulfides for methyl mercury production in contaminated sediments, Environ. Sci. Technol., 41, 2270–2276, doi:10.1021/es061724z, 2007.

Du, H., Ma, M., Igarashi, Y., and Wang, D.: Biotic and Abiotic Degradation of Methylmercury in Aquatic Ecosystems: A Review, Bull Environ Contam Toxicol, 102, 605–611, doi:10.1007/s00128-018-2530-2, 2019.

Duan, Y., Han, D. S., Batchelor, B., and Abdel-Wahab, A.: Synthesis, characterization, and application of pyrite for removal of mercury, Colloids and Surfaces A: Physicochemical and Engineering Aspects, 490, 326–335, doi:10.1016/j.colsurfa.2015.11.057, 2016.

Dublet, G., Worms, I., Frutschi, M., Brown, A., Zünd, G. C., Bartova, B., Slaveykova, V. I., and Bernier-Latmani, R.: Colloidal Size and Redox State of Uranium Species in the Porewater of a Pristine Mountain Wetland, Environmental science & technology, 53, 9361–9369, doi:10.1021/acs.est.9b01417, 2019.

Eagles-Smith, C. A., Silbergeld, E. K., Basu, N., Bustamante, P., Diaz-Barriga, F., Hopkins, W. A., Kidd, K. A., and Nyland, J. F.: Modulators of mercury risk to wildlife and humans in the context of rapid global change, Ambio, 47, 170–197, doi:10.1007/s13280-017-1011-x, 2018.

Eckley, C. S., Luxton, T. P., Goetz, J., and McKernan, J.: Water-level fluctuations influence sediment porewater chemistry and methylmercury production in a flood-control reservoir, Environmental pollution (Barking, Essex 1987), 222, 32–41, doi:10.1016/j.envpol.2017.01.010, 2017.

Eckley, C. S., Luxton, T. P., Stanfield, B., Baldwin, A., Holloway, J., McKernan, J., and Johnson, M. G.: Effect of organic matter concentration and characteristics on mercury mobilization and methylmercury production at an abandoned mine site, Environmental pollution (Barking, Essex 1987), 271, 116369, doi:10.1016/j.envpol.2020.116369, 2021.

Edwards, B. A., Kushner, D. S., Outridge, P. M., and Wang, F.: Fifty years of volcanic mercury emission research: Knowledge gaps and future directions, The Science of the total environment, 757, 143800, doi:10.1016/j.scitotenv.2020.143800, 2021.

Eklöf, K., Bishop, K., Bertilsson, S., Björn, E., Buck, M., Skyllberg, U., Osman, O. A., Kronberg, R.-M., and Bravo, A. G.: Formation of mercury methylation hotspots as a consequence of forestry operations, The Science of the total environment, 613-614, 1069–1078, doi:10.1016/j.scitotenv.2017.09.151, 2018.

Erhardt, T., Jensen, C. M., Borovinskaya, O., and Fischer, H.: Single Particle Characterization and Total Elemental Concentration Measurements in Polar Ice Using Continuous Flow Analysis-Inductively Coupled Plasma Time-of-Flight Mass Spectrometry, Environmental science & technology, 53, 13275–13283, doi:10.1021/acs.est.9b03886, 2019.

Falter, R.: Experimental study on the unintentional abiotic methylation of inorganic mercury during analysis: Part 1: Localisation of the compounds effecting the abiotic mercury methylation, Chemosphere, 39, 1051–1073, doi:10.1016/S0045-6535(99)00178-2, 1999a.

Falter, R.: Experimental study on the unintentional abiotic methylation of inorganic mercury during analysis: Part 2: Controlled laboratory experiments to elucidate the mechanism and critical discussion of the species specific isotope addition correction method, Chemosphere, 39, 1075–1091, doi:10.1016/S0045-6535(99)00179-4, 1999b.

Fernández-Martínez, R., Larios, R., Gómez-Pinilla, I., Gómez-Mancebo, B., López-Andrés, S., Loredo, J., Ordóñez, A., and Rucandio, I.: Mercury accumulation and speciation in plants and soils from abandoned cinnabar mines, Geoderma, 253-254, 30–38, doi:10.1016/j.geoderma.2015.04.005, 2015.

Fitzgerald, W. F., Lamborg, C. H., and Hammerschmidt, C. R.: Marine biogeochemical cycling of mercury, Chemical reviews, 107, 641–662, doi:10.1021/cr050353m, 2007.

Frohne, T., Rinklebe, J., Diaz-Bone, R. A., and Du Laing, G.: Controlled variation of redox conditions in a floodplain soil: Impact on metal mobilization and biomethylation of arsenic and antimony, Geoderma, 160, 414–424, doi:10.1016/j.geoderma.2010.10.012, 2011.

Frohne, T., Rinklebe, J., Langer, U., Du Laing, G., Mothes, S., and Wennrich, R.: Biogeochemical factors affecting mercury methylation rate in two contaminated floodplain soils, Biogeosciences, 9, 493–507, doi:10.5194/bg-9-493-2012, 2012.

Frossard, A., Donhauser, J., Mestrot, A., Gygax, S., Bååth, E., and Frey, B.: Long- and short-term effects of mercury pollution on the soil microbiome, Soil Biology and Biochemistry, 120, 191–199, doi:10.1016/j.soilbio.2018.01.028, 2018.

Fu, X., Zhu, W., Zhang, H., Sommar, J., Yu, B., Yang, X., Wang, X., Lin, C.-J., and Feng, X.: Depletion of atmospheric gaseous elemental mercury by plant uptake at Mt. Changbai, Northeast China, Atmos. Chem. Phys., 16, 12861–12873, doi:10.5194/acp-16-12861-2016, 2016.

Fujiki, M. and Tajima, S.: The Pollution of Minamata Bay by Mercury, Water Science and Technology, 25, 133–140, doi:10.2166/wst.1992.0284, 1992.

Gallorini, A. and Loizeau, J.-L.: Mercury methylation in oxic aquatic macro-environments: a review, Journal of Limnology, 2021.

Gallorini, A. and Loizeau, J.-L.: Lake snow as a mercury methylation micro-environment in the oxic water column of a deep peri-alpine lake, Chemosphere, 299, 134306, doi:10.1016/j.chemosphere.2022.134306, 2022.

Geier, D. A., King, P. G., Hooker, B. S., Dórea, J. G., Kern, J. K., Sykes, L. K., and Geier, M. R.: Thimerosal: clinical, epidemiologic and biochemical studies, Clinica chimica acta; international journal of clinical chemistry, 444, 212–220, doi:10.1016/j.cca.2015.02.030, 2015.

Gerbig, C. A., Kim, C. S., Stegemeier, J. P., Ryan, J. N., and Aiken, G. R.: Formation of nanocolloidal metacinnabar in mercury-DOM-sulfide systems, Environmental science & technology, 45, 9180–9187, doi:10.1021/es201837h, 2011.

Gfeller, L., Caplette, J. N., Frossard, A., and Mestrot, A.: Organo-mercury species in a polluted agricultural flood plain: Combining speciation methods and polymerase chain reaction to investigate pathways of contamination, Environmental pollution (Barking, Essex 1987), 311, 119854, doi:10.1016/j.envpol.2022.119854, 2022.

Gfeller, L., Weber, A., Worms, I., Slaveykova, V. I., and Mestrot, A.: Mercury mobility, colloid formation and methylation in a polluted Fluvisol as affected by manure application and flooding–draining cycle, Biogeosciences, 18, 3445–3465, doi:10.5194/bg-18-3445-2021, 2021.

Gilli, R., Karlen, C., Weber, M., Rüegg, J., Barmettler, K., Biester, H., Boivin, P., and Kretzschmar, R.: Speciation and Mobility of Mercury in Soils Contaminated by Legacy Emissions from a Chemical Factory in the Rhône Valley in Canton of Valais, Switzerland, Soil Syst., 2, 44, doi:10.3390/soilsystems2030044, 2018.

Gilmour, C. C., Podar, M., Bullock, A. L., Graham, A. M., Brown, S. D., Somenahally, A. C., Johs, A., Hurt, R. A., Bailey, K. L., and Elias, D. A.: Mercury methylation by novel microorganisms from new environments, Environmental science & technology, 47, 11810–11820, doi:10.1021/es403075t, 2013.

Glenz, C. and Escher, J.-R.: Voruntersuchung von belasteten Standorten: Historische Untersuchung Objekt Grossgrundkanal, FUAG-Forum Umwelt AG, Visp, Switzerland, 89 pp., 2011.

Golding, G. R., Sparling, R., and Kelly, C. A.: Effect of pH on intracellular accumulation of trace concentrations of Hg(II) in Escherichia coli under anaerobic conditions, as measured using a mer-lux bioreporter, Applied and Environmental Microbiology, 74, 667–675, doi:10.1128/AEM.00717-07, 2008.

Graham, A. M., Aiken, G. R., and Gilmour, C. C.: Dissolved organic matter enhances microbial mercury methylation under sulfidic conditions, Environmental science & technology, 46, 2715–2723, doi:10.1021/es203658f, 2012.

Graham, A. M., Aiken, G. R., and Gilmour, C. C.: Effect of dissolved organic matter source and character on microbial Hg methylation in Hg-S-DOM solutions, Environ. Sci. Technol., 47, 5746–5754, doi:10.1021/es400414a, 2013.

Grangeon, S., Guédron, S., Asta, J., Sarret, G., and Charlet, L.: Lichen and soil as indicators of an atmospheric mercury contamination in the vicinity of a chlor-alkali plant (Grenoble, France), Ecological Indicators, 13, 178–183, doi:10.1016/j.ecolind.2011.05.024, 2012.

Gray, J. E., Hines, M. E., Higueras, P. L., Adatto, I., and Lasorsa, B. K.: Mercury speciation and microbial transformations in mine wastes, stream sediments, and surface waters at the Almadén Mining District, Spain, Environmental science & technology, 38, 4285–4292, doi:10.1021/es040359d, 2004.

Graydon, J. A., St Louis, V. L., Hintelmann, H., Lindberg, S. E., Sandilands, K. A., Rudd, J. W. M., Kelly, C. A., Hall, B. D., and Mowat, L. D.: Long-term wet and dry deposition of total and methyl mercury in the remote boreal ecoregion of Canada, Environmental science & technology, 42, 8345–8351, doi:10.1021/es801056j, 2008.

Grégoire, D. S. and Poulain, A. J.: Shining light on recent advances in microbial mercury cycling, FACETS, 3, 858–879, doi:10.1139/facets-2018-0015, 2018.

Grigg, A. R. C., Kretzschmar, R., Gilli, R. S., and Wiederhold, J. G.: Mercury isotope signatures of digests and sequential extracts from industrially contaminated soils and sediments, The Science of the total environment, 636, 1344–1354, doi:10.1016/j.scitotenv.2018.04.261, 2018.

Gruber, A., Schwab, P., Wächter, D., Meuli, R. G., and Keller, A.: Ergebnisse der Nationalen Bodenbeobachtung (NABO) 1985-2009: Zustand und Veränderung anorganischer Schadstoffe und Begleitparameter, Bundesamt für Umwelt BAFU, Bern, Umwelt-Zustand, 1507, 81 pp., 2015.

Guedron, S., Grangeon, S., Lanson, B., and Grimaldi, M.: Mercury speciation in a tropical soil association; Consequence of gold mining on Hg distribution in French Guiana, Geoderma, 153, 331–346, doi:10.1016/j.geoderma.2009.08.017, 2009.

Guédron, S., Grangeon, S., Jouravel, G., Charlet, L., and Sarret, G.: Atmospheric mercury incorporation in soils of an area impacted by a chlor-alkali plant (Grenoble, France): contribution of canopy uptake, The Science of the total environment, 445-446, 356–364, doi:10.1016/j.scitotenv.2012.12.084, 2013.

Guney, M., Akimzhanova, Z., Kumisbek, A., Beisova, K., Kismelyeva, S., Satayeva, A., Inglezakis, V., and Karaca, F.: Mercury (Hg) Contaminated Sites in Kazakhstan: Review of Current Cases and Site Remediation Responses, International journal of environmental research and public health, 17, doi:10.3390/ijerph17238936, 2020.

Gustin, M. S., Dunham-Cheatham, S. M., Harper, J. F., Choi, W.-G., Blum, J. D., and Johnson, M. W.: Investigation of the biochemical controls on mercury uptake and mobility in trees, The Science of the total environment, 851, 158101, doi:10.1016/j.scitotenv.2022.158101, 2022.

Gygax, S.: Mercury methylation in a polluted floodplain of the Canton of Valais, Switzerland: Influence of flooding and agricultural practices, Master Thesis, Universität Bern, Bern, 55 pp., 2015.

Gygax, S., Gfeller, L., Wilcke, W., and Mestrot, A.: Emerging investigator series: mercury mobility and methylmercury formation in a contaminated agricultural flood plain: influence of flooding and manure addition, Environmental science. Processes & impacts, 21, 2008–2019, doi:10.1039/c9em00257j, 2019.

Haitzer, M., Aiken, G. R., and Ryan, J. N.: Binding of mercury(II) to dissolved organic matter: the role of the mercury-to-DOM concentration ratio, Environmental science & technology, 36, 3564–3570, doi:10.1021/es025699i, 2002.

Hammerschmidt, C. R. and Fitzgerald, W. F.: Formation of Artifact Methylmercury during Extraction from a Sediment Reference Material, Anal. Chem., 73, 5930–5936, doi:10.1021/ac010721w, 2001.

Han, S. and Gill, G. A.: Determination of mercury complexation in coastal and estuarine waters using competitive ligand exchange method, Environmental science & technology, 39, 6607–6615, doi:10.1021/es048667z, 2005.

Han, Y., Kingston, H. M., Boylan, H. M., Rahman, G. M. M., Shah, S., Richter, R. C., Link, D. D., and Bhandari, S.: Speciation of mercury in soil and sediment by selective solvent and acid extraction, Analytical and bioanalytical chemistry, 375, 428–436, doi:10.1007/s00216-002-1701-4, 2003.

Hellmann, C., Costa, R. D., and Schmitz, O. J.: How to Deal with Mercury in Sediments? A Critical Review About Used Methods for the Speciation of Mercury in Sediments, Chromatographia, 82, 125–141, doi:10.1007/s10337-018-3625-y, 2019.

Hight, S. C. and Cheng, J.: Determination of methylmercury and estimation of total mercury in seafood using high performance liquid chromatography (HPLC) and inductively coupled plasma-mass spectrometry (ICP-MS): Method development and validation, ANALYTICA CHIMICA ACTA, 567, 160–172, doi:10.1016/j.aca.2006.03.048, 2006.

Higueras, P., Oyarzun, R., Biester, H., Lillo, J., and Lorenzo, S.: A first insight into mercury distribution and speciation in soils from the Almadén mining district, Spain, Journal of Geochemical Exploration, 80, 95–104, doi:10.1016/S0375-6742(03)00185-7, 2003.

Hindersmann, I., Hippler, J., Hirner, A. V., and Mansfeldt, T.: Mercury volatilization from a floodplain soil during a simulated flooding event, J Soils Sediments, 14, 1549–1558, doi:10.1007/s11368-014-0908-2, 2014.

Hintelmann, H., Falter, R., Ilgen, G., and Evans, D. R.: Determination of artifactual formation of monomethylmercury (CH3Hg+) in environmental samples using stable Hg2+ isotopes with ICP-MS detection: Calculation of contents applying species specific isotope addition, Fresenius Journal of Analytical Chemistry, 358, 363–370, 1997.

Hintelmann, H., Hempel, M., and WILKEN, R. D.: Observation of unusual organic mercury species in soils and sediments of industrially contaminated sites, Environ. Sci. Technol., 29, 1845–1850, doi:10.1021/es00007a023, 1995.

Hintelmann, H. and Wilken, R.-D.: The analysis of organic mercury compounds using liquid chromatography with on-line atomic fluorescence spectrometric detection, Applied Organometallic Chemistry, 7, 173–180, 1993.

Hissler, C. and Probst, J.-L.: Impact of mercury atmospheric deposition on soils and streams in a mountainous catchment (Vosges, France) polluted by chlor-alkali industrial activity: the important trapping role of the organic matter, The Science of the total environment, 361, 163–178, doi:10.1016/j.scitotenv.2005.05.023, 2006.

Hofacker, A. F., Behrens, S., Voegelin, A., Kaegi, R., Lösekann-Behrens, T., Kappler, A., and Kretzschmar, R.: Clostridium Species as Metallic Copper-Forming Bacteria in Soil under Reducing Conditions, GEOMICROBIOLOGY JOURNAL, 32, 130–139, doi:10.1080/01490451.2014.933287, 2015.

Hofacker, A. F., Voegelin, A., Kaegi, R., and Kretzschmar, R.: Mercury mobilization in a flooded soil by incorporation into metallic copper and metal sulfide nanoparticles, Environmental science & technology, 47, 7739–7746, doi:10.1021/es4010976, 2013.

Hojdová, M., Rohovec, J., Chrastný, V., Penížek, V., and Navrátil, T.: The influence of sample drying procedures on mercury concentrations analyzed in soils, Bulletin of environmental contamination and toxicology, 94, 570–576, doi:10.1007/s00128-015-1521-9, 2015.

Horowitz, H. M., Jacob, D. J., Amos, H. M., Streets, D. G., and Sunderland, E. M.: Historical Mercury releases from commercial products: global environmental implications, Environmental science & technology, 48, 10242–10250, doi:10.1021/es501337j, 2014.

Horvat, M., Liang, L., and Bloom, N. S.: Comparison of distillation with other current isolation methods for the determination of methyl mercury compounds in low level environmental samples, ANALYTICA CHIMICA ACTA, 282, 153–168, doi:10.1016/0003-2670(93)80364-Q, 1993.

Horvat, M., Nolde, N., Fajon, V., Jereb, V., Logar, M., Lojen, S., Jacimovic, R., Falnoga, I., Liya, Q., Faganeli, J., and Drobne, D.: Total mercury, methylmercury and selenium in mercury polluted areas in the province Guizhou, China, Science of The Total Environment, 304, 231–256, doi:10.1016/S0048-9697(02)00572-7, 2003.

Hsu-Kim, H., Eckley, C. S., Achá, D., Feng, X., Gilmour, C. C., Jonsson, S., and Mitchell, C. P. J.: Challenges and opportunities for managing aquatic mercury pollution in altered landscapes, Ambio, 47, 141–169, doi:10.1007/s13280-017-1006-7, 2018.

Hsu-Kim, H., Kucharzyk, K. H., Zhang, T., and Deshusses, M. A.: Mechanisms regulating mercury bioavailability for methylating microorganisms in the aquatic environment: a critical review, Environmental science & technology, 47, 2441–2456, doi:10.1021/es304370g, 2013.

Hu, H., Li, M., Wang, G., Drosos, M., Li, Z., Hu, Z., and Xi, B.: Water-soluble mercury induced by organic amendments affected microbial community assemblage in mercury-polluted paddy soil, Chemosphere, 236, 124405, doi:10.1016/j.chemosphere.2019.124405, 2019.

Huang, J.-H.: Artifact formation of methyl- and ethyl-mercury compounds from inorganic mercury during derivatization using sodium tetra(n-propyl)borate, ANALYTICA CHIMICA ACTA, 532, 113–120, doi:10.1016/j.aca.2004.10.057, 2005.

Imseng, M., Wiggenhauser, M., Müller, M., Keller, A., Frossard, E., Wilcke, W., and Bigalke, M.: The Fate of Zn in Agricultural Soils: A Stable Isotope Approach to Anthropogenic Impact, Soil Formation, and Soil-Plant Cycling, Environmental science & technology, 53, 4140–4149, doi:10.1021/acs.est.8b03675, 2019.

IUSS Working Group WRB: World Reference Base for Soil Resources 2014, update 2015: International soil classification system for naming soils and creating legends for soil maps., FOOD AND AGRICULTURE ORGANIZATION OF THE UNITED NATIONS, Rome, World Soil Resources Reports, 106, 203 pp., 2015.

Jagtap, R. and Maher, W.: Measurement of mercury species in sediments and soils by HPLC–ICPMS, Microchemical Journal, 121, 65–98, doi:10.1016/j.microc.2015.01.010, 2015.

Jiang, T., Skyllberg, U., Wei, S., Wang, D., Lu, S., Jiang, Z., and Flanagan, D. C.: Modeling of the structure-specific kinetics of abiotic, dark reduction of Hg(II) complexed by O/N and S functional groups in humic acids while accounting for time-dependent structural rearrangement, Geochimica et Cosmochimica Acta, 154, 151–167, doi:10.1016/j.gca.2015.01.011, 2015.

Jiskra, M., Heimbürger-Boavida, L.-E., Desgranges, M.-M., Petrova, M. V., Dufour, A., Ferreira-Araujo, B., Masbou, J., Chmeleff, J., Thyssen, M., Point, D., and Sonke, J. E.: Mercury stable isotopes constrain atmospheric sources to the ocean, Nature, 597, 678–682, doi:10.1038/s41586-021-03859-8, 2021.

Jiskra, M., Sonke, J. E., Obrist, D., Bieser, J., Ebinghaus, R., Myhre, C. L., Pfaffhuber, K. A., Wängberg, I., Kyllönen, K., Worthy, D., Martin, L. G., Labuschagne, C., Mkololo, T., Ramonet, M., Magand, O., and Dommergue, A.: A vegetation control on seasonal variations in global atmospheric mercury concentrations, Nature Geosci, 11, 244–250, doi:10.1038/s41561-018-0078-8, 2018.

Jiskra, M., Wiederhold, J. G., Skyllberg, U., Kronberg, R.-M., and Kretzschmar, R.: Source tracing of natural organic matter bound mercury in boreal forest runoff with mercury stable isotopes, Environmental science. Processes & impacts, 19, 1235–1248, doi:10.1039/c7em00245a, 2017.

Jones, M. E., Nico, P. S., Ying, S., Regier, T., Thieme, J., and Keiluweit, M.: Manganese-Driven Carbon Oxidation at Oxic-Anoxic Interfaces, Environ. Sci. Technol., 52, 12349–12357, doi:10.1021/acs.est.8b03791, 2018.

Jonsson, S., Skyllberg, U., Nilsson, M. B., Westlund, P.-O., Shchukarev, A., Lundberg, E., and Björn, E.: Mercury methylation rates for geochemically relevant Hg(II) species in sediments, Environmental science & technology, 46, 11653–11659, doi:10.1021/es3015327, 2012.

José Manuel Barroso: COMMISSION REGULATION (EU) No 848/2012: amending Annex XVII to Regulation (EC) No 1907/2006 of the European Parliament and of the Council on the Registration, Evaluation, Authorisation and Restriction of Chemicals (REACH) as regards phenylmercury compounds, Official Journal of the European Union, Brussels, 3 pp., 2012.

Kelly, C. A., Rudd, J. W. M., and Holoka, M. H.: Effect of pH on mercury uptake by an aquatic bacterium: implications for Hg cycling, Environmental science & technology, 37, 2941–2946, doi:10.1021/es026366o, 2003.

Kentisbeer, J., Leeson, S. R., Malcolm, H. M., Leith, I. D., Braban, C. F., and Cape, J. N.: Patterns and source analysis for atmospheric mercury at Auchencorth Moss, Scotland, Environmental science. Processes & impacts, 16, 1112–1123, doi:10.1039/C3EM00700F, 2014.

King, J. K., Harmon, S., Fu, T. T., and Gladden, J. B.: Mercury removal, methylmercury formation, and sulfate-reducing bacteria profiles in wetland mesocosms, Chemosphere, 46, 859–870, doi:10.1016/S0045-6535(01)00135-7, 2002.

Kodamatani, H., Maeda, C., Balogh, S. J., Nollet, Y. H., Kanzaki, R., and Tomiyasu, T.: The influence of sample drying and storage conditions on methylmercury determination in soils and sediments, Chemosphere, 173, 380–386, doi:10.1016/j.chemosphere.2017.01.053, 2017.

Kodamatani, H., Shigetomi, A., Akama, J., Kanzaki, R., and Tomiyasu, T.: Distribution, alkylation, and migration of mercury in soil discharged from the Itomuka mercury mine, The Science of the total environment, 815, 152492, doi:10.1016/j.scitotenv.2021.152492, 2022.

Kronberg, R.-M., Jiskra, M., Wiederhold, J. G., Björn, E., and Skyllberg, U.: Methyl Mercury Formation in Hillslope Soils of Boreal Forests: The Role of Forest Harvest and Anaerobic Microbes, Environmental science & technology, 50, 9177–9186, doi:10.1021/acs.est.6b00762, 2016.

Lakshmanan, S. and Murugesan, T.: The chlor-alkali process: Work in Progress, Clean Techn Environ Policy, 16, 225–234, doi:10.1007/s10098-013-0630-6, 2014.

Landis, M. S., Keeler, G. J., Al-Wali, K. I., and Stevens, R. K.: Divalent inorganic reactive gaseous mercury emissions from a mercury cell chlor-alkali plant and its impact on near-field atmospheric dry deposition, Atmospheric Environment, 38, 613–622, doi:10.1016/j.atmosenv.2003.09.075, 2004.

Langford, N. and Ferner, R.: Toxicity of mercury, J Hum Hypertens, 13, 651–656, doi:10.1038/sj.jhh.1000896, 1999.

Lavoie, R. A., Jardine, T. D., Chumchal, M. M., Kidd, K. A., and Campbell, L. M.: Biomagnification of mercury in aquatic food webs: a worldwide meta-analysis, Environ. Sci. Technol., 47, 13385–13394, doi:10.1021/es403103t, 2013.

Lazareva, O., Sparks, D. L., Landis, R., Ptacek, C. J., and Ma, J.: Investigation of legacy industrial mercury in floodplain soils: South River, Virginia, USA, Environ Earth Sci, 78, 276, doi:10.1007/s12665-019-8253-9, 2019.

Leermakers, M., Nguyen, H. L., Kurunczi, S., Vanneste, B., Galletti, S., and Baeyens, W.: Determination of methylmercury in environmental samples using static headspace gas chromatography and atomic fluorescence detection after aqueous phase ethylation, Analytical and bioanalytical chemistry, 377, 327–333, doi:10.1007/s00216-003-2116-6, 2003.

Li, C., Xu, Z., Luo, K., Chen, Z., Xu, X., Xu, C., and Qiu, G.: Biomagnification and trophic transfer of total mercury and methylmercury in a sub-tropical montane forest food web, southwest China, Chemosphere, 277, 130371, doi:10.1016/j.chemosphere.2021.130371, 2021a.

Li, H., Zheng, D., Zhang, X., Niu, Z., Ma, H., Zhang, S., and Wu, C.: Total and Methylmercury of Suaeda heteroptera Wetland Soil Response to a Salinity Gradient Under Wetting and Drying Conditions, Bulletin of environmental contamination and toxicology, 104, 778–785, doi:10.1007/s00128-020-02874-1, 2020.

Li, M., Drosos, M., Hu, H., He, X., Wang, G., Zhang, H., Hu, Z., and Xi, B.: Organic amendments affect dissolved organic matter composition and mercury dissolution in pore waters of mercury-polluted paddy soil, Chemosphere, 232, 356–365, doi:10.1016/j.chemosphere.2019.05.234, 2019.

Li, R., Qi, L., Ibeanusi, V., Badisa, V., Brooks, S., and Chen, G.: Reduction and bacterial adsorption of dissolved mercuric ion by indigenous bacteria at the Oak Ridge Reservation site, Chemosphere, 280, 130629, doi:10.1016/j.chemosphere.2021.130629, 2021b.

Lian, P., Mou, Z., Cooper, C. J., Johnston, R. C., Brooks, S. C., Gu, B., Govind, N., Jonsson, S., and Parks, J. M.: Mechanistic Investigation of Dimethylmercury Formation Mediated by a Sulfide Mineral Surface, The journal of physical chemistry. A, 125, 5397–5405, doi:10.1021/acs.jpca.1c04014, 2021.

Liang, L., Horvat, M., Feng, X., Shang, L., Li, H., and Pang, P.: Re-evaluation of distillation and comparison with HNO3 leaching/solvent extraction for isolation of methylmercury compounds from sediment/soil samples, Appl. Organometal. Chem., 18, 264–270, doi:10.1002/aoc.617, 2004.

Liang, X., Lu, X., Zhao, J., Liang, L., Zeng, E. Y., and Gu, B.: Stepwise Reduction Approach Reveals Mercury Competitive Binding and Exchange Reactions within Natural Organic Matter and Mixed Organic Ligands, Environmental science & technology, 53, 10685–10694, doi:10.1021/acs.est.9b02586, 2019.

Lide, D. R.: CRC Handbook of Chemistry and Physics, 85th Edition, CRC Press, 2004.

Lima, C. A. I. de, Almeida, M. G. de, Pestana, I. A., Bastos, W. R., do Nascimento Recktenvald, M. C. N., Souza, C. M. M. de, and Pedrosa, P.: Impact of Land Use on the Mobility of Hg Species in Different Compartments of a Tropical Watershed in Brazil, Archives of environmental contamination and toxicology, doi:10.1007/s00244-017-0449-y, 2017.

Liu, J., Zhao, L., Kong, K., Abdelhafiz, M. A., Tian, S., Jiang, T., Meng, B., and Feng, X.: Uncovering geochemical fractionation of the newly deposited Hg in paddy soil using a stable isotope tracer, Journal of hazardous materials, 433, 128752, doi:10.1016/j.jhazmat.2022.128752, 2022.

Liu, S., Wang, J., Pu, S., Blagodatskaya, E., Kuzyakov, Y., and Razavi, B. S.: Impact of manure on soil biochemical properties: A global synthesis, The Science of the total environment, 745, 141003, doi:10.1016/j.scitotenv.2020.141003, 2020.

Liu, Y.-R., Dong, J.-X., Han, L.-L., Zheng, Y.-M., and He, J.-Z.: Influence of rice straw amendment on mercury methylation and nitrification in paddy soils, Environmental pollution (Barking, Essex 1987), 209, 53–59, doi:10.1016/j.envpol.2015.11.023, 2016.

Liu, Y.-R., Johs, A., Bi, L., Lu, X., Hu, H.-W., Sun, D., He, J.-Z., and Gu, B.: Unraveling Microbial Communities Associated with Methylmercury Production in Paddy Soils, Environmental science & technology, 52, 13110–13118, doi:10.1021/acs.est.8b03052, 2018.

Liu, Y.-R., Yu, R.-Q., Zheng, Y.-M., and He, J.-Z.: Analysis of the microbial community structure by monitoring an Hg methylation gene (hgcA) in paddy soils along an Hg gradient, Applied and Environmental Microbiology, 80, 2874–2879, doi:10.1128/AEM.04225-13, 2014.

Lyman, S. N. and Jaffe, D. A.: Formation and fate of oxidized mercury in the upper troposphere and lower stratosphere, Nature Geosci, 5, 114–117, doi:10.1038/ngeo1353, 2012.

Ma, D., Wu, J., Yang, P., and Zhu, M.: Coupled Manganese Redox Cycling and Organic Carbon Degradation on Mineral Surfaces, Environ. Sci. Technol., 54, 8801–8810, doi:10.1021/acs.est.0c02065, 2020.

Malta, G., Freakley, S. J., Kondrat, S. A., and Hutchings, G. J.: Acetylene hydrochlorination using Au/carbon: a journey towards single site catalysis, Chemical communications (Cambridge, England), 53, 11733–11746, doi:10.1039/c7cc05986h, 2017.

Manceau, A., Lemouchi, C., Enescu, M., Gaillot, A.-C., Lanson, M., Magnin, V., Glatzel, P., Poulin, B. A., Ryan, J. N., Aiken, G. R., Gautier-Luneau, I., and Nagy, K. L.: Formation of Mercury Sulfide from Hg(II)-Thiolate Complexes in Natural Organic Matter, Environmental science & technology, 49, 9787–9796, doi:10.1021/acs.est.5b02522, 2015.

Manceau, A., Nagy, K. L., Marcus, M. A., Lanson, M., Geoffroy, N., Jacquet, T., and Kirpichtchikova, T.: Formation of metallic copper nanoparticles at the soil-root interface, Environmental science & technology, 42, 1766–1772, doi:10.1021/es072017o, 2008.

Mantovi, P., Bonazzi, G., Maestri, E., and Marmiroli, N.: Accumulation of copper and zinc from liquid manure in agricultural soils and crop plants., Plant and Soil, 250, 249–257, doi:10.1023/A:1022848131043, 2003.

Mao, Y., Yin, Y., Li, Y., Liu, G., Feng, X., Jiang, G., and Cai, Y.: Occurrence of monoethylmercury in the Florida Everglades: identification and verification, Environmental pollution (Barking, Essex 1987), 158, 3378–3384, doi:10.1016/j.envpol.2010.07.031, 2010.

Marvin-DiPasquale, M., Windham-Myers, L., Agee, J. L., Kakouros, E., Le Kieu, H., Fleck, J. A., Alpers, C. N., and Stricker, C. A.: Methylmercury production in sediment from agricultural and non-agricultural wetlands in the Yolo Bypass, California, USA, The Science of the total environment, 484, 288–299, doi:10.1016/j.scitotenv.2013.09.098, 2014.

Matsumoto, H., Koya, G., and Takeuchi, T.: Fetal Minamata Disease: A Neuropathological Study of Two Cases of Intrauterine Intoxi cation by a Methyl Mercury Compound, Journal of Neuropathology and Experimental Neurology, 24, 563–574, doi:10.1097/00005072-196510000-00002, 1965.

Matthews, D. A., Babcock, D. B., Nolan, J. G., Prestigiacomo, A. R., Effler, S. W., Driscoll, C. T., Todorova, S. G., and Kuhr, K. M.: Whole-lake nitrate addition for control of methylmercury in mercury-contaminated Onondaga Lake, NY, Environmental research, 125, 52–60, doi:10.1016/j.envres.2013.03.011, 2013.

McLagan, D. S., Osterwalder, S., and Biester, H.: Temporal and spatial assessment of gaseous elemental mercury concentrations and emissions at contaminated sites using active and passive measurements, Environ. Res. Commun., 3, 51004, doi:10.1088/2515-7620/abfe02, 2021.

McLagan, D. S., Schwab, L., Wiederhold, J. G., Chen, L., Pietrucha, J., Kraemer, S. M., and Biester, H.: Demystifying mercury geochemistry in contaminated soil-groundwater systems with complementary mercury stable isotope, concentration, and speciation analyses, Environmental science. Processes & impacts, 24, 1406–1429, doi:10.1039/d1em00368b, 2022.

Mesko, M. F., Hartwig, C. A., Bizzi, C. A., Pereira, J. S., Mello, P. A., and Flores, E. M.: Sample preparation strategies for bioinorganic analysis by inductively coupled plasma mass spectrometry, International Journal of Mass Spectrometry, 307, 123–136, doi:10.1016/j.ijms.2011.03.002, 2011.

Miller, C. L., Mason, R. P., Gilmour, C. C., and Heyes, A.: Influence of dissolved organic matter on the complexation of Hg under sulfidic conditions., Environmental Toxicology and Chemistry, 26, 624–633, 2007.

Miller, C. L., Southworth, G., Brooks, S., Liang, L., and Gu, B.: Kinetic controls on the complexation between mercury and dissolved organic matter in a contaminated environment, Environmental science & technology, 43, 8548–8553, doi:10.1021/es901891t, 2009.

Millhollen, A. G., Obrist, D., and Gustin, M. S.: Mercury accumulation in grass and forb species as a function of atmospheric carbon dioxide concentrations and mercury exposures in air and soil, Chemosphere, 65, 889–897, doi:10.1016/j.chemosphere.2006.03.008, 2006.

Mitchell, C. P. J., Branfireun, B. A., and Kolka, R. K.: Methylmercury dynamics at the upland-peatland interface: Topographic and hydrogeochemical controls, Water Resour. Res., 45, doi:10.1029/2008WR006832, 2009.

Monperrus, M., Krupp, E., Amouroux, D., Donard, O., and Rodríguez Martín-Doimeadios, R.: Potential and limits of speciated isotope-dilution analysis for metrology and assessing environmental reactivity, TrAC Trends in Analytical Chemistry, 23, 261–272, doi:10.1016/S0165-9936(04)00313-9, 2004.

Monperrus, M., Rodriguez Gonzalez, P., Amouroux, D., Garcia Alonso, J. I., and Donard, O. F. X.: Evaluating the potential and limitations of double-spiking species-specific isotope dilution analysis for the accurate quantification of mercury species in different environmental matrices, Analytical and bioanalytical chemistry, 390, 655–666, doi:10.1007/s00216-007-1598-z, 2008.

Monperrus, M., Zuloaga, O., Krupp, E., Amouroux, D., Wahlen, R., Fairman, B., and Donard, O. F. X.: Rapid, accurate and precise determination of tributyltin in sediments and biological samples by species specific isotope dilution-microwave extraction-gas chromatography-ICP mass spectrometry, J. Anal. At. Spectrom., 18, 247–253, doi:10.1039/b203242m, 2003.

Moore, C. and Carpi, A.: Mechanisms of the emission of mercury from soil: Role of UV radiation, J. Geophys. Res., 110, doi:10.1029/2004JD005567, 2005.

Mudry, A.: Quecksilberbelastungen im Raum Visp - Niedergesteln: Weitere Ergebnisse im Siedlungsgebiet, Sion, 2 pp., 2016.

Muresan, B., Cossa, D., Jézéquel, D., Prévot, F., and Kerbellec, S.: The biogeochemistry of mercury at the sediment–water interface in the Thau lagoon. 1. Partition and speciation, Estuarine, Coastal and Shelf Science, 72, 472–484, doi:10.1016/j.ecss.2006.11.015, 2007.

Nagase, H., Ose, Y., Sato, T., and Ishikawa, T.: Mercury methylation by compounds in humic material, Science of The Total Environment, 32, 147–156, doi:10.1016/0048-9697(84)90127-X, 1984.

Neculita, C.-M., Zagury, G. J., and Deschênes, L.: Mercury speciation in highly contaminated soils from chlor-alkali plants using chemical extractions, Journal of Environmental Quality, 34, 255–262, 2005.

Nriagu, J. and Becker, C.: Volcanic emissions of mercury to the atmosphere: global and regional inventories, Science of The Total Environment, 304, 3–12, doi:10.1016/S0048-9697(02)00552-1, 2003.

Obrist, D.: Mercury distribution across 14 U.S. forests. Part II: Patterns of methyl mercury concentrations and areal mass of total and methyl mercury, Environmental science & technology, 46, 5921–5930, doi:10.1021/es2045579, 2012.

Obrist, D., Johnson, D. W., and Lindberg, S. E.: Mercury concentrations and pools in four Sierra Nevada forest sites, and relationships to organic carbon and nitrogen, Biogeosciences Discuss., 6, 1777–1809, doi:10.5194/bgd-6-1777-2009, 2009.

Obrist, D., Johnson, D. W., Lindberg, S. E., Luo, Y., Hararuk, O., Bracho, R., Battles, J. J., Dail, D. B., Edmonds, R. L., Monson, R. K., Ollinger, S. V., Pallardy, S. G., Pregitzer, K. S., and Todd, D. E.: Mercury distribution across 14 U.S. Forests. Part I: spatial patterns of concentrations in biomass, litter, and soils, Environmental science & technology, 45, 3974–3981, doi:10.1021/es104384m, 2011.

Obrist, D., Kirk, J. L., Zhang, L., Sunderland, E. M., Jiskra, M., and Selin, N. E.: A review of global environmental mercury processes in response to human and natural perturbations: Changes of emissions, climate, and land use, Ambio, 47, 116–140, doi:10.1007/s13280-017-1004-9, 2018.

O'Connor, D., Peng, T., Li, G., Wang, S., Duan, L., Mulder, J., Cornelissen, G., Cheng, Z., Yang, S., and Hou, D.: Sulfur-modified rice husk biochar: A green method for the remediation of mercury contaminated soil, The Science of the total environment, 621, 819–826, doi:10.1016/j.scitotenv.2017.11.213, 2018.

OSHA Hazard Information Bulletins Dimethylmercury | Occupational Safety and Health Administration: https://www.osha.gov/publications/hib19980309, last access: 8 January 2023.

Osterwalder, S., Huang, J.-H., Shetaya, W. H., Agnan, Y., Frossard, A., Frey, B., Alewell, C., Kretzschmar, R., Biester, H., and Obrist, D.: Mercury emission from industrially contaminated soils in relation to chemical, microbial, and meteorological factors, Environmental pollution (Barking, Essex 1987), 250, 944–952, doi:10.1016/j.envpol.2019.03.093, 2019.

Osterwalder, S., Sommar, J., Åkerblom, S., Jocher, G., Fritsche, J., Nilsson, M. B., Bishop, K., and Alewell, C.: Comparative study of elemental mercury flux measurement techniques over a Fennoscandian boreal peatland, Atmospheric Environment, 172, 16–25, doi:10.1016/j.atmosenv.2017.10.025, 2018.

Panagos, P., Jiskra, M., Borrelli, P., Liakos, L., and Ballabio, C.: Mercury in European topsoils: Anthropogenic sources, stocks and fluxes, Environmental research, 201, 111556–111567, doi:10.1016/j.envres.2021.111556, 2021.

Parks, J. M., Guo, H., Momany, C., Liang, L., Miller, S. M., Summers, A. O., and Smith, J. C.: Mechanism of Hg-C protonolysis in the organomercurial lyase MerB, Journal of the American Chemical Society, 131, 13278–13285, doi:10.1021/ja9016123, 2009.

Parks, J. M., Johs, A., Podar, M., Bridou, R., Hurt, R. A. [., Smith, S. D., Tomanicek, S. J., Qian, Y., Brown, S. D., Brandt, C. C., Palumbo, A. V., Smith, J. C., Wall, J. D., Elias, D. A., and Liang, L.: The Genetic Basis for Bacterial Mercury Methylation, Science, 339, 1332–1335, 2013.

Pfiffner, L. and Luka, H.: Evaluation Ökomassnahmen Biodiversität: Biodiversitä Effekte ökologischer Ausgleichsflächen auf die Laufkäferfauna, AGRARForschung, 7, 205–217, 2000.

Pham, A. L.-T., Morris, A., Zhang, T., Ticknor, J., Levard, C., and Hsu-Kim, H.: Precipitation of nanoscale mercuric sulfides in the presence of natural organic matter: Structural properties, aggregation, and biotransformation, Geochimica et Cosmochimica Acta, 133, 204–215, doi:10.1016/j.gca.2014.02.027, 2014.

Pickhardt, P. C. and Fisher, N. S.: Accumulation of inorganic and methylmercury by freshwater phytoplankton in two contrasting water bodies, Environmental science & technology, 41, 125–131, doi:10.1021/es060966w, 2007.

Podar, M., Gilmour, C. C., Brandt, C. C., Soren, A., Brown, S. D., Crable, B. R., Palumbo, A. V., Somenahally, A. C., and Elias, D. A.: Global prevalence and distribution of genes and microorganisms involved in mercury methylation, Science advances, 1, e1500675, doi:10.1126/sciadv.1500675, 2015.

Ponting, J., Kelly, T. J., Verhoef, A., Watts, M. J., and Sizmur, T.: The impact of increased flooding occurrence on the mobility of potentially toxic elements in floodplain soil - A review, The Science of the total environment, 754, 142040, doi:10.1016/j.scitotenv.2020.142040, 2020.

Poulain, A. J. and Barkay, T.: Cracking the Mercury Methylation Code, Science (New York, N.Y.), 339, 1280–1281, doi:10.1126/science.1235591, 2013.

Poulin, B. A., Aiken, G. R., Nagy, K. L., Manceau, A., Krabbenhoft, D. P., and Ryan, J. N.: Mercury transformation and release differs with depth and time in a contaminated riparian soil during simulated flooding, Geochimica et Cosmochimica Acta, 176, 118–138, doi:10.1016/j.gca.2015.12.024, 2016.

Poulin, B. A., Gerbig, C. A., Kim, C. S., Stegemeier, J. P., Ryan, J. N., and Aiken, G. R.: Effects of Sulfide Concentration and Dissolved Organic Matter Characteristics on the Structure of Nanocolloidal Metacinnabar, Environmental science & technology, 51, 13133–13142, doi:10.1021/acs.est.7b02687, 2017.

Qiu, G., Feng, X., Wang, S., and Shang, L.: Mercury and methylmercury in riparian soil, sediments, mine-waste calcines, and moss from abandoned Hg mines in east Guizhou province, southwestern China, Applied Geochemistry, 20, 627–638, doi:10.1016/j.apgeochem.2004.09.006, 2005.

Quenvauviller, P. and Horvat, M.: Letter to the Editor: Artifact formation of methylmercury in sediments, Analytical chemistry, 71, 155A, doi:10.1021/ac990222j, 1999.

Qvarnström, J. and Frech, W.: Mercury species transformations during sample pre-treatment of biological tissues studied by HPLC-ICP-MS, J. Anal. At. Spectrom., 17, 1486–1491, doi:10.1039/B205246F, 2002.

Ravichandran, M.: Interactions between mercury and dissolved organic matter--a review, Chemosphere, 55, 319–331, doi:10.1016/j.chemosphere.2003.11.011, 2004.

Ravichandran, M., Aiken, G. R., Reddy, M. M., and Ryan, J. N.: Enhanced Dissolution of Cinnabar (Mercuric Sulfide) by Dissolved Organic Matter Isolated from the Florida Everglades, Environ. Sci. Technol., 32, 3305–3311, doi:10.1021/es9804058, 1998.

Ravichandran, M., Aiken, G. R., Ryan, J. N., and Reddy, M. M.: Inhibition of Precipitation and Aggregation of Metacinnabar (Mercuric Sulfide) by Dissolved Organic Matter Isolated from the Florida Everglades, Environ. Sci. Technol., 33, 1418–1423, doi:10.1021/es9811187, 1999.

Reimann, C. and Caritat, P. de: Distinguishing between natural and anthropogenic sources for elements in the environment: regional geochemical surveys versus enrichment factors, The Science of the total environment, 337, 91–107, doi:10.1016/j.scitotenv.2004.06.011, 2005.

Remucal, C. K., Cory, R. M., Sander, M., and McNeill, K.: Low molecular weight components in an aquatic humic substance as characterized by membrane dialysis and orbitrap mass spectrometry, Environ. Sci. Technol., 46, 9350–9359, doi:10.1021/es302468q, 2012.

Remucal, C. K. and Ginder-Vogel, M.: A critical review of the reactivity of manganese oxides with organic contaminants, Environmental science. Processes & impacts, 16, 1247–1266, doi:10.1039/c3em00703k, 2014.

Richner, W. and Sinaj, S.: Grundlagen für die Düngung landwirtschaflticher Kulturen in der Schweiz (GRUD 2017), Agroscope, Bern, Schweiz, 276 pp., 2017.

Rieder, S. R., Brunner, I., Horvat, M., Jacobs, A., and Frey, B.: Accumulation of mercury and methylmercury by mushrooms and earthworms from forest soils, Environmental pollution (Barking, Essex 1987), 159, 2861–2869, doi:10.1016/j.envpol.2011.04.040, 2011.

Rimmer, C. C., Miller, E. K., McFarland, K. P., Taylor, R. J., and Faccio, S. D.: Mercury bioaccumulation and trophic transfer in the terrestrial food web of a montane forest, Ecotoxicology (London, England), 19, 697–709, doi:10.1007/s10646-009-0443-x, 2010.

Rivera, N. A., Bippus, P. M., and Hsu-Kim, H.: Relative Reactivity and Bioavailability of Mercury Sorbed to or Coprecipitated with Aged Iron Sulfides, Environ. Sci. Technol., 53, 7391–7399, doi:10.1021/acs.est.9b00768, 2019.

Roberts, H., Price, R., Brombach, C.-C., and Pichler, T.: Mercury in the hydrothermal fluids and gases in Paleochori Bay, Milos, Greece, Marine Chemistry, 233, 103984, doi:10.1016/j.marchem.2021.103984, 2021.

Rodríguez Martín, J. A. and Nanos, N.: Soil as an archive of coal-fired power plant mercury deposition, Journal of hazardous materials, 308, 131–138, doi:10.1016/j.jhazmat.2016.01.026, 2016.

Rogers, R. D.: Methylation of Mercury in Agricultural Soils, J. environ. qual., 5, 454–458, doi:10.2134/jeq1976.00472425000500040028x, 1976.

Rogers, R. D.: Abiological Methylation of Mercury in Soil, J. environ. qual., 6, 463–467, doi:10.2134/jeq1977.00472425000600040029x, 1977.

Rothenberg, S. E. and Feng, X.: Mercury cycling in a flooded rice paddy, J. Geophys. Res., 117, doi:10.1029/2011JG001800, 2012.

RStudio Team: RStudio: Integrated Development for R., RStudio Team, PBC, Boston, MA, 2020.

Sannac, S., Chen, Y.-H., Wahlen, R., and McCurdy, E.: Benefits of HPLC-ICP-MS coupling for mercury speciation in food: Application note, Food testing, Agilent Technologies, 5991-D066EN, 1–6, 2017.

Sannac, S., Fisicaro, P., Labarraque, G., Pannier, F., and Potin-Gautier, M.: Development of a reference measurement procedure for the determination of methylmercury in fish products, Accred Qual Assur, 14, 263–267, doi:10.1007/s00769-009-0509-8, 2009.

Schaefer, J. K. and Morel, F. M. M.: High methylation rates of mercury bound to cysteine by Geobacter sulfurreducens, Nature Geosci, 2, 123–126, doi:10.1038/NGEO412, 2009.

Schaefer, J. K., Rocks, S. S., Zheng, W., Liang, L., Gu, B., and Morel, F. M. M.: Active transport, substrate specificity, and methylation of Hg(II) in anaerobic bacteria, Proceedings of the National Academy of Sciences of the United States of America, 108, 8714–8719, doi:10.1073/pnas.1105781108, 2011.

Schaefer, K., Elshorbany, Y., Jafarov, E., Schuster, P. F., Striegl, R. G., Wickland, K. P., and Sunderland, E. M.: Potential impacts of mercury released from thawing permafrost, Nat Commun, 11, 4650, doi:10.1038/s41467-020-18398-5, 2020.

Schlueter, K.: Review: evaporation of mercury from soils. An integration and synthesis of current knowledge, Environmental Geology, 39, 249–271, doi:10.1007/s002540050005, 2000.

Schroeder, W. H. and Munthe, J.: Atmospheric mercury—An overview, Atmospheric Environment, 32, 809–822, doi:10.1016/S1352-2310(97)00293-8, 1998.

Schuster, P. F., Schaefer, K. M., Aiken, G. R., Antweiler, R. C., Dewild, J. F., Gryziec, J. D., Gusmeroli, A., Hugelius, G., Jafarov, E., Krabbenhoft, D. P., Liu, L., Herman-Mercer, N., Mu, C., Roth, D. A., Schaefer, T., Striegl, R. G., Wickland, K. P., and Zhang, T.: Permafrost Stores a Globally Significant Amount of Mercury, Geophys. Res. Lett., 45, 1463–1471, doi:10.1002/2017GL075571, 2018.

Shanley, J. B., Marvin-DiPasquale, M., Lane, O., Arendt, W., Hall, S., and McDowell, W. H.: Resolving a paradox-high mercury deposition, but low bioaccumulation in northeastern Puerto Rico, Ecotoxicology (London, England), 29, 1207–1220, doi:10.1007/s10646-019-02108-z, 2020.

Sheehan, M. C., Burke, T. A., Navas-Acien, A., Breysse, P. N., McGready, J., and Fox, M. A.: Global methylmercury exposure from seafood consumption and risk of developmental neurotoxicity: a systematic review, Bull World Health Organ, 92, 254-269F, doi:10.2471/BLT.12.116152, 2014.

Siemens, J. and Kaupenjohann, M.: Dissolved organic carbon is released from sealings and glues of pore-water samplers, Soil Science Society of America Journal, 67, 795–797, 2003.

Singer, M. B., Harrison, L. R., Donovan, P. M., Blum, J. D., and Marvin-DiPasquale, M.: Hydrologic indicators of hot spots and hot moments of mercury methylation potential along river corridors, The Science of the total environment, 568, 697–711, doi:10.1016/j.scitotenv.2016.03.005, 2016.

Skerfving, S. B. and Copplestone, J. F.: Poisoning caused by the consumption of organomercury-dressed seed in Iraq, Bulletin of the World Health Organization, 54, 101–112, 1976.

Skyllberg, U.: Competition among thiols and inorganic sulfides and polysulfides for Hg and MeHg in wetland soils and sediments under suboxic conditions: Illumination of controversies and implications for MeHg net production, J. Geophys. Res., 113, n/a-n/a, doi:10.1029/2008JG000745, 2008.

Skyllberg, U., Bloom, P. R., Qian, J., Lin, C.-M., and Bleam, W. F.: Complexation of mercury(II) in soil organic matter: EXAFS evidence for linear two-coordination with reduced sulfur groups, Environmental science & technology, 40, 4174–4180, doi:10.1021/es0600577, 2006.

Skyllberg, U. and Drott, A.: Competition between disordered iron sulfide and natural organic matter associated thiols for mercury(II)-an EXAFS study, Environmental science & technology, 44, 1254–1259, doi:10.1021/es902091w, 2010.

Smeds, J., Öquist, M., Nilsson, M. B., and Bishop, K.: A Simplified Drying Procedure for Analysing Hg Concentrations, Water Air Soil Pollut, 233, doi:10.1007/s11270-022-05678-7, 2022.

Smith-Downey, N. V., Sunderland, E. M., and Jacob, D. J.: Anthropogenic impacts on global storage and emissions of mercury from terrestrial soils: Insights from a new global model, J. Geophys. Res., 115, doi:10.1029/2009JG001124, 2010.

Song, Y., Jiang, T., van Liem-Nguyen, Sparrman, T., Björn, E., and Skyllberg, U.: Thermodynamics of Hg(II) Bonding to Thiol Groups in Suwannee River Natural Organic Matter Resolved by Competitive Ligand Exchange, Hg LIII-Edge EXAFS and 1H NMR Spectroscopy, Environ. Sci. Technol., 52, 8292–8301, doi:10.1021/acs.est.8b00919, 2018.

Stoichev, T., Tessier, E., Coelho, J. P., Lobos Valenzuela, M. G., Pereira, M. E., and Amouroux, D.: Multiple regression analysis to assess the spatial distribution and speciation of mercury in surface sediments of a contaminated lagoon, Journal of hazardous materials, 367, 715–724, doi:10.1016/j.jhazmat.2018.12.109, 2018.

Sunda, W. G. and Kieber, D. J.: Oxidation of humic substances by manganese oxides yields low-molecular-weight organic substrates, Nature, 367, 62–64, doi:10.1038/367062a0, 1994.

Sunderland, E. M. and Mason, R. P.: Human impacts on open ocean mercury concentrations, Global Biogeochem. Cycles, 21, n/a-n/a, doi:10.1029/2006GB002876, 2007.

Tang, W., Hintelmann, H., Gu, B., Feng, X., Liu, Y., Gao, Y., Zhao, J., Zhu, H., Lei, P., and Zhong, H.: Increased Methylmercury Accumulation in Rice after Straw Amendment, Environ. Sci. Technol., 53, 6144–6153, doi:10.1021/acs.est.8b07145, 2019.

Tang, Z., Fan, F., Wang, X., Shi, X., Deng, S., and Wang, D.: Mercury in rice (Oryza sativa L.) and rice-paddy soils under long-term fertilizer and organic amendment, Ecotoxicology and environmental safety, 150, 116–122, doi:10.1016/j.ecoenv.2017.12.021, 2018.

Tian, L., Guan, W., Ji, Y., He, X., Chen, W., Alvarez, P. J. J., and Zhang, T.: Microbial methylation potential of mercury sulfide particles dictated by surface structure, Nat. Geosci., 14, 409–416, doi:10.1038/s41561-021-00735-y, 2021.

Ticknor, J. L., Kucharzyk, K. H., Porter, K. A., Deshusses, M. A., and Hsu-Kim, H.: Thiol-Based Selective Extraction Assay to Comparatively Assess Bioavailable Mercury in Sediments, Environmental engineering science, 32, 564–573, doi:10.1089/ees.2014.0526, 2015.

Tomiyasu, T., Kodamatani, H., Imura, R., Matsuyama, A., Miyamoto, J., Akagi, H., Kocman, D., Kotnik, J., Fajon, V., and Horvat, M.: The dynamics of mercury near Idrija mercury mine, Slovenia: Horizontal and vertical distributions of total, methyl, and ethyl mercury concentrations in soils, Chemosphere, 184, 244–252, doi:10.1016/j.chemosphere.2017.05.123, 2017.

Tsz-Ki Tsui, M., Liu, S., Brasso, R. L., Blum, J. D., Kwon, S. Y., Ulus, Y., Nollet, Y. H., Balogh, S. J., Eggert, S. L., and Finlay, J. C.: Controls of Methylmercury Bioaccumulation in Forest Floor Food Webs, Environmental science & technology, 53, 2434–2440, doi:10.1021/acs.est.8b06053, 2019.

Ukonmaanaho, L., Starr, M., Kantola, M., Laurén, A., Piispanen, J., Pietilä, H., Perämäki, P., Merilä, P., Fritze, H., Tuomivirta, T., Heikkinen, J., Mäkinen, J., and Nieminen, T. M.: Impacts of forest harvesting on mobilization of Hg and MeHg in drained peatland forests on black schist or felsic bedrock, Environ Monit Assess, 188, 228, doi:10.1007/s10661-016-5210-x, 2016.

Ullrich, S. M., Tanton, T. W., and Abdrashitova, S. A.: Mercury in the Aquatic Environment: A Review of Factors Affecting Methylation, Critical Reviews in Environmental Science and Technology, 31, 241–293, doi:10.1080/20016491089226, 2001.

UNEP: Report of the Conference of the Parties to the Minamata Convention on Mercury on the work of its first meeting: UNEP/MC/COP.1/29, UNEP, Geneva, Conference of the Parties to the Minamata Convention on Mercury, First meeting, 85 pp., 2017.

UNEP: Global Mercury Assessment 2018, Geneva, Switzerland, 62 pp., 2019.

UNEP and AMAP: Technical Background Report for the Global Mercury Assessment 2018, Arctic Monitoring and Assessment Programme, Oslo, Norway/UN Environment Programme, Chemicals and Health Branch, Geneva, Switzerland, Geneva, Switzerland, 426 pp., 2019.

Untersuchung der Quecksilberbelastung im Boden: https://www.vs.ch/de/web/sen/untersuchungen, last access: 1 December 2016.

Untersuchung der Quecksilberbelastung im Boden: Gesamtüberblick der Quecksilbergehalte: https://www.vs.ch/de/web/sen/untersuchungen, last access: 12 December 2021.

US EPA: Method 3200: Mercury Species Fractionation and Quantification by Microwave Assisted Extraction, Selective Solvent Extraction and/or Solid Phase Extraction, part of Test Methods for Evaluating Solid Waste, Physical/Chemical Methods, SW-846 Update V, OSWER; Office of Resource Conservation and Recovery, 34 pp., 2014.

Vähätalo, A. V., Aarnos, H., and Mäntyniemi, S.: Biodegradability continuum and biodegradation kinetics of natural organic matter described by the beta distribution, Biogeochemistry, 100, 227–240, doi:10.1007/s10533-010-9419-4, 2010.

van Liem-Nguyen, Skyllberg, U., and Björn, E.: Thermodynamic Modeling of the Solubility and Chemical Speciation of Mercury and Methylmercury Driven by Organic Thiols and Micromolar Sulfide Concentrations in Boreal Wetland Soils, Environ. Sci. Technol., 51, 3678–3686, doi:10.1021/acs.est.6b04622, 2017.

Vigneron, A., Cruaud, P., Aubé, J., Guyoneaud, R., and Goñi-Urriza, M.: Transcriptomic evidence for versatile metabolic activities of mercury cycling microorganisms in brackish microbial mats, NPJ biofilms and microbiomes, 7, 83, doi:10.1038/s41522-021-00255-y, 2021.

Vlassopoulos, D., Kanematsu, M., Henry, E. A., Goin, J., Leven, A., Glaser, D., Brown, S. S., and O'Day, P. A.: Manganese(iv) oxide amendments reduce methylmercury concentrations in sediment porewater, Environmental science. Processes & impacts, 20, 1746–1760, doi:10.1039/c7em00583k, 2018.

Vos, H. C., Karst, I. G., Eckardt, F. D., Fister, W., and Kuhn, N. J.: Influence of Crop and Land Management on Wind Erosion from Sandy Soils in Dryland Agriculture, Agronomy, 12, 457, doi:10.3390/agronomy12020457, 2022.

Wang, A. O., Ptacek, C. J., Mack, E. E., and Blowes, D. W.: Impact of multiple drying and rewetting events on biochar amendments for Hg stabilization in floodplain soil from South River, VA, Chemosphere, 262, 127794, doi:10.1016/j.chemosphere.2020.127794, 2021a.

Wang, A. O., Ptacek, C. J., Paktunc, D., Mack, E. E., and Blowes, D. W.: Application of biochar prepared from ethanol refinery by-products for Hg stabilization in floodplain soil: Impacts of drying and rewetting, Environmental pollution (Barking, Essex 1987), 267, 115396, doi:10.1016/j.envpol.2020.115396, 2020.

Wang, B., Zhong, S., Bishop, K., Nilsson, M. B., Hu, H., Eklöf, K., Bravo, A. G., Åkerblom, S., Bertilsson, S., Björn, E., and Skyllberg, U.: Biogeochemical influences on net methylmercury formation proxies along a peatland chronosequence, Geochimica et Cosmochimica Acta, 308, 188–203, doi:10.1016/j.gca.2021.06.010, 2021b.

Wang, X., Bao, Z., Lin, C.-J., Yuan, W., and Feng, X.: Assessment of Global Mercury Deposition through Litterfall, Environ. Sci. Technol., 50, 8548–8557, doi:10.1021/acs.est.5b06351, 2016a.

Wang, Y., Chen, Z., Wu, Y., and Zhong, H.: Comparison of methylmercury accumulation in wheat and rice grown in straw-amended paddy soil, The Science of the total environment, 697, 134143, doi:10.1016/j.scitotenv.2019.134143, 2019.

Wang, Y., Dang, F., Zhong, H., Wei, Z., and Li, P.: Effects of sulfate and selenite on mercury methylation in a mercury-contaminated rice paddy soil under anoxic conditions, Environmental science and pollution research international, 23, 4602–4608, doi:10.1007/s11356-015-5696-8, 2016b.

Wängberg, I., Edner, H., Ferrara, R., Lanzillotta, E., Munthe, J., Sommar, J., Sjöholm, M., Svanberg, S., and Weibring, P.: Atmospheric mercury near a chlor-alkali plant in Sweden, Science of The Total Environment, 304, 29–41, doi:10.1016/S0048-9697(02)00554-5, 2003.

Weber, F.-A., Voegelin, A., Kaegi, R., and Kretzschmar, R.: Contaminant mobilization by metallic copper and metal sulphide colloids in flooded soil, Nature Geoscience, 2, 267–271, doi:10.1038/ngeo476, 2009.

Weiss-Penzias, P. S., Bank, M. S., Clifford, D. L., Torregrosa, A., Zheng, B., Lin, W., and Wilmers, C. C.: Marine fog inputs appear to increase methylmercury bioaccumulation in a coastal terrestrial food web, Scientific reports, 9, 17611, doi:10.1038/s41598-019-54056-7, 2019.

West, J., Gindorf, S., and Jonsson, S.: Photochemical Degradation of Dimethylmercury in Natural Waters, Environ. Sci. Technol., 56, 5920–5928, doi:10.1021/acs.est.1c08443, 2022.

Wilken, R.-D., Nitschke, F., and Falter, R.: Possible interferences of mercury sulfur compounds with ethylated and methylated mercury species using HPLC-ICP-MS, Analytical and bioanalytical chemistry, 377, 149–153, doi:10.1007/s00216-003-2090-z, 2003.

Windham-Myers, L., Marvin-DiPasquale, M., Kakouros, E., Agee, J. L., Le Kieu, H., Stricker, C. A., Fleck, J. A., and Ackerman, J. T.: Mercury cycling in agricultural and managed wetlands of California, USA: Seasonal influences of vegetation on mercury methylation, storage, and transport, The Science of the total environment, 484, 308–318, doi:10.1016/j.scitotenv.2013.05.027, 2014.

Wohlgemuth, L., Rautio, P., Ahrends, B., Russ, A., Vesterdal, L., Waldner, P., Timmermann, V., Eickenscheidt, N., Fürst, A., Greve, M., Roskams, P., Thimonier, A., Nicolas, M., Kowalska, A., Ingerslev, M., Merilä, P., Benham, S., Iacoban, C.,

Hoch, G., Alewell, C., and Jiskra, M.: Physiological and climate controls on foliar mercury uptake by European tree species, 19 pp., 2021.

Xu, X., Lin, Y., Meng, B., Feng, X., Xu, Z., Jiang, Y., Zhong, W., Hu, Y., and Qiu, G.: The impact of an abandoned mercury mine on the environment in the Xiushan region, Chongqing, southwestern China, Applied Geochemistry, 88, 267–275, doi:10.1016/j.apgeochem.2017.04.005, 2018.

Yin, D., He, T., Yin, R., and Zeng, L.: Effects of soil properties on production and bioaccumulation of methylmercury in rice paddies at a mercury mining area, China, Journal of environmental sciences (China), 68, 194–205, doi:10.1016/j.jes.2018.04.028, 2018.

Yu, X., Driscoll, C. T., Warby, R. A. F., Montesdeoca, M., and Johnson, C. E.: Soil mercury and its response to atmospheric mercury deposition across the northeastern United States, Ecological Applications, 24, 812–822, doi:10.1890/13-0212.1, 2014.

Zhang, L., Wu, S., Zhao, L., Lu, X., Pierce, E. M., and Gu, B.: Mercury Sorption and Desorption on Organo-Mineral Particulates as a Source for Microbial Methylation, Environmental science & technology, 53, 2426–2433, doi:10.1021/acs.est.8b06020, 2019.

Zhang, T., Kim, B., Levard, C., Reinsch, B. C., Lowry, G. V., Deshusses, M. A., and Hsu-Kim, H.: Methylation of mercury by bacteria exposed to dissolved, nanoparticulate, and microparticulate mercuric sulfides, Environmental science & technology, 46, 6950–6958, doi:10.1021/es203181m, 2012.

Zhang, T., Kucharzyk, K. H., Kim, B., Deshusses, M. A., and Hsu-Kim, H.: Net methylation of mercury in estuarine sediment microcosms amended with dissolved, nanoparticulate, and microparticulate mercuric sulfides, Environmental science & technology, 48, 9133–9141, doi:10.1021/es500336j, 2014.

Zhang, Y., Liu, Y.-R., Lei, P., Wang, Y.-J., and Zhong, H.: Biochar and nitrate reduce risk of methylmercury in soils under straw amendment, The Science of the total environment, 619-620, 384–390, doi:10.1016/j.scitotenv.2017.11.106, 2018.

Zhao, J.-Y., Ye, Z.-H., and Zhong, H.: Rice root exudates affect microbial methylmercury production in paddy soils, Environmental pollution (Barking, Essex 1987), 242, 1921–1929, doi:10.1016/j.envpol.2018.07.072, 2018.

Zhao, L., Chen, H., Lu, X., Lin, H., Christensen, G. A., Pierce, E. M., and Gu, B.: Contrasting Effects of Dissolved Organic Matter on Mercury Methylation by Geobacter sulfurreducens PCA and Desulfovibrio desulfuricans ND132, Environmental science & technology, 51, 10468–10475, doi:10.1021/acs.est.7b02518, 2017.

Zhao, L., Qiu, G., Anderson, C. W. N., Meng, B., Wang, D., Shang, L., Yan, H., and Feng, X.: Mercury methylation in rice paddies and its possible controlling factors in the Hg mining area, Guizhou province, Southwest China, Environmental pollution (Barking, Essex 1987), 215, 1–9, doi:10.1016/j.envpol.2016.05.001, 2016.

Zheng, N., Wang, S., Dong, W., Hua, X., Li, Y., Song, X., Chu, Q., Hou, S., and Li, Y.: The Toxicological Effects of Mercury Exposure in Marine Fish, Bull Environ Contam Toxicol, 102, 714–720, doi:10.1007/s00128-019-02593-2, 2019.

Zhou, J., Obrist, D., Dastoor, A., Jiskra, M., and Ryjkov, A.: Vegetation uptake of mercury and impacts on global cycling, Nat Rev Earth Environ, 2, 269–284, doi:10.1038/s43017-021-00146-y, 2021.

Zhu, H., Zhong, H., and Wu, J.: Incorporating rice residues into paddy soils affects methylmercury accumulation in rice, Chemosphere, 152, 259–264, doi:10.1016/j.chemosphere.2016.02.095, 2016.